Investigations into the Nature of the Endosomal System in *Plasmodium falciparum*

Priscilla Marilyn Krai

Dissertation submitted to the faculty of the Virginia Polytechnic Institute and State University in partial fulfillment of the requirements for the degree of

Doctor of Philosophy
In
Biochemistry

Michael Klemba, Chair
Daniela Cimini
Richard Helm
Marcy Hernick

August 9th, 2013
Blacksburg, VA

Keywords: Plasmodium falciparum, malaria, retromer complex, Rab7, FYVE domain, endosome, food vacuole, protein trafficking

Investigations into the Nature of the Endosomal System in *Plasmodium falciparum*

Priscilla Marilyn Krai

ABSTRACT

The parasite *Plasmodium falciparum* causes the most virulent form of human malaria and is responsible for the vast majority of malaria-related deaths. During the asexual intraerythrocytic stage, the parasite must transport newly synthesized proteins and endocytosed cargo to a variety of organelles, many of which are formed *de novo* and have no human equivalent. This process in mammalian cells would utilize an endosomal protein trafficking system, but no endosomal structures or proteins have been described in the parasite. Prior work on the parasite genome indicated that several proteins, which could potentially coordinate an endosomal network, were encoded in the genome and expressed during the asexual parasite stages. In this study, we have localized and attempted to further characterize these proteins in the context of the endosomal system. Two well-conserved protein components of the late endosome, the retromer cargo-selective complex and Rab7, were found on a previously un-described inherited structure adjacent to the parasite Golgi apparatus and in close opposition to nascent rhoptries (specialized secretory organelles required for invasion). The retromer cargo-selective complex was also in close proximity to its putative cargo, a *P. falciparum* homolog of the sortilin family of protein sorting receptors, PfSortilin. Another protein, PfFCP, the sole FYVE domain-containing protein in the *P. falciparum* genome, was localized to the membrane of a specialized acidic organelle, known as the food vacuole, where the parasite catabolizes the majority of its host cell hemoglobin. We analyzed the effects of a PfFCP dominant negative mutant and found that it altered food vacuole morphology and trafficking. A previous report localized the early endosome phosphoinositide, phosphatidylinositol 3-phosphate, to the food vacuole membrane,

and in conjunction with our studies on PfFCP, this has raised doubts about the food vacuole as a lysosome equivalent in the parasite. The combination of both early and late endosome protein homologs in the parasite, and their potential function, has led to a new model of protein trafficking within the parasite that includes the food vacuole as a terminal early endosome and the apical organelles as lysosome equivalents.

TABLE OF CO NTENTS

LIST OF FIGURES

LIST OF TABLES

LIST OF ABBREVIATIONS

10C	YFP variant "10C"
ACC	7-amino-4-carbamoylcoumarin
ACP	acyl carrier protein
ADP	adenosine diphosphate
AMC	7-amino-4-methylcoumarin
AP	clathrin adaptor protein complex
APP	amyloid precursor protein
ARF	ADP-ribosylation factor
BAR	Bin-Amphiphysin-Rvs protein dimerization domains
CIE	clathrin independent endocytosis
CI-MPR	cation-independent mannose-6-phosphate receptor (MPR)
CIT	YFP variant “Citrine”
CME	clathrin mediated endocytosis
COP	coat protein complex
CORVET	class C core vacuole/endosome tethering complex
CPY	carboxypeptidase Y
CSC	cargo-selective complex of retromer consisting of Vps26, Vps29 and Vps35
DD	destabilization domain
DKO	double-crossover homologous recombination knock out
DM	dominant negative mutant
DPAP	dipeptidyl aminopeptidase
DV	digestive vacuole (also called food vacuole)
EBA	erythrocyte-binding antigen
EEA1	early endosome autoantigen 1
EPM	erythrocyte plasma membrane
ER	endoplasmic reticulum
ESCRT	endosomal sorting complexes required for transport
FP-2	falcipain-2
FV	food vacuole (also called digestive vacuole)
FYVE	phosphoinositide-binding domain found in Fab1p, YOTB, Vac1p, and EEA1
GAP	GTPase activating protein
GEEC	GPI-AP-enriched early endosomal compartments
GEF	guanine nucleotide exchange factors
GFP	green fluorescent protein
GPI	glycosylphosphatidylinositol
GRASP	golgi reassembly and stacking protein
GRP	glucose-regulated protein
HA	hemagglutinin epitope tag
hDHFR	human dihydrofolate reductase
HMW	high molecular weight complex of rhoptry proteins
HOPS	homotypic fusion and vacuole protein sorting
LCEA	last common eukaryotic ancestor

LMW	low molecular weight complex of rhoptry proteins
MBP	maltose binding protein
MPR	mannose-6-phosphate receptor
MVB	multivesicular body
nDPAP1	native partially purified DPAP1
PfA-M1/ PfAMPN	M1-family aminopeptidase/ aminopeptidase N in *Plasmodium falciparum*
PfAPP	aminopeptidase P in *Plasmodium falciparum*
PfFCP	FYVE-domain containing protein in *Plasmodium falciparum*
PI	phosphoinositide
PI(3,5)P_2	phosphatidylinositol-3,5-bisphosphate
PI(4,5)P_2	phosphatidylinositol-4,5-bisphosphate
PI3P	phosphatidylinositol 3-phosphate
PPM	parasite plasma membrane of *Plasmodium falciparum*
PSL	positional scanning libraries
PV	parasitophorous vacuole
PVC	prevacuolar compartment
PVM	parasitophorous vacuole membrane
PX	phosphoinositide-binding domain first found in phagocytic oxidase (phox)
rDPAP1	recombinantly expressed and purified DPAP1
RE	restriction endonuclease
RFP	red fluorescent protein
RING	really interesting new gene zinc finger domain
SDPM	serine decarboxylase-phosphoethanolamine methyltransferase pathway
SERA	serine repeat antigen
SNARE	soluble N-ethylmaleimide-sensitive factor attachment protein receptors
SNX	sorting nexin
TEV	tobacco etch virus
TGN	*trans*-Golgi network
TgSORTLR	sortilin-like receptor in *Toxoplasma gondii*
TMP	trimethoprim
UTR	untranslated region
VPS	vacuolar protein sorting
WHO	World Health Organization
yDHOD	yeast dihydroorotate dehydrogenase
YFP	yellow fluorescent protein

CHAPTER 1:

Introduction

Malaria is an ancient disease and remains a global health threat today with an estimated 2 to 3 hundred million malaria cases per year, resulting in nearly one million deaths [1]. Human malaria is caused by five different members of *Plasmodium* spp., but *P. falciparum* is the cause of the vast majority of cases and malaria-related deaths [1]. Great progress has been made in the past decade thanks to increased funding [2]. The World Health Organization (WHO) estimates cases have decreased globally by 17%, and mortality rates by 26%, from 2000 to 2010 [1]. These gains are fragile though and subject to proper program implementation and available funding, which is expected to be reduced in the coming years [1,3]. Parasite resistance to current drugs is also a reasonable concern, especially given that *P. falciparum* strains have been discovered for which many anti-malarial drugs are no longer effective. These include the once ubiquitous chloroquine [4]. The danger exists that the most recent accomplishments will suffer the same fate as the malaria Global Eradication Program of the previous century, which resulted in resurgence in some areas and an increase in infant mortality [4]. Resistance to the highly effective frontline artemisinin-based combination therapies have recently been reported in southeast Asia [5]. Concerns center on the devastating effects these strains could have if containment failed and they reached sub-Saharan Africa where the malaria burden is much higher [6,7]. With the anticipated availability of a malaria vaccine still several years away [8], new anti-malarial therapies are urgently needed. Development of these treatments will require a much deeper understanding of parasite biology to exploit vulnerabilities and optimally implement new treatments in the field [4].

The parasite life cycle between the parasite's human host and insect vector presents multiple targets for drug development ([9], Fig. 1-1). The *P. falciparum* parasite first enters its human host as a motile sporozoite when an infected *Anopheles* mosquito takes a blood meal. From there it enters the bloodstream and invades liver hepatocytes where over the course of one to two weeks, it generates thousands of daughter merozoites. This small parasite form egresses and invades erythrocytes to begin the asexual erythrocyte cycle wherein clinical symptoms of malaria manifest. Over the course of approximately 48 hours, the parasite grows and replicates to produce 8-32 progeny that egress and invade fresh erythrocytes to begin the cycle anew. Some parasites differentiate into male and female sexual forms, also called gametocytes, due to various stimuli. These forms are taken up by another mosquito when it bites the infected human. Within the mosquito gut, gametocytes develop into male and female reproductive cells (gametes), which fuse to form a zygote. The zygote continues to develop into an ookinete, which crosses the wall of the gut to form an oocyst filled with sporozoites. When the oocyst bursts, the sporozoites move to the insect's salivary glands. Here they are ready to infect another human host to complete the cycle [10-12].

During the asexual erythrocyte stages, the parasite must complete the tasks of host cell modification and *de novo* development of multiple parasite-specific organelles that are important for parasite growth and subsequent invasion. This requires a powerful and agile protein synthesis and trafficking system with potentially exploitable elements that we are only beginning to understand.

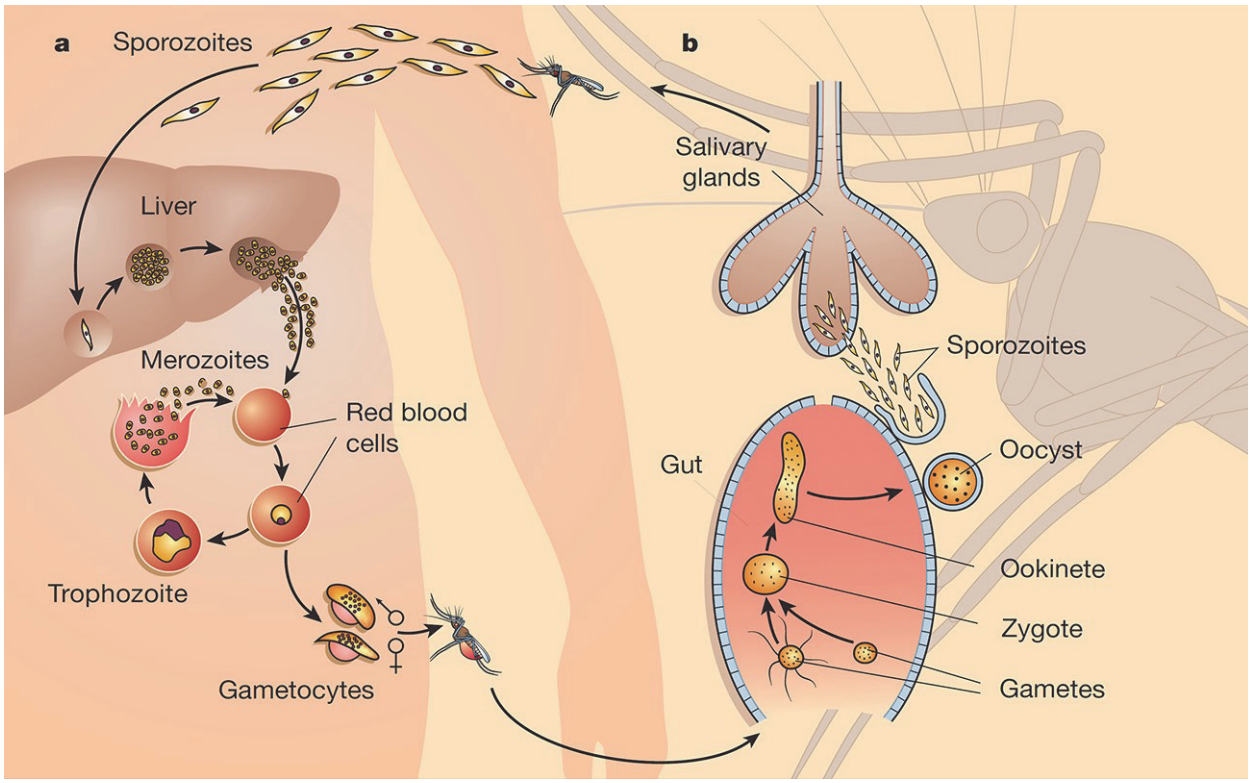

Figure 1-1. Life cycle of the parasite *Plasmodium falciparum*. The parasite progresses through multiple stages during its time within its A) human host and B) *Anopheles* mosquito vector. Individual stages are described in the text. Reprinted by permission from Macmillan Publishers Ltd: Nature [11], copyright 2002.

In the chapters to follow, I discuss our work towards understanding the components of the *P. falciparum* protein trafficking endomembrane system. Chapter 2 reviews what is known about *P. falciparum* protein trafficking and how it compares with model systems. Curiously, despite possessing a rudimentary early secretory pathway, an endosomal system has never been described in the parasite. To define the endosome and its role in protein trafficking, in Chapter 3 we localized and attempted to characterize homologs of the retromer cargo-selective complex and Rab7, which both localize to the late endosome in mammals [13]. In mammals, endocytosed cargo enters the endosomal system through the early endosome [14], where proteins containing a FYVE domain are routinely localized [15]. I present our results of a study exploring the role of

the only phosphatidylinositol 3-phosphate (PI3P)-binding FYVE-domain containing protein, PfFCP, in Chapter 4. In Chapter 5, I present our ideas on how endocytic and biosynthetic pathways have differentiated in the parasite. This work as a whole offers insight into the unique cell biology and protein trafficking pathways in *P. falciparum*, insight that may aid in the understanding and prevention of parasite drug resistance and development of new antimalarial treatments.

References

1. Organization WH (2012) World Malaria Report 2012. In: Organization WH, editor. Geneva, Switzerland: World Health Organization (WHO).
2. Organization WH (2010) World Malaria Report 2010. In: Organization WH, editor. Geneva, Switzerland: World Health Organization (WHO).
3. Cohen JM, Smith DL, Cotter C, Ward A, Yamey G, et al. (2012) Malaria resurgence: a systematic review and assessment of its causes. Malar J 11: 122.
4. Greenwood BM, Fidock DA, Kyle DE, Kappe SH, Alonso PL, et al. (2008) Malaria: progress, perils, and prospects for eradication. J Clin Invest 118: 1266-1276.
5. Ringwald P (2012) Update on artemisinin resistance
6. Organization WH (2013) Emergency response to artemisinin resistance in the Greater Mekong subregion: Regional Framework for Action 2013-2015. In: Organization WH, editor.
7. Dondorp AM, Fairhurst RM, Slutsker L, Macarthur JR, Breman JG, et al. (2011) The threat of artemisinin-resistant malaria. N Engl J Med 365: 1073-1075.
8. Riley EM, Stewart VA (2013) Immune mechanisms in malaria: new insights in vaccine development. Nat Med 19: 168-178.
9. Delves M, Plouffe D, Scheurer C, Meister S, Wittlin S, et al. (2012) The activities of current antimalarial drugs on the life cycle stages of Plasmodium: a comparative study with human and rodent parasites. PLoS Med 9: e1001169.
10. Sherman IW (2005) Molecular approaches to malaria. Washington, D.C.: ASM Press. xviii, 542 p. p.
11. Wirth DF (2002) Biological revelations. Nature 419: 495-496.
12. Miller LH, Ackerman HC, Su XZ, Wellems TE (2013) Malaria biology and disease pathogenesis: insights for new treatments. Nat Med 19: 156-167.
13. Balderhaar HJ, Arlt H, Ostrowicz C, Brocker C, Sundermann F, et al. (2010) The Rab GTPase Ypt7 is linked to retromer-mediated receptor recycling and fusion at the yeast late endosome. J Cell Sci 123: 4085-4094.
14. Huotari J, Helenius A (2011) Endosome maturation. EMBO J 30: 3481-3500.
15. Gillooly DJ, Simonsen A, Stenmark H (2001) Cellular functions of phosphatidylinositol 3-phosphate and FYVE domain proteins. Biochem J 355: 249-258.

CHAPTER 2:

Literature Review

Protein Sorting and Transport Challenges Facing the Malaria Parasite

During the asexual intraerythrocytic stage (Fig. 2-1), the malaria parasite *Plasmodium falciparum* has multiple trafficking challenges that it must overcome to grow and produce progeny. Newly synthesized proteins must be directed to a variety of destinations both within the parasite's plasma membrane and outside to its host (Fig. 2-1 inset). In contrast to related species like *Toxoplasma gondii* that invade nucleated cells and can hijack their metabolic machinery [1], the human erythrocyte has no nucleus, protein synthesis or trafficking capability. The asexual parasite must supply all the necessary tools to the erythrocyte cytoplasm and membrane for its own survival, as well as sort cargo to its own unique organelles within its plasma membrane. These include the apicoplast, food vacuole (FV), and apical secretory organelles. Trafficking to both the erythrocyte and the apicoplast has been reviewed in detail [2,3]. We have no evidence that protein transport to these compartments is relevant to the topics explored in this study. Therefore, trafficking mechanisms to these compartments will not be included in this review.

The FV and apical organelles are formed *de novo* in the parasite, but at different stages in development. Less than 12 hours after invasion, small endocytic vesicles containing host cell cytoplasm and acidic hydrolases fuse together to form the FV [4]. This acidic organelle (pH 5.5) [5] is the site of hemoglobin catabolism to amino acids, an important process required for parasite growth and proliferation [6-10]. A byproduct of hemoglobin catabolism is toxic free heme, which is sequestered in a non-toxic crystalline lattice known as hemozoin in the FV [11].

Many questions remain about the process of bringing erythrocyte cytoplasm and new acidic hydrolases into the FV. These are discussed below.

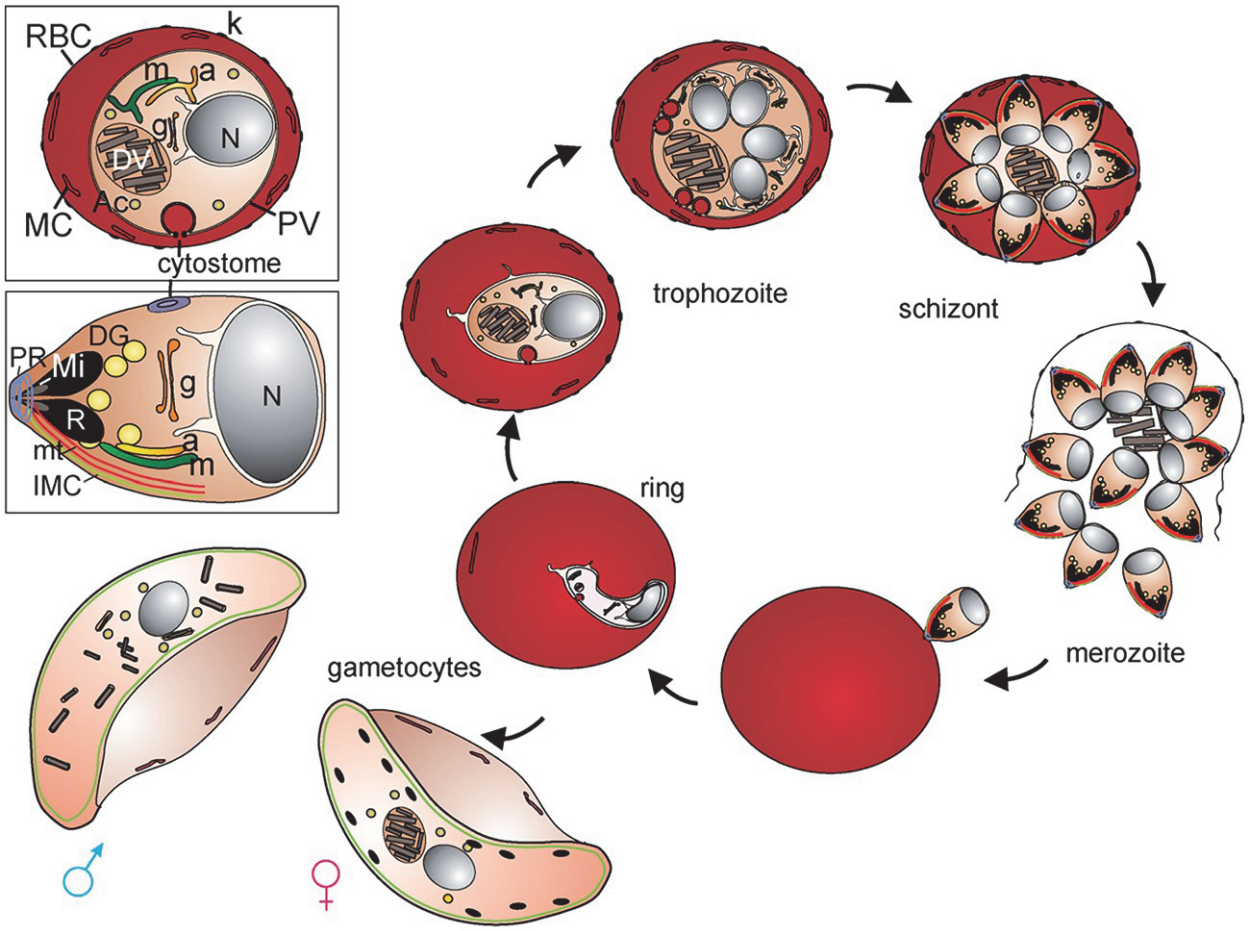

Figure 2-1: Schematic representation of the intraerythrocytic cycle of *P. falciparum*. After invading a new RBC, the parasite may differentiate into male and female gametocytes that can infect mosquitoes. The majority of parasites, however, continue the asexual cycle by developing into a mononuclear trophozoite stage with a hemozoin crystal and later a schizont stage, which undergoes nuclear division and merozoite development. Fully formed merozoites egress the spent RBC to begin the cycle anew. The upper inset illustrates a trophozoite with the nucleus (N), Golgi (g), digestive/food vacuole (DV), mitochondrion (m), apicoplast (a), acidocalcisomes (Ac), cytostomal invagination, parasitophorous vacuole (PV), Maurer's clefts (MC) and knobs (k) indicated. The lower inset illustrates a merozoite with nucleus (N), Golgi (g), mitochondrion (m), apicoplast (a), rhoptries (R), micronemes (Mi), dense granules (DG), polar rings (PR), inner membrane complex (IMC) and lateral microtubules (mt) indicated. Reprinted from [12] Int J Biochem Cell Biol, 43, Tilley, L., Dixon, M. W. & Kirk, K., The *Plasmodium falciparum*-infected red blood cell, 839-42, Copyright (2011), with permission from Elsevier.

The apical secretory organelles include several compartments formed *de novo* by budding from the Golgi apparatus or nearby organelles [13] during the late trophozoite and schizont stages. These include rhoptries, micronemes, dense granules, exonemes and mononemes. The apical organelles facilitate egress of a daughter merozoite from the spent erythrocyte and its attachment, invasion and establishment into its new host [14,15]. The process of apical organelle formation and their contents will be discussed below.

Trafficking to both the FV and apical organelles occurs along the secretory and endocytic pathways. Our understanding of protein trafficking in the parasite has grown considerably in recent years, yet much is still undefined, especially beyond the Golgi apparatus [16]. Studies suggest a highly streamlined and simplified system relative to its counterparts in model organisms. The unique targets within the parasitized erythrocyte have given rise to specific transport needs, and potentially have necessitated new or modified pathways.

The Early Secretory Pathway in *P. falciparum*

What is known about the *P. falciparum* protein trafficking and sorting system indicates that many components of the early secretory pathway are conserved between the parasite and model organisms; these include the perinuclear and transitional ER and the Golgi apparatus (reviewed previously [2,16,17]). The scope of the next few sections will include properties and structures that are unique to the parasite, and trafficking within the parasite plasma membrane beyond the *trans*-face of the Golgi apparatus.

The early secretory pathway in eukaryotes follows a set of sequential and regulated steps within the ER and Golgi apparatus before proteins are directed to the extracellular space or to the cell's organelles (Fig. 2-2). In *P. falciparum*, many features of this system are simplified,

modified or even missing entirely (Table 2-1). Entry into the ER is governed by the translocon multi-protein complex [18]. The parasite genome encodes translocon core subunits and accessory proteins [19]. The locations of the majority of these proteins have not been directly studied, but two, PfSec61, a translocon core subunit, and PfBiP, an ER chaperone, have been found in the perinuclear ER [20,21]. Similar to model systems, the parasite translocon recognizes an N-terminal hydrophobic amino acid sequence of variable length known as a signal peptide. Parasite proteins may also have recessed signal peptides, or export proteins that have no recognizable sequence [22]. Whether the different types of signal peptides serve additional functions has yet to be shown.

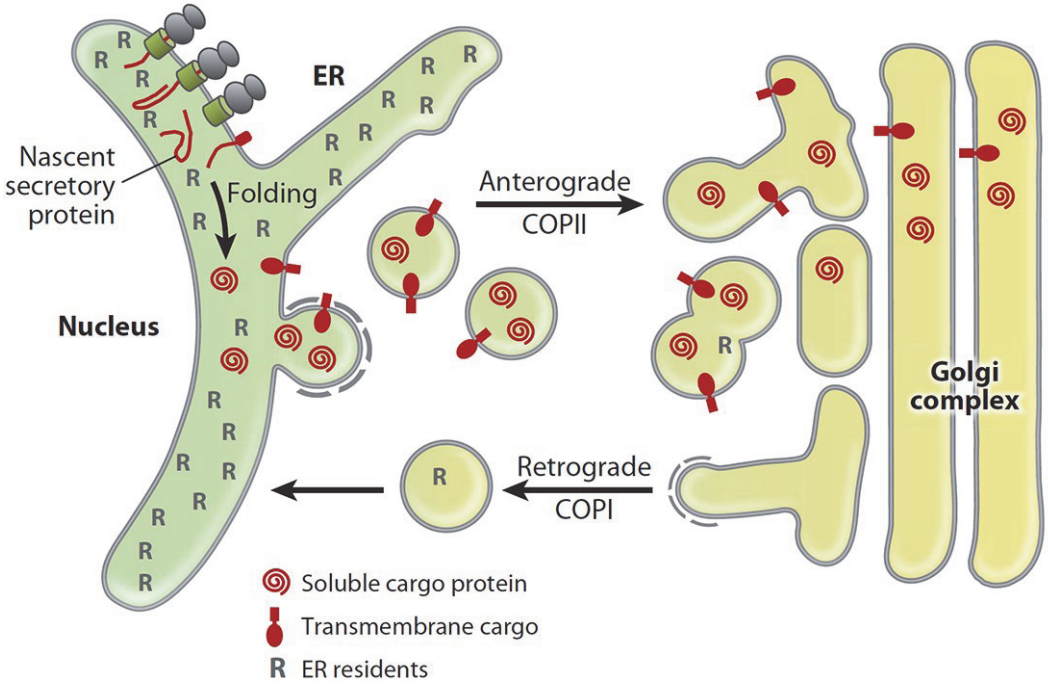

Figure 2-2: Model of the mammalian early secretory pathway. Integral membrane and soluble secretory proteins (in red) with signal peptides are translated and folded at the ER where they are exported to the Golgi apparatus in coat protein complex II (COPII)-formed transport vesicles to fuse with or form pre-Golgi compartments. COPI coated vesicles traveling in a retrograde fashion contain resident proteins (R) that have escaped the ER. Republished with permission of Annu. Rev. Biochem., from [23] Protein Sorting Receptors in the Early Secretory Pathway, Julia Dancourt & Charles Barlowe, 79 and 2010; permission conveyed through Copyright Clearance Center, Inc.

Structural components of the ER and Golgi apparatus, as well as transportation systems between the two, are present and functional in the parasite (Table 2-1). These include budding, transport, docking and fusion machinery of the COPI- and COPII-mediated pathways [24-26]. PfRab1 [27] and PfRab2 [28] have also been found to facilitate vesicle traffic between the ER and Golgi apparatus. Protein modification and quality control functions of these two organelles are simplified, however. Molecular chaperones that regulate "quality control" processes in the ER sequester and eventually degrade improperly folded proteins [29,30]. The *P. falciparum* genome does encode for homologs of some of these, namely BiP [21], glucose-regulated protein (Grp) 94 [31,32], peptidyl prolyl isomerase [33] and protein disulfide isomerase [34,35], indicating that the parasite retains primary quality control ability and ER retention. Interestingly, calnexin and calreticulin, also ER chaperones, are missing from the parasite genome [33]. Both of these proteins are involved in quality control of glycoproteins [30]. Their absence is in agreement with experimental evidence that the parasite lacks most, if not all, N-glycosylation machinery [33,36-38].

The parasite Golgi apparatus has an unusual ultrastructure and that O-glycosylated proteins are rare [17]. It consists of a single compartment [39], rather than stacked cisternae found in other eukaryotes. Several homologs of Golgi apparatus proteins in model systems are conserved. These include the *cis*-Golgi located ER receptor, PfERD2 [40]; Golgi matrix proteins, PfGRASP1/2 [41]; Golgi-docking protein, PfBet3 [42]; and *trans*-Golgi located, PfRab6 [39]. In mammals, Rab6 is important for trans-Golgi trafficking and organization of the Golgi stack [43], but its function in the parasite is still uncertain [39,44-46]. These proteins have been localized to spatially discrete subdomains, suggesting that *cis*- and *trans*-faces may be compositionally distinct even within the single Golgi compartment [47].

Table 2-1: Selected early secretory proteins and their putative homologs in *P. falciparum*

Protein/Complex	Function	Mammalian Protein Name	Gene in *P. falciparum*[1]	Ref(s)
Protein Translocation Pathway				
Signal recognition particle (SRP) complex	binds to signal sequence & blocks translation	SRP9	MAL7P1.158	[19]
		SRP14	PFL0160w	[19]
		SRP19	PFL0785c	[19]
		SRP54	PF14_0477	[19]
		SRP68	n/f	[19]
		SRP72	n/f	[19]
SRP receptor (SRPR) complex	binds to SRP at ER membrane	SRPRα	PF13_0350	[19]
		SRPRβ	PFL2245w	[19]
Translocon/secretory (Sec) complex	forms a protein conducting channel at the ER membrane	Sec61α	MAL13P1.231	[19,20]
		Sec61β	MAL8P1.51	[19]
		Sec61γ	PFB0450w	[19]
		Sec62	PF14_0361	[19]
		Sec63	PF13_0102	[19]
Translocation associated membrane protein (TRAM)	regulates which regions of nascent protein are available to the cytosol during translocation	TRAM	PF14_0034	[19]
ER Lumen Protein Quality Control and Modification				
Chaperones (for a more complete list of parasite chaperones in the genome see [33])	binds newly synthesized proteins & promotes proper folding	Bip	PFI0875w	[33,48,49]
		Grp94	PFL1070c	[31-33]
	catalyzes cis-trans isomerization of proline	peptidyl prolyl isomerase (PPI)	PF08_0121, PF11_0164	[33]
	catalyzes formation & breakage of cysteine disulfide bonds	protein disulfide isomerase (PDI)	MAL8P1.17	[33-35]
	prevent Golgi transport of improperly folded glycoproteins	calnexin	n/f	[33]
		calreticulin	n/f	[33]
ER-resident calcium (ERC) binding protein	maintains calcium gradient between ER & cytosol	reticulocalbin	PF11_0098	[50]
ER lumen resident glycosyltransferase	synthesizes dolichol-PP-oligosaccarides	Alg3	n/f	[51]
		Alg9	n/f	[51]
		Alg12	n/f	[51]
		Alg6	n/f	[51]
		Alg8	n/f	[51]
		Alg10	n/f	[51]
Sugar donor synthesizing enzymes	synthesizes dolichol-P-Glc	Alg5	n/f	[51]
	synthesizes dolichol-P-Man	Dpm1	PF11_0427[2]	[51]

Antereograde Protein Transport from the ER to the Golgi Apparatus

COPII Coat Complex	coat protein complex for ER to Golgi sorting found at ER exit sites	Sar1	PFD0810w	[52]
		Sec23	PF08_0036	[53]
		Sec24 a/b	PF13_0324 PFD0250c	[54]
		Sec13	PFL1480w	[47]
		Sec31	PFB0640c	[55]
	Sar1 GEF (ER membrane)	Sec12	PF11_0171	[54]
COPII vesicle tethering	recruits p115 to COPII vesicles	Rab1 GTPase a/b	PFE0690c PFE0625w	[27]
	tethers COPII vesicles	p115	n/d	
COPII vesicle SNAREs	Qa-SNARE	Sed5	n/d	
	Qb-SNARE	Bos1	n/d	
	Qc-SNARE	Bet1	PF14_0500 PFE1505w	[56]
	R-SNARE	Ykt6	PFI0515W MAL13P1.135	[56]
TRAPPI complex	tethers COPII-derived vesicles to Golgi membranes & may act as Rab1 GEF	Trs20/sedlin	PF13_0174	[57]
		Trs23/sybindin	PFC0445w	[57]
		Trs31	PF14_0358[3]	[57]
		Trs33	PFF0905w[3]	[57]
		Bet5	PF14_0049[3]	[57]
		Bet3	PFD0895c PF14_0358[3]	[57]

Retrograde Transport from the Golgi Apparatus to the ER

ER resident protein receptor	KDEL receptor at the Golgi	ERD2	PF13_0280	[39,40]
COPI complex	coat protein complex for sorting within the Golgi & between the Golgi & the ER	αCOP/Sec33/Ret1	PFF0330w	[24]
		βCOP/β'COP	PF14_0277 PFI0290c	[58]
		γCOP/Sec21	PF11_0463	
		δCOP/Ret2	PF11_0359	
		εCOP/Sec28	MAL8P1.121	
		ζCOP/Ret3	PFD0745c	
COPI Complex Recruitment	recruits COPI subunits	ARF1 GTPase	PF10_0203	[59,60]
	deactivate ARF GTPase	ARF GAP	PFL2140c	[61,62]
	activate ARF GTPase	ARF1 GEF	PF14_0407	[63,64]
	recruits ARF GTPase	Sys1	n/d	
	regulates traffic & may recruit COPI subunits	Rab2 GTPase	PFL1500w	[28]
Dsl1 Complex	tethers COPI vesicles at the ER membrane	Dsl1	n/f	[57]
		Tip20	n/f	[57]
COPI vesicle & Dsl1 complex SNAREs	Qb-SNARE	Sec20	MAL13P1.87	[57]
	Qa-SNARE	Ufe1	n/d	
	Qc-SNARE	Use1/Slt1	n/d	

	R-SNARE	Sec22	PFC0890w	[56]
TRAPPII complex	tethers Golgi cisternae & interacts with COPI vesicles	TRAPPI subunits plus	see above	[57]
		Trs65	n/f	[57]
		Trs120	n/f	[57]
		Trs130	n/f	[57]
Protein Components, Quality Control and Modification at the Golgi Apparatus				
trans-Golgi Rab GTPase	retrograde transport within the Golgi and to the ER	Rab6 GTPase	PF11_0461	[39,47]
Golgi reassembly stacking proteins	structural proteins	GRASP1	PF10_0168	[41]
		GRASP2	PF10_0168 (splice variant)	[45]
Serine derived phosphatidylecholine (SDPM) pathway	phosphatidylecholine synthesis in the *trans*-Golgi	phosphoethanolamine methyltransferase	MAL13P1.214	[65]
Postranslational modification enzymes	transfers of palmitoyl group for membrane association	palmitoyl transferase	PFC0160w	[66,67]

n/d: Presence or absence of *P. falciparum* homologs has not yet been determined.
n/f: Homolog(s) not found *P. falciparum* genome in cited reference.

[1]: PlasmoDB Gene ID for *P. falciparum* homolog(s) either as stated in reference or as gene is annotated.
[2]: N-glycosylation activity has not been detected during *P. falciparum* intraerythrocytic stages. These genes have not been further characterized to confirm involvement in this pathway.
[3]: PlasmoDB ID not specified in reference or annotated in genome, but found via BLAST search results with high degree of certainty using *S. cerevisiae* or human homolog as query.

Within the Golgi apparatus, two enzymes with recognizable functions have been localized. These enzymes are involved in the synthesis of phospholipids and addition of fatty acids to proteins. The parasite can use serine as a precursor in phosphatidylecholine production in the plant-like serine decarboxylase-phosphoethanolamine methyltransferase (SDPM) pathway. One of the enzymes required for synthesis is phosphoethanolamine methyltransferase, which has been localized to the PfRab6-positive Golgi apparatus [65]. In addition, one of twelve potential palmitoyl transferases has been experimentally characterized and localized to the Golgi apparatus in mature parasites [66,67].

In model systems the *trans*-Golgi network functions as a transit nexus for cargo to a wide variety of destinations (reviewed in [68,69]). Secreted proteins can be directed to the plasma membrane through secretory granules or constitutively secreted to the plasma membrane [70]. Cargo destined for the lysosome, such as acidic hydrolases, travels a third route through the endosomal system [71]. In *Plasmodium* we have little understanding about post-Golgi trafficking [16]. Whether cargo reaches its target directly or passes through intermediate compartments has yet to be determined. There is a growing body of evidence, including microscopy studies, that supports vesicle-mediated transport [13]. While this has never been directly investigated, the presence of Rab GTPase, SNARE, clathrin and clathrin adaptor homologs in the *P. falciparum* genome support this theory.

Despite our limited understanding of trafficking, targeting sequences to specific post-Golgi organelles have been identified. If a protein lacks a targeting sequence, the default destination after entering the secretory pathway is the parasitophorous vacuole (PV) [16]. Targeting sequences assist in the transport of many proteins beyond the parasitophorous vacuolar membrane (PVM) and into the erythrocyte (reviewed in [2]). For some proteins, the PV is an intermediate step before being brought back into the parasite through hemoglobin endocytosis.

Hemoglobin Uptake and Food Vacuole Transport

The food vacuole (FV) is a large (2 to 3 μm) [72] acidic organelle in *P. falciparum* in which two-thirds of host erythrocyte hemoglobin (~97% its dry weight) is degraded by multiple acidic hydrolases [73,74]. This produces individual amino acids, which have multiple fates [75-77]. A minority (~16%) of these amino acids is incorporated into parasite proteins [74]; the remainder is released into the medium to make space for the growing parasite and relieve

osmotic pressure [7,78,79]. A byproduct of hemoglobin catabolism is toxic free heme [80]. To prevent the generation of reactive oxygen species the parasite sequesters heme in a crystalline lattice known as hemozoin [81]. Both hemoglobin catabolism and hemozoin generation in the FV are essential processes for the parasite [7,9]. For this reason, trafficking of hemoglobin and enzymes to the FV and FV biogenesis are topics that have received much attention.

According to current models, the FV is not inherited with each invasion, but formed *de novo* though endocytic vesicle fusion (Fig. 2-3, [4]) . The organelle changes shape throughout the asexual blood stages. Abu Bakar and colleagues recently studied the formation of the FV during the early stages of parasite development [4]. They found that initial uptake of erythrocyte cytoplasm occurs through vesicle transport 10 to 12 hours after host cell invasion. Hemoglobin-containing vesicles form at electron dense pores on the parasite membrane, known as the cytostomes. These small compartments are already acidic and separate from the host cytoplasm [4]. They also contained the acidic hydrolase plasmepsin II (PM2), and by late ring stage hemozoin crystals, suggesting that hemoglobin catabolism had already begun before the generation of a large food vacuole [4].

A larger acidic compartment was not consolidated until the late ring and early trophozoite stage [4]. In mature parasites, extra-FV compartments were also observed often near the FV [4]. These other compartments were acidic and housed acidic hydrolases. Similar structures have also been seen when localizing the chloroquine resistance transporter (PfCRT) an integral FV membrane protein [82]. It is unknown yet when or if the extra FV compartment merges with the main FV. During the schizont stage, the FV, along with enclosed hemozoin crystal, becomes closely compact [83]. A lipid body appears near the FV, which could potentially account for loss

of membrane [84]. When merozoites egress from the spent host cell, the FV residual body, including hemozoin and its membrane, is left behind [83,85].

Many aspects of the process of hemoglobin uptake remain unknown. While we know that vesicles appear to form at cytostomes, the structural components of the cytostome have yet to be identified. The endocytic process used by the parasite has proven difficult to unravel. Invaginations form at the cytostome bound by two membranes, the PPM and the PVM. The current model suggests that these invaginations then pinch off into double membrane vesicles (Fig. 2-3). Current evidence suggests that parasite phosphatidylinositol 3-phosphate (PI3P) plays a role in hemoglobin endocytosis [86-90]. The characteristic clathrin electron dense coat does not surround nascent hemoglobin-containing vesicles, suggesting that classical clathrin mediated endocytosis (CME) mechanisms are not employed. Homologs of CME components are present in the parasite genome but may have functions in other aspects of protein trafficking, such as secretion, or at different stages in parasite development [16]. Despite this, both dynamin and actin, components of CME, have been implicated in hemoglobin uptake. The dynamin inhibitor, dynasore, appears to inhibit hemoglobin uptake into the parasite [91]. It is possible that one of the two dynamin homologs in the parasite is involved with hemoglobin vesicle fission. Disrupting normal actin dynamics with polymerization inhibitors and stabilizers also prevents proper hemoglobin trafficking. In parasites treated with these compounds, vesicles did not fuse to the FV, but endocytosis and vesicle formation was not inhibited [92]. It has been suggested that actin may function in directing newly formed vesicles towards the FV [16]. The small GTPase PfRab5a has been localized to the membrane of these hemoglobin-containing vesicles [93], tempting comparisons with early endosomal trafficking (discussed below). However, the

localization of PfRab5a was using overexpressed constitutively active mutant and therefore may not reflect the location of the endogenous enzyme.

In order for hemoglobin catabolism to occur, multiple acidic hydrolases must reach the FV lumen. Generally, in model systems, resident soluble enzymes of an acidic degradative organelle are trafficked from the TGN to the late endosome on their way to lysosome or vacuole by vesicle fusion or endosome maturation [71]. No study on the presence or function of the parasite endosomal system has yet been published. There is, however, some information on the paths enzymes take on their way to the FV. Trafficking of plasmepsin II (PM2), falcipain-2 (FP-2), and dipeptidyl aminopeptidase 1 (DPAP1) are the best studied.

The aspartic protease plasmepsin II (PM2) catalyzes the release of globin peptides from hemoglobin [94]. PM2 enters the early secretory system as an integral membrane protein [76]. It is thought to be transported to cytostome-derived vesicles before being delivered to the FV [95]. Within the acidic environment of the FV, PM2 is proteolytically cleaved to release it from the membrane by other proteases [96] or itself [95], a process called autocatalytic maturation. The cysteine protease FP-2 is also initially expressed with a transmembrane domain and both cytosolic and lumenal regions. Most of the propeptide, including sections from all three regions, is necessary for trafficking to the FV [77]. Dipeptidyl aminopeptidase 1 (DPAP1) is involved in hemoglobin catabolism downstream of PM2 and FP-2; it cleaves dipeptides from hemoglobin derived oligopeptides. It is trafficked differently than the previous two enzymes. Accumulations of DPAP1are not observed around cytostomal vesicles. Instead, DPAP1 is found in the PV during the asexual stages, suggesting that it is transported to the FV along with endocytosed hemoglobin. However, a direct route cannot be ruled out at this time. Both PM2 and FP-2 require components of vesicle trafficking to reach the cytostome and DPAP1 within the PV is likely

actively incorporated into the hemoglobin-containing vesicle. None of the components for these processes has been characterized.

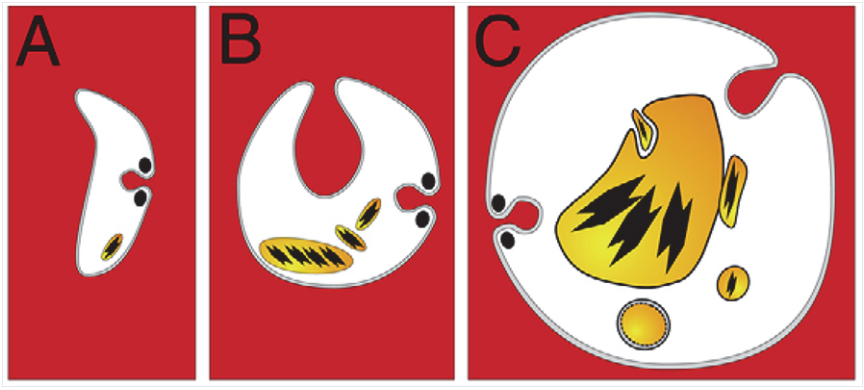

Figure 2-3: Current model of FV biogenesis and hemoglobin endocytosis. A) In ring stage parasites, the cytostome is actively involved in hemoglobin uptake. These vesicles form pre-FV compartments. B) Later in development, endocytosis at the cytostome continues and these pre-FV compartments fuse to form a single FV. C) In the trophozoite stage, endocytosis of hemoglobin continues and vesicles fuse to form a large FV structure along with longer-lived extra-FV compartments in which hemoglobin catabolism may occur. Republished with permission of J. Cell Sci. from [4] Digestive-vacuole genesis and endocytic processes in the early intraerythrocytic stages of *Plasmodium falciparum*, Abu Bakar, N., Klonis, N., Hanssen, E., Chan, C., & Tilley, L., 123, 3, 2011; permission conveyed through Copyright Clearance Center, Inc.

Trafficking to the Apical Secretory Organelles

The apical secretory organelles include rhoptries, micronemes, dense granules, exonemes and mononemes (Fig. 2-1 bottom inset). These organelles have diverse contents and shapes, but are all likely formed *de novo* after each invasion. Not much is known about this process, but there is some evidence that suggests rhoptries are formed via vesicle budding from either the Golgi apparatus or parasite endosome ([13], Chapter 3). The apical organelles work in conjunction to allow a new merozoite to leave the depleted host and to invade a fresh erythrocyte [15]. Apical organelle proteins enter the secretory system and likely reach their destination

through vesicle-mediated trafficking (Fig. 2-4, [16,97]). Determining what protein coats and receptors are used, and how cargo distinguishes between organelles or its subcompartments, has yet to be elucidated.

Rhoptries, the largest of these organelles, are pear -shaped structures at the apical tip of a merozoite. The contents of the rhoptry are not homogeneous; the bulb and neck regions have different compositions. Upon attachment and invasion, rhoptries release their contents in a regulated fashion to establish binding to the target cell plasma membrane and then form the tight (or moving) junction (reviewed in [98]). Some rhoptry proteins, such as RAP1 and RhopH1/2/3, are found in the PV and erythrocyte after invasion, suggesting that they have roles in defining these compartments as well [15,99].

Most apical organelle proteins are not expressed until the parasite has begun nuclear division, or even later after apical organelle formation has commenced [100]. Rhoptry-associated membrane antigen (RAMA) is a GPI-anchored protein that is an important exception to this rule [101,102]. Expressed during the late trophozoite stage, it remains at the ER and Golgi before being transported to the rhoptries [103]. Due to early expression, membrane association and interaction with other soluble rhoptry proteins, RAMA is thought to be important for rhoptry formation and sorting [103]. RAMA has been shown to associate with rhoptry associated protein 1 (RAP1), part of the low molecular weight (LMW) complex. Interaction occurs at a ~30 amino acid segment of the propeptide region of RAP1 [104]. RAP1 in turn associates with, and is required for, RAP2 and RAP3 transport [105]. Potentially, RAMA may form a complex with the high molecular weight (HMW) complex components, RhopH1/2/3, as well [104,106]. Both RAMA and RAP1 undergo proteolytic cleavage [104]. For RAMA this is quite extensive, removing almost 50% of the protein before it reaches the rhoptries [103]. Processing may have

importance for proper trafficking, complex formation or stability. The C-terminus of RAMA is embedded in the lipid bilayer and is not cytosol accessible [107]. Consequently, it is unlikely to act alone in targeting rhoptry proteins.

Proteins are also targeted to the cytosolic face of the rhoptries. One of these was described in a recent study on PfARO, a conserved protein in *P. falciparum* with armadillo repeats and an unknown function at the rhoptries. Targeting of PfARO to the rhoptry membrane requires two acylation motifs within the first 20 amino acids [108]. Interestingly, similar sequences are found in other proteins that localize to the apical organelles, inner membrane complex or parasite plasma membrane (PPM) [108]. The dual acylation motif may act as a novel parasite-specific signal sequence.

Micronemes are smaller than rhoptries. These organelles are the first to release their contents and establish erythrocyte attachment [97,109]. A few *P. falciparum* microneme proteins also possess propeptides [110-112], but their role in trafficking is difficult to interpret. The microneme-localized merozoite surface sheddase, PfSUB2, is expressed as precursor zymogen that enters the secretory pathway [113]. Autocatalytic maturation, transmembrane and cytosolic domains are necessary for release from the ER and microneme transport [113]. In contrast, microneme proteins like erythrocyte-binding antigen (EBA)-140, EBA-175 and EBA-180 all contain transmembrane domains and cytosolic tails, which could act in sorting. Curiously, none of these proteins requires their cytosolic tails for microneme transport. A cysteine-rich ectodomain and a sequence upstream of it are required for microneme trafficking [114-116]. Timing of expression is also important; if expressed earlier (pre-32 hours after invasion), EBA proteins followed the default pathway to the PV [114]. This suggests that the machinery for microneme trafficking is not fully functional until late in parasite development.

Despite understanding some of the motifs necessary for transport of rhoptry and microneme proteins, many of the targeting signals are not cytosolic and thus do not fit into our current understanding of receptor-mediated vesicle trafficking. No sorting receptor or protein coat has yet to be identified for either rhoptries or micronemes in *P. falciparum*. In the related species *Toxoplasma gondii*, a transmembrane sorting receptor homolog of sortilin, TgSORTLR, has been implicated in apical organelle trafficking [117]. It has been proposed that a yet to be identified AP adaptor and sortilin homolog may have a similar role in *P. falciparum* [97]. Proteins identified as requiring TgSORTLR for trafficking do not have direct homologs in *P. falciparum*. Alternatively, the RAMA complex is associated with lipid rafts [100,103], which can facilitate sorting without coats or adaptors [118]. This type of protein sorting has not yet been demonstrated in *P. falciparum*.

Much less is known about dense granules, exonemes and mononemes, both their contents and trafficking. Dense granules release their cargo to assist in establishing the parasite and its PV [97,119]. The exoneme protease, PfSUB1 [120], is released after merozoite formation. Both PfSUB1 and the cysteine protease, DPAP3, catalyze important protein processing events necessary for merozoite egress [121-123]. These events include the activation of SERAs (serine repeat antigens) that break down the cellular membranes [121,122]. Trafficking to dense granules or the exonemes has yet to be characterized. Mononemes contain the protease PfROM1, which is necessary for cleavage of transmembrane domains of invasion proteins [124]. As a whole, very little is known about the components necessary for apical organelle trafficking, but it may resemble the endosomal pathway established in model systems.

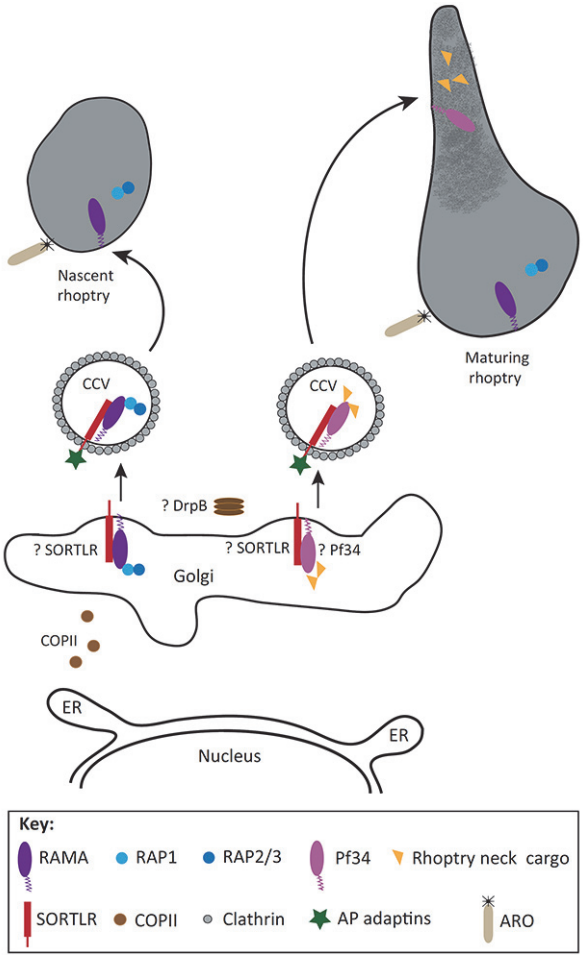

Figure 2-4: Model of rhoptry protein sorting in *P. falciparum*. Proteins destined for the rhoptries enter the early secretory system via a signal peptide at the ER and are transported to the Golgi apparatus in COPII-coated vesicles. Early in rhoptry development, GPI-anchored RAMA associates with bulb cargo, such as the RAP1 LMW complex, at the Golgi apparatus or parasite endosome. PfSortilin, a parasite sortilin homolog, may act as a sorting receptor to recruit adapter proteins (AP) and the cytosolic trafficking machinery. These regions ultimately bud off as rhoptry-destined potentially clathrin-coated vesicles (CCV). The CCVs fuse at the target membrane to release cargo into nascent rhoptries. Here, proteolytic processing of the rhoptry cargo facilitates their release from the trafficking complex. A bulb-retention motif in the RAP complex prevents their dispersal throughout the entire rhoptry as it matures and develops a neck region. The GPI-anchored rhoptry neck protein Pf34 may perform a similar role to RAMA later in rhoptry development. The function of the armadillo repeats-only (ARO) protein has not been characterized, but is targeted to the rhoptry membrane. Reprinted from [97] Trends in parasitology, 29, Counihan, N. A., Kalanon, M., Coppel, R. L., & de Koning-Ward, T. F., *Plasmodium* rhoptry proteins: why order is important, 228-36, Copyright (2013), with permission from Elsevier.

Role of the Endosome in Endocytic and Biosynthetic Pathways in Model Systems

The endosomal system includes many varied membrane bound compartments, which connect endocytic and biosynthetic pathways (Fig. 2-5). This organization was present before the last common eukaryotic ancestor (LCEA) [125]. As such, pathways and components of these routes may still be present and functional in *P. falciparum*. In addition, the parasite genome encodes for many endosome-specific homologs. These include three Rab5 isoforms, Rab7 and the retromer complex (Chapter 3), and an early endosome PI3-kinase, Vps34 [87]. Given our limited understanding of protein trafficking within the parasite itself, it may be useful to pursue these endosome protein homologs, identify their distribution, and function within the parasite.

The mammalian endosome is a tubular-vesicular network that acts as a crossroads for endocytic traffic from and to the plasma membrane, and biosynthetic traffic from the Golgi apparatus on its way to the lysosome [71]. Curiously, no mention of a *P. falciparum* endosome or endosome-like organelle exists in the current literature. The only endosome protein homolog that has been described in the parasite is PfVps4 [126]. Yeast Vps4p is found at the late-endosome/multivesicular body (MVB) where it is involved in protein sorting and causes the disassembly of the ESCRT-III complex [127-129]. Localization studies found that although wild type PfVps4 was cytosolic, an ATP hydrolysis deficient mutant was localized to punctate structures. No colocalization studies were performed in *P. falciparum*, but the PfVps4 mutant was expressed in *T. gondii* [126], where it was found on a MVB-like structure. It is therefore possible that *P. falciparum* utilizes some endosome protein homologs in trafficking and that an endosome-like organelle may exist in the parasite.

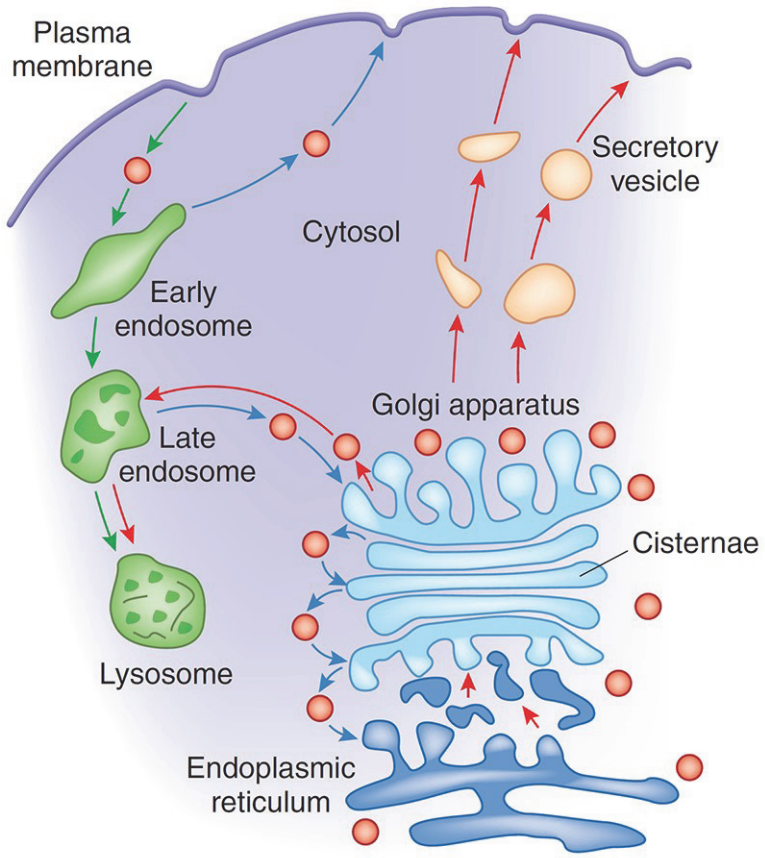

Figure 2-5: Schematic of the endosome/lysosome system in mammals. Endocytic vesicles deliver their contents and membrane components to the early endosome where they can travel to the late endosome and ultimately lysosome for degradation (green arrows) or be recycled to the plasma membrane (blue arrows). Biosynthetic cargo enters the secretory system at the ER and transported through the Golgi apparatus cisternae. At the trans-Golgi network, biosynthetic cargo may be secreted directly to the PM, to the cell's organelles (not shown), or in the case of newly synthesized lysosomal hydrolases and membrane components to the endosomal system via the late endosome. Late endosomes also carry a selected subset of both endocytosed and biosynthetic cargo. They undergo homotypic fusion reactions, growth, and a maturation process to deliver components to lysosomes. Reprinted by permission from Macmillan Publishers Ltd: Nature Chemical Biology [130], copyright (2009)

Even in genetically more tractable organisms, endosomes are difficult to characterize. Mammalian endosomes exist as a continuum of many small heterogeneous compartments scattered throughout the cytoplasm [131]. They are continually undergoing fusion, fission and maturation (reviewed in [71]). Endosomes act at the center of two circuits and receive influx from the *trans*-Golgi network. One circuit connects to the plasma membrane where internalized

cargo and integral membrane proteins brought into the cell can be sequestered or recycled back to the plasma membrane through the early and recycling endosomes. Cargo brought into the cell through clathrin mediated endocytosis (CME) and clathrin independent endocytosis (CIE) methods, such as caveolar-, GEEC-, and ARF6-dependent pathways, is received by the early endosome [132]. This organelle acts as the main sorting station along the endocytic pathway and as such is heterogeneous in terms of not only composition and function, but also location and morphology. A portion of endocytosed cargo enters the degradation circuit via early endosome maturation or vesicular transport to the late endosome. Endosome maturation occurs when the early endosome receives cargo destined for degradation by ubiquitination and sequestration in internal vesicles, beginning the process of multi-vesicular body (MVB) formation. Maturation of this pre-MVB to a late endosome proceeds through membrane protein changes and internal acidification. Late endosomes formed through early endosome maturation eventually fuse to, or become, lysosomes [133].

The *trans*-Golgi network connects to the endosomal system through the late endosome. It provides protein cargo to the lysosome, including new acidic hydrolases and membrane proteins. New endocytic biosynthetic vesicles from the TGN must be recognized and fuse to the appropriate subdomain of the late endosome. This often occurs through receptor-mediated vesicle trafficking. Some of the best-studied receptors are vacuolar hydrolase receptors of the Vps10-family. In yeast, the type I transmembrane protein Vps10 facilitates carboxypeptidase Y transport from the TGN to the MVB [134], by binding its cargo and recruiting AP-1 adaptors to form a clathrin coated vesicle. In mammals, retromer was found to recycle not only the several Vps10p homologs but also mannose-6-phosphate receptors [135,136]. The first discovered was cation-independent mannose-6-phosphate receptor (CI-MPR) which has a similar role for

mannose-6-phosphate labeled lysosomal cargo as Vps10p. Retrograde transport to recycle receptors at the late endosome back to the TGN is facilitated by the retromer complex and Rab7 [137,138].

The endosomal pathways are active in many eukaryotes including mammals, yeast [139], fungi [140], insects [141] and flat worms [141-143]. They are also important in plants, but appear to have diverged from their mammalian and yeast counterparts. The plant TGN is a distinct structure, separate from the Golgi apparatus and is the first compartment to receive endocytic cargo. These observations have prompted the theory that the compartment also acts as an early endosome equivalent [144-148]. Even though a parasite endosome has not been described, many important elements of the endosomal system are encoded in the *P. falciparum* genome. To understand if these proteins are sufficient to form a functional endosomal system similar to that observed in model systems, is a major objective of this thesis.

Endosomal Maturation: the Role of Phosphoinositides and Small Rab GTPases

Transport through the endosomal system can occur via endosome maturation or vesicle trafficking. The role of phosphoinositides and Rab GTPases is especially important in the process of endosome maturation. Vesicle traffic throughout the endosomal system is governed by phosphoinositides and Rab GTPases, as well as tethering components and fusion factors known as SNAREs (soluble *N*-ethylmaleimide-sensitive factor attachment protein receptors).

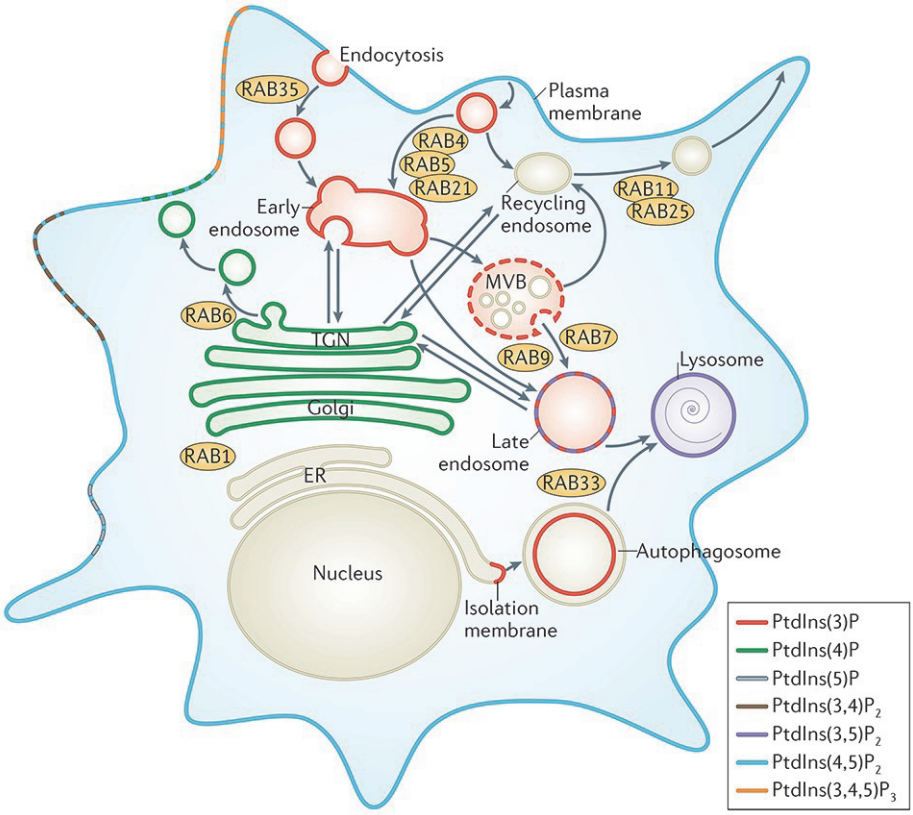

Figure 2-6: Distribution of selected Rab GTPases and phosphoinositides in a mammalian cell. Specifically of interest are the locations of PI3P/Rab5 at the early endosome and their conversion to PI(3,5)P_2/Rab7 at the late endosome and lysosome. Reprinted by permission from Macmillan Publishers Ltd: Nature Reviews: Molecular Cell Biology [149], copyright (2012).

In most eukaryotes, inositol phospholipids are concentrated at the cytosolic surface of membranes (Fig. 2-6); though there is some evidence that *P. falciparum* is an exception to the rule [150,151]. Each inositol ring can be reversibly phosphorylated at positions 3, 4 and/or 5 to produce seven different phosphoinositide combinations [152]. While phosphoinositides make up less than 15% of the total phospholipids in mammalian cells they can have a profound effect on membrane traffic [152]. Each type of phosphoinositide has specific distribution, often predominating a subset of membranes to assist in recruitment of proteins that contain PI-binding domains (Fig. 2-6, [153]). At least ten protein domains have been identified as interacting with phosphoinositides [153-155]. Generally, single protein-PI interactions are of low affinity and

require at least one additional contact with the membrane to be stable, producing a coincidence detection code for membrane-protein interactions [156,157]. The detection-code is also flexible; each PI can be interconverted from one PI to another through a set of kinases and phosphatases.

The endosomal system in mammals employs multiple PIs to identify compartments. The majority of the plasma membrane contains $PI(4,5)P_2$, but portions of the membrane actively involved in endocytosis are often labeled with PI3P. These PI3P labeled vesicles more easily fuse with the similarly labeled early endosome. Through the process of endosome maturation, the endosome membrane loses PI3P labeling in exchange for $PI(3,5)P_2$, which is characteristic of the lysosome.

The process of endosome maturation and PI-conversion is facilitated by Ras-family of small Rab GTPases. The majority of these proteins share a common structure: a GTPase domain followed by a hypervariable region and, at the far C-terminus, a motif with two cysteines (CCXX, CC or CXC) to which geranylgeranyl moieties are covalently attached [158]. Conserved regions of amino acids, named F1 to F5, differentiate Rab GTPases from other members of the Ras family [159]. Rabs can be further divided into subfamilies by other regions, called SF1 to SF4 motifs [159]. Rab GTPases act as membrane-bound molecular switches that shift between a GTP-bound active and GDP-bound inactive form [160] . GTP hydrolysis and GTP loading are assisted by GTPase activating proteins (GAPs) and guanine nucleotide exchange factors (GEFs) respectively [158]. While active, the Rab GTPases can recruit effectors to the membrane, sometimes in conjunction with phosphoinositides. The combination of Rab GTPases and PIs to a subdomain of a membrane facilitates high affinity and specific binding.

Both PIs and Rab GTPases coordinate endosome maturation. The small GTPase Rab5 on the early endosome membrane recruits Vps34 and p150, a phosphatidylinositol 3-kinase (PI3-

kinase) and its regulator, which results in phosphorylation of membrane inositol phospholipids [156,161,162]. These three components define the early endosome. For endosome conversion to occur, Mon1 (alone or in complex with Ccz1) binds to GTP-Rab5 and recruits Rab7 (Fig. 2-7, [163,164]). Recruitment of Rab7 is thought to stimulate GTP-Rab5 hydrolysis, which is in turn necessary for late endosomal conversion [163] and causes Rab5 effectors to dissociate from the membrane [163]. The HOPs complex may also interact with Rab7 as a GEF to stimulate other Rab7 effectors that bring about further maturation of the endosome [71]. PI conversion from PI3P to PI(3,5)P_2 is catalyzed by PIKfyve (Fab1p) recruited to the membrane, in part, through interaction of its FYVE domain and PI3P on the membrane [71].

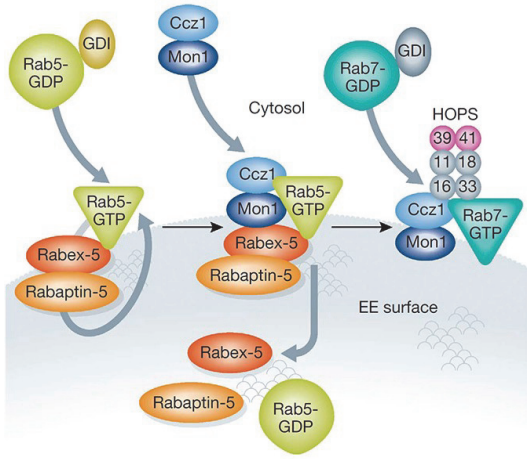

Figure 2-7 The Rab5/Rab7 switch during endosome maturation. Rab5 is activated by the GEF Rabex-5 on early endosome membranes. Rabaptin-5, a Rab5 effector, binds to Rabex-5 and promotes the activation of Rab5. This initiates a positive feedback loop. To begin Rab5 to Rab7 conversion, Mon1 (alone or in complex with Ccz1) binds to Rab5, PI3P, and Rabex-5, resulting in disassociation of Rabex-5 from the membrane. With the feedback loop terminated, Rab5 inactivates and dissociates from the membrane. The Mon1–Ccz1 complex also promotes the recruitment and activation of Rab7. Members of the HOPS complex bind both Rab7 and the Mon1–Ccz1 complex to mediate membrane tethering and fusion with other late endosomes and lysosomes. Reprinted by permission from Macmillan Publishers Ltd: EMBO J. [71], copyright (2011).

The *P. falciparum* genome encodes for homologs of endosome proteins: Rab5a/b/c [165], Rab7 [165], HOPS core subunits [57] and Mon1 (GeneID: PF3D7_1352800 annotated as "vacuolar fusion protein MON1"). The distribution of two of the three PfRab5 isoforms was

found to be isoprenoid dependent [166], but they have not been fully characterized. The functions of the other proteins have not been investigated to determine if they have similar functions to their mammalian homologs. As for related PIs, PI3P has been detected in the parasite around the FV, apicoplast and in the ER lumen [86,150]. The PI characteristic of the late endosome PI(3,5)P_2, however, was not detected in a phosphoinositide profile of *P. falciparum*-infected red blood cells.[86]. In addition, the only FYVE domain containing protein, PfFCP, does not contain a kinase domain and is not likely involved in PI3P to PI(3,5)P_2 conversion [89]. It is intriguing that the parasite encodes for proteins that are characteristic of a mammalian endosome, but does not appear to have an active early to late endosome maturation process.

Vesicle Fusion within the Endosomal System

Cargo from the early endosome can also be transported to the late endosome via vesicle-mediated transport. This mechanism is also used to transport cargo to and from the TGN and late endosome. Some questions arise when examining vesicle transport: (1) how do vesicles recognize and position themselves near the target membrane, and (2) how do target membranes and vesicles merge before cargo release? This process involves a number of components including previously mentioned phosphoinositides and Rab GTPases.

Close association of vesicles to a target membrane is called docking or tethering (reviewed in [167,168]). This process requires at least two additional components not previously described. Docking proteins create contacts between the target and vesicle membranes prior to vesicle fusion. This process is reversible and Rab GTPase-dependent. To maintain stable complexes, many docking proteins also interact directly with SNAREs (soluble N-ethylmaleimide-sensitive factor activating protein receptor). In some instances, the Rab GTPase

itself can act as a docking factor [169]. Once the vesicle is within range, SNAREs on both the target membrane and vesicle form "transSNARE" complexes to facilitate membrane fusion (reviewed in [170]).

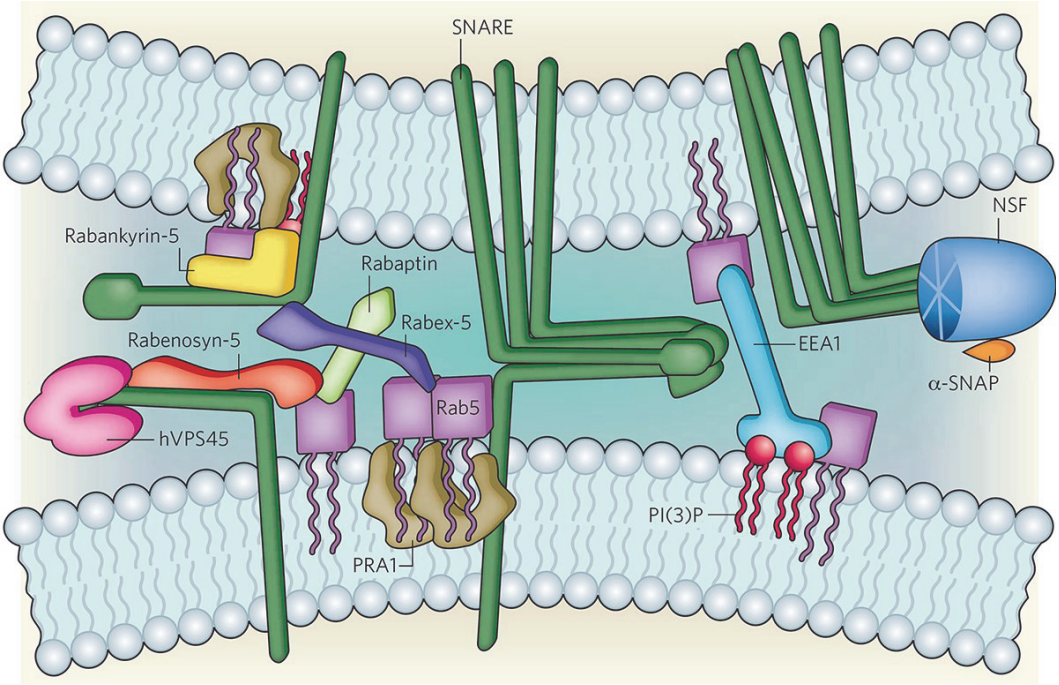

Figure 2-8: Endosomal membrane fusion is facilitated by many components. Rab5 GTPase and SNARE proteins (and their accessory proteins) work synergistically to facilitate vesicle fusion at the early endosome. to drive endosomal fusion. Rab5 effectors include rabankyrin-5, rabenosyn-5, rabaptin, rabex-5 and EEA1. SNARE accessory factors include α-SNAP, NSF and hVPS45. The recruitment of Rab5 effectors is stabilized by SNARE proteins and SNARE-protein accessory factors. Reprinted by permission from Macmillan Publishers Ltd: Nature [171], copyright (2009)

One of the best-characterized fusion reactions is the homotypic fusion of early endosome vesicles (Fig. 2-8, [162]). This process illustrates how multiple factors are engaged. The small GTPase Rab5, PI3P and the PI3-kinase complex (Vps34/p150) on early endosomes are actively involved [172,173]. For fusion events, Rab5 must exist in a complex with rabex-5, its GEF, and rabaptin-5, a Rab5 effector which slows GTP hydrolysis [174-177]. Two docking proteins are active in this process. The best characterized is early endosome autoantigen 1 (EEA1). More

recently another docking protein, Rabenosyn-5, has also been identified [178]. EEA1 and Rabenosyn-5 have been localized to the early endosome and both contain a C_2H_2 RING and a FYVE domain [178]. EEA1 is recruited only to the early endosome membrane through coincidence detection of both PI3P and Rab5. Rabenosyn-5 interacts with hVPS45, suggesting that it acts as a bridge between Rab5 and endosomal SNAREs [178]. Rabenosyn-5 is required for both endocytic and homotypic fusion [178]. Early endosome-specific SNAREs contribute to vesicle fusion and are able to impart another layer of specificity to the process [173]. SNAREs also contribute to complex recruitment and stability, but are not sufficient alone [173].

The *P. falciparum* genome encodes for 18 SNARE homologs [56]. Only four have been localized in the parasite [56]; all these were found to act at the ER-Golgi interface. No SNAREs have been found at either the FV or parasite endosome. In addition, no docking protein has yet to be identified in the parasite. Cargo and regulatory proteins involved in vesicle traffic, but not destined to be degraded, are removed from the endosomal system at the late endosome to the TGN by coordination of Rab7 and the retromer complex.

Discovery and Function o f the Retromer Cargo-Selective Complex

The retromer complex was first discovered using yeast mutant screens. Three of these screens focused on targeting proteins to the vacuole, and affected genes were consolidated into one list of vacuolar protein sorting (vps) mutants [179] . Further study led to the discovery of a new intermediate prevacuolar compartment (PVC)/Class E compartment, which became prominent in some mutants [180]. This was later recognized as the equivalent of the late endosome in mammals. The model vacuolar hydrolase, carboxypeptidase Y (CPY), was found to traverse the PVC en route to the vacuole [181]. In the landmark paper by Marcusson and

colleagues, it was found proper targeting of CPY to the vacuole was dependent on Vps10p, a type I transmembrane sorting receptor [134]. Vps10p cycles between the yeast Golgi apparatus and the PVC, and this behavior is dependent on its cytoplasmic tail [182]. Many CPY missorting errors were a direct result of failures of the cell to transport and recycle Vps10p by AP-1 clathrin adaptor and the retromer complex respectively [182-185].

In yeast, the retromer complex itself is composed of five subunits consisting of two subcomplexes: a Vps5p and Vps17p PX-BAR domain sorting nexin dimer, along with a Vps26p/29p/35p trimer, also known as the cargo-selective complex (CSC) [186-189]. The sorting nexin BAR domain is able to sense and promote membrane curvature [190,191]. The PX domain binds PI3P and directs the complex to the endosomal membrane [192,193]. Disruption of the early endosome PI3-kinase (Vps34p), and thus generation of PI3P, results in errors in retromer-dependent sorting [194].

While the function of yeast retromer may be limited to the recycling of Vps10p from the PVC, in mammalian cells the picture becomes more complicated. The mammalian retromer cargo selective complex consists of Vps26, Vps29, and Vps35 [195-197], but to date at least three isoforms of Vps26 [198,199] and two isoforms of Vps29 have been found to be incorporated into separate complexes. Sorting nexin 1 (SNX1) was identified as a Vps5p homolog and its involvement in trafficking to the lysosome was documented [186,200]. However, a clear Vps17p was difficult to find and the propensity of SNX1 towards self-assembly does not mirror Vps5p behavior [201]. In addition, the mammalian retromer CSC does not associate with sorting nexins as tightly as it did yeast [202,203], suggesting marked differences between the two species. Sorting nexins that interact with the mammalian retromer CSC have since expanded to include other PX-BAR sorting nexins (SNX2, 5 and 6) that can form

homodimer and heterodimer combinations with each other and SNX1 [204]. The first identified recycled cargo protein was the cation independent mannose-6-phosphate receptor, CI-MPR, which is also an important component in lysosome trafficking [196,197]. Mammalian retromer also recycles other sorting receptors, like sorLA, the sorting receptor for amyloid precursor protein, APP [135,205]. More recently, the PX-only sorting nexin, SNX3, was found to form a complex with retromer CSC to recycle the Wnt sorting receptor, Wntls, and the transferrin receptor [206,207].

Retromer recruitment to the late endosome requires both its cargo and Rab7 (Fig. 2-9, [208]). Recognition of retromer cargo is primarily through the central subunit, Vps35, at various sites on the protein [189]. Sorting nexins coordinate binding of PI3P through their PX domain for specific membrane targeting. The retromer complex is important for maintaining equilibrium along the early to late endosome continuum and disruption can easily result in downstream effects.

The *P. falciparum* genome encodes all three subunits of the retromer CSC [209] and a homolog of Rab7 [165]. To our knowledge, these proteins have never been investigated. They may help define the endosomal compartments and contribute to protein sorting in the parasite. Curiously, sorting nexins appear to be absent from the *P. falciparum* genome [209]. It is uncertain whether membrane curvature induction and sensing is required in the parasite or is performed by another protein.

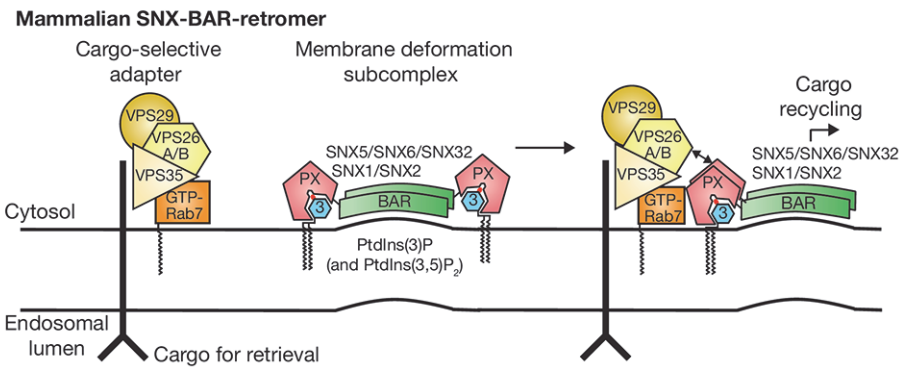

Figure 2-9: The cargo-selective complex and membrane deformation subunits of the mammalian SNX-BAR-retromer. The retromer CSC is recruited to the cytosolic leaflet of the endosomal membrane by Rab7 and primarily Vps35-cargo interactions. The sorting nexin dimer is directed to the endosomal membrane through PX-PI interactions and its membrane curvature sensing BAR domain. These two subcomplexes interact to drive tubule/vesicle formation towards the TGN. Reprinted by permission from Macmillan Publishers Ltd: Nature Cell Biology [210], copyright (2012).

Summary

The malaria parasite, *P. falciparum,* sorts synthesized proteins to multiple compartments, many of which are unique to the parasite. It is apparent that the parasite uses an early secretory pathway very similar to model systems for both FV and apical organelle sorting (Fig. 2-10). Many of these proteins pass through a simplified Golgi apparatus on their way to their target, but beyond this point very little information is available. Current data suggests vesicle-mediated transport is employed, but how those vesicles form, are directed and eventually fuse with their target, is still unknown. Vesicles formed and trafficked in a receptor-mediated fashion often take advantage of coat complexes. The only coating complexes identified in the parasite act at the interface of the ER and Golgi apparatus. Apical secretory organelles or FV sorting receptors have also not been identified.

The parasite genome encodes for many proteins that are homologous to endosomal proteins in mammals, but most have not been characterized or even localized. An endosome

compartment that sorts traffic to either the FV or apical organelles would be in agreement with sequential proteolytic cleavage important for trafficking. It is possible that the simplicity of the parasite trafficking system has been overestimated and the presence of a unique parasite endosomal system has been overlooked. Thus far, no studies have been conducted on the retromer cargo-selective complex or Rab7 in *P. falciparum*. The FYVE-domain containing protein, PfFCP, is a potential EEA1 homolog, but only one study has been published on it and we find it difficult to interpret their results. In this dissertation, we attempt to dissect the endosomal system in the malaria parasite by looking at both early and late endosomal proteins.

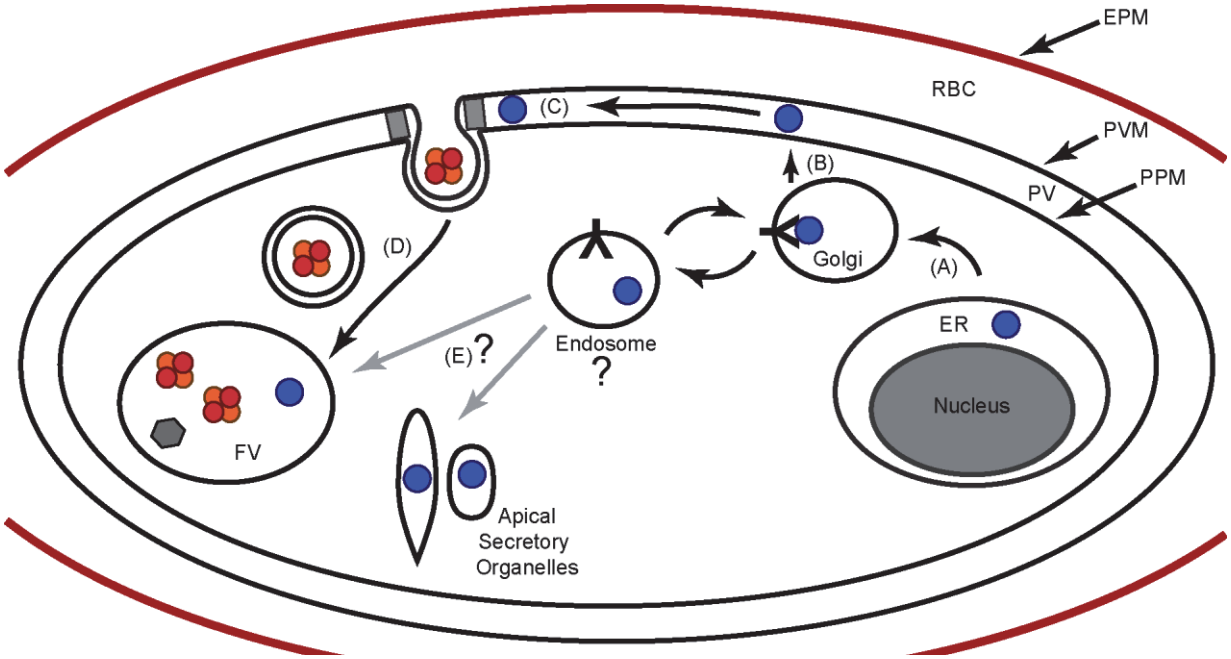

Figure 2-10: Model of potential endosomal sorting in *P. falciparum*. The parasite exists within three membranes: the erythrocyte plasma membrane (EPM, red line), the parasitophorous vacuolar membrane (PVM), and the parasite plasma membrane (PPM). Current understanding of protein trafficking (black arrows) is limited to the early secretory pathway (A) between the ER and Golgi apparatus. Food vacuole (FV) resident proteins may be trafficked through the parasitophours vacuole (PV) (B), endocytic vesicles (C), before their fusion to the FV (D). Given the precence of endosomal homologs in the parasite genome, a post-Golgi endosome-like compartment may exist and be involved in trafficking to both the FV and apical secretory organelles (grey arrows).

References

1. Coppens I, Dunn JD, Romano JD, Pypaert M, Zhang H, et al. (2006) Toxoplasma gondii sequesters lysosomes from mammalian hosts in the vacuolar space. Cell 125: 261-274.
2. Lingelbach K, Przyborski JM (2006) The long and winding road: protein trafficking mechanisms in the Plasmodium falciparum infected erythrocyte. Mol Biochem Parasitol 147: 1-8.
3. Tonkin CJ, Kalanon M, McFadden GI (2008) Protein targeting to the malaria parasite plastid. Traffic 9: 166-175.
4. Abu Bakar N, Klonis N, Hanssen E, Chan C, Tilley L (2010) Digestive-vacuole genesis and endocytic processes in the early intraerythrocytic stages of Plasmodium falciparum. J Cell Sci 123: 441-450.
5. Klonis N, Tan O, Jackson K, Goldberg D, Klemba M, et al. (2007) Evaluation of pH during cytostomal endocytosis and vacuolar catabolism of haemoglobin in Plasmodium falciparum. Biochem J 407: 343-354.
6. Rosenthal PJ (2011) Falcipains and other cysteine proteases of malaria parasites. Adv Exp Med Biol 712: 30-48.
7. Liu J, Istvan ES, Gluzman IY, Gross J, Goldberg DE (2006) Plasmodium falciparum ensures its amino acid supply with multiple acquisition pathways and redundant proteolytic enzyme systems. Proc Natl Acad Sci U S A 103: 8840-8845.
8. Goldberg DE (2013) Complex nature of malaria parasite hemoglobin degradation [corrected]. Proc Natl Acad Sci U S A 110: 5283-5284.
9. Rosenthal PJ (1995) Plasmodium falciparum: effects of proteinase inhibitors on globin hydrolysis by cultured malaria parasites. Exp Parasitol 80: 272-281.
10. Olson JE, Lee GK, Semenov A, Rosenthal PJ (1999) Antimalarial effects in mice of orally administered peptidyl cysteine protease inhibitors. Bioorg Med Chem 7: 633-638.
11. Slater AF (1992) Malaria pigment. Exp Parasitol 74: 362-365.
12. Tilley L, Dixon MW, Kirk K (2011) The Plasmodium falciparum-infected red blood cell. Int J Biochem Cell Biol 43: 839-842.
13. Bannister LH, Hopkins JM, Fowler RE, Krishna S, Mitchell GH (2000) Ultrastructure of rhoptry development in *Plasmodium falciparum* erythrocytic schizonts. Parasitology 121: 273-287.
14. Cowman AF, Berry D, Baum J (2012) The cellular and molecular basis for malaria parasite invasion of the human red blood cell. J Cell Biol 198: 961-971.
15. Riglar DT, Richard D, Wilson DW, Boyle MJ, Dekiwadia C, et al. (2011) Super-resolution dissection of coordinated events during malaria parasite invasion of the human erythrocyte. Cell Host Microbe 9: 9-20.
16. Deponte M, Hoppe HC, Lee MC, Maier AG, Richard D, et al. (2012) Wherever I may roam: protein and membrane trafficking in *P. falciparum*-infected red blood cells. Mol Biochem Parasitol 186: 95-116.
17. van Dooren GG, Waller RF, Joiner KA, Roos DS, McFadden GI (2000) Traffic jams: protein transport in Plasmodium falciparum. Parasitol Today 16: 421-427.
18. Johnson AE, van Waes MA (1999) The translocon: a dynamic gateway at the ER membrane. Annu Rev Cell Dev Biol 15: 799-842.
19. Tuteja R (2007) Unraveling the components of protein translocation pathway in human malaria parasite Plasmodium falciparum. Arch Biochem Biophys 467: 249-260.

20. Couffin S, Hernandez-Rivas R, Blisnick T, Mattei D (1998) Characterisation of PfSec61, a Plasmodium falciparum homologue of a component of the translocation machinery at the endoplasmic reticulum membrane of eukaryotic cells. Mol Biochem Parasitol 92: 89-98.
21. Kumar N, Koski G, Harada M, Aikawa M, Zheng H (1991) Induction and localization of Plasmodium falciparum stress proteins related to the heat shock protein 70 family. Mol Biochem Parasitol 48: 47-58.
22. Cooke BM, Lingelbach K, Bannister LH, Tilley L (2004) Protein trafficking in Plasmodium falciparum-infected red blood cells. Trends Parasitol 20: 581-589.
23. Dancourt J, Barlowe C (2010) Protein sorting receptors in the early secretory pathway. Annu Rev Biochem 79: 777-802.
24. Foley M, Tilley L (1998) Protein trafficking in malaria-infected erythrocytes. Int J Parasitol 28: 1671-1680.
25. Taraschi TF, Trelka D, Martinez S, Schneider T, O'Donnell ME (2001) Vesicle-mediated trafficking of parasite proteins to the host cell cytosol and erythrocyte surface membrane in Plasmodium falciparum infected erythrocytes. Int J Parasitol 31: 1381-1391.
26. Przyborski JM, Wickert H, Krohne G, Lanzer M (2003) Maurer's clefts--a novel secretory organelle? Mol Biochem Parasitol 132: 17-26.
27. Elias M, Patron NJ, Keeling PJ (2009) The RAB family GTPase Rab1A from Plasmodium falciparum defines a unique paralog shared by chromalveolates and rhizaria. J Eukaryot Microbiol 56: 348-356.
28. Daubenberger CA, Tisdale EJ, Curcic M, Diaz D, Silvie O, et al. (2003) The N'-terminal domain of glyceraldehyde-3-phosphate dehydrogenase of the apicomplexan Plasmodium falciparum mediates GTPase Rab2-dependent recruitment to membranes. Biol Chem 384: 1227-1237.
29. Kleizen B, Braakman I (2004) Protein folding and quality control in the endoplasmic reticulum. Curr Opin Cell Biol 16: 343-349.
30. Ellgaard L, Helenius A (2003) Quality control in the endoplasmic reticulum. Nat Rev Mol Cell Biol 4: 181-191.
31. Banumathy G, Singh V, Pavithra SR, Tatu U (2003) Heat shock protein 90 function is essential for Plasmodium falciparum growth in human erythrocytes. J Biol Chem 278: 18336-18345.
32. Kumar R, Musiyenko A, Barik S (2003) The heat shock protein 90 of Plasmodium falciparum and antimalarial activity of its inhibitor, geldanamycin. Malar J 2: 30.
33. Pavithra SR, Kumar R, Tatu U (2007) Systems analysis of chaperone networks in the malarial parasite Plasmodium falciparum. PLoS Comput Biol 3: 1701-1715.
34. Mahajan B, Noiva R, Yadava A, Zheng H, Majam V, et al. (2006) Protein disulfide isomerase assisted protein folding in malaria parasites. Int J Parasitol 36: 1037-1048.
35. Mouray E, Moutiez M, Girault S, Sergheraert C, Florent I, et al. (2007) Biochemical properties and cellular localization of Plasmodium falciparum protein disulfide isomerase. Biochimie 89: 337-346.
36. Dieckmann-Schuppert A, Bender S, Odenthal-Schnittler M, Bause E, Schwarz RT (1992) Apparent lack of N-glycosylation in the asexual intraerythrocytic stage of Plasmodium falciparum. Eur J Biochem 205: 815-825.
37. Gowda DC, Gupta P, Davidson EA (1997) Glycosylphosphatidylinositol anchors represent the major carbohydrate modification in proteins of intraerythrocytic stage Plasmodium falciparum. J Biol Chem 272: 6428-6439.

38. Gowda DC, Davidson EA (1999) Protein glycosylation in the malaria parasite. Parasitol Today 15: 147-152.
39. Van Wye J, Ghori N, Webster P, Mitschler RR, Elmendorf HG, et al. (1996) Identification and localization of rab6, separation of rab6 from ERD2 and implications for an 'unstacked' Golgi, in Plasmodium falciparum. Mol Biochem Parasitol 83: 107-120.
40. Elmendorf HG, Haldar K (1993) Identification and localization of ERD2 in the malaria parasite Plasmodium falciparum: separation from sites of sphingomyelin synthesis and implications for organization of the Golgi. Embo Journal 12: 4763-4773.
41. Struck NS, de Souza Dias S, Langer C, Marti M, Pearce JA, et al. (2005) Re-defining the Golgi complex in Plasmodium falciparum using the novel Golgi marker PfGRASP. J Cell Sci 118: 5603-5613.
42. Adisa A, Frankland S, Rug M, Jackson K, Maier AG, et al. (2007) Re-assessing the locations of components of the classical vesicle-mediated trafficking machinery in transfected Plasmodium falciparum. Int J Parasitol 37: 1127-1141.
43. Storrie B, Micaroni M, Morgan GP, Jones N, Kamykowski JA, et al. (2012) Electron tomography reveals Rab6 is essential to the trafficking of trans-Golgi clathrin and COPI-coated vesicles and the maintenance of Golgi cisternal number. Traffic 13: 727-744.
44. de Castro FA, Ward GE, Jambou R, Attal G, Mayau V, et al. (1996) Identification of a family of Rab G-proteins in Plasmodium falciparum and a detailed characterisation of pfrab6. Mol Biochem Parasitol 80: 77-88.
45. Struck NS, Herrmann S, Langer C, Krueger A, Foth BJ, et al. (2008) *Plasmodium falciparum* possesses two GRASP proteins that are differentially targeted to the Golgi complex via a higher- and lower-eukaryote-like mechanism. J Cell Sci 121: 2123-2129.
46. Ming M, VanWye J, Janse CJ, Waters AP, Haldar K (1999) Gene organization of rab6, a marker for the novel Golgi of Plasmodium. Mol Biochem Parasitol 100: 217-222.
47. Struck NS, Herrmann S, Schmuck-Barkmann I, de Souza Dias S, Haase S, et al. (2008) Spatial dissection of the *cis*- and *trans*-Golgi compartments in the malaria parasite *Plasmodium falciparum*. Mol Microbiol 67: 1320-1330.
48. Kumar N, Syin CA, Carter R, Quakyi I, Miller LH (1988) Plasmodium falciparum gene encoding a protein similar to the 78-kDa rat glucose-regulated stress protein. Proc Natl Acad Sci U S A 85: 6277-6281.
49. van Dooren GG, Marti M, Tonkin CJ, Stimmler LM, Cowman AF, et al. (2005) Development of the endoplasmic reticulum, mitochondrion and apicoplast during the asexual life cycle of *Plasmodium falciparum*. Mol Microbiol 57: 405-419.
50. La Greca N, Hibbs AR, Riffkin C, Foley M, Tilley L (1997) Identification of an endoplasmic reticulum-resident calcium-binding protein with multiple EF-hand motifs in asexual stages of Plasmodium falciparum. Molecular and Biochemical Parasitology 89: 283-293.
51. Samuelson J, Banerjee S, Magnelli P, Cui J, Kelleher DJ, et al. (2005) The diversity of dolichol-linked precursors to Asn-linked glycans likely results from secondary loss of sets of glycosyltransferases. Proc Natl Acad Sci U S A 102: 1548-1553.
52. Albano FR, Berman A, La Greca N, Hibbs AR, Wickham M, et al. (1999) A homologue of Sar1p localises to a novel trafficking pathway in malaria-infected erythrocytes. Eur J Cell Biol 78: 453-462.
53. Wickert H, Rohrbach P, Scherer SJ, Krohne G, Lanzer M (2003) A putative Sec23 homologue of Plasmodium falciparum is located in Maurer's clefts. Mol Biochem Parasitol 129: 209-213.

54. Lee MC, Moura PA, Miller EA, Fidock DA (2008) Plasmodium falciparum Sec24 marks transitional ER that exports a model cargo via a diacidic motif. Mol Microbiol 68: 1535-1546.
55. Adisa A, Albano FR, Reeder J, Foley M, Tilley L (2001) Evidence for a role for a Plasmodium falciparum homologue of Sec31p in the export of proteins to the surface of malaria parasite-infected erythrocytes. J Cell Sci 114: 3377-3386.
56. Ayong L, Pagnotti G, Tobon AB, Chakrabarti D (2007) Identification of Plasmodium falciparum family of SNAREs. Mol Biochem Parasitol 152: 113-122.
57. Koumandou VL, Dacks JB, Coulson RM, Field MC (2007) Control systems for membrane fusion in the ancestral eukaryote; evolution of tethering complexes and SM proteins. BMC Evol Biol 7: 29.
58. Adisa A, Rug M, Foley M, Tilley L (2002) Characterisation of a delta-COP homologue in the malaria parasite, Plasmodium falciparum. Mol Biochem Parasitol 123: 11-21.
59. Stafford WH, Stockley RW, Ludbrook SB, Holder AA (1996) Isolation, expression and characterization of the gene for an ADP-ribosylation factor from the human malaria parasite, Plasmodium falciparum. Eur J Biochem 242: 104-113.
60. Cook WJ, Smith CD, Senkovich O, Holder AA, Chattopadhyay D (2010) Structure of Plasmodium falciparum ADP-ribosylation factor 1. Acta Crystallogr Sect F Struct Biol Cryst Commun 66: 1426-1431.
61. Cook WJ, Senkovich O, Chattopadhyay D (2011) Structure of the catalytic domain of Plasmodium falciparum ARF GTPase-activating protein (ARFGAP). Acta Crystallogr Sect F Struct Biol Cryst Commun 67: 1339-1344.
62. Senkovich O, Chattopadhyay D (2004) Plasmodium falciparum ARFGAP: expression and crystallization of the catalytic domain. Biochim Biophys Acta 1698: 127-130.
63. Baumgartner F, Wiek S, Paprotka K, Zauner S, Lingelbach K (2001) A point mutation in an unusual Sec7 domain is linked to brefeldin A resistance in a Plasmodium falciparum line generated by drug selection. Mol Microbiol 41: 1151-1158.
64. Wiek S, Cowman AF, Lingelbach K (2004) Double cross-over gene replacement within the sec 7 domain of a GDP-GTP exchange factor from Plasmodium falciparum allows the generation of a transgenic brefeldin A-resistant parasite line. Mol Biochem Parasitol 138: 51-55.
65. Witola WH, Pessi G, El Bissati K, Reynolds JM, Mamoun CB (2006) Localization of the phosphoethanolamine methyltransferase of the human malaria parasite Plasmodium falciparum to the Golgi apparatus. J Biol Chem 281: 21305-21311.
66. Seydel KB, Gaur D, Aravind L, Subramanian G, Miller LH (2005) Plasmodium falciparum: characterization of a late asexual stage golgi protein containing both ankyrin and DHHC domains. Exp Parasitol 110: 389-393.
67. Jones ML, Tay CL, Rayner JC (2012) Getting stuck in: protein palmitoylation in Plasmodium. Trends Parasitol 28: 496-503.
68. Gu F, Crump CM, Thomas G (2001) Trans-Golgi network sorting. Cell Mol Life Sci 58: 1067-1084.
69. Santiago-Tirado FH, Bretscher A (2011) Membrane-trafficking sorting hubs: cooperation between PI4P and small GTPases at the trans-Golgi network. Trends Cell Biol 21: 515-525.
70. Blazquez M, Shennan KI (2000) Basic mechanisms of secretion: sorting into the regulated secretory pathway. Biochem Cell Biol 78: 181-191.

71. Huotari J, Helenius A (2011) Endosome maturation. EMBO J 30: 3481-3500.
72. Dluzewski AR, Ling IT, Hopkins JM, Grainger M, Margos G, et al. (2008) Formation of the food vacuole in Plasmodium falciparum: a potential role for the 19 kDa fragment of merozoite surface protein 1 (MSP1(19)). PLoS One 3: e3085.
73. Weed RI, Reed CF, Berg G (1963) Is hemoglobin an essential structural component of human erythrocyte membranes? J Clin Invest 42: 581-588.
74. Krugliak M, Zhang J, Ginsburg H (2002) Intraerythrocytic Plasmodium falciparum utilizes only a fraction of the amino acids derived from the digestion of host cell cytosol for the biosynthesis of its proteins. Mol Biochem Parasitol 119: 249-256.
75. Dasaradhi PV, Korde R, Thompson JK, Tanwar C, Nag TC, et al. (2007) Food vacuole targeting and trafficking of falcipain-2, an important cysteine protease of human malaria parasite Plasmodium falciparum. Mol Biochem Parasitol 156: 12-23.
76. Francis SE, Banerjee R, Goldberg DE (1997) Biosynthesis and maturation of the malaria aspartic hemoglobinases plasmepsins I and II. J Biol Chem 272: 14961-14968.
77. Subramanian S, Sijwali PS, Rosenthal PJ (2007) Falcipain cysteine proteases require bipartite motifs for trafficking to the Plasmodium falciparum food vacuole. J Biol Chem 282: 24961-24969.
78. Martin RE, Kirk K (2007) Transport of the essential nutrient isoleucine in human erythrocytes infected with the malaria parasite Plasmodium falciparum. Blood 109: 2217-2224.
79. Lew VL, Tiffert T, Ginsburg H (2003) Excess hemoglobin digestion and the osmotic stability of Plasmodium falciparum-infected red blood cells. Blood 101: 4189-4194.
80. Goldberg DE (2005) Hemoglobin Degradation. In: Compans RW, Cooper MD, Honjo T, Koprowski H, Melchers F et al., editors. Malaria: Drugs, Disease and Post-genomic Biology: Springer Berlin Heidelberg. pp. 275-291.
81. Egan TJ, Combrinck JM, Egan J, Hearne GR, Marques HM, et al. (2002) Fate of haem iron in the malaria parasite Plasmodium falciparum. Biochem J 365: 343-347.
82. Ehlgen F, Pham JS, de Koning-Ward T, Cowman AF, Ralph SA (2012) Investigation of the Plasmodium falciparum food vacuole through inducible expression of the chloroquine resistance transporter (PfCRT). PLoS One 7: e38781.
83. Bannister LH, Hopkins JM, Fowler RE, Krishna S, Mitchell GH (2000) A brief illustrated guide to the ultrastructure of Plasmodium falciparum asexual blood stages. Parasitol Today 16: 427-433.
84. Jackson KE, Klonis N, Ferguson DJ, Adisa A, Dogovski C, et al. (2004) Food vacuole-associated lipid bodies and heterogeneous lipid environments in the malaria parasite, Plasmodium falciparum. Mol Microbiol 54: 109-122.
85. Dasari P, Reiss K, Lingelbach K, Baumeister S, Lucius R, et al. (2011) Digestive vacuoles of Plasmodium falciparum are selectively phagocytosed by and impair killing function of polymorphonuclear leukocytes. Blood 118: 4946-4956.
86. Tawk L, Chicanne G, Dubremetz JF, Richard V, Payrastre B, et al. (2010) Phosphatidylinositol 3-phosphate, an essential lipid in Plasmodium, localizes to the food vacuole membrane and the apicoplast. Eukaryot Cell 9: 1519-1530.
87. Vaid A, Ranjan R, Smythe WA, Hoppe HC, Sharma P (2010) PfPI3K, a phosphatidylinositol-3 kinase from Plasmodium falciparum, is exported to the host erythrocyte and is involved in hemoglobin trafficking. Blood 115: 2500-2507.

88. Elabbadi N, Ancelin ML, Vial HJ (1994) Characterization of phosphatidylinositol synthase and evidence of a polyphosphoinositide cycle in Plasmodium-infected erythrocytes. Mol Biochem Parasitol 63: 179-192.
89. McIntosh MT, Vaid A, Hosgood HD, Vijay J, Bhattacharya A, et al. (2007) Traffic to the malaria parasite food vacuole: a novel pathway involving a phosphatidylinositol 3-phosphate-binding protein. J Biol Chem 282: 11499-11508.
90. Wengelnik K, Vial HJ (2007) Characterisation of the phosphatidylinositol synthase gene of Plasmodium species. Res Microbiol 158: 51-59.
91. Zhou HC, Gao YH, Zhong X, Wang H (2009) Dynamin like protein 1 participated in the hemoglobin uptake pathway of Plasmodium falciparum. Chin Med J (Engl) 122: 1686-1691.
92. Lazarus MD, Schneider TG, Taraschi TF (2008) A new model for hemoglobin ingestion and transport by the human malaria parasite Plasmodium falciparum. J Cell Sci 121: 1937-1949.
93. Elliott DA, McIntosh MT, Hosgood HD, 3rd, Chen S, Zhang G, et al. (2008) Four distinct pathways of hemoglobin uptake in the malaria parasite Plasmodium falciparum. Proc Natl Acad Sci U S A 105: 2463-2468.
94. Gluzman IY, Francis SE, Oksman A, Smith CE, Duffin KL, et al. (1994) Order and specificity of the Plasmodium falciparum hemoglobin degradation pathway. J Clin Invest 93: 1602-1608.
95. Klemba M, Beatty W, Gluzman I, Goldberg DE (2004) Trafficking of plasmepsin II to the food vacuole of the malaria parasite Plasmodium falciparum. J Cell Biol 164: 47-56.
96. Drew ME, Banerjee R, Uffman EW, Gilbertson S, Rosenthal PJ, et al. (2008) Plasmodium food vacuole plasmepsins are activated by falcipains. J Biol Chem 283: 12870-12876.
97. Counihan NA, Kalanon M, Coppel RL, de Koning-Ward TF (2013) Plasmodium rhoptry proteins: why order is important. Trends Parasitol 29: 228-236.
98. Proellocks NI, Coppel RL, Waller KL (2010) Dissecting the apicomplexan rhoptry neck proteins. Trends Parasitol 26: 297-304.
99. Vincensini L, Fall G, Berry L, Blisnick T, Braun Breton C (2008) The RhopH complex is transferred to the host cell cytoplasm following red blood cell invasion by Plasmodium falciparum. Mol Biochem Parasitol 160: 81-89.
100. Sanders PR, Cantin GT, Greenbaum DC, Gilson PR, Nebl T, et al. (2007) Identification of protein complexes in detergent-resistant membranes of Plasmodium falciparum schizonts. Mol Biochem Parasitol 154: 148-157.
101. Topolska AE, Black CG, Coppel RL (2004) Identification and characterisation of RAMA homologues in rodent, simian and human malaria species. Mol Biochem Parasitol 138: 237-241.
102. Sanders PR, Kats LM, Drew DR, O'Donnell RA, O'Neill M, et al. (2006) A set of glycosylphosphatidyl inositol-anchored membrane proteins of Plasmodium falciparum is refractory to genetic deletion. Infect Immun 74: 4330-4338.
103. Topolska AE, Lidgett A, Truman D, Fujioka H, Coppel RL (2004) Characterization of a membrane-associated rhoptry protein of Plasmodium falciparum. J Biol Chem 279: 4648-4656.
104. Richard D, Kats LM, Langer C, Black CG, Mitri K, et al. (2009) Identification of rhoptry trafficking determinants and evidence for a novel sorting mechanism in the malaria parasite Plasmodium falciparum. PLoS Pathog 5: e1000328.

105. Baldi DL, Andrews KT, Waller RF, Roos DS, Howard RF, et al. (2000) RAP1 controls rhoptry targeting of RAP2 in the malaria parasite Plasmodium falciparum. EMBO J 19: 2435-2443.
106. Ghoneim A, Kaneko O, Tsuboi T, Torii M (2007) The Plasmodium falciparum RhopH2 promoter and first 24 amino acids are sufficient to target proteins to the rhoptries. Parasitol Int 56: 31-43.
107. Topolska AE, Richie TL, Nhan DH, Coppel RL (2004) Associations between responses to the rhoptry-associated membrane antigen of Plasmodium falciparum and immunity to malaria infection. Infect Immun 72: 3325-3330.
108. Cabrera A, Herrmann S, Warszta D, Santos JM, John Peter AT, et al. (2012) Dissection of minimal sequence requirements for rhoptry membrane targeting in the malaria parasite. Traffic 13: 1335-1350.
109. Besteiro S, Dubremetz JF, Lebrun M (2011) The moving junction of apicomplexan parasites: a key structure for invasion. Cell Microbiol 13: 797-805.
110. Hackett F, Sajid M, Withers-Martinez C, Grainger M, Blackman MJ (1999) PfSUB-2: a second subtilisin-like protein in Plasmodium falciparum merozoites. Mol Biochem Parasitol 103: 183-195.
111. Healer J, Crawford S, Ralph S, McFadden G, Cowman AF (2002) Independent translocation of two micronemal proteins in developing Plasmodium falciparum merozoites. Infect Immun 70: 5751-5758.
112. Harris PK, Yeoh S, Dluzewski AR, O'Donnell RA, Withers-Martinez C, et al. (2005) Molecular identification of a malaria merozoite surface sheddase. PLoS Pathog 1: 241-251.
113. Child MA, Harris PK, Collins CR, Withers-Martinez C, Yeoh S, et al. (2013) Molecular determinants for subcellular trafficking of the malarial sheddase PfSUB2. Traffic.
114. Treeck M, Struck NS, Haase S, Langer C, Herrmann S, et al. (2006) A conserved region in the EBL proteins is implicated in microneme targeting of the malaria parasite Plasmodium falciparum. J Biol Chem 281: 31995-32003.
115. Sakura T, Yahata K, Kaneko O (2013) The upstream sequence segment of the C-terminal cysteine-rich domain is required for microneme trafficking of Plasmodium falciparum erythrocyte binding antigen 175. Parasitol Int 62: 157-164.
116. Gilberger TW, Thompson JK, Reed MB, Good RT, Cowman AF (2003) The cytoplasmic domain of the Plasmodium falciparum ligand EBA-175 is essential for invasion but not protein trafficking. J Cell Biol 162: 317-327.
117. Sloves PJ, Delhaye S, Mouveaux T, Werkmeister E, Slomianny C, et al. (2012) *Toxoplasma* sortilin-like receptor regulates protein transport and is essential for apical secretory organelle biogenesis and host infection. Cell Host Microbe 11: 515-527.
118. Surma MA, Klose C, Simons K (2012) Lipid-dependent protein sorting at the trans-Golgi network. Biochim Biophys Acta 1821: 1059-1067.
119. Aikawa M, Torii M, Sjolander A, Berzins K, Perlmann P, et al. (1990) Pf155/RESA antigen is localized in dense granules of Plasmodium falciparum merozoites. Exp Parasitol 71: 326-329.
120. Yeoh S, O'Donnell RA, Koussis K, Dluzewski AR, Ansell KH, et al. (2007) Subcellular discharge of a serine protease mediates release of invasive malaria parasites from host erythrocytes. Cell 131: 1072-1083.

121. Arastu-Kapur S, Ponder EL, Fonovic UP, Yeoh S, Yuan F, et al. (2008) Identification of proteases that regulate erythrocyte rupture by the malaria parasite Plasmodium falciparum. Nat Chem Biol 4: 203-213.
122. Lee MC, Fidock DA (2008) Arresting malaria parasite egress from infected red blood cells. Nat Chem Biol 4: 161-162.
123. Bowyer PW, Simon GM, Cravatt BF, Bogyo M (2011) Global profiling of proteolysis during rupture of Plasmodium falciparum from the host erythrocyte. Mol Cell Proteomics 10: M110 001636.
124. Singh S, Plassmeyer M, Gaur D, Miller LH (2007) Mononeme: a new secretory organelle in *Plasmodium falciparum* merozoites identified by localization of rhomboid-1 protease. Proc Natl Acad Sci USA 104: 20043-20048.
125. Dacks JB, Peden AA, Field MC (2009) Evolution of specificity in the eukaryotic endomembrane system. Int J Biochem Cell Biol 41: 330-340.
126. Yang M, Coppens I, Wormsley S, Baevova P, Hoppe HC, et al. (2004) The *Plasmodium falciparum* Vps4 homolog mediates multivesicular body formation. J Cell Sci 117: 3831-3838.
127. Babst M, Wendland B, Estepa EJ, Emr SD (1998) The Vps4p AAA ATPase regulates membrane association of a Vps protein complex required for normal endosome function. EMBO J 17: 2982-2993.
128. Kumar A, Agarwal S, Heyman JA, Matson S, Heidtman M, et al. (2002) Subcellular localization of the yeast proteome. Genes Dev 16: 707-719.
129. Babst M, Katzmann DJ, Estepa-Sabal EJ, Meerloo T, Emr SD (2002) Escrt-III: an endosome-associated heterooligomeric protein complex required for mvb sorting. Dev Cell 3: 271-282.
130. Xu D, Esko JD (2009) A Golgi-on-a-chip for glycan synthesis. Nat Chem Biol 5: 612-613.
131. Von Bartheld CS, Altick AL (2011) Multivesicular bodies in neurons: distribution, protein content, and trafficking functions. Prog Neurobiol 93: 313-340.
132. Mayor S, Pagano RE (2007) Pathways of clathrin-independent endocytosis. Nat Rev Mol Cell Biol 8: 603-612.
133. Luzio JP, Pryor PR, Bright NA (2007) Lysosomes: fusion and function. Nat Rev Mol Cell Biol 8: 622-632.
134. Marcusson EG, Horazdovsky BF, Cereghino JL, Gharakhanian E, Emr SD (1994) The sorting receptor for yeast vacuolar carboxypeptidase Y is encoded by the VPS10 gene. Cell 77: 579-586.
135. Hermey G (2009) The Vps10p-domain receptor family. Cell Mol Life Sci 66: 2677-2689.
136. Lane RF, St George-Hyslop P, Hempstead BL, Small SA, Strittmatter SM, et al. (2012) Vps10 family proteins and the retromer complex in aging-related neurodegeneration and diabetes. J Neurosci 32: 14080-14086.
137. Bonifacino JS, Hurley JH (2008) Retromer. Curr Opin Cell Biol 20: 427-436.
138. Attar N, Cullen PJ (2010) The retromer complex. Adv Enzyme Regul 50: 216-236.
139. Pelham HR (2002) Insights from yeast endosomes. Curr Opin Cell Biol 14: 454-462.
140. Penalva MA (2010) Endocytosis in filamentous fungi: Cinderella gets her reward. Curr Opin Microbiol 13: 684-692.
141. Michelet X, Djeddi A, Legouis R (2010) Developmental and cellular functions of the ESCRT machinery in pluricellular organisms. Biol Cell 102: 191-202.
142. Grant BD, Sato M (2006) Intracellular trafficking. WormBook: 1-9.

143. Poteryaev D, Datta S, Ackema K, Zerial M, Spang A (2010) Identification of the switch in early-to-late endosome transition. Cell 141: 497-508.
144. Irani NG, Russinova E (2009) Receptor endocytosis and signaling in plants. Curr Opin Plant Biol 12: 653-659.
145. Foresti O, Denecke J (2008) Intermediate organelles of the plant secretory pathway: identity and function. Traffic 9: 1599-1612.
146. Dettmer J, Hong-Hermesdorf A, Stierhof YD, Schumacher K (2006) Vacuolar H+-ATPase activity is required for endocytic and secretory trafficking in Arabidopsis. Plant Cell 18: 715-730.
147. Niemes S, Labs M, Scheuring D, Krueger F, Langhans M, et al. (2010) Sorting of plant vacuolar proteins is initiated in the ER. Plant J 62: 601-614.
148. Niemes S, Langhans M, Viotti C, Scheuring D, San Wan Yan M, et al. (2010) Retromer recycles vacuolar sorting receptors from the trans-Golgi network. Plant J 61: 107-121.
149. Jean S, Kiger AA (2012) Coordination between RAB GTPase and phosphoinositide regulation and functions. Nat Rev Mol Cell Biol 13: 463-470.
150. Bhattacharjee S, Speicher KD, Stahelin RV, Speicher DW, Haldar K (2012) PI(3)P-independent and -dependent pathways function together in a vacuolar translocation sequence to target malarial proteins to the host erythrocyte. Mol Biochem Parasitol 185: 106-113.
151. Bhattacharjee S, Stahelin RV, Speicher KD, Speicher DW, Haldar K (2012) Endoplasmic reticulum PI(3)P lipid binding targets malaria proteins to the host cell. Cell 148: 201-212.
152. Di Paolo G, De Camilli P (2006) Phosphoinositides in cell regulation and membrane dynamics. Nature 443: 651-657.
153. Lemmon MA (2003) Phosphoinositide recognition domains. Traffic 4: 201-213.
154. Misra S, Miller GJ, Hurley JH (2001) Recognizing phosphatidylinositol 3-phosphate. Cell 107: 559-562.
155. Hurley JH, Meyer T (2001) Subcellular targeting by membrane lipids. Curr Opin Cell Biol 13: 146-152.
156. Behnia R, Munro S (2005) Organelle identity and the signposts for membrane traffic. Nature 438: 597-604.
157. Wenk MR, De Camilli P (2004) Protein-lipid interactions and phosphoinositide metabolism in membrane traffic: insights from vesicle recycling in nerve terminals. Proc Natl Acad Sci U S A 101: 8262-8269.
158. Hutagalung AH, Novick PJ (2011) Role of Rab GTPases in membrane traffic and cell physiology. Physiol Rev 91: 119-149.
159. Pereira-Leal JB, Seabra MC (2000) The mammalian Rab family of small GTPases: definition of family and subfamily sequence motifs suggests a mechanism for functional specificity in the Ras superfamily. J Mol Biol 301: 1077-1087.
160. Kabcenell AK, Goud B, Northup JK, Novick PJ (1990) Binding and hydrolysis of guanine nucleotides by Sec4p, a yeast protein involved in the regulation of vesicular traffic. J Biol Chem 265: 9366-9372.
161. Christoforidis S, Miaczynska M, Ashman K, Wilm M, Zhao L, et al. (1999) Phosphatidylinositol-3-OH kinases are Rab5 effectors. Nat Cell Biol 1: 249-252.
162. Zerial M, McBride H (2001) Rab proteins as membrane organizers. Nat Rev Mol Cell Biol 2: 107-117.

163. Rink J, Ghigo E, Kalaidzidis Y, Zerial M (2005) Rab conversion as a mechanism of progression from early to late endosomes. Cell 122: 735-749.
164. Vonderheit A, Helenius A (2005) Rab7 associates with early endosomes to mediate sorting and transport of Semliki forest virus to late endosomes. PLoS Biol 3: e233.
165. Quevillon E, Spielmann T, Brahimi K, Chattopadhyay D, Yeramian E, et al. (2003) The Plasmodium falciparum family of Rab GTPases. Gene 306: 13-25.
166. Howe R, Kelly M, Jimah J, Hodge D, Odom AR (2013) Isoprenoid biosynthesis inhibition disrupts Rab5 localization and food vacuolar integrity in Plasmodium falciparum. Eukaryot Cell 12: 215-223.
167. Jackson LP, Kummel D, Reinisch KM, Owen DJ (2012) Structures and mechanisms of vesicle coat components and multisubunit tethering complexes. Curr Opin Cell Biol 24: 475-483.
168. Brown FC, Pfeffer SR (2010) An update on transport vesicle tethering. Mol Membr Biol 27: 457-461.
169. Lo SY, Brett CL, Plemel RL, Vignali M, Fields S, et al. (2012) Intrinsic tethering activity of endosomal Rab proteins. Nat Struct Mol Biol 19: 40-47.
170. Risselada HJ, Grubmuller H (2012) How SNARE molecules mediate membrane fusion: recent insights from molecular simulations. Curr Opin Struct Biol 22: 187-196.
171. Collins RN, Zimmerberg J (2009) Cell biology: A score for membrane fusion. Nature 459: 1065-1066.
172. Lippe R, Miaczynska M, Rybin V, Runge A, Zerial M (2001) Functional synergy between Rab5 effector Rabaptin-5 and exchange factor Rabex-5 when physically associated in a complex. Mol Biol Cell 12: 2219-2228.
173. Ohya T, Miaczynska M, Coskun U, Lommer B, Runge A, et al. (2009) Reconstitution of Rab- and SNARE-dependent membrane fusion by synthetic endosomes. Nature 459: 1091-1097.
174. Stenmark H, Vitale G, Ullrich O, Zerial M (1995) Rabaptin-5 is a direct effector of the small GTPase Rab5 in endocytic membrane fusion. Cell 83: 423-432.
175. Horiuchi H, Lippe R, McBride HM, Rubino M, Woodman P, et al. (1997) A novel Rab5 GDP/GTP exchange factor complexed to Rabaptin-5 links nucleotide exchange to effector recruitment and function. Cell 90: 1149-1159.
176. Rybin V, Ullrich O, Rubino M, Alexandrov K, Simon I, et al. (1996) GTPase activity of Rab5 acts as a timer for endocytic membrane fusion. Nature 383: 266-269.
177. Lippe R, Horiuchi H, Runge A, Zerial M (2001) Expression, purification, and characterization of Rab5 effector complex, rabaptin-5/rabex-5. Methods Enzymol 329: 132-145.
178. Nielsen E, Christoforidis S, Uttenweiler-Joseph S, Miaczynska M, Dewitte F, et al. (2000) Rabenosyn-5, a novel Rab5 effector, is complexed with hVPS45 and recruited to endosomes through a FYVE finger domain. J Cell Biol 151: 601-612.
179. Klionsky DJ, Herman PK, Emr SD (1990) The fungal vacuole: composition, function, and biogenesis. Microbiol Rev 54: 266-292.
180. Raymond CK, Howald-Stevenson I, Vater CA, Stevens TH (1992) Morphological classification of the yeast vacuolar protein sorting mutants: evidence for a prevacuolar compartment in class E vps mutants. Mol Biol Cell 3: 1389-1402.

181. Vida TA, Huyer G, Emr SD (1993) Yeast vacuolar proenzymes are sorted in the late Golgi complex and transported to the vacuole via a prevacuolar endosome-like compartment. J Cell Biol 121: 1245-1256.
182. Cooper AA, Stevens TH (1996) Vps10p cycles between the late-Golgi and prevacuolar compartments in its function as the sorting receptor for multiple yeast vacuolar hydrolases. J Cell Biol 133: 529-541.
183. Cereghino JL, Marcusson EG, Emr SD (1995) The cytoplasmic tail domain of the vacuolar protein sorting receptor Vps10p and a subset of VPS gene products regulate receptor stability, function, and localization. Mol Biol Cell 6: 1089-1102.
184. Canuel M, Lefrancois S, Zeng J, Morales CR (2008) AP-1 and retromer play opposite roles in the trafficking of sortilin between the Golgi apparatus and the lysosomes. Biochem Biophys Res Commun 366: 724-730.
185. Bowers K, Stevens TH (2005) Protein transport from the late Golgi to the vacuole in the yeast Saccharomyces cerevisiae. Biochim Biophys Acta 1744: 438-454.
186. Horazdovsky BF, Davies BA, Seaman MN, McLaughlin SA, Yoon S, et al. (1997) A sorting nexin-1 homologue, Vps5p, forms a complex with Vps17p and is required for recycling the vacuolar protein-sorting receptor. Mol Biol Cell 8: 1529-1541.
187. Seaman MN, McCaffery JM, Emr SD (1998) A membrane coat complex essential for endosome-to-Golgi retrograde transport in yeast. J Cell Biol 142: 665-681.
188. Seaman MN, Marcusson EG, Cereghino JL, Emr SD (1997) Endosome to Golgi retrieval of the vacuolar protein sorting receptor, Vps10p, requires the function of the VPS29, VPS30, and VPS35 gene products. J Cell Biol 137: 79-92.
189. Nothwehr SF, Bruinsma P, Strawn LA (1999) Distinct domains within Vps35p mediate the retrieval of two different cargo proteins from the yeast prevacuolar/endosomal compartment. Mol Biol Cell 10: 875-890.
190. Peter BJ, Kent HM, Mills IG, Vallis Y, Butler PJ, et al. (2004) BAR domains as sensors of membrane curvature: the amphiphysin BAR structure. Science 303: 495-499.
191. Carlton J, Bujny M, Peter BJ, Oorschot VM, Rutherford A, et al. (2004) Sorting nexin-1 mediates tubular endosome-to-TGN transport through coincidence sensing of high-curvature membranes and 3-phosphoinositides. Curr Biol 14: 1791-1800.
192. Yu JW, Lemmon MA (2001) All phox homology (PX) domains from Saccharomyces cerevisiae specifically recognize phosphatidylinositol 3-phosphate. J Biol Chem 276: 44179-44184.
193. Cozier GE, Carlton J, McGregor AH, Gleeson PA, Teasdale RD, et al. (2002) The phox homology (PX) domain-dependent, 3-phosphoinositide-mediated association of sorting nexin-1 with an early sorting endosomal compartment is required for its ability to regulate epidermal growth factor receptor degradation. J Biol Chem 277: 48730-48736.
194. Burda P, Padilla SM, Sarkar S, Emr SD (2002) Retromer function in endosome-to-Golgi retrograde transport is regulated by the yeast Vps34 PtdIns 3-kinase. J Cell Sci 115: 3889-3900.
195. Haft CR, de la Luz Sierra M, Bafford R, Lesniak MA, Barr VA, et al. (2000) Human orthologs of yeast vacuolar protein sorting proteins Vps26, 29, and 35: assembly into multimeric complexes. Mol Biol Cell 11: 4105-4116.
196. Seaman MN (2004) Cargo-selective endosomal sorting for retrieval to the Golgi requires retromer. J Cell Biol 165: 111-122.

197. Arighi CN, Hartnell LM, Aguilar RC, Haft CR, Bonifacino JS (2004) Role of the mammalian retromer in sorting of the cation-independent mannose 6-phosphate receptor. J Cell Biol 165: 123-133.
198. Bugarcic A, Zhe Y, Kerr MC, Griffin J, Collins BM, et al. (2011) Vps26A and Vps26B subunits define distinct retromer complexes. Traffic 12: 1759-1773.
199. Kerr MC, Bennetts JS, Simpson F, Thomas EC, Flegg C, et al. (2005) A novel mammalian retromer component, Vps26B. Traffic 6: 991-1001.
200. Kurten RC, Cadena DL, Gill GN (1996) Enhanced degradation of EGF receptors by a sorting nexin, SNX1. Science 272: 1008-1010.
201. Kurten RC, Eddington AD, Chowdhury P, Smith RD, Davidson AD, et al. (2001) Self-assembly and binding of a sorting nexin to sorting endosomes. J Cell Sci 114: 1743-1756.
202. Rojas R, Kametaka S, Haft CR, Bonifacino JS (2007) Interchangeable but essential functions of SNX1 and SNX2 in the association of retromer with endosomes and the trafficking of mannose 6-phosphate receptors. Mol Cell Biol 27: 1112-1124.
203. Harbour ME, Breusegem SY, Antrobus R, Freeman C, Reid E, et al. (2010) The cargo-selective retromer complex is a recruiting hub for protein complexes that regulate endosomal tubule dynamics. J Cell Sci 123: 3703-3717.
204. Wassmer T, Attar N, Harterink M, van Weering JR, Traer CJ, et al. (2009) The retromer coat complex coordinates endosomal sorting and dynein-mediated transport, with carrier recognition by the trans-Golgi network. Dev Cell 17: 110-122.
205. Fjorback AW, Seaman M, Gustafsen C, Mehmedbasic A, Gokool S, et al. (2012) Retromer binds the FANSHY sorting motif in SorLA to regulate amyloid precursor protein sorting and processing. J Neurosci 32: 1467-1480.
206. Harterink M, Port F, Lorenowicz MJ, McGough IJ, Silhankova M, et al. (2011) A SNX3-dependent retromer pathway mediates retrograde transport of the Wnt sorting receptor Wntless and is required for Wnt secretion. Nat Cell Biol 13: 914-923.
207. Chen C, Garcia-Santos D, Ishikawa Y, Seguin A, Li L, et al. (2013) Snx3 regulates recycling of the transferrin receptor and iron assimilation. Cell Metab 17: 343-352.
208. Rojas R, van Vlijmen T, Mardones GA, Prabhu Y, Rojas AL, et al. (2008) Regulation of retromer recruitment to endosomes by sequential action of Rab5 and Rab7. J Cell Biol 183: 513-526.
209. Koumandou VL, Klute MJ, Herman EK, Nunez-Miguel R, Dacks JB, et al. (2011) Evolutionary reconstruction of the retromer complex and its function in *Trypanosoma brucei*. J Cell Sci 124: 1496-1509.
210. Cullen PJ, Korswagen HC (2012) Sorting nexins provide diversity for retromer-dependent trafficking events. Nat Cell Biol 14: 29-37.

CHAPTER 3:

Evidence for a Golgi-to-endosome protein sorting pathway in *Plasmodium falciparum*

Priscilla Krai, Seema Dalal and Michael Klemba

This chapter has been submitted for publication to PLOS ONE.

Author Contributions:

Priscilla Krai performed all research except experiments mentioned below and helped write the article

Seema Dalal generated PfSortilin-HA expressing parasites and performed imaging and immunoblot.

Michael Klemba oversaw and directed the research and helped write the article.

Abstract:

During the asexual intraerythrocytic stage, the malaria parasite *Plasmodium falciparum* must traffic newly-synthesized proteins to a broad array of destinations within and beyond the parasite's plasma membrane. In this study, we have localized two well-conserved protein components of eukaryotic endosomes, the retromer complex and the small GTPase Rab7, to define a previously-undescribed endosomal compartment in *P. falciparum*. Retromer and Rab7 co-localized to a small number of punctate structures within parasites. These structures, which we refer to as endosomes, lie in close proximity to the Golgi apparatus and, like the Golgi apparatus, are inherited by daughter merozoites. However, the endosome is clearly distinct from

the Golgi apparatus as neither retromer nor Rab7 redistributed to the endoplasmic reticulum upon brefeldin A treatment. Nascent rhoptries (specialized secretory organelles required for invasion) developed adjacent to endosomes, an observation that suggests a role for the endosome in rhoptry biogenesis. A *P. falciparum* homolog of the sortilin family of protein sorting receptors (PfSortilin) was localized to the Golgi apparatus. Together, these results elaborate a putative Golgi-to-endosome protein sorting pathway in asexual blood stage parasites and suggest that one role of retromer is to mediate the retrograde transport of PfSortilin from the endosome to the Golgi apparatus.

Introduction

The human malaria parasite *Plasmodium falciparum* is responsible for approximately one million deaths annually [1]. The pathology of malaria is caused by infection of the host's erythrocytes. Within the erythrocyte, the parasite undergoes a ~48 hour replication cycle, generating 8-26 daughter merozoites that egress from the spent host cell and invade fresh erythrocytes [2]. During this cycle, the parasite must replicate its heritable organelles (the nucleus, endoplasmic reticulum, Golgi apparatus, mitochondrion and apicoplast) and generate others *de novo.* Of the latter group, the food vacuole, rhoptries, micronemes, and dense granules are the best characterized [3,4] but other compartments (exonemes and mononemes) have also been reported [5,6]. The food vacuole is an acidic organelle in which endocytosed host cell hemoglobin is degraded to amino acids; it is also the site of action of quinoline anti-malarials such as chloroquine. Rhoptries, micronemes and dense granules are specialized, apically oriented secretory organelles that discharge their contents during and shortly after host cell invasion.

Intraerythrocytic *P. falciparum* must accurately sort and traffic newly-synthesized proteins to all of these intracellular organelles, several of which are not present in well-studied eukaryotic model organisms. In addition to intracellular protein trafficking, the parasite exports endogenous proteins beyond its plasma membrane, first into the parasitophorous vacuole and then in some cases into the host cell [7]. There is abundant evidence that the parasite relies heavily on its endomembrane (or secretory) system to sort and traffic both intracellular and extracellular proteins to their proper destinations (recently reviewed in [8]). Many proteins targeted to the food vacuole, apicoplast, rhoptries, micronemes, dense granules and outside of the parasite possess a canonical "signal peptide", a short sequence of hydrophobic amino acids near the amino terminus of the protein, that specifies co-translational import into the endoplasmic reticulum (ER). In intraerythrocytic *P. falciparum*, the ER is largely perinuclear with a couple of "horn-like" projections [9]. From the ER, most proteins appear to be transported to the parasite Golgi apparatus (the exceptions being apicoplast-targeted proteins, which bypass the Golgi [10]). These conclusions are largely drawn from experiments that demonstrate the inhibition of trafficking by brefeldin A, a fungal metabolite that blocks anterograde ER-to-Golgi traffic and causes Golgi proteins to redistribute to the ER [11,12].

There have been conflicting reports regarding the nature of the Golgi apparatus in blood-stage *P. falciparum*. In many eukaryotic organisms, the Golgi apparatus is composed of several biochemically distinct compartments called cisternae (designated *cis*-, medial-, and *trans*-). These cisternae are closely apposed or "stacked" in mammalian cells but may also exist as unstacked cisternae as is the case in *Saccharomyces cerevisiae* [13]. Localization studies using antibodies against *P. falciparum* homologs of proteins that reside in the *cis*-Golgi (ERD2 and Bet3p) and the *trans*-Golgi (Rab6) cisternae of mammalian cells have suggested that the Golgi

apparatus in *P. falciparum* is composed of dispersed, unstacked *cis*- and *trans*-cisternae [14,15]. In contrast, localization of fluorescent protein-tagged versions of the *cis*-Golgi marker PfGRASP and the *trans*-Golgi marker PfRab6 in live cells has indicated that these two proteins are in close proximity [16], although whether they label the same or different compartments has not yet been fully resolved. Numerous ultrastructural studies of intraerythrocytic parasites, including those that have employed serial sectioning and three dimensional reconstruction, have failed to detect stacked Golgi cisternae in the parasite [17-19], which raises the possibility that the plasmodial Golgi apparatus is a "stripped-down" form of the organelle consisting of a single compartment. It has been speculated that the absence of N-linked glycosylation in *P. falciparum* [20] renders unnecessary the presence of biochemically distinct Golgi compartments [21].

The multi-compartment endosomal network is a key constituent of the endomembrane system. The mammalian endosomal network consists of discrete compartments (early, late and recycling endosomes) that collectively serve as a "hub" of cellular protein traffic [22]. Early endosomes are generated from endocytic vesicles and are characterized by the presence of phosphatidylinositol-3-phosphate (PI3P) and the small GTPase Rab5 at the cytosolic leaflet of the membrane. Early endosomes undergo a process of maturation that involves the replacement of Rab5 with Rab7 and the conversion of PI3P to phosphatidylinositol-3,5-bisphosphate [23]. Biosynthetic traffic intersects with the endosomal network during the transition from early to late endosomes. Late endosomes ultimately fuse with lysosomes, delivering their biosynthetic cargo to its final destination. This endosomal maturation pathway is also used to deliver membrane proteins (*e.g.* signaling receptors) from the plasma membrane to the lysosome for degradation. Some membrane proteins avoid degradation and are cycled back to the plasma membrane *via* so-called recycling endosomes. The nature of the endosomal network in *P. falciparum* has, to our

knowledge, not yet been investigated. Structures resembling the multi-vesicular bodies of mammalian endosomes have been observed in parasites expressing a dominant negative mutant of the GTPase Vps4 [24]; however, it is not clear whether these structures are present in wild-type parasites.

The aim of this study was first to define endosomal compartments in intraerythrocytic *P. falciparum* and then to interrogate their contribution to protein sorting and trafficking. We focused our investigation on two highly conserved species found on the cytosolic leaflet of the endosomal membrane: the retromer cargo-selective complex and the small GTPase Rab7. The retromer cargo-selective complex is comprised of three proteins, termed Vps26, Vps29 and Vps35, which associate into a stable trimeric assembly [25]. The retromer cargo-selective complex is recruited to the mammalian endosomal membrane by prenylated, GTP-bound Rab7 [26,27]. One role of retromer that is conserved from yeast to mammalian cells is the recycling of protein sorting receptors from the endosome to the Golgi apparatus [25]. Interaction of membrane-associated retromer with the cytosolic tail of its cargo (*i.e.*, sorting receptors) triggers transport back to the Golgi apparatus. In yeast and mammalian cells, retromer function also requires a heterodimer of sorting nexins, which are rigid, curved BAR (Bin-Amphiphysin-Rvs) domain proteins capable of deforming membranes and stabilizing endosomal tubules [28]. However, sorting nexins are not universally conserved in eukaryotes and appear to be absent from *P. falciparum* (Results and [29]).

We localized the retromer cargo-selective complex and PfRab7 in asexual blood-stage *P. falciparum* to a putative endosomal compartment. The spatial relationship of the endosome to other subcellular compartments in the parasite was characterized. We describe attempts to perturb protein traffic through the endosome by conditional destabilization of retromer subunits

and by the expression of PfRab7 dominant negative and constitutively active mutants. The effect of blocking COPI-dependent vesicular traffic on endosomal structure was determined by treating parasites with brefeldin A. To gain insight into a possible role for retromer in recycling protein sorting receptors, we characterized the subcellular distribution of the sole *P. falciparum* homolog of the Vps10/sortilin family of protein sorting receptors. Together, these studies define a new compartment in the *P. falciparum* secretory system with a likely role in protein sorting and organelle biogenesis.

Results

The P. falciparum genome encodes the three retromer cargo-selective subunits

The genome of *P. falciparum* clone 3D7 encodes a single homolog of each retromer cargo-selective subunit: PfVps26 (GeneID PF3D7_1250300), PfVps29 (GeneID PF3D7_1406700), and PfVps35 (GeneID PF3D7_1110500). PfVps26, PfVps29 and PfVps35 share 53, 47 and 30% identity at non-gap positions with the human orthologs Vps26 (isoform A or B), Vps29 and Vps35, respectively (Fig. 3-3 and 3-S1). Residues that contribute to interactions between cargo-selective subunits in human retromer are generally well conserved in the *P. falciparum* sequences (Fig. 3-S1). Transcriptomic data indicate that expression of all three retromer cargo-selective subunits peaks between early trophozoite and late schizont stages [30-32].

In addition to the cargo-selective complex, a second component of the retromer complex in mammals and yeast is a PX-BAR sorting nexin dimer, which binds to PI3P through the Phox (PX) domains and induces or stabilizes membrane curvature with the BAR domains [22,33-35]. We attempted to identify parasite sorting nexins using PSI-BLAST searches with human sorting

nexin 1 and *S. cerevisiae* Vps5p as queries but were unable to find any *P. falciparum* homologs. When we restricted the search to the PX domains, we found two PX domain-containing proteins in the *P. falciparum* genome but neither appeared to be followed by a BAR domain (data not shown). Our results are consistent with a previous report that sorting nexins are likely absent from *P. falciparum* and other pathogenic protozoa [29].

P. falciparum retromer labels a putative endosome in asexual blood-stage parasites

To determine whether retromer is associated with an endosome-like compartment in blood-stage *P. falciparum*, we attempted to independently modify the endogenous PfVps26, PfVps29 and PfVps35 loci to encode C-terminal fusions to the enhanced yellow fluorescent protein (YFP) variant "Citrine" [36]. Parasite lines expressing PfVps29-YFP and PfVps35-YFP were obtained (Fig. 3-S2); however, we were unable to introduce a tag (either YFP or the 9-residue hemagglutinin tag) at the C-terminus of PfVps26.

Both PfVps29-YFP and PfVps35-YFP were expressed throughout the asexual blood stage (Fig. 3-1). In live parasites expressing PfVps35-YFP, punctate structures were observed in trophozoites and schizonts amid a background of diffuse, presumably cytosolic fluorescence (Fig. 3-1A). One to two puncta were present in trophozoite stages. As the parasites matured, the puncta became more numerous until in segmenting schizonts there appeared to be one retromer-labeled punctum for each daughter nucleus. Single puncta were present in egressed merozoites, which indicates that the retromer-labeled compartment is inherited. Surprisingly, the PfVps35-YFP-labeled puncta were no longer visible in early ring-stage parasites. The distribution of PfVps29-YFP across the asexual cycle was essentially identical to that of PfVps35-YFP (Fig. 3-1B). To determine whether PfVps35 and PfVps29 are present on the same structures, a

transposable PfVps29-mCherry expression cassette was introduced into the genome of the parasite line expressing PfVps35-YFP. The two fluorescent proteins co-localized to the same punctate structures in trophozoites and schizonts (Fig. 3-1C).

To establish the position of the retromer-labeled compartment in relation to other known organelles, PfVps35-YFP was co-localized with organellar markers (Fig. 3-1D). Localization of the Golgi apparatus with antibodies against ERD2 revealed that this organelle and the PfVps35-YFP-labeled compartment are distinct structures with a close spatial relationship (Fig. 3-1D). A similar result was obtained with the Golgi-specific protein PfRab6 as described below. Thus, the PfVps35-YFP-labeled compartment appears to be adjacent to yet distinct from the *P. falciparum* Golgi apparatus. There was no apparent overlap of PfVps35-YFP with markers for the endoplasmic reticulum, apicoplast or mitochondrion (Fig. 3-1D).

Figure 3-1 (next page). The retromer cargo-selective complex localizes to a novel, heritable subcellular compartment in intraerythrocytic *P. falciparum*. A) Wide-field epifluorescence images of live parasites expressing PfVps35-YFP. Parasites are shown at ring (R), trophozoite (T), schizont (Sz), segmenter (Sg), and extracellular merozoite (M) stages. Hoechst 33342 fluorescence (DNA) is pseudocolored red. B) Images of live parasites expressing PfVps29-YFP. C) Images of live parasites co-expressing PfVps35-YFP and PfVps29-mCherry ("PfVps29-mC") in trophozoite (T) and schizont (Sz) stages. mCherry fluorescence is pseudocolored red. D) Co-localization of PfVps35-YFP and organellar markers in paraformaldehyde-fixed parasites (except for MitoTracker, which was imaged live). PMV, plasmepsin V; ACP, acyl carrier protein; MT, MitoTracker Red CM-H2Xros; RAP1, rhoptry associated protein 1; EBA175, erythrocyte binding antigen 175. Organelles labeled by the markers are indicated in parenthesis. Marker-derived fluorescence is pseudocolored red. E) PfVps35-YFP is adjacent to developing rhoptries in a 2N parasite. Hoechst 33342 fluorescence (DNA) is pseudocolored cyan. In all panels, YFP fluorescence is pseudocolored green. Scale bar, 2 μm.

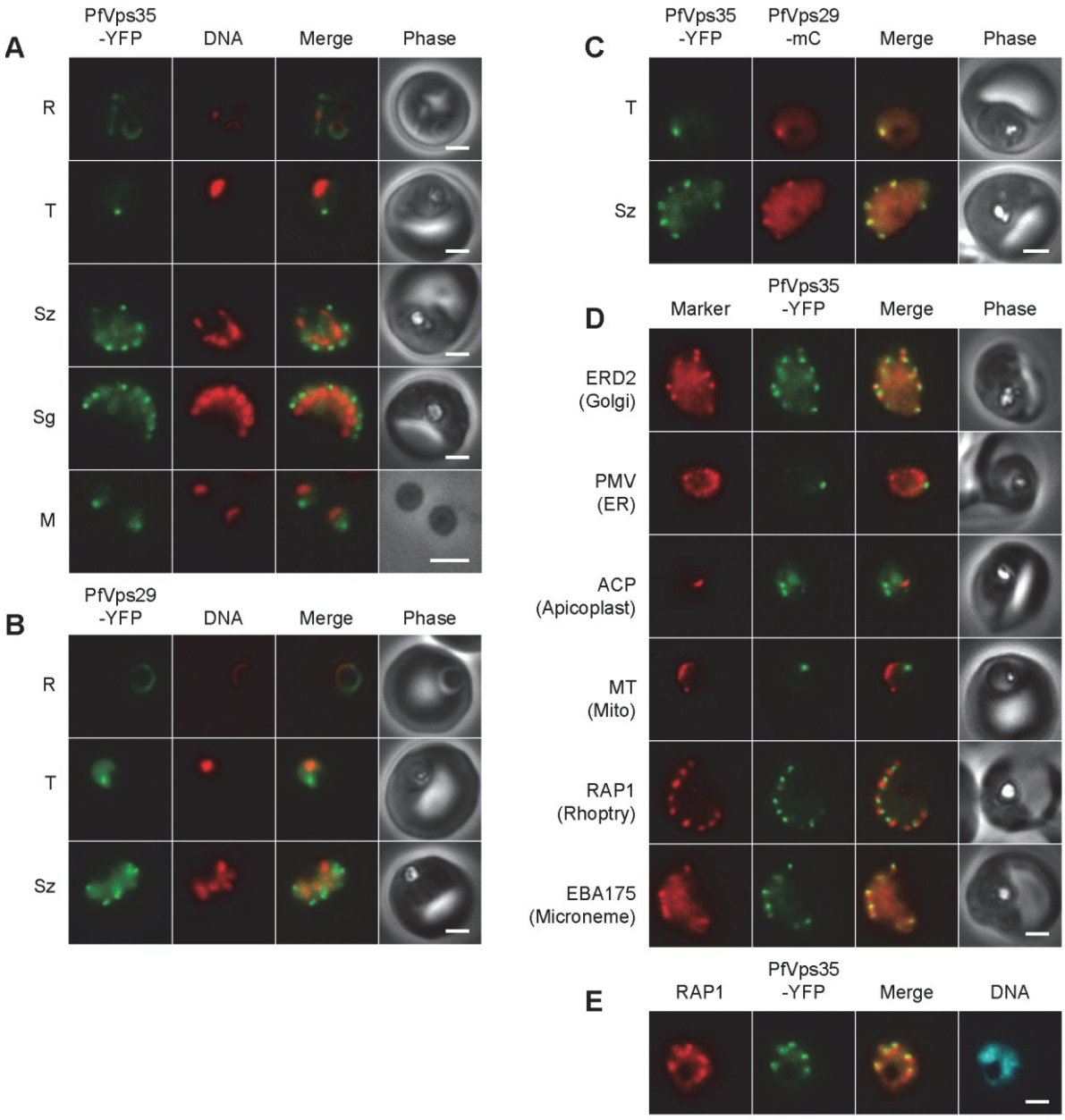
A
PfVps35 -YFP
DNA
Merge
Phase
R
T
Sz
Sg
M
B
PfVps29 -YFP
DNA
Merge
Phase
R
T
Sz
C
PfVps35 -YFP
PfVps29 -mC
Merge
Phase
T
Sz
D
Marker
PfVps35 -YFP
Merge
Phase
ERD2 (Golgi)
PMV (ER)
ACP (Apicoplast)
MT (Mito)
RAP1 (Rhoptry)
EBA175 (Microneme)
E
RAP1
PfVps35 -YFP
Merge
DNA

In the schizont stage, the rhoptries and micronemes are generated *de novo*. Interestingly, the PfVps35-YFP-labeled compartment was consistently found in close proximity to the rhoptry (Fig. 3-1D and 3-1E). This spatial relationship was observed at the earliest time points at which the rhoptry marker, rhoptry-associated protein 1 (RAP1), was visible (*i.e.*, as nuclear division commenced) and before the organelles segregated into individual merozoites (Fig. 3-1E). Micronemes also appeared to develop in close proximity to the retromer-labeled compartment (Fig. 3-1D). Taken together, the localization studies reveal that *P. falciparum* retromer is located on a subcellular compartment that is distinct from known components of the *P. falciparum* endomembrane system. On the basis of its association with the retromer cargo-selective complex, we term this compartment the "*P. falciparum* endosome". Close spatial proximity to the Golgi apparatus and to developing rhoptries and micronemes raises the intriguing possibility that the endosome plays a role in protein trafficking to the apical organelles.

Attempts to perturb retromer function

To establish the importance of retromer in asexual blood stages and gain insight into the role of the endosome in protein trafficking, we attempted to disrupt the coding sequence of PfVps35 using double-crossover homologous recombination coupled with positive and negative selection [37]. This strategy would replace the sequence coding for residues 244 to 817 with a drug selection cassette (Fig. 3-S2). PfVps35 was chosen for disruption because it is the central component of the retromer cargo-selective complex and interacts with both PfVps29 and PfVps26 [38]. Thus, the absence of full-length PfVps35 would preclude the formation of a functional retromer complex. Three independent sets of transfected parasites were subjected to multiple rounds of positive-selection drug cycling followed by negative selection, with the result

that the PfVps35 sequence remained intact (Fig. 3-S2). The inability to disrupt the PfVps35 coding sequence suggests that the retromer cargo-selective complex could be important for efficient asexual blood-stage growth.

We next attempted to manipulate steady-state levels of PfVps29 and PfVps35 by generating fusions of the endogenous sequences with YFP followed by a regulatable *Escherichia coli* dihydrofolate reductase (DHFR) "destabilization domain" (DD) [39]. This strategy has been successfully used in *P. falciparum* to conditionally regulate protein levels [40]. Independent parasite lines expressing PfVps35-YFP-DD and PfVps29-YFP-DD were obtained. When cultured in medium containing the DD stabilizing agent trimethoprim, the distribution of the labeled retromer components, as judged by YFP fluorescence, was indistinguishable from those described in Fig. 3-1 for PfVps35-YFP and PfVps29-YFP (data not shown). Upon removal of the stabilizing ligand, little or no change in fluorescence pattern or intensity was observed for either PfVps35-YFP-DD or PfVps29-YFP-DD. Furthermore, there was no apparent growth defect associated with expression of PfVps35-YFP-DD and PfVps29-YFP-DD in the absence of the stabilizing ligand (data not shown). These results suggest that the addition of a C-terminal destabilization domain did not effectively reduce the steady-state levels PfVps29 or PfVps35. We did not further characterize these parasite lines.

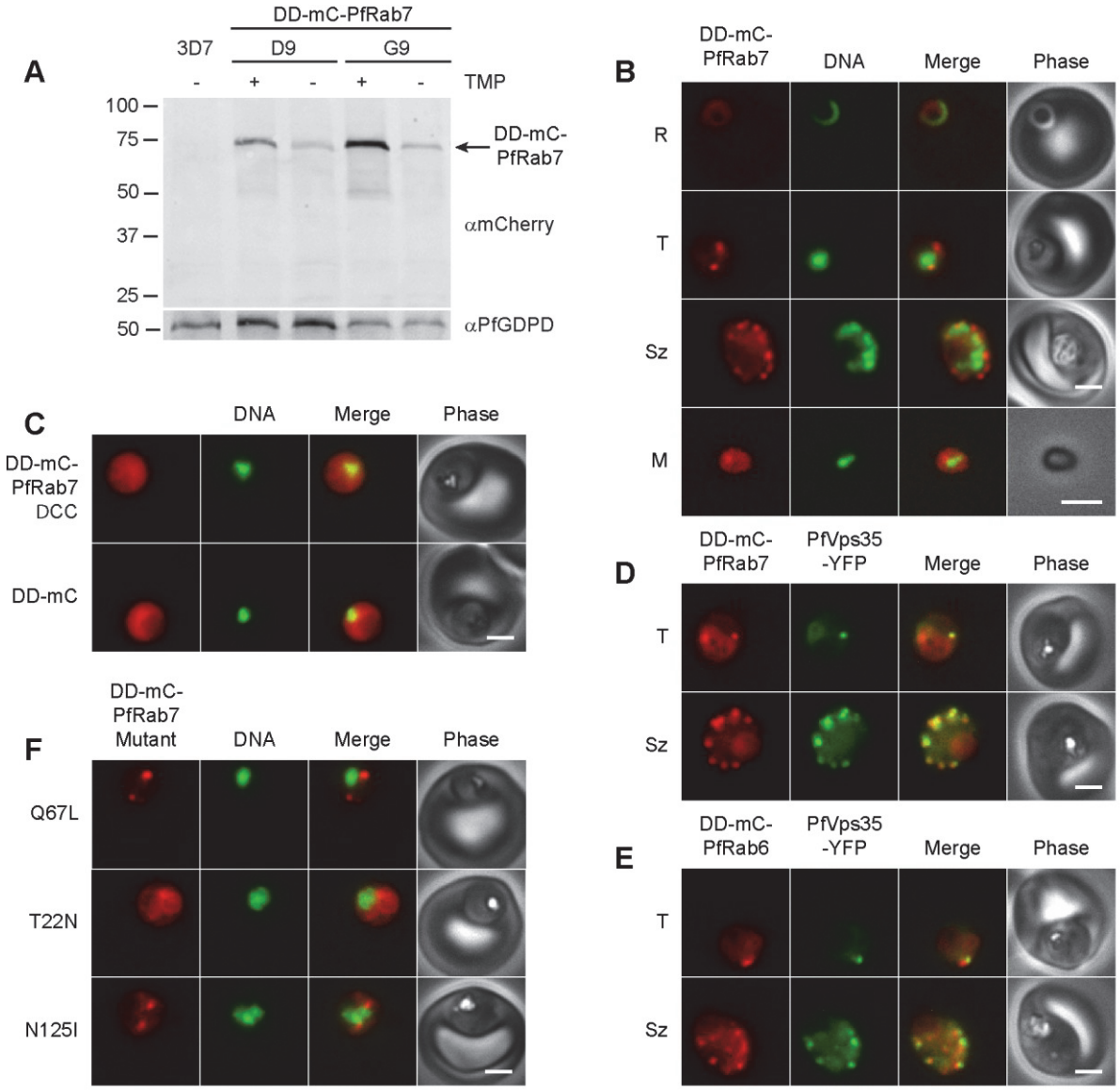

Figure 3-2. PfRab7 localizes to the same compartment as the retromer cargo-selective complex. A) Effect of the DD-stabilizing agent trimethroprim (TMP) on the steady-state levels of DD-mCherry-PfRab7 in clonal parasite lines D9 (one expression cassette per genome) and G9 (two expression cassettes per genome). 3D7 is the untransfected parental parasite line. Upper: Anti-mCherry immunoblot. Lower: The membrane was reprobed with anti-glycerophosphoester phosphodiesterase (PfGDPD) antibodies for a loading control. The sizes of protein markers in kDa are indicated at left. B) Images of DD-mCherry-PfRab7 ("DD-mC-PfRab7") in live clone G9 parasites. Stages shown are ring (R), trophozoite (T), schizont (Sz), and extracellular merozoite (M). C) Live parasites expressing DD-mCherry-PfRab7ΔCC ("DD-mC-Rab7ΔCC") and DD-mCherry ("DD-mC"). D) Live parasites co-expressing PfVps35-YFP and DD-mCherry-PfRab7 ("DD-mC-PfRab7"). E) Live parasites co-expressing PfVps35-YFP and DD-mCherry-PfRab6 ("DD-mC-PfRab6"). F) Live parasites expressing DD-mCherry-PfRab7 mutants. T22N

and N125I are predicted to be "GDP-locked" and Q67L is predicted to be "GTP-locked". 5' UTR sequences driving expression are *pfrab7* for N125I and Q67L and *pfapp* (aminopeptidase P) for T22N. In panels B, C and F, Hoechst 33342 fluorescence (DNA) is pseudocolored green and in panels D and E YFP fluorescence is pseudocolored green. In panels B-F, parasites were cultured in the presence of 10 μM trimethoprim. mCherry fluorescence is pseudocolored red. Scale bar, 2 μm.

The small GTPase PfRab7 co-localizes with retromer to the endosome

In light of our inability to perturb retromer function, we sought an alternate means of disrupting protein traffic through the *P. falciparum* endosome. Dominant negative and constitutively active mutants of Rab family GTPases are useful tools for interrogating trafficking pathways in yeast and mammalian systems. Rab7 is a well-established marker of the late endosome in mammalian cells and is required for recruitment of the retromer cargo-selective complex to the endosomal membrane [26,27,41,42]. The *P. falciparum* genome encodes one Rab7 homolog, designated as PfRab7 (GeneID PF3D7_0903200) for which transcription is maximal in trophozoite and early schizont stages [43-45]. Thus, we investigated the subcellular distribution of PfRab7 and explored whether the expression of PfRab7 mutants could provide insight into the role of the putative *P. falciparum* endosome.

We first determined whether steady-state levels of mCherry-PfRab7 expressed from a transposable cassette in *P. falciparum* could be regulated by N-terminal fusion to the *E. coli* DHFR destabilization domain (DD). Regulated expression would be necessary to mitigate any deleterious effects of PfRab7 mutants during parasite transfection and selection. A transposable DD-mCherry-PfRab7 expression cassette under the control of the PfRab7 promoter was generated and transfected into wild-type parasites. Two clonal parasite lines were obtained (Fig. 3-S2). One line (D9) contained one copy of the transposon expression cassette, whereas the other line (G9) possessed two copies. In both clones, steady-state levels of the DD-mCherry-PfRab7

fusion were ~5-fold higher in the presence of the DD-stabilizing ligand trimethoprim (Fig. 3-2A). Full-length DD-mCherry-PfRab7 (predicted size 69 kDa) was the major species detected with anti-mCherry antibodies in both parasite lines.

DD-mCherry-PfRab7 exhibited a dual cytosolic-punctate distribution in the presence of trimethoprim (Fig. 3-2B). In trophozoites one to two punctate structures were observed. These puncta multiplied as parasites matured and were segregated to daughter merozoites in segmented schizonts. In free merozoites, concentrated foci of DD-mCherry-PfRab7 could be observed; however, as in the case of PfVps35-YFP, no puncta were found in ring-stage parasites. The cytosolic fluorescence likely reflects the distribution of inactive, GDP-bound PfRab7 whereas the punctate distribution is presumably attributable to the membrane-bound PfRab7-GTP complex. To confirm that the puncta were labeled with prenylated, membrane-bound DD-mCherry-PfRab7, we expressed a truncated variant of PfRab7 lacking the C-terminal two-amino acid prenylation motif required for membrane insertion (DD-mCherry-PfRab7ΔCC; Fig. 3-S1). In the presence of trimethoprim, DD-mCherry-PfRab7ΔCC fluorescence was distributed throughout the parasite cytosol and no puncta were observed (Fig. 3-2C). This distribution was indistinguishable from that of DD-mCherry expressed alone (Fig. 3-2C). We conclude that the puncta observed with DD-mCherry-PfRab7 reflect the distribution of the active, membrane-bound PfRab7-GTP complex.

To determine whether PfRab7 was present on the same subcellular structures as the retromer cargo-selective complex, the DD-mCherry-PfRab7 transposable expression cassette was introduced into the genome of the parasite line expressing PfVps35-YFP. Substantial overlap of mCherry and YFP fluorescence was observed in trophozoite- and schizont-stage parasites (Fig. 3-2D). To confirm that this co-localization was specific for PfRab7, we also

generated parasites co-expressing the Golgi protein PfRab6 (expressed as a DD-mCherry-PfRab6 fusion from the *pfrab6* promoter) and PfVps35-YFP. As described above for the Golgi marker ERD2, PfVps35-YFP-labeled puncta were located adjacent to DD-mCherry-PfRab6-labeled Golgi compartments but the two proteins did not co-localize (Fig. 3-2E). Together, these results indicate that PfRab7 and retromer are both found on the *P. falciparum* endosome and confirm the close spatial proximity of this compartment to the parasite's Golgi apparatus.

Expression of PfRab7 dominant negative and constitutively active mutants in P. falciparum

Dominant negative mutants of Rab7 are impaired for GTP binding [46,47] and exert their effects by sequestering Rab effector proteins. In contrast, constitutively active mutants exhibit greatly reduced intrinsic GTPase activity [46,48] and persist in an activated, membrane- and GTP-bound state. Both types of mutants can potentially disrupt specific vesicle trafficking pathways and provide insight into the role of the endogenous Rab protein. By reference to the literature on Rab7 mutants cited above and sequence alignments, we identified T22N and N125I as potential dominant negative mutants and Q67L as a potential constitutively active mutant of PfRab7 (Fig. 3-S1). We generated transposable cassettes to express DD-mCherry fusions of the three PfRab7 mutants and introduced them into parasites. Expression of the fusions was driven by either the native *pfrab7* promoter or, to potentially increase the steady-state levels, by the stronger *P. falciparum* aminopeptidase P promoter (S. Dalal and M. Klemba, unpublished data). Parasite lines conditionally expressing all three PfRab7 mutants were obtained with both promoters (Fig. 3-2F and data not shown).

When expressed in mammalian cells, Rab7 dominant negative mutants (T22N and N125I) are found in the cytosol and have a profound effect on late endosome-to-lysosome

trafficking and lysosome morphology [46,49,50]. Lysosome-bound vesicular transport requires multiple effectors that interact with active GTP-bound Rab7. For example, dominant negative Rab7 mutants prevent complex formation with dynein-dynactin motors that direct minus-end trafficking on microtubules towards the lysosome [51,52]. As a result, the lysosome becomes dispersed into small vesicles that have reduced acidity and are not accessible to endocytic traffic [46]. When expressed in *P. falciparum* from either the *pfrab7* or the *pfapp* promoter and stabilized with trimethoprim, the T22N mutant had the expected cytosolic distribution (Fig. 3-2F), which suggests that it exists to a greater extent in the GDP-bound state than wild-type PfRab7. Surprisingly, the N125I mutant was present in a punctate distribution that resembled that of wild-type PfRab7, an observation that suggests that this mutant persisted in a GTP-bound state (Fig. 3-2F). Neither PfRab7 mutant inhibited parasite growth or altered the morphology of the lysosome-like food vacuole as assessed by phase contrast microscopy (data not shown).

The constitutively active Q67L mutant of human Rab7 associates with the lysosomal membrane and increases the rate of endosome-to-lysosome fusion, resulting in an enlarged perinuclear acidic organelle labeled with both lysosome and late endosomal proteins [46,53]. In this study, DD-mCherry-PfRab7Q67L exhibited a very similar distribution to that of wild-type PfRab7 (Fig. 3-2F). Microscopic inspection of live parasites indicated that food vacuole morphology was normal. Live-cell fluorescence and immunofluorescence experiments revealed that DD-mCherry-PfRab7-Q67L had not redistributed to the Golgi apparatus, rhoptries or food vacuole (data not shown). To all appearances, PfRab7Q67L behaved indistinguishably from wild-type PfRab7.

PfRab6 but not PfRab7 or retromer redistributes to the ER upon brefeldin A treatment

The fungal metabolite brefeldin A is widely used to interrogate endomembrane trafficking pathways. Addition of brefeldin A to mammalian cells rapidly induces the reversible collapse of the Golgi apparatus into the ER [54,55], endosome tubulation [56-58] and recycling endosome fusion to the *trans*-Golgi network [59,60]. Early-to-late endosome maturation is also disrupted [56,61,62]. The mechanism of action involves the inhibition of three guanine nucleotide exchange factors (GEFs) that act on small GTPases of the ADP-ribosylation factor (Arf) family at the *cis*- or *trans*-Golgi cisternae and *trans*-Golgi network [63-66]. Brefeldin A also stabilizes the inactive GDP-Arf GTPase and Arf-GEF complexes [64,67], which can no longer properly recruit COP1 or AP-1/clathrin coat proteins [68].

We compared the effects of brefeldin A on the *P. falciparum* Golgi apparatus and endosome by treating parasites lines expressing DD-mCherry-PfRab6 and PfVps35-YFP or DD-mCherry-PfRab7 with 5 μg/mL brefeldin A for one hour. As expected, the Golgi marker DD-mCherry-PfRab6 redistributed to the perinuclear ER (Fig. 3-3A). After the one hour brefeldin A treatment, fewer than 3% of parasites contained a DD-mCherry-PfRab6-labeled punctum, compared to 80% in the untreated control (Fig. 3-3C). In addition, the number of parasites exhibiting DD-mCherry-PfRab6 fluorescence at the perinuclear ER doubled (Fig. 3-2B). The effect of brefeldin A on the endosome was much less pronounced. We observed a reduction in the number of PfVps35-YFP- and DD-mCherry-PfRab7-labeled puncta, but such structures persisted in about half of the parasites (Fig. 3-3C). Association with the perinuclear ER was not observed for either protein (Fig. 3-3A). The contrasting responses of the Golgi apparatus and endosome to brefeldin A treatment reveal differences in the dynamics of vesicular traffic to and from these compartments.

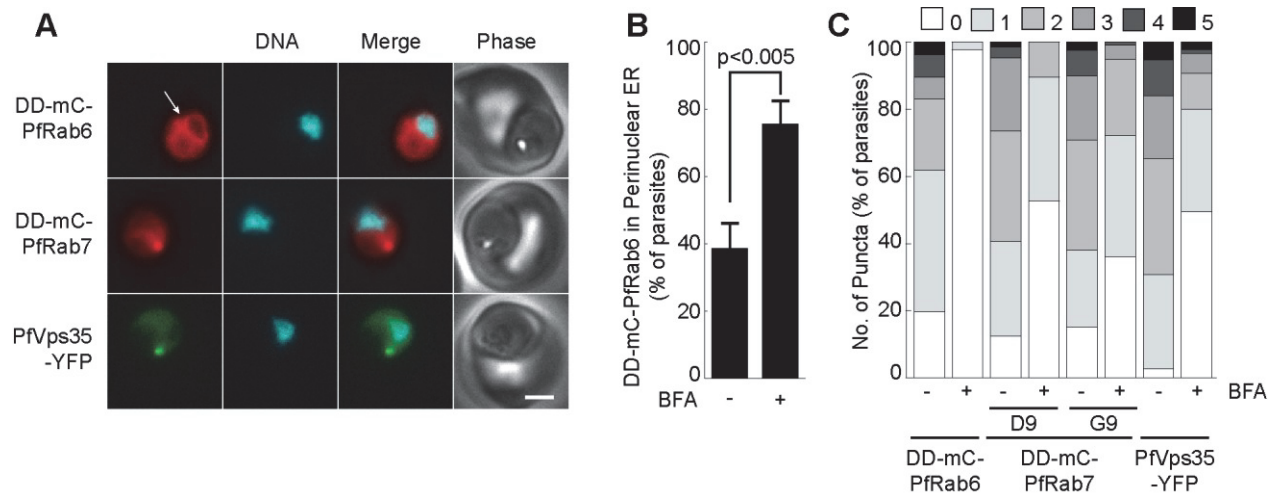

Figure 3-3. PfRab6 but not PfRab7 or retromer rapidly redistributes to the ER upon brefeldin A treatment. A) Distributions of DD-mCherry-PfRab6 ("DD-mC-PfRab6"), DD-mCherry-PfRab7 ("DD-mC-PfRab7") and PfVps35-YFP in live parasites after one hour in the presence of 5 µg/mL brefeldin A. Redistribution of DD-mCherry-PfRab6 to the perinuclear ER is indicated with an arrow. mCherry fluorescence is pseudocolored red, YFP fluorescence is pseudocolored green and Hoechst 33342 fluorescence is pseudocolored cyan. Scale bar, 2 µm. B) Effect of brefeldin A (5 µg /mL, 1 hour) on the percentage of parasites exhibiting ER-associated DD-mCherry-PfRab6 fluorescence. Results are an average of three experiments, n = 75 to 85 parasites per condition. The *p*-value was determined using a two-tailed Student's t-test. C) Effect of Brefeldin A (5 µg/mL, 1 hour) on the number of puncta labeled with DD-mCherry-PfRab6, DD-mCherry-PfRab7 (clones D9 and G9) or PfVps35-YFP. Results are an average of three experiments, n = 50 to 70 parasites per condition.

PfSortilin, a putative retromer cargo, is located in the Golgi apparatus

A major role for the cargo-selective retromer complex in yeast and mammalian cells involves the recycling of protein sorting receptors such as the mannose-6-phosphate receptor (MPR) and the Vps10p-domain-containing sorting receptors known as sortilins from the endosome back to the Golgi apparatus [69]. To assess whether this might be a plausible role for retromer in *P. falciparum*, we searched the parasite genome for MPR and sortilin homologs. We found one sortilin homolog, referred to here as PfSortilin (GeneID: PF3D7_1451800, annotated as "sortilin, putative") but could not identify any MPR homologs. The PfSortilin open reading

frame codes for a 102 kDa protein with a putative signal peptide, a Vps10 domain, a putative single-pass transmembrane sequence, and a C-terminal tail (Fig. 3-4A). Transcriptomic data indicate that PfSortilin is maximally expressed from about 20 to 40 hours post-invasion (*i.e.*, during the trophozoite and schizont stages) [30-32].

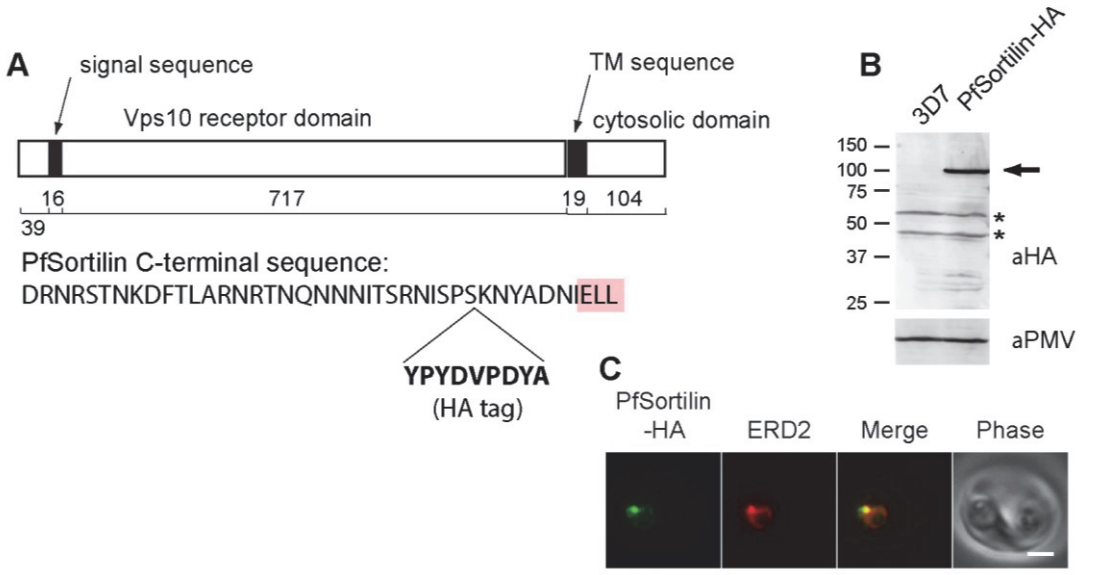

Figure 3-4. The putative protein sorting receptor PfSortilin localizes to the *P. falciparum* Golgi apparatus. A) Schematic diagram of the domain organization of PfSortilin with the number of amino acids in each domain indicated below. At bottom is the C-terminal sequence of PfSortilin with the site of incorporation of the HA tag indicated. Three C-terminal residues that are conserved in Apicomplexan sortilin homologs are indicated with pink shading. TM, transmembrane. B) Anti-HA immunoblot of the membrane fraction of parasites expressing PfSortilin-HA (clone C9) and of the parental 3D7 parasite line. The membrane was reprobed with anti-PMV antibodies for a loading control. The sizes of protein markers in kDa are indicated at left. Two cross-reacting species are present in both lanes (asterisks). C) Co-localization of PfSortilin-HA and ERD2 in aldehyde-fixed clone C9 parasites. Scale bar, 2 μm.

To localize PfSortilin in asexual blood-stage parasites, we attempted to modify the endogenous locus by single-crossover recombination to encode a C-terminal fusion to YFP. We were unable to obtain parasites with the desired integration and considered the possibility that a C-terminal YFP tag interfered with the normal function of PfSortilin. We therefore attempted to introduce a hemagglutinin epitope tag at an internal position 10 amino acids away from the C-

terminus (Fig. 3-4A), which is a region of low conservation in Apicomplexan sortilin homologs, and obtained the desired recombination event (Fig. 3-S3).

A protein of the size expected for PfSortilin-HA was detected in the membrane fraction of transgenic but not parental parasites upon immunoblotting with an anti-HA antibody (Fig. 3-4B). In asexual blood-stage parasites, PfSortilin-HA localized to puncta that were also recognized by antibodies to the Golgi marker ERD2 (Fig. 3-4C). No Golgi labeling with anti-HA antibodies was observed in wild-type parasites. Thus, at steady state the putative protein sorting receptor PfSortilin is present mainly in the parasite's Golgi apparatus where it presumably interacts with and sorts proteins transiting the endomembrane system.

Discussion

We have shown that *P. falciparum* homologs of the retromer cargo-selective complex and of the small GTPase Rab7 localize to an intracellular compartment that, to our knowledge, has not been previously described. This compartment appears to be a component of the parasite's endomembrane system and we propose to call it the "*P. falciparum* endosome". In terms of its Rab identity, it resembles the mammalian late (Rab7) endosome [22]. It is not clear whether the early endosome, which in mammalian cells is decorated with the lipid PI3P and Rab5, exists as a discrete compartment in *P. falciparum*. PI3P has been localized to the food vacuole, the apicoplast and the luminal face of the ER [70,71], none of which appears to represent a canonical early endosome. Three Rab5 isoforms are encoded in the *P. falciparum* genome [44] but their distributions in the parasite have not yet been reported.

In contrast to the abundance of late endosomes present in mammalian cells (e.g., [26]), we observe only one or two endosomes in trophozoite stage parasites. This compartment

multiplies during schizogony and is inherited by daughter merozoites. In this regard, it behaves more like a Golgi cisterna than like the mammalian late endosome, which terminates its independent existence by fusing with the lysosome. Curiously, the punctate concentrations of the retromer cargo-selective complex and PfRab7 that define the parasite endosome are not visible during the ring stage of the asexual cycle. This may reflect the dissociation of retromer and PfRab7 from the endosome membrane during this stage; alternately, the endosome may undergo a cycle of destruction and regeneration early in the asexual cycle.

Our observations suggest that the *P. falciparum* endosome plays a role in protein trafficking. This compartment resides in close proximity to the Golgi apparatus (as defined by PfRab6 or PfERD2) during the trophozoite and schizont stages of the asexual intraerythrocytic cycle. The Golgi apparatus, in turn, has been shown to be close to transitional ER sites where cargo is organized for delivery to the Golgi [21]. The close spatial organization of the transitional ER, Golgi apparatus and endosome could serve to limit the distance that coated vesicles (COPII-coated from the ER, COPI- or clathrin-coated from the Golgi apparatus) must travel between compartments, thus increasing the efficiency of vesicular traffic. Our observations also suggest that there is a tethering mechanism that holds the endosome close to the Golgi apparatus. In mammalian cells, there is evidence that Golgi reassembly stacking proteins (GRASPs) are in part responsible for interactions between Golgi cisternae (*i.e.*, stacking) [72]. We speculate that the *P. falciparum* GRASP homolog, which exists in two isoforms [73], may contribute to tethering the Golgi apparatus and the endosome. Whether or not the two compartments are tethered, the dynamics of vesicular traffic into and out of these compartments are clearly distinct. This was illustrated by treatment of *P. falciparum* with brefeldin A, which caused redistribution of PfRab6 but not PfRab7 or PfVps35 to the endoplasmic reticulum.

The idea that vesicular traffic occurs between the Golgi apparatus and the endosome is supported by our identification of a putative protein sorting pathway between these compartments. We have shown that a *P. falciparum* homolog of the sortilin/Vps10 class of sorting receptor localizes to the Golgi apparatus. In *S. cerevisiae* and mammalian cells, sortilin cycles between the *trans*-Golgi network and the endosome, with the retrograde pathway dependent on the interaction of the cytoplasmic tail of sortilin with the retromer complex [74]. Given the presence of the retromer cargo-selective complex on the *P. falciparum* endosome, we speculate that PfSortilin sorts specific cargo from the Golgi to the endosome, with subsequent recycling to the Golgi mediated by the plasmodial retromer cargo-selective complex. Yeast and mammalian retromer interact with a short hydrophobic motif in the cytosolic tail of the respective sortilin homologs (FYVFSN in yeast, FLV in mammals) [25]. Although neither of these sequences is found in the cytosolic tail of PfSortilin, there are similar hydrophobic sequences (e.g. LFYNY) that could fulfill the same role. Additionally, S-palmitoylation of the cytosolic tail of human sortilin is important for efficient retromer-mediated retrieval to the Golgi apparatus [75]. The sidechain of Cys791 of PfSortilin, which immediately follows the transmembrane domain and is the sole cysteine residue in the cytosolic tail, could potentially be available for palmitoylation. This residue is conserved in primate and rodent malaria species (not shown).

The question then arises as to what biosynthetic cargo passes through endosome, and to where. In the course of our immunofluorescence studies, we noticed that the rhoptry bulb protein RAP1 consistently localized to a position in the cell close to the endosome. This proximity was observed in maturing parasites that had not yet begun to segregate organelles into daughter merozoites. Thus, the close proximity of the endosome and the nascent rhoptries did not appear

to be merely a consequence of being restricted to a small space (*i.e.*, at the apical end of the merozoite). Based on these observations we suggest a role for the endosome in rhoptry biogenesis. One intriguing possibility is that rhoptry proteins are transported to the endosome by PfSortilin and from the endosome proceed by vesicular traffic to the rhoptry. This idea is supported by the recent finding that the *Toxoplasma gondii* sortilin homolog (TgSORTLR) sorts rhoptry and microneme proteins in this organism [76]. Although the specific rhoptry cargo molecules that were found to interact with TgSORTLR do not have close homologs in *P. falciparum*, it is likely that a subset of conserved rhoptry proteins interacts with sortilin in both organisms. Unfortunately, none of our several attempts to perturb protein trafficking through the endosome was successful and we do not at this time have direct evidence for the trafficking of rhoptry proteins through the *P. falciparum* endosome.

It has been previously suggested on the basis of electron microscopic analyses that the rhoptry is formed through vesicle budding from a cisternal structure that was, based on morphological considerations, presumed to be the Golgi apparatus [17]. Our epifluorescence images suggest that the Golgi apparatus and the endosome are of comparable size and shape and in close proximity; therefore, without organellar markers it would probably be difficult to unambiguously identify these structures in electron micrographs. We consider it possible that the structure identified as the "Golgi apparatus" by Bannister et al. [17] is in fact the endosomal compartment; however, further studies would be needed to decisively resolve this question.

Although the *P. falciparum* endosome and the mammalian late endosome are both decorated with Rab7, we suspect that their roles in the respective organisms are quite different. The close association of the *P. falciparum* endosome with the Golgi apparatus throughout the cell cycle (excepting the early ring stage) suggests that this compartment is dedicated to sorting

biosynthetic protein traffic. Also, the *P. falciparum* endosome does not appear to fuse in its entirety with other organelles, as does the mammalian late endosome with lysosomes. The loss of ESCRT I and II complexes in *P. falciparum* [77] suggests that the parasite does not downregulate cell surface proteins through ubiquitin-dependent sequestration into multivesicular bodies in late endosomes. These considerations are consistent with the prevailing view that the malaria parasite possesses a "minimal" or "stripped-down" endomembrane system [8]. Further studies will be required to better elaborate the form and functions of the *P. falciparum* endosome network.

Experimental Procedures

Construction of plasmids for P. falciparum transfection

Plasmids for the generation of chimeras between the chromosomal coding sequences of PfVps26, PfVps29 or PfVps35 and that of yellow fluorescent protein (YFP) through single-crossover homologous recombination were produced as follows (see also Fig. 3-S2). One kilobase of the 3' end (excluding the stop codon) of PfVps26, PfVps29 and PfVps35 coding sequences was PCR amplified from *P. falciparum* 3D7 genomic DNA using oligos 428/429, 334/335, and 352/353, respectively. (All oligonucleotides used in this study are listed in Table 3-S1). The PCR product was introduced into the XhoI and AvrII sites of pPM2CIT2 [78], yielding pPfVps26-YFP, pPfVps29-YFP and pPfVps35-YFP. Plasmids for the generation of chimeras between the chromosomal coding sequences of each retromer subunit and those of YFP and *E. coli* DHFR destabilization domain (DD) were produced in a similar fashion. The DD sequence was PCR amplified from pBMN YFP-DHFR(DD) [39] using oligos 486/487 and cloned into the NheI/NotI sites of pGDPD-YFP-CAD [79]. Next, the 3' coding sequences of PfVps26, PfVps29

and PfVps35 generated above were introduced into the XhoI and AvrII sites to yield pPfVps26-YFP-DD, pPfVps29-YFP-DD and pPfVps35-YFP-DD. To introduce a hemagglutinin (HA) tag into the PfSortilin locus, a PCR product encompassing bases 2476 to 3106 of the genomic PfSortilin sequence was amplified with oligos 276/283 and introduced into the XhoI/AvrII sites of plasmid pPM2CIT2. A pair of annealed oligonucleotides (286/287) containing the sequence of the HA tag and bases 3107 – 3139 of PfSortilin was subsequently introduced into the AvrII/NotI sites to generate pSortilin-HA.

A construct for double-crossover recombination at the PfVps35 locus was produced by PCR amplification of 5′ (bases 368-938) and 3′ (bases 2661-3238) fragments of the PfVps35 open reading frame using oligo pairs 344/345 and 346/347, respectively. These PCR products were cloned into the SacII/SpeI and NcoI/AvrII sites, respectively, in the plasmid pCC-1 [80] to produce pPfVps35-DKO (Fig. 3-S2).

Plasmids for transposon-based expression were constructed from pXL-BacII-DHFR [81]. First, a linker (oligos 245/246) was cloned into the XhoI site to introduce unique KasI and XmaI sites while maintaining a unique downstream XhoI site. Next the XhoI-BglII restriction fragment (containing internal AvrII and NotI sites) from pPM2CIT2 [78] was cloned into the same sites in the modified pXL-BacII-DHFR, yielding pSD-DHFR. To generate an expression cassette for PfVps29-mCherry, the complete coding sequence of PfVps29 (without a stop codon) was PCR amplified with oligos 456/457 and introduced into the XhoI/AvrII sites of pSD-DHFR. The sequence for mCherry (encoding for an N-terminal tobacco etch virus protease site but no start codon) was amplified with oligos 460/461 from pRSET$_B$-mCherry [82] and cloned into the AvrII/NotI sites. Approximately 800 nucleotides of the 5’ UTR of PfVps29 were PCR amplified with oligos 458/459 and introduced into the XmaI/XhoI sites to yield pPfVps29-mCherry. N-

terminal DHFR destabilization domain-mCherry (DD-mCherry) as fusions to PfRab6 and PfRab7 were constructed as follows. The *E. coli* DHFR destabilization domain (DD) coding sequence (omitting the stop codon) was PCR amplified from pBMN DHFR(DD)-YFP [39] using oligos 470/471 and cloned into XhoI/AvrII sites of pSD-DHFR. The sequence for mCherry (omitting the start and stop codons) was PCR amplified with oligos 484/485 to contain 5' AvrII and 3' SacII/NotI sites and was cloned into AvrII/NotI sites. Approximately 800 nucleotides of the 5' UTR for PfRab6 and PfRab7 were amplified using oligos 480/481 and 476/477, respectively, and cloned into XmaI/XhoI sites. cDNA sequences for PfRab6 and PfRab7 were obtained by SuperScript II reverse transcriptase/PCR (Invitrogen) using unsynchronized *P. falciparum* 3D7 total RNA and gene-specific primers. PfRab6 and PfRab7 sequences were then amplified using oligo pairs 482/483 and 478/479, respectively, and cloned into SacII/NotI sites to yield pDD-mCherry-PfRab6 and pDD-mCherry-PfRab7. To generate pDD-mCherry-PfRab7ΔCC, the wild-type PfRab7 coding sequence was replaced with a PfRab7 sequence lacking the codons for the two C-terminal cysteine residues that was obtained by PCR amplification of PfRab7 cDNA using oligos 478/598 (Fig. 3-S1). To obtain plasmid pDD-mCherry, the mCherry sequence (omitting the start codon but containing a stop codon) was PCR amplified with oligos 484/597 and cloned into AvrII/NotI sites of pDD-mCherry-PfRab7. Finally, the hDHFR cassette in selected transposon expression constructs was excised from the BglII/EcoRI sites and replaced with a yDHOD expression cassette amplified from pUF-1 [83] with oligos 501/502 to yield pPfVps29-mCherry-yDHOD, pDD-mCherry-PfRab6-yDHOD and pDD-mCherry-PfRab7-yDHOD.

To generate point mutants of PfRab7, the coding sequence was PCR amplified with oligos 599/600 to contain 5' BamHI/SacII and 3' NotI/XhoI sites and cloned into the

BamH1/XhoI sites of pSP72 (Promega). Site-directed mutagenesis was performed using the Quikchange II XL kit (Agilent) and oligo pairs 591/592 for PfRab7T22N, 593/594 for PfRab7Q67L and 595/596 for PfRab7N125I. Mutated sequences were excised with SacII and NotI and cloned into the same sites in pDD-mCherry-PfRab7 to yield pDD-mCherry-PfRab7T22N, pDD-mCherry-PfRab7Q67L, and pDD-mCherry-PfRab7N125I. A second set of mutant PfRab7 mutant expression cassettes with transcription driven by the promoter sequence of *P. falciparum* aminopeptidase P (GeneID PF3D7_1454400) was constructed by replacing the PfRab7 5' UTR with a PCR product (oligos 251/144) containing bases -865 to -39 of the PfAPP 5' UTR.

All coding sequences that were subjected to PCR amplification were verified by DNA sequencing. Plasmids used in this study are listed in Table 3-S2.

Parasite culture and transfection

P. falciparum 3D7 parasites were cultured in human O^+ erythrocytes (Interstate Blood Bank; 2% hematocrit) in RPMI 1640 medium (Life Technologies) supplemented with 27 mM sodium bicarbonate, 11 mM, glucose, 0.37 mM hypoxanthine, 10 μg/ml gentamicin, and 5 g/liter Albumax I (Invitrogen). Parasites were synchronized by 5% sorbitol treatment [84]. Parasites used for immunoblotting were isolated from intact red blood cells by treatment with 1.5 mg/ml saponin in phosphate buffered saline.

For experiments involving homologous recombination, ring-stage 3D7 parasites were transfected with 100 μg of plasmid DNA by electroporation using low voltage conditions [85]. Transfected parasites were selected with 2.5 nM WR99210. Drug-resistant parasites were subjected to a drug cycling protocol whereby parasites were cultured without selection for 3

weeks followed by re-selection. To attempt to isolate parasites that had undergone double-crossover homologous recombination at the PfVps35 locus, the negative selection agent 300 nM 5-fluorocytosine [37] was added to cultures. To introduce plasmids carrying expression cassettes on the *piggyBac* transposon, uninfected erythrocytes were transfected with 100 µg of transposon-containing plasmid and 50 µg of the helper plasmid pHTH [81]. Late-stage parasites were purified using a MACS magnetic column (Miltenyi Biotec) and electroporated erythrocytes were seeded with 2.5-5 x 10^5 parasites/mL. Drug selection with WR99210 (2.5-10 nM) or DSM-1 (1.5 µM) was initiated two days after transfection and drug-resistant parasites appeared after about 18 days. Clonal parasite lines were generated by limiting dilution

Southern blot analysis

Genomic DNA was isolated from saponin-treated parasites using the QiaAmp DNA Mini kit (Qiagen) and digested with one or two restriction enzymes as indicated in Fig. 3-S2. DNA fragments were resolved on a 0.6% agarose gel, transferred to positively-charged nylon membrane and hybridized to labeled probes overnight. Probe labeling and detection were carried out using the AlkPhos direct labeling kit (GE Biosciences) or BrightStar Psoralen-Biotin Non-isotopic labeling kit (Ambion) according to the manufacturer's instructions.

Immunofluorescence assays and live cell imaging

For live cell imaging, parasites in culture were resuspended and placed under a coverslip following a short (<30 minute) incubation with the vital nuclear stain Hoechst 33342 (5 µM). Images were collected on a Zeiss AxioImager equipped with an MRm Axiocam digital camera using a 100×/1.4NA objective lens. For immunofluorescence assays, parasites were fixed and

permeabilized as described previously [78] and incubated with organelle-specific antibodies followed by Alexa 488-or 594-conjugated rabbit or mouse secondary antibodies diluted to 2 μg/mL (Invitrogen). The primary antibodies used were: rabbit anti-ERD2 [11], 1:500; mouse anti-plasmepsin V [86], 1:10; rabbit anti-acyl carrier protein [87], 1:5000; mouse anti-rhoptry associated protein 1 (RAP1) monoclonal antibody 7H8/50 [88], 1:200; rabbit anti-erythrocyte binding antigen (EBA) 175 antibody R617 [89], 1:250; and anti-HA monoclonal antibody 16B12 (Covance), 2 μg /mL. DNA was stained with 1 μM Hoechst 33342. For colocalization with mitochondria, parasites were incubated in culture medium containing 100 nM MitoTracker Red CM-H2XRos (Invitrogen) for 15 minutes at 37 °C. Cells were then washed into MitoTracker-free medium containing 5 μM Hoechst 33342 and were imaged live.

For analysis of the effects of brefeldin A, live parasites expressing DD-mCherry-PfRab7 or co-expressing DD-mCherry-PfRab6 and PfVps35-YFP were cultured in media containing 10 μM trimethoprim and 0.2% DMSO with or without 5 μg/mL brefeldin A for 1 hour. To ensure that parasites of a similar stage of development were compared, only single-parasite infected erythrocytes with one to two nuclei (as determined by Hoechst 33342 fluorescence) and a visible hemozoin crystal (*i.e.*, trophozoite stage) were included in the analysis. The numbers of fluorescent puncta and the association of fluorescence with the perinuclear ER were determined by visual inspection of images.

For figure preparation, images were converted to TIF files and contrast was adjusted using Adobe Photoshop CS6.

Immunoblotting

Saponin parasite pellets were lysed by sonication in phosphate buffered saline with protease inhibitors (10 μM E-64, 10 μM pepstatin A and 1 mM 4-(2-aminoethyl)benzenesulfonyl fluoride). Lysates were centrifuged at 16,100 x *g* for 10 minutes at 4 °C to remove hemozoin. Samples from parasites expressing PfSortilin-HA were further centrifuged at 100,000 x *g* for 1 hour at 4 °C to isolate the membrane fraction, which was solubilized in reducing, SDS-containing Laemmli buffer. Proteins were resolved on polyacrylamide gels and blotted to nitrocellulose. Antibodies used were anti-RFP (Rockland), 0.3 μg/mL; anti-HA monoclonal antibody 16B12 (Covance), 1 μg/mL; anti-plasmepsin V [86], 1:400; and affinity purified rat anti-GDPD [79], 1:5000. Signal was detected by chemiluminescence using horseradish peroxidase-conjugated anti-rabbit or anti-mouse secondary antibodies. Blots were developed using ECL Plus (GE Biosciences) and imaged on a Storm 840 imager (GE Biosciences) or on film.

Acknowledgments

We are grateful to T. Wandless for supplying *E. coli* DHFR-DD plasmids, A. Vaidya for pUF-1 and the selection agent DSM-1, A. Cowman for anti-RAP1 and anti-EBA175 antibodies and plasmid pCC-1, R. Tsien for pRSET$_B$-mCherry, D. Goldberg for anti-plasmepsin V antibodies, G. McFadden for anti-ACP antibodies and D. Jacobus (Jacobus Pharmaceuticals) for WR99210. PfERD2 antiserum was obtained through the MR4 as part of the BEI Resources Repository, NIAID, NIH: PfERD2 Rabbit Antiserum, MRA-1, deposited by J. H. Adams.

References

1. Wellems TE, Hayton K, Fairhurst RM (2009) The impact of malaria parasitism: from corpuscles to communities. J Clin Invest 119: 2496-2505.
2. Reilly HB, Wang H, Steuter JA, Marx AM, Ferdig MT (2007) Quantitative dissection of clone-specific growth rates in cultured malaria parasites. Int J Parasitol 37: 1599-1607.
3. Gubbels MJ, Duraisingh MT (2012) Evolution of apicomplexan secretory organelles. Int J Parasitol 42: 1071-1081.
4. Wunderlich J, Rohrbach P, Dalton JP (2012) The malaria digestive vacuole. Front Biosci 4: 1424-1448.
5. Singh S, Plassmeyer M, Gaur D, Miller LH (2007) Mononeme: a new secretory organelle in *Plasmodium falciparum* merozoites identified by localization of rhomboid-1 protease. Proc Natl Acad Sci USA 104: 20043-20048.
6. Yeoh S, O'Donnell RA, Koussis K, Dluzewski AR, Ansell KH, et al. (2007) Subcellular discharge of a serine protease mediates release of invasive malaria parasites from host erythrocytes. Cell 131: 1072-1083.
7. Maier AG, Cooke BM, Cowman AF, Tilley L (2009) Malaria parasite proteins that remodel the host erythrocyte. Nat Rev Microbiol 7: 341-354.
8. Deponte M, Hoppe HC, Lee MC, Maier AG, Richard D, et al. (2012) Wherever I may roam: protein and membrane trafficking in *P. falciparum*-infected red blood cells. Mol Biochem Parasitol 186: 95-116.
9. van Dooren GG, Marti M, Tonkin CJ, Stimmler LM, Cowman AF, et al. (2005) Development of the endoplasmic reticulum, mitochondrion and apicoplast during the asexual life cycle of *Plasmodium falciparum*. Mol Microbiol 57: 405-419.
10. Tonkin CJ, Struck NS, Mullin KA, Stimmler LM, McFadden GI (2006) Evidence for Golgi-independent transport from the early secretory pathway to the plastid in malaria parasites. Mol Microbiol 61: 614-630.
11. Elmendorf HG, Haldar K (1993) Identification and localization of ERD2 in the malaria parasite Plasmodium falciparum: separation from sites of sphingomyelin synthesis and implications for organization of the Golgi. EMBO J 12: 4763-4773.
12. Klausner RD, Donaldson JG, Lippincott-Schwartz J (1992) Brefeldin A: insights into the control of membrane traffic and organelle structure. J Cell Biol 116: 1071-1080.
13. Glick BS, Nakano A (2009) Membrane traffic within the Golgi apparatus. Annu Rev Cell Dev Biol 25: 113-132.
14. Adisa A, Frankland S, Rug M, Jackson K, Maier AG, et al. (2007) Re-assessing the locations of components of the classical vesicle-mediated trafficking machinery in transfected Plasmodium falciparum. Int J Parasitol 37: 1127-1141.
15. Van Wye J, Ghori N, Webster P, Mitschler RR, Elmendorf HG, et al. (1996) Identification and localization of rab6, separation of rab6 from ERD2 and implications for an 'unstacked' Golgi, in Plasmodium falciparum. Mol Biochem Parasitol 83: 107-120.
16. Struck NS, Herrmann S, Schmuck-Barkmann I, de Souza Dias S, Haase S, et al. (2008) Spatial dissection of the *cis*- and *trans*-Golgi compartments in the malaria parasite *Plasmodium falciparum*. Mol Microbiol 67: 1320-1330.
17. Bannister LH, Hopkins JM, Fowler RE, Krishna S, Mitchell GH (2000) Ultrastructure of rhoptry development in *Plasmodium falciparum* erythrocytic schizonts. Parasitology 121: 273-287.

18. Bannister LH, Hopkins JM, Margos G, Dluzewski AR, Mitchell GH (2004) Three-dimensional ultrastructure of the ring stage of *Plasmodium falciparum*: evidence for export pathways. Microsc Microanal 10: 551-562.
19. Langreth SG, Jensen JB, Reese RT, Trager W (1978) Fine structure of human malaria in vitro. J Protozool 25: 443-452.
20. von Itzstein M, Plebanski M, Cooke BM, Coppel RL (2008) Hot, sweet and sticky: the glycobiology of *Plasmodium falciparum*. Trends Parasitol 24: 210-218.
21. Lee MC, Moura PA, Miller EA, Fidock DA (2008) Plasmodium falciparum Sec24 marks transitional ER that exports a model cargo via a diacidic motif. Mol Microbiol 68: 1535-1546.
22. Seaman MN (2008) Endosome protein sorting: motifs and machinery. Cell Mol Life Sci 65: 2842-2858.
23. Huotari J, Helenius A (2011) Endosome maturation. EMBO J 30: 3481-3500.
24. Yang M, Coppens I, Wormsley S, Baevova P, Hoppe HC, et al. (2004) The *Plasmodium falciparum* Vps4 homolog mediates multivesicular body formation. J Cell Sci 117: 3831-3838.
25. Seaman MN (2012) The retromer complex - endosomal protein recycling and beyond. J Cell Sci 125: 4693-4702.
26. Rojas R, van Vlijmen T, Mardones GA, Prabhu Y, Rojas AL, et al. (2008) Regulation of retromer recruitment to endosomes by sequential action of Rab5 and Rab7. J Cell Biol 183: 513-526.
27. Seaman MN, Harbour ME, Tattersall D, Read E, Bright N (2009) Membrane recruitment of the cargo-selective retromer subcomplex is catalysed by the small GTPase Rab7 and inhibited by the Rab-GAP TBC1D5. J Cell Sci 122: 2371-2382.
28. Cullen PJ, Korswagen HC (2012) Sorting nexins provide diversity for retromer-dependent trafficking events. Nat Cell Biol 14: 29-37.
29. Koumandou VL, Klute MJ, Herman EK, Nunez-Miguel R, Dacks JB, et al. (2011) Evolutionary reconstruction of the retromer complex and its function in *Trypanosoma brucei*. J Cell Sci 124: 1496-1509.
30. Bozdech Z, Llinas M, Pulliam BL, Wong ED, Zhu J, et al. (2003) The transcriptome of the intraerythrocytic developmental cycle of *Plasmodium falciparum*. PLoS Biology 1: 85-100.
31. Bartfai R, Hoeijmakers WA, Salcedo-Amaya AM, Smits AH, Janssen-Megens E, et al. (2010) H2A.Z demarcates intergenic regions of the *Plasmodium falciparum* epigenome that are dynamically marked by H3K9ac and H3K4me3. PLoS Pathog 6: e1001223.
32. Le Roch KG, Zhou Y, Blair PL, Grainger M, Moch JK, et al. (2003) Discovery of gene function by expression profiling of the malaria parasite life cycle. Science 301: 1503-1508.
33. Griffin CT, Trejo J, Magnuson T (2005) Genetic evidence for a mammalian retromer complex containing sorting nexins 1 and 2. Proc Natl Acad Sci USA 102: 15173-15177.
34. Wassmer T, Attar N, Bujny MV, Oakley J, Traer CJ, et al. (2007) A loss-of-function screen reveals SNX5 and SNX6 as potential components of the mammalian retromer. J Cell Sci 120: 45-54.
35. Haft CR, de la Luz Sierra M, Bafford R, Lesniak MA, Barr VA, et al. (2000) Human orthologs of yeast vacuolar protein sorting proteins Vps26, 29, and 35: assembly into multimeric complexes. Mol Biol Cell 11: 4105-4116.

36. Griesbeck O, Baird GS, Campbell RE, Zacharias DA, Tsien RY (2001) Reducing the environmental sensitivity of yellow fluorescent protein. Mechanism and applications. J Biol Chem 276: 29188-29194.
37. Maier AG, Braks JA, Waters AP, Cowman AF (2006) Negative selection using yeast cytosine deaminase/uracil phosphoribosyl transferase in *Plasmodium falciparum* for targeted gene deletion by double crossover recombination. Mol Biochem Parasitol 150: 118-121.
38. Hierro A, Rojas AL, Rojas R, Murthy N, Effantin G, et al. (2007) Functional architecture of the retromer cargo-recognition complex. Nature 449: 1063-1067.
39. Iwamoto M, Bjorklund T, Lundberg C, Kirik D, Wandless TJ (2010) A general chemical method to regulate protein stability in the mammalian central nervous system. Chem Biol 17: 981-988.
40. Muralidharan V, Oksman A, Iwamoto M, Wandless TJ, Goldberg DE (2011) Asparagine repeat function in a Plasmodium falciparum protein assessed via a regulatable fluorescent affinity tag. Proc Natl Acad Sci U S A 108: 4411-4416.
41. Balderhaar HJ, Arlt H, Ostrowicz C, Brocker C, Sundermann F, et al. (2010) The Rab GTPase Ypt7 is linked to retromer-mediated receptor recycling and fusion at the yeast late endosome. J Cell Sci 123: 4085-4094.
42. Liu TT, Gomez TS, Sackey BK, Billadeau DD, Burd CG (2012) Rab GTPase regulation of retromer-mediated cargo export during endosome maturation. Mol Biol Cell 23: 2505-2515.
43. Spielmann T, Beck HP (2000) Analysis of stage-specific transcription in *Plasmodium falciparum* reveals a set of genes exclusively transcribed in ring stage parasites. Mol Biochem Parasitol 111: 453-458.
44. Quevillon E, Spielmann T, Brahimi K, Chattopadhyay D, Yeramian E, et al. (2003) The Plasmodium falciparum family of Rab GTPases. Gene 306: 13-25.
45. Langsley G, van Noort V, Carret C, Meissner M, de Villiers EP, et al. (2008) Comparative genomics of the Rab protein family in Apicomplexan parasites. Microbes Infect 10: 462-470.
46. Bucci C, Thomsen P, Nicoziani P, McCarthy J, van Deurs B (2000) Rab7: a key to lysosome biogenesis. Mol Biol Cell 11: 467-480.
47. Feng Y, Press B, Wandinger-Ness A (1995) Rab 7: an important regulator of late endocytic membrane traffic. J Cell Biol 131: 1435-1452.
48. Meresse S, Gorvel JP, Chavrier P (1995) The rab7 GTPase resides on a vesicular compartment connected to lysosomes. J Cell Sci 108: 3349-3358.
49. Feng Y, Press B, Chen W, Zimmerman J, Wandinger-Ness A (2001) Expression and properties of Rab7 in endosome function. Methods Enzymol 329: 175-187.
50. Cantalupo G, Alifano P, Roberti V, Bruni CB, Bucci C (2001) Rab-interacting lysosomal protein (RILP): the Rab7 effector required for transport to lysosomes. EMBO J 20: 683-693.
51. Johansson M, Rocha N, Zwart W, Jordens I, Janssen L, et al. (2007) Activation of endosomal dynein motors by stepwise assembly of Rab7-RILP-p150Glued, ORP1L, and the receptor betalll spectrin. J Cell Biol 176: 459-471.
52. Wang T, Ming Z, Xiaochun W, Hong W (2011) Rab7: role of its protein interaction cascades in endo-lysosomal traffic. Cell Signal 23: 516-521.

53. Taub N, Teis D, Ebner HL, Hess MW, Huber LA (2007) Late endosomal traffic of the epidermal growth factor receptor ensures spatial and temporal fidelity of mitogen-activated protein kinase signaling. Mol Biol Cell 18: 4698-4710.
54. Lippincott-Schwartz J, Yuan LC, Bonifacino JS, Klausner RD (1989) Rapid redistribution of Golgi proteins into the ER in cells treated with brefeldin A: evidence for membrane cycling from Golgi to ER. Cell 56: 801-813.
55. Fujiwara T, Oda K, Yokota S, Takatsuki A, Ikehara Y (1988) Brefeldin A causes disassembly of the Golgi complex and accumulation of secretory proteins in the endoplasmic reticulum. J Biol Chem 263: 18545-18552.
56. Lippincott-Schwartz J, Yuan L, Tipper C, Amherdt M, Orci L, et al. (1991) Brefeldin A's effects on endosomes, lysosomes, and the TGN suggest a general mechanism for regulating organelle structure and membrane traffic. Cell 67: 601-616.
57. Hunziker W, Whitney JA, Mellman I (1991) Selective inhibition of transcytosis by brefeldin A in MDCK cells. Cell 67: 617-627.
58. Wood SA, Park JE, Brown WJ (1991) Brefeldin A causes a microtubule-mediated fusion of the *trans*-Golgi network and early endosomes. Cell 67: 591-600.
59. Roa M, Cornet V, Yang CZ, Goud B (1993) The small GTP-binding protein rab6p is redistributed in the cytosol by brefeldin A. J Cell Sci 106: 789-802.
60. Boal F, Stephens DJ (2010) Specific functions of BIG1 and BIG2 in endomembrane organization. PLoS One 5: e9898.
61. Gu F, Aniento F, Parton RG, Gruenberg J (1997) Functional dissection of COP-I subunits in the biogenesis of multivesicular endosomes. J Cell Biol 139: 1183-1195.
62. Daro E, Sheff D, Gomez M, Kreis T, Mellman I (1997) Inhibition of endosome function in CHO cells bearing a temperature-sensitive defect in the coatomer (COPI) component epsilon-COP. J Cell Biol 139: 1747-1759.
63. D'Souza-Schorey C, Chavrier P (2006) ARF proteins: roles in membrane traffic and beyond. Nat Rev Mol Cell Biol 7: 347-358.
64. Jackson CL, Casanova JE (2000) Turning on ARF: the Sec7 family of guanine-nucleotide-exchange factors. Trends Cell Biol 10: 60-67.
65. Donaldson JG, Finazzi D, Klausner RD (1992) Brefeldin A inhibits Golgi membrane-catalysed exchange of guanine nucleotide onto ARF protein. Nature 360: 350-352.
66. Helms JB, Rothman JE (1992) Inhibition by brefeldin A of a Golgi membrane enzyme that catalyses exchange of guanine nucleotide bound to ARF. Nature 360: 352-354.
67. Peyroche A, Antonny B, Robineau S, Acker J, Cherfils J, et al. (1999) Brefeldin A acts to stabilize an abortive ARF-GDP-Sec7 domain protein complex: involvement of specific residues of the Sec7 domain. Mol Cell 3: 275-285.
68. Donaldson JG, Lippincott-Schwartz J, Klausner RD (1991) Guanine nucleotides modulate the effects of brefeldin A in semipermeable cells: regulation of the association of a 110-kD peripheral membrane protein with the Golgi apparatus. J Cell Biol 112: 579-588.
69. Attar N, Cullen PJ (2010) The retromer complex. Adv Enzyme Regul 50: 216-236.
70. Bhattacharjee S, Stahelin RV, Speicher KD, Speicher DW, Haldar K (2012) Endoplasmic reticulum PI(3)P lipid binding targets malaria proteins to the host cell. Cell 148: 201-212.
71. Tawk L, Chicanne G, Dubremetz JF, Richard V, Payrastre B, et al. (2010) Phosphatidylinositol 3-phosphate, an essential lipid in Plasmodium, localizes to the food vacuole membrane and the apicoplast. Eukaryot Cell 9: 1519-1530.

72. Vinke FP, Grieve AG, Rabouille C (2011) The multiple facets of the Golgi reassembly stacking proteins. Biochem J 433: 423-433.
73. Struck NS, Herrmann S, Langer C, Krueger A, Foth BJ, et al. (2008) *Plasmodium falciparum* possesses two GRASP proteins that are differentially targeted to the Golgi complex via a higher- and lower-eukaryote-like mechanism. J Cell Sci 121: 2123-2129.
74. Johannes L, Popoff V (2008) Tracing the retrograde route in protein trafficking. Cell 135: 1175-1187.
75. McCormick PJ, Dumaresq-Doiron K, Pluviose AS, Pichette V, Tosato G, et al. (2008) Palmitoylation controls recycling in lysosomal sorting and trafficking. Traffic 9: 1984-1997.
76. Sloves PJ, Delhaye S, Mouveaux T, Werkmeister E, Slomianny C, et al. (2012) *Toxoplasma* sortilin-like receptor regulates protein transport and is essential for apical secretory organelle biogenesis and host infection. Cell Host Microbe 11: 515-527.
77. Leung KF, Dacks JB, Field MC (2008) Evolution of the multivesicular body ESCRT machinery; retention across the eukaryotic lineage. Traffic 9: 1698-1716.
78. Dalal S, Klemba M (2007) Roles for two aminopeptidases in vacuolar hemoglobin catabolism in Plasmodium falciparum. J Biol Chem 282: 35978-35987.
79. Denloye T, Dalal S, Klemba M (2012) Characterization of a glycerophosphodiesterase with an unusual tripartite distribution and an important role in the asexual blood stages of *Plasmodium falciparum*. Mol Biochem Parasitol 186: 29-37.
80. Maier AG, Rug M, O'Neill MT, Brown M, Chakravorty S, et al. (2008) Exported proteins required for virulence and rigidity of *Plasmodium falciparum*-infected human erythrocytes. Cell 134: 48-61.
81. Balu B, Shoue DA, Fraser MJ, Jr., Adams JH (2005) High-efficiency transformation of Plasmodium falciparum by the lepidopteran transposable element piggyBac. Proc Natl Acad Sci U S A 102: 16391-16396.
82. Shaner NC, Campbell RE, Steinbach PA, Giepmans BN, Palmer AE, et al. (2004) Improved monomeric red, orange and yellow fluorescent proteins derived from *Discosoma* sp. red fluorescent protein. Nat Biotechnol 22: 1567-1572.
83. Ganesan SM, Morrisey JM, Ke H, Painter HJ, Laroiya K, et al. (2011) Yeast dihydroorotate dehydrogenase as a new selectable marker for Plasmodium falciparum transfection. Mol Biochem Parasitol 177: 29-34.
84. Lambros C, Vanderberg JP (1979) Synchronization of *Plasmodium falciparum* erythrocytic stages in culture. J Parasitol 65: 418-420.
85. Fidock DA, Wellems TE (1997) Transformation with human dihydrofolate reductase renders malaria parasites insensitive to WR99210 but does not affect the intrinsic activity of proguanil. Proc Natl Acad Sci USA 94: 10931-10936.
86. Klemba M, Goldberg DE (2005) Characterization of plasmepsin V, a membrane-bound aspartic protease homolog in the endoplasmic reticulum of *Plasmodium falciparum*. Mol Biochem Parasitol 143: 183-191.
87. Waller RF, Reed MB, Cowman AF, McFadden GI (2000) Protein trafficking to the plastid of *Plasmodium falciparum* is via the secretory pathway. EMBO J 19: 1794-1802.
88. Schofield L, Bushell GR, Cooper JA, Saul AJ, Upcroft JA, et al. (1986) A rhoptry antigen of *Plasmodium falciparum* contains conserved and variable epitopes recognized by inhibitory monoclonal antibodies. Mol Biochem Parasitol 18: 183-195.

89. Reed MB, Caruana SR, Batchelor AH, Thompson JK, Crabb BS, et al. (2000) Targeted disruption of an erythrocyte binding antigen in *w* is associated with a switch toward a sialic acid-independent pathway of invasion. Proc Natl Acad Sci USA 97: 7509-7514.
90. O'Sullivan O, Suhre K, Abergel C, Higgins DG, Notredame C (2004) 3DCoffee: combining protein sequences and structures within multiple sequence alignments. J Mol Biol 340: 385-395.
91. Poirot O, Suhre K, Abergel C, O'Toole E, Notredame C (2004) 3DCoffee@igs: a web server for combining sequences and structures into a multiple sequence alignment. Nucleic Acids Res 32: W37-40.
92. Notredame C, Higgins DG, Heringa J (2000) T-Coffee: A novel method for fast and accurate multiple sequence alignment. J Mol Biol 302: 205-217.
93. Waterhouse AM, Procter JB, Martin DM, Clamp M, Barton GJ (2009) Jalview Version 2--a multiple sequence alignment editor and analysis workbench. Bioinformatics 25: 1189-1191.

Supplementary Information

Figure 3-S1: Sequence alignments of *Plasmodium falciparum* retromer subunits and Rab7 with human and *Saccharomyces cerevisiae* homologs. Multiple sequence alignments were generated using the Clustal W algorithm in MegAlign 10.0.3 (DNAstar) and T-Coffee Expresso [268-270]. Alignments were manually edited and shaded in Jalview 11.0 [271]. Light grey shading indicates identity between two sequences whereas dark gray shading indicates identity among all three sequences. Residue numbers are indicated at left and right. A. Vps29 alignment. Residues important for Vps35 binding are indicated with black squares. The leucine residue critical for Vps5p (yeast) or TBC1D5 Rab GAP binding (human) is indicated with a black star. B. Vps26 alignment. The interdomain loop is indicated with a black bar and the region which interacts with Vps35 is indicated with a double red line. C. Vps35 alignment. The conserved Vps26-interacting motif is indicated with a black bar. D. Rab7 alignment. Residues mutated in this study are indicated with a square (T22N), circle (Q67L) and star (N125I). The C-terminal prenylation motif is indicated with a red box.

A. Vps29

```
PfVps29       1 MSGKLEDIGELVLLIGDFHSPIRNLGLPDCFKELL-KTDKIKHVLCTGN-VG 50
HsVps29-1     1 ---------MLVLVLGDLHIPHRCNSLPAKFKKLL-VPGKIQHILCTGN-LC 41
ScVps29       1 ---------MLLLALSDAHIPDRATDLPVKFKKLLSVPDKISQVALLGNSTK 43

PfVps29      51 CNENLELLKNIADSVHITKGDMDDN-----------------FDFPEDITLC 85
HsVps29-1    42 TKESYDYLKTLAGDVHIVRGDFDEN-----------------LNYPEQKVVT 76
ScVps29      44 SYDFLKFVNQISNNITIVRGEFDNGHLPSTKKDKASDNSRPMEEIPMNSIIR 95
                                ■■■■       ■
PfVps29      86 IGDFKISLIHGHQIIPWGDMNALLQWQKKYDSDIIISGHTHKNSIVQYEGKY 137
HsVps29-1    77 VGQFKIGLIHGHQVIPWGDMASLALLQRQFDVDILISGHTHKFEAFEHENKF 128
ScVps29      96 QGALKIGCCSGYTVVPKNDPLSLLALARQLDVDILLWGGTHNVEAYTLEGKF 147
                    ■
PfVps29     138 FINPGSVTGAFQ---------------------------------------- 149
HsVps29-1   129 YINPGSATGAYN---------------------------------------- 140
ScVps29     148 FVNPGSCTGAFNTDWPIVFDVEDSDEAVTSEVDKPTKENQSEDDDAKGGSTG 199
                                                      ■■
PfVps29     150 ----------------------------------------PWLSEPTPTFI 160
HsVps29-1   141 ----------------------------------------ALETNIIPSFV 151
ScVps29     200 KEQPGSYTPKEGTAGERENENESNVKPENQFKEDEVDMSDSDINGSNSPSFC 251
                 ★
PfVps29     161 LMAVAKSNIVLYVYEEKNGKTNVEMSELHKSTVI                   194
HsVps29-1   152 LMDIQASTVVTYVYQLIGDDVKVERIEYKKP                     182
ScVps29     252 LLDIQGNTCTLYIYLYVNGEVKVDKVVYEKE                     282
```

Figure 3-S1 (continued)

B. Vps26

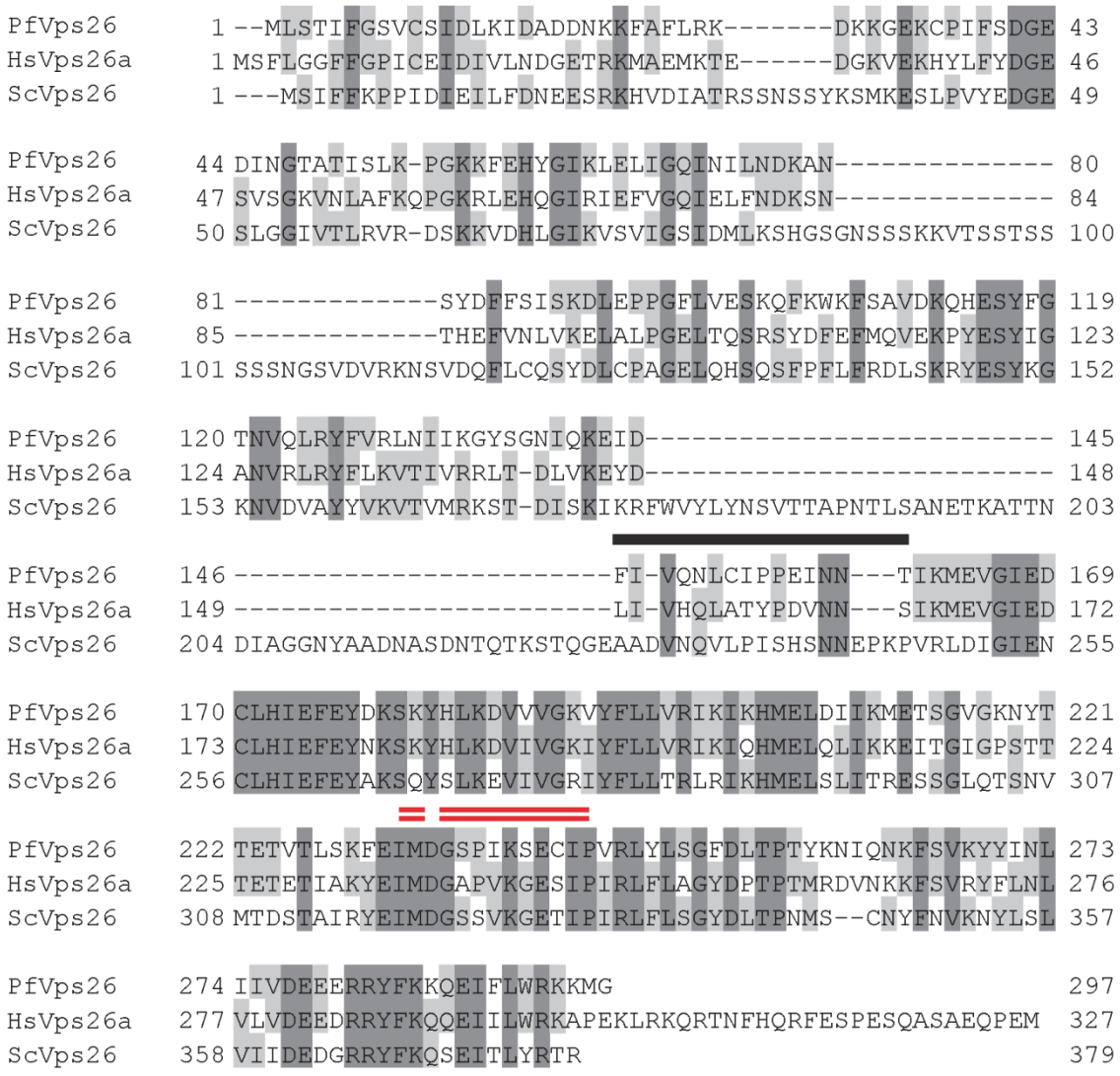

Figure 3-S1 (continued)

C. Vps35

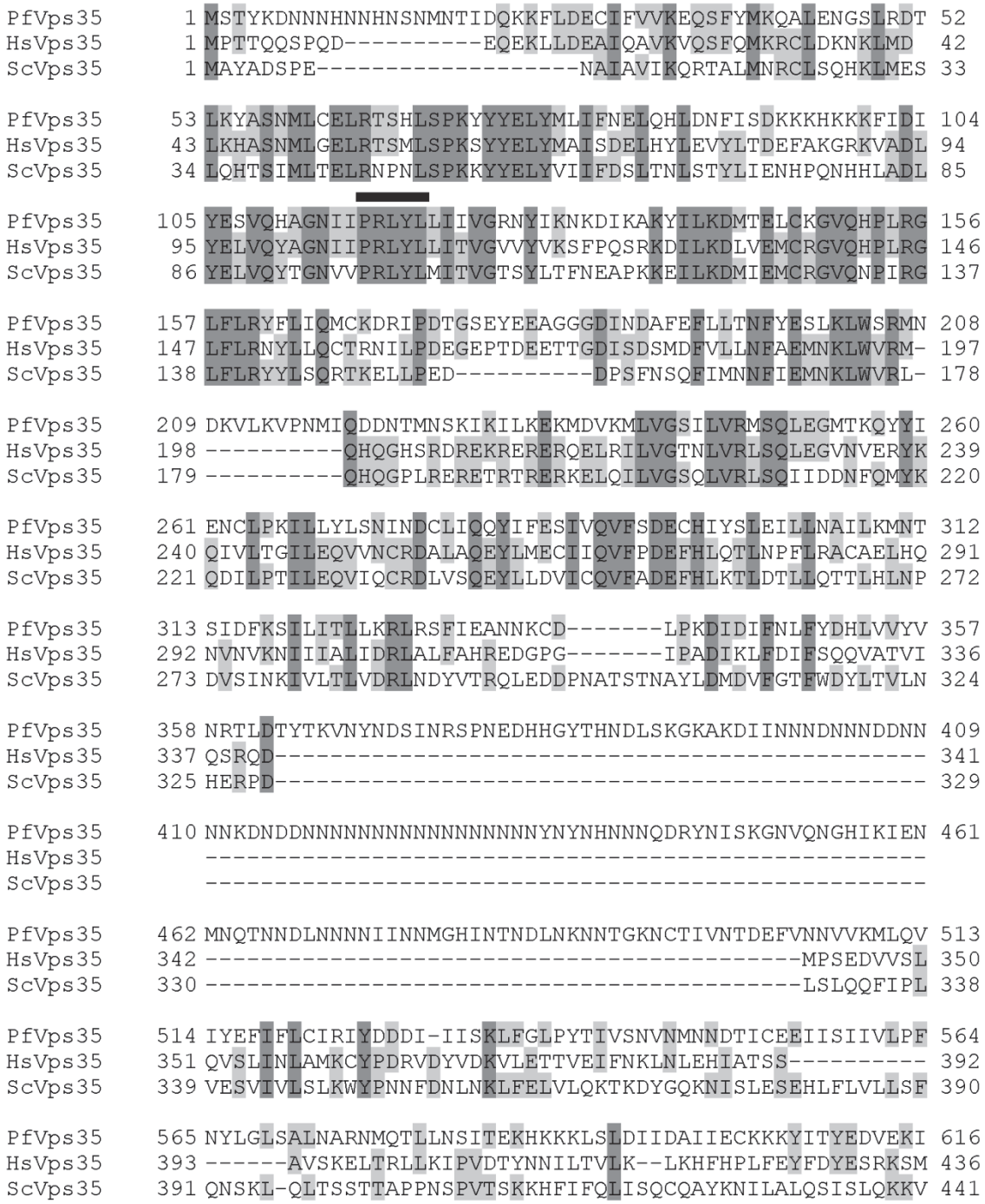

Figure 3-S1 (continued)

C. Vps35 (continued)

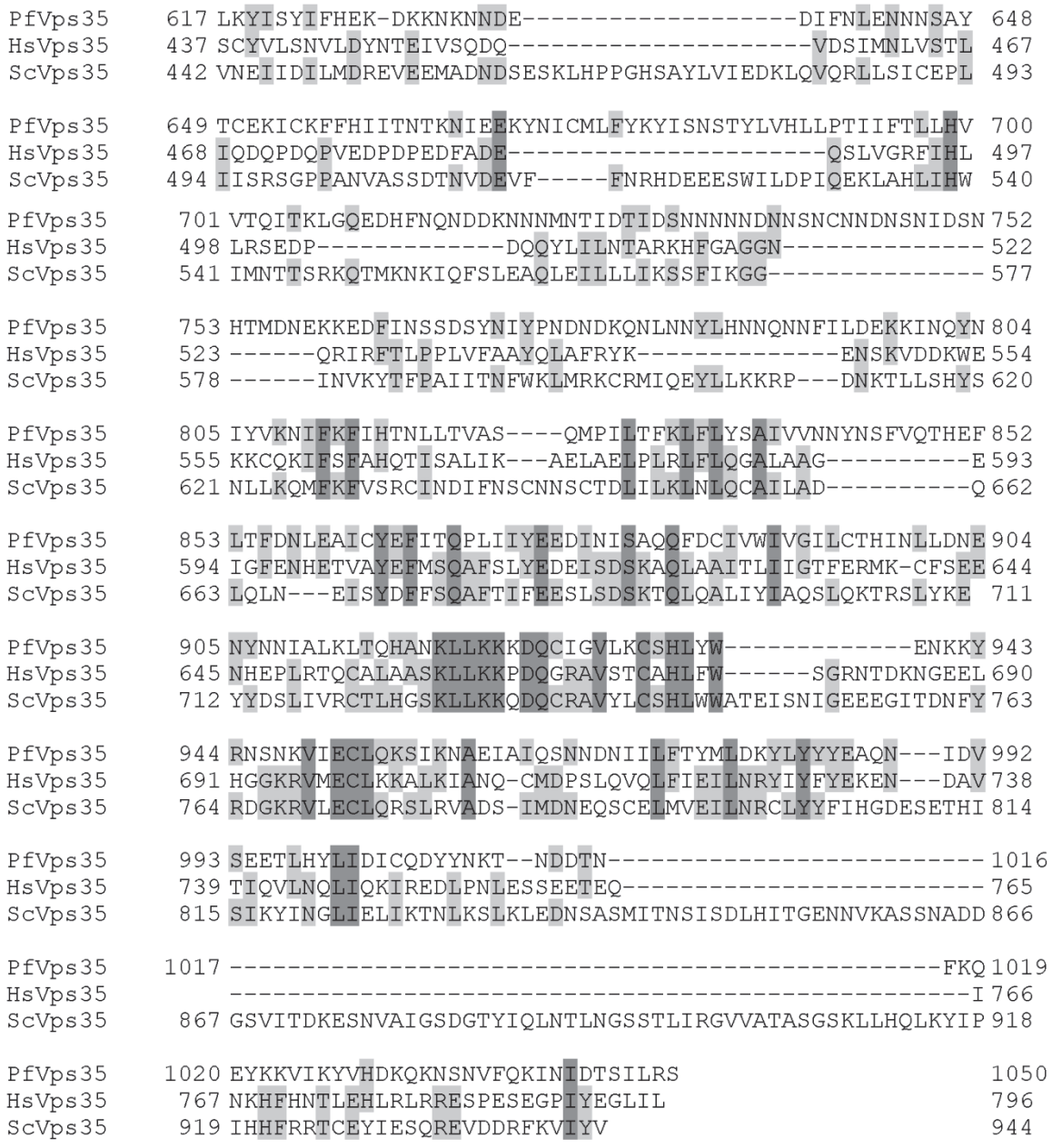

Figure 3-S1 (continued)

D. Rab7

Figure 3-S2 (following pages): Genotype analysis of transfected parasite lines.
A. Parasite line expressing PfVps29-YFP following single-crossover recombination with pPfVPs29pYFP. B. Parasite line expressing PfVps35-YFP following single-crossover recombination with pPfVps35-YFP. C. Parasite line transfected with pPfVps35-DKO and selected for double-crossover disruption of the PfVps35 allele. D. Two clonal parasite lines (D9 and G9) transfected with a plasmid carrying a transposable DD-mCherry-PfRab7 expression cassette. For all panels, a schematic diagram of the product of recombination or transposition is provided on the left. The predicted sizes of DNA fragments upon digestion with the indicated restriction enzyme are shown. The red bar indicates the position of the probe used for Southern blotting. "X" indicates the expected site(s) of homologous recombination, where applicable. Figures are not drawn to scale. Southern blots of genomic DNA of parental and transformed parasite lines are shown on the right. Each blot was performed on a single membrane. For clarity some lanes are shown as individual strips but all strips originate from the same exposure. Sizes of DNA markers in kilobases are indicated at left. Arrows at right identify the positions of the expected bands. The presence of "plasmid" in the panels A and B likely reflects the integration of concatameric episomes. Abbreviations: hDHFR, human dihydrofolate reductase; YFP, yellow fluorescent protein; CD, cytosine deaminase; DD, *E. coli* DHFR destabilization domain.

Figure 3-S2 (continued)

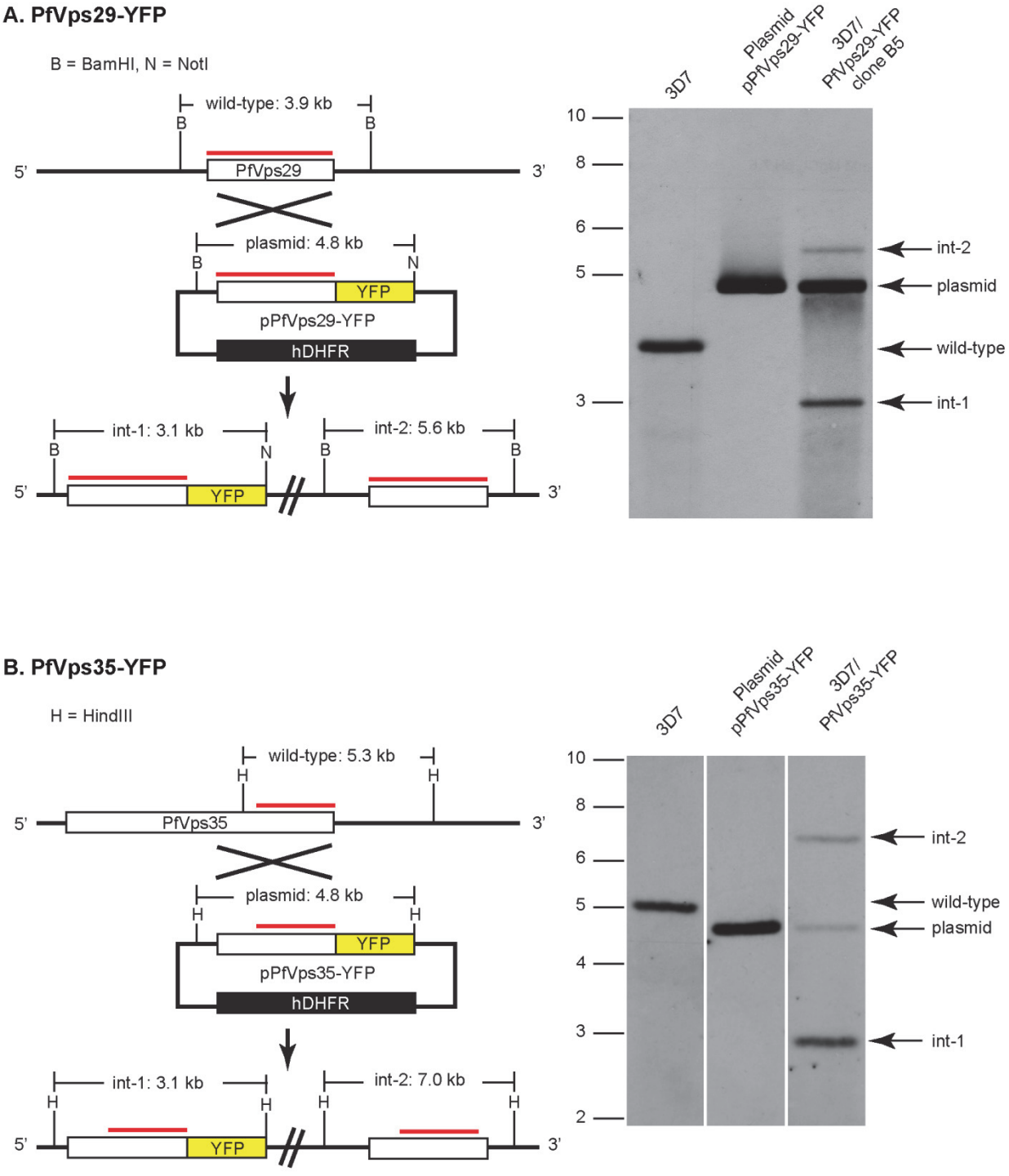

Figure 3-S2 (continued)

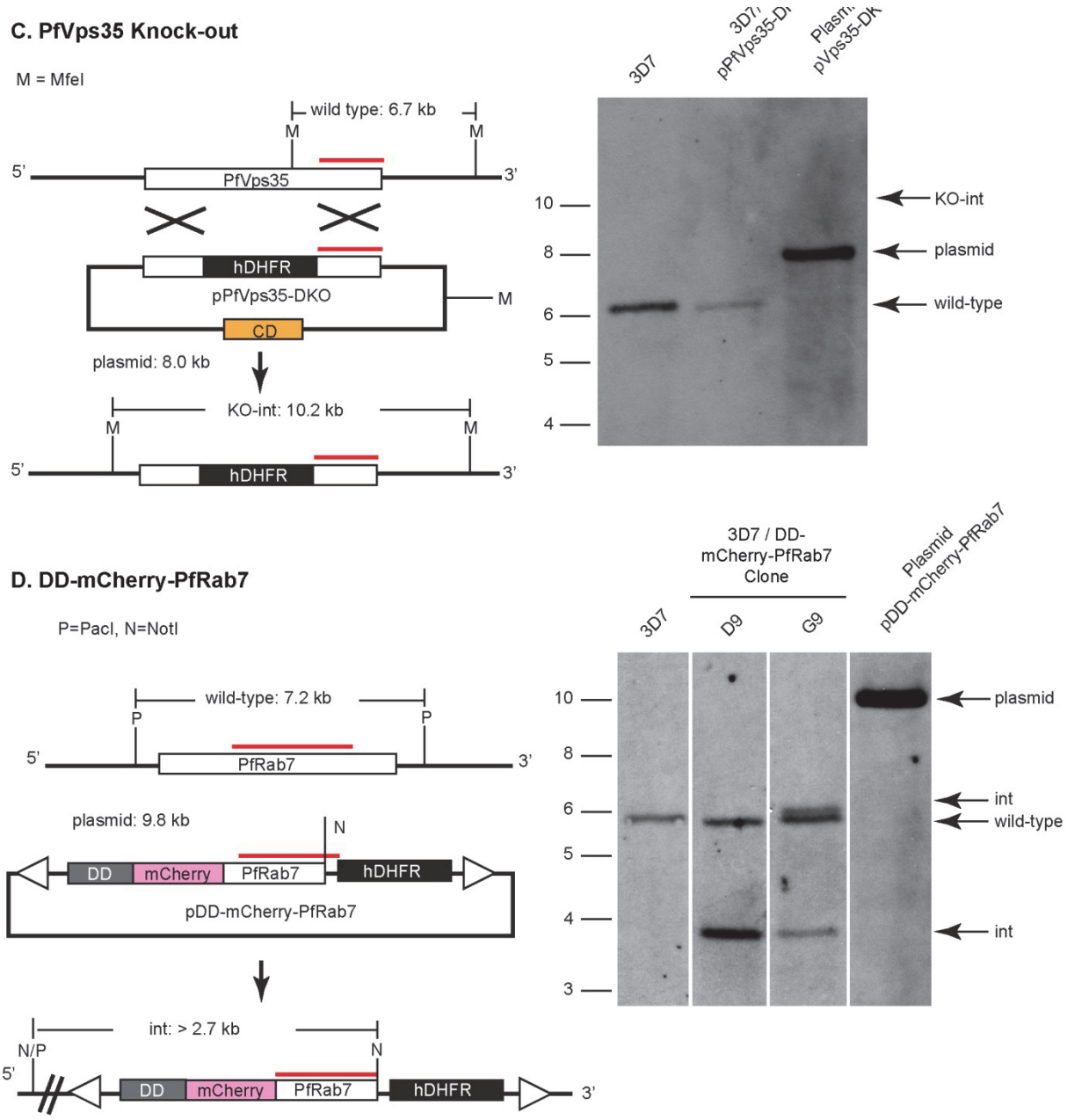

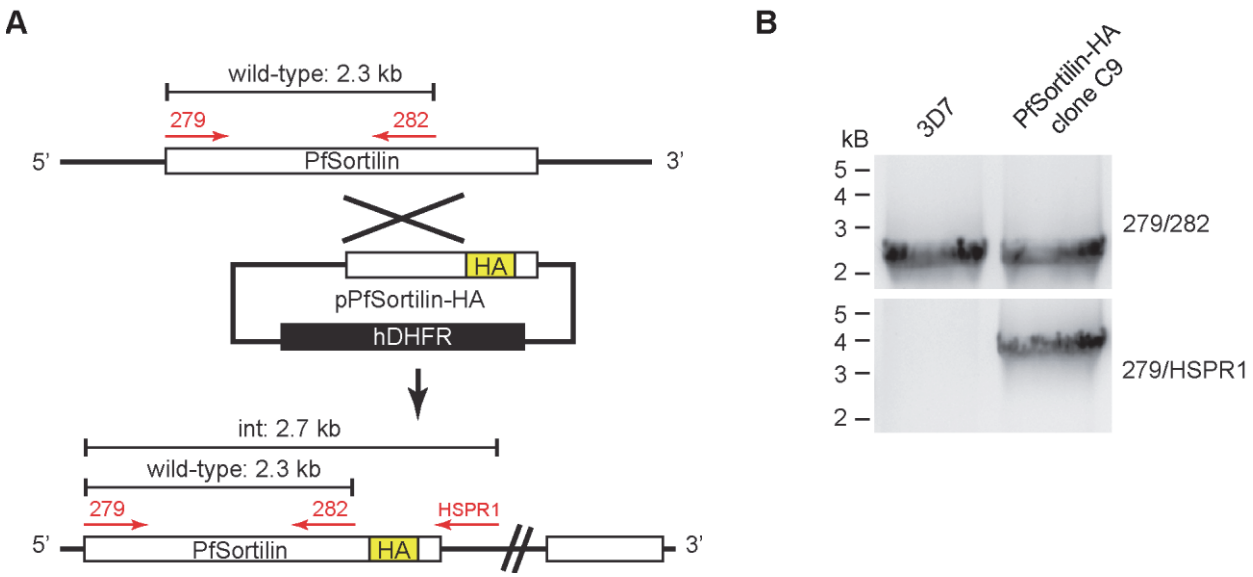

Figure 3-S3: Generation of a parasite line expressing PfSortilin-HA. A. Schematic diagram of the single-crossover strategy for modifying the PfSortilin chromosomal locus. The yellow box indicates the hemagglutinin (HA) tag and the green box indicates that the 3' end of the PfSortilin coding sequence was codon-altered region to prevent recombination downstream of the HA tag. Primers used for PCR analysis are indicated with red arrows and predicted sizes of amplified regions are shown. The figure is not drawn to scale. hDHFR, human dihydrofolate reductase.B. PCR analysis of genomic DNA obtained from parasite clonal line C9 expressing PfSortilin-HA and from the parental 3D7 line using primers indicated in A. Sizes of DNA markers are shown at left.

Table 3-S1: Sequences of oligonucleotides used in this study. Restriction sites are underlined. Where two restriction sites are present, the second is double underlined. RE, restriction endonuclease; UTR, untranslated region; RFP, red fluorescent protein; DD, *E. coli dihydrofolate reductase* destabilization domain; DM, dominant mutant; HA, hemagglutinin epitope tag.

Name	Oligonucleotide Sequence (5' to 3')	RE site	Purpose
334	GCACGCTCGAGAGTGGGAAATTGGAAGATATTGG	XhoI	PCR: PfVps29 bases 4 to 582
335	GCACGCCTAGGTATAACTGTTGACTTATGTAGTTCAC	AvrII	
352	GCACGCTCGAGATACCAATTTATTAACAGTAGCTAGC	XhoI	PCR: PfVps35 bases 2444 to 3150
353	GCACGCCTAGGTGATCTCAATATGGATGTATCTATATTAATTTTCTG	AvrII	
428	GCACGCTCGAGCTATATCAAAAGATC	XhoI	PCR: PfVps26 bases 257 to 891
429	GCACGCCTAGGACCCATTTTTTTTCG	AvrII	
344	GTACGCCGCGGAAAATATGCCTCAAATATGCTGTGC	SacII	PCR: PfVps35 bases 368 to 938
345	GTACGACTAGTAGATCCAACTAACATTTTTACATCC	SpeI	
346	GTACGCCATGGTTATTAACAGTAGCTAGCCAAATGC	NcoI	PCR: PfVps35 bases 2661 to 3238
347	GTACGCCTAGGTTATTGTAATAATCTTGGCATATGTC	AvrII	
456	GCACGCTCGAGCCGTGTTATTATTTAAAGATGAGTGG	XhoI	PCR: PfVps29 bases 1 to 582
457	GTACGCCTAGGTATAACTGTTGACTTATGTAGTTCAC	AvrII	
458	GCACGCCCGGGTCTATTTTCTGTTTTCAATTTTTCACAC	XmaI	PCR: PfVps29 5' UTR (-800 to -20)
459	CACGGCTCGAGAAAAAAAAAAAAAATATATGAAAATA	XhoI	
460	GTACGCCTAGGGAAAATTTATATTTTCAAAGTGTGAGCAAGGGCGAGGAGGATAAC	AvrII	PCR: mCherry RFP bases 4 to 711
461	GTACGGCGGCCGCTTACTTGTACAGCTCGTCCATGC	NotI	
486	GTACGGCTAGCATCAGTCTGATTGCGGCGTTAG	NheI	PCR: ecDHFR-DD bases 4 to 480
487	GTACGGCGGCCGCTTACCGCCGCTCCAGAATCTC	NotI	
470	GTACGCTCGAGCTTAAAAGAATAATAATGATCAGTCTGATTGCGGCGTTAG	XhoI	PCR: ecDHFR DD bases 1 to 474
471	GTACGCCTAGGTCCTCCTCCTCCTCCCCGCCGCTCCAGAATCTCAAAGC	AvrII	
484	GTACGCCTAGGGTGAGCAAGGGCGAGGAGGATAAC	AvrII	PCR: mCherry bases 4 to 708
485	GTACGGCGGCCGCTACTCCGCGGACTTTGAAAATATAAATTTTCCTTGTACAGCTCGTCCATGCCGC	SacII/NotI	
476	GTACGCCCGGGAATAAAACATTTTAATTGCACATGTGTG	XmaI	PCR: PfRab7 5' UTR (-880 to -17)
477	GTACGCTCGAGTTGTTCTTTTTTTTTTTTTTTTTTTTATTAAAATTTGATTTTAC	XhoI	

478 479	GTACGCCGCGGTCAAATAAAAAAAGAACCATATTAAAAG GTACGGCGGCCGCTTAACAACAACGACTTTTGTACATTTTTTG	SacII NotI	PCR: PfRab7 bases 4 to 621
480 481	GTACGCCCGGGTTTCTTTTGTTTGAATTTAAAATATTTTAGAG GTACGCTCGAGAAAATAAAAAAATATTTTTAATTAAGAATTAGTC	XmaI XhoI	PCR: PfRab6 5' UTR (-806 to -16)
482 483	GTACGCCGCGGGATGAATTTCAAAACTCGGGAC GTACGGCGGCCGCTTAACATAAACATTTACTTAACATATTTTTG	SacII NotI	PCR: PfRab6 bases 4 to 624
597 598	GTACGGCGGCCGCTTACTTGTACAGCTCGTCCATGC GTACGGCGGCCGCTTAACGACTTTTGTACATTTTTTGTTCG	NotI NotI	PCR: mCherry with 3' stop codon PCR: PfRab7□CC bases 4 to 612
599 600	GTACGAGATCTTACTCCGCGGTCAAATAAAAAAAGAACCATATTAAAAG GTACGCTCGAGTACTGCGGCCGCTTAACAACAACGACTTTTGTACATTTTTTG	BglII/SacII XhoI/NotI	PCR: PfRab7 transfer to pSP72
591 592	CTTGGAGATAGTGGTGTTGGTAAAAATTCATTAATGAATCAATATGTG CACATATTGATTCATTAATGAATTTTTACCAACACCACTATCTCCAAG	none none	Quikchange: PfRab7 T22N
593 594	GATATGGGATACTGCAGGACTAGAACGTTTTCAAAGTTTAGGAG CTCCTAAACTTTGAAAACGTTCTAGTCCTGCAGTATCCCATATC	none none	Quikchange: PfRab7 Q67L
595 596	GAAAATTTTCCTTTTGTTATTATTGGACTTAAAGTTGATGAAACAAATAAAAG CTTTTATTTGTTTCATCAACTTTAAGTCCAATAATAACAAAAGGAAAATTTTC	none none	Quikchange: PfRab7 N125I
251 144	GTACGCCCGGGTAAGTTTTTTTTTTATTTGATATAGAAAC GCACGCTCGAGATTTAAAAAAAAAAAAAGAAAGAAGAAG	XmaI XhoI	PCR: PfAPP 5' UTR (-865 to -39)
HSPR1	TATATATGTATATTGGGGTGATG	none	Sequencing: HSP86 Primer
276 283	GCACGCTCGAGGTCAATATTATTTATAATATTTATCATGG GTACGCCTAGGTGAAGGTGATATATTCCTTGAGGT	XhoI AvrII	PCR: PfSortilin bases 2476 to 3106
286	CTAGGTATCCATATGATGTACCAGATTATGCAAAAAATTATGCAGATAATATTGAATTATTATAAGC	AvrII/NotI	Annealing oligos: HA tag and PfSortilin bases 3107 to 3139
287	GGCCGCTTATAATAATTCAATATTATCTGCATAATTTTTTGCATAATCTGGTACATCATATGGATAC	AvrII/NotI	
501 502	CTACGAGATCTCATTTTGTAAAAAAAATTAAAATATATTTATAT CTACGGAATTCTTTAATAAATATGTTCTTATATATAATGAG	BglII EcoRI	PCR: yDHOD cassette
245 246	TCGAAGGCGCCATATACCCGGGATATAC TCGAGTATATCCCGGGTATATGGCGCCT	KasI/XmaI XmaI/KasI	Annealing oligos: pXL-BacII linker

Table 3-S2: Plasmids constructed in this study. YFP, yellow fluorescent protein; DD, *E. coli* dihydrofolate reductase destabilization domain; HA, hemagglutinin epitope tag; RFP, red fluorescent protein; hDHFR, human *dihydrofolate reductase*; yDHOD, yeast *dihydroorotate dehydrogenase*; DKO, double-crossover knockout.

Plasmids for Chromosomal Integration

Gene of Interest	Modification(s)	Drug Resistance	Name of Plasmid
PfVps29	C-terminal YFP	hDHFR	pPfVps29-YFP
	C-terminal YFP / C-terminal DD	hDHFR	pPfVps29-YFP-DD
PfVps26	C-terminal YFP	hDHFR	pPfVps26-YFP
	C-terminal YFP / C-terminal DD	hDHFR	pPfVps26-YFP-DD
PfVps35	C-terminal YFP	hDHFR	pPfVps35-YFP
	C-terminal YFP / C-terminal DD	hDHFR	pPfVps35-YFP-DD
	Double cross-over recombination for knock out	hDHFR	pPfVps35-DKO
PfSortillin	Internal HA tag and codon-altered C-terminal tail	hDHFR	pPfSortillin-HA

Plasmids for Transposon Expression

Gene of Interest	Modification(s)	Drug Resistance	Name of Plasmid
PfVps29	C-terminal mCherry RFP	hDHFR	pPfVps29-mCherry
	C-terminal mCherry RFP	yDHOD	pPfVps29-mCherry-yDHOD
PfRab7	N-terminal DD / mCherry RFP	hDHFR	pDD-mCherry
	N-terminal DD / N-terminal mCherry RFP	hDHFR	pDD-mCherry-PfRab7
	N-terminal DD / N-terminal mCherry RFP	yDHOD	pDD-mCherry-PfRab7-yDHOD
	N-terminal DD / N-terminal mCherry RFP/ PfRab7 C-terminal truncation (prenylation motif removed)	hDHFR	pDD-mCherry-PfRab7□ΔCC
	N-terminal DD / N-terminal mCherry RFP / PfRab7 (T22N) / PfRab7 promoter	hDHFR	pDD-mCherry-PfRab7T22N
	N-terminal DD / N-terminal mCherry RFP / PfRab7 (N125I) / PfRab7 promoter	hDHFR	pDD-mCherry-PfRab7N125I
	N-terminal DD / N-terminal mCherry RFP / PfRab7 (Q67L) / PfRab7 promoter	hDHFR	pDD-mCherry-PfRab7Q67L
	N-terminal DD / N-terminal mCherry RFP / PfRab7 (T22N) / PfAPP promoter	hDHFR	pPfAPPp-DD-mCherry-PfRab7T22N
	N-terminal DD / N-terminal mCherry RFP / PfRab7 (N125I) / PfAPP promoter	hDHFR	pPfAPPp-DD-mCherry-PfRab7N125I
	N-terminal DD / N-terminal mCherry RFP / PfRab7 (Q67L) / PfAPP promoter	hDHFR	pPfAPPp-DD-mCherry-PfRab7Q67L
PfRab6	N-terminal DD / N-terminal mCherry RFP	hDHFR	pDD-mCherry-PfRab6
	N-terminal DD / N-terminal mCherry RFP	yDHOD	pDD-mCherry-PfRab6-yDHOD

CHAPTER 4:

The *P. falciparum* FYVE-domain containing protein, PfFCP, participates in trafficking to the food vacuole

Priscilla Krai, Titilola Denloye and Michael Klemba

Author Contributions:

Priscilla Krai performed all research except experiments mentioned below and wrote the article.
Titilola Denloye generated CIT-PfFCP, PfFCP-IntHA, and DD-HA-PfFCPΔFYVE expressing parasites and performed pull-down of CIT-PfFCP parasite lysate.
Michael Klemba oversaw and directed the research, generated PM2-CIT and PM2-10C expressing parasites and helped edit the article.

Abstract

During the asexual intraerythrocytic stage, the human malaria parasite *Plasmodium falciparum* catabolizes the majority of its host cell hemoglobin in a lysosome-like food vacuole (FV). According to the currently accepted model, hemoglobin endocytosis and transport to the FV occurs via a vesicle-dependent process [1]. The components of this process are poorly understood, but likely involve phosphatidylinositol 3-phosphate (PI3P) and its binding proteins [2]. The zinc finger domain, known as FYVE, is highly specific for PI3P. In this study, we have localized the sole FYVE-domain containing protein in the parasite genome to the food vacuole membrane where it is present as a homodimer. We have also generated a regulatable, lethal dominant negative mutant that alters FV morphology and trafficking of both host cell

hemoglobin and acidic hydrolases. We find evidence of a previously unreported role of PfFCP in trafficking to the FV.

Introduction

The malaria parasites of *Plasmodium* spp. are responsible for at least 800 thousand deaths annually, mostly young children [3]. Of the five species that can infect humans, *P. falciparum* accounts for the majority of cases worldwide and is by far the most virulent [3]. The clinical manifestations of disease are caused by replication within, and release from, the host's erythrocytes [4,5]. Over the course of ~48 hrs, the parasite grows and divides to form daughter merozoites that egress and invade new cells. During this process about three quarters of host cell soluble protein, consisting mostly of hemoglobin, is catabolized within a lysosome-like organelle known as the food vacuole (FV) [6,7]. This provides a source of amino acids while creating space for parasite growth and relieving osmotic stress [8-10]. Given that hemoglobin catabolism is essential to parasite growth in cell culture and animal models [8,11-14], acidic hydrolases which reside within the FV and catalyze the reaction are attractive drug targets. Several proteins involved in hemoglobin endocytosis and vesicle fusion identified in the *P. falciparum* genome [15-20] have been overlooked. Preliminary studies, however, indicate dynamin and AP-2 subunit homologs may be involved in these important processes and are connected in emerging artemisinin resistance [21,22].

The process by which the FV is formed and hemoglobin brought into the parasite has been of interest for decades. Analysis by several laboratories has resulted in multiple conflicting theories of FV biogenesis in the literature, from an initial ring-stage "big gulp," to elongated cytostomal tubules which remained connected with the host cell cytoplasm (Fig. 4-1A and 4-1B)

[23,24]. Within the past half decade, however, strong evidence has been published that all hemoglobin uptake occurs via vesicle-mediated processes mostly through an electron dense pore, the cytostome (Fig. 4-1C) [1,25]. Parasites begin to ingest host cell cytoplasm as early as mid-ring stage (10 to 12 hrs after invasion) into multiple compartments that can independently digest hemoglobin before the development of a single larger FV [1,25]. Evidence of larger extra-FV acidic compartments containing both hemoglobin and biosynthetic cargo, which may ultimately merge with the existing FV, have also been reported [1,26].

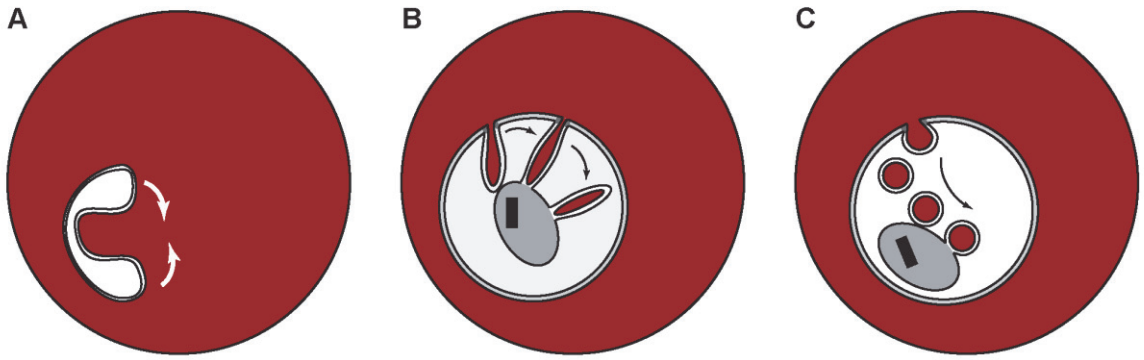

Fig 4-1: Models of hemoglobin uptake and food vacuole biogenesis. A) Ring stage "big gulp" to form the FV. B) Trophozoite stage elogated tubule connected to the erythrocyte cytosol. C) Vesicle-mediated model.

If hemoglobin uptake occurs primarily via a vesicle-mediated process (reviewed in [27,28]), which parasite components are involved in vesicle fission, trafficking and fusion? It appears that generation and transport of hemoglobin-containing vesicles is clathrin, AP-2 and dynamin dependent [15,17,21,23,24]. This is similar to clathrin mediated endocytic processes in model systems (reviewed in [29,30]). After vesicle formation, the parasite would need to direct newly formed vesicles and their cargo to the FV. In mammalian cells, endocytic cargo slated for delivery to the lysosome must first traverse the early and then late endosome. Similarly, biosynthetic cargo headed towards the lysosome is also sorted at the late endosome. Equivalent

intermediate steps remain poorly defined in *P. falciparum*. We have previously reported the existence of a plasmodial endosome separate from the Golgi apparatus, which shares some common features of the mammalian late endosome (Chapter 3). Whether the parasite possesses an early endosome equivalent that undergoes maturation, or is involved in hemoglobin uptake, remains an open question.

One characteristic of early endosomes is the presence of phosphatidylinositol 3-phosphate (PI3P) on the cytosolic face of the membrane [31]. In *P. falciparum,* PI3P has been localized to the FV, ER lumen and apicoplast [2,32,33] . None of these compartments fit the classical definition of an early endosome, and the purpose of this phosphoinositide on the FV membrane is unclear. Identifying FV membrane proteins that can interact with PI3P may give us some clues. Several protein domains have the potential to bind phosphoinositides, but none is as specific for PI3P as the FYVE [31,34-36], a zinc finger domain named after four proteins: Fab1p, YOTB, Vac1p, and EEA1, in which it has been found [36]. The number and structure of proteins containing FYVE domains varies widely throughout eukaryotes with yeast possessing only five and humans at least 26 [34,37]. They often share a functional role in endomembrane traffic as part of complexes either at the early endosome or prevacuolar compartments [37]. The parasite genome encodes only a single FYVE-domain containing protein, PfFCP (GeneID: PF3D7_1460100). The FYVE domain is situated at the N-terminus, followed by a coiled-coil domain and a C-terminal region (Fig. 4-2A, PfFCP) [38]. This domain structure does not have an easily recognizable homolog in model systems. This is especially true for the C-terminal region, which has multiple cysteine residues similar to a truncated zinc-finger but otherwise bears little resemblance to other protein domains and has yet to be characterized. McIntosh and colleagues [38] have reported that PfFCP and its FYVE domain retain the capacity to bind PI3P *in vitro*.

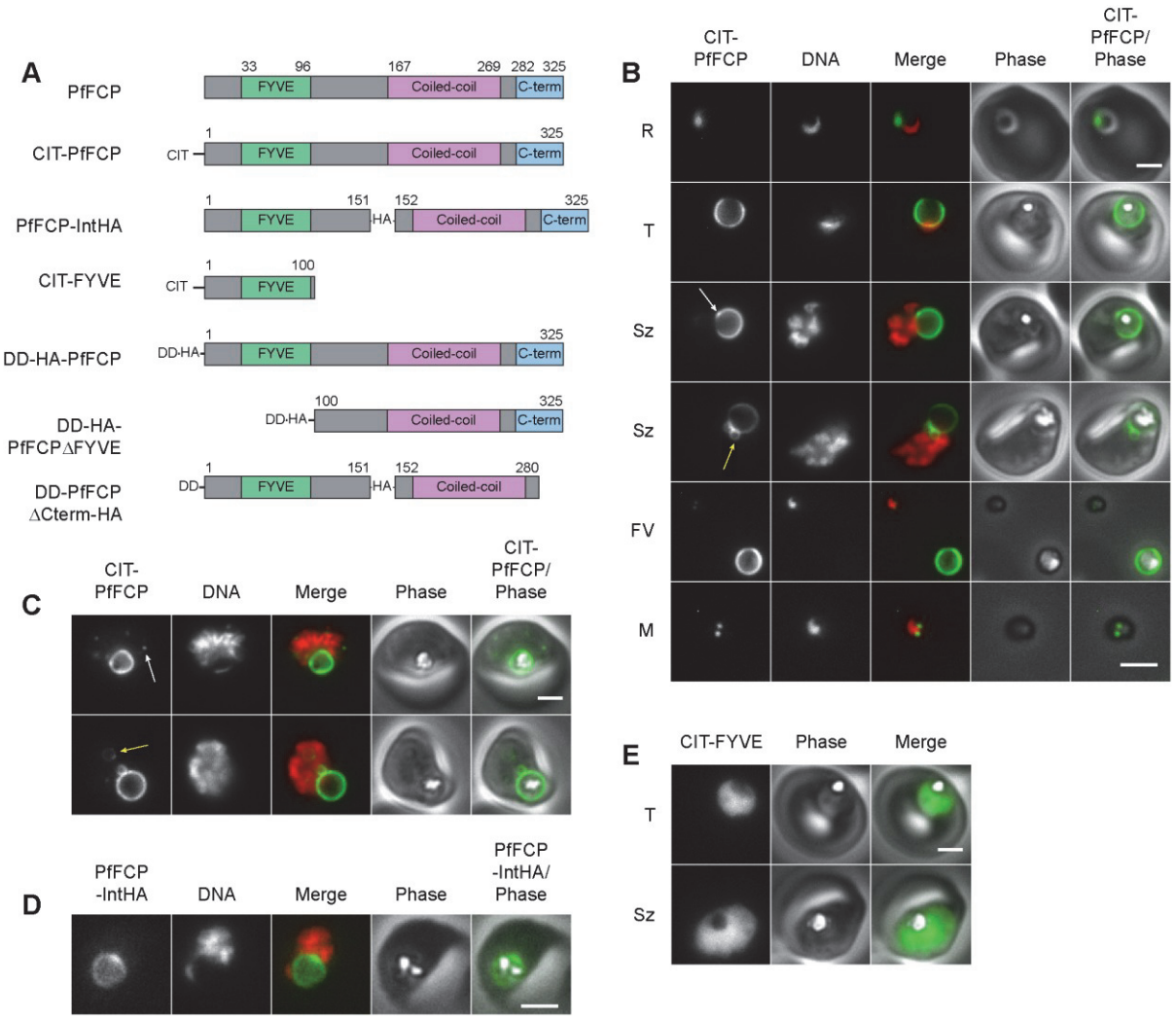

Figure 4-2: The FYVE-domain containing protein PfFCP localizes to the FV membrane and compartments in intraerythrocytic *P. falciparum*. A) Schematic representation of endogenous PfFCP and PfFCP variants used in this study. B) Wide-field epifluorescence images of live parasites expressing CIT-PfFCP (clone B8). Parasites are shown at ring (R), trophozoite (T), schizont (Sz), segmenter (Sg), and merozoite (M) stages, along with the extracellular FV (residual body, (FV)). Arrows indicate points of brighter fluorescence on the FV membrane (white) and secondary compartments attached to the FV (yellow). C) Images show that in some parasites the CIT-PfFCP punctate structures near nascent merozoites (white arrow) and additional compartments that are not in association with the FV (yellow arrow). D) Wide-field epifluorescence paraformaldehyde-fixed and mounted parasites expressing PfFCP-IntHA. Wide-field epifluorescence images of live parasites expressing CIT-FYVE. In merged parasite images, PfFCP is pseudocolored green and Hoechst 33342 or DAPI fluorescence (DNA) is pseudocolored red. Scale bar, 2 μm.

Surprisingly, they reported finding PfFCP within the FV lumen [38,39], which is not a reported location of PI3P. No such distribution pattern has ever been reported for a FYVE-domain containing protein before, and is therefore of special interest. They also reported that deletion of the FYVE domain has a dominant negative effect on FV formation, although technical issues made this difficult to characterize [38].

In this study we sought to establish the role of PfFCP in endomembrane traffic. We used stably integrated transposed expression cassettes to establish the distribution of PfFCP in both live and fixed cells. We have also generated a regulatable dominant negative variant of PfFCP to study its effects on parasite growth, FV biogenesis and trafficking, and hemoglobin catabolism. Our evidence suggests that the PfFCP homodimer acts at the FV membrane to regulate for inbound traffic.

Results

The P. falciparum *FYVE-domain containing protein, PfFCP, is associated with the food vacuole membrane*

The phosphoinositide, PI3P, in the parasite has been found in such diverse locations as the food vacuole (FV) membrane, apicoplast and ER lumen [2,32,33] and the FYVE domain is highly specific for this phosphoinositide. We sought to determine the distribution of the only *P. falciparum* FYVE-domain containing protein, PfFCP, in relation to these features by attempting to modify the endogenous PfFCP locus to encode a C-terminal fusion to the enhanced yellow fluorescent protein (YFP) variant “Citrine" (CIT) ([40,41], Fig. 4-S1A). We were unable to obtain parasites with the desired modification (data not shown). The C-terminal addition of YFP may obstruct protein function. Therefore, we generated parasites that expressed PfFCP as fusion

to an N-terminal YFP variant "Citrine" from a transposable cassette under control of the PfFCP promoter, CIT-PfFCP (Fig. 4-2A, 4-S1B and 4-S1C). From two independent transfections, clonal lines F9 and B8 were obtained and their genotype determined by Southern blot (Fig.4-S1B and 4-S1C). In both parasite lines, multiple unique transposition events had occurred. In the F9 clone, we found three separate integration events compared with only two in the B8 clone. In the B8 line there was an unexpected size shift of the chromosomal PfFCP band. This was determined to be the product of an unintentional single crossover recombination event at the PfFCP locus, which would not result in modification to the coding sequence (Fig. 4-S1C). Despite CIT-PfFCP overexpression and changes to the endogenous locus, no growth rate or morphological changes were observed in either parasite line relative to parental wild type 3D7 (data not shown).

The CIT-PfFCP distribution pattern was the same in both clonal parasite lines (Fig. 4-2B, 4-2C and 4-S2A). The B8 clonal line was used in all localization studies. CIT-PfFCP was observed throughout the asexual blood stage (Fig. 4-2B). In live recently invaded ring stage parasites expressing CIT-PfFCP, fluorescence was present and not cytosolic, but confined to regions within the parasite consistent with a compartmental localization pattern (Fig, 2B, R). A circular structure partially or completely encompassing the FV and hemozoin crystal was observed in trophozoites and schizonts (Fig. 4-2B, T and Sz). Fluorescence was not evenly distributed around the FV but appeared to be more concentrated at small points along the ring. These points often coincided with the intersection of secondary smaller compartments that were observed with increasing frequency as the parasite matured. In some schizonts, CIT-PfFCP was observed on circular compartments and puncta not in direct contact with the FV membrane (Fig. 4-2C). Secondary compartments suggest that CIT-PfFCP is associated with extra-FV membranes similar to the pattern seen for the chloroquine resistance transporter, PfCRT, a FV integral

membrane protein [1,26]. The secondary compartments were no longer apparent in segmenting schizonts. Punctate structures persisted, however, and were distributed around the parasite periphery. This distribution is consistent with association with nascent daughter merozoites (Fig. 4-2C). After egress, the FV residual body continued to be labeled with CIT-PfFCP (Fig. 4-2B, FV). Puncta in each merozoite were observed, indicating that structures containing CIT-PfFCP is inherited (Fig. 4-2B, M).

Fusion to large proteins, such as YFP, can potentially alter the distribution of a protein and may account for some of our observations of CIT-PfFCP. Beyond this concern, due to multiple integrations and recombination events seen in the CIT-PfFCP clones, we needed to confirm that the distribution of CIT-PfFCP was not aberrant or artifactual. Therefore, we generated parasites that expressed PfFCP with an internal small hemagglutinin (HA) epitope tag from a transposable cassette, PfFCP-IntHA (Fig. 4-2A and 4-S1D). Immunofluorescence analysis of PfFCP-IntHA-expressing parasites agreed with CIT-PfFCP localization around the FV (Fig. 4-2D). Secondary compartments and punctate structures were not observed in any parasites, indicating that these structures may not be stabilized by paraformaldehyde fixation methods or may be artifacts of YFP fusion.

The PfFCP FYVE domain is not sufficient for membrane association

One of the best studied FYVE-domain containing proteins is the early endosome autoantigen 1 (EEA1) in mammals. By expressing EEA1 fragments it was found that the C-terminal FYVE domain is necessary, but insufficient for membrane binding [42,43]. In addition, expression of this fragment acted as a dominant negative and inhibited fusion of early endosomes in mammalian cells [44].

To determine what effect the FYVE domain alone would have in parasites and if it was sufficient for membrane association, we expressed an N-terminal fragment of PfFCP including the complete FYVE domain as a fusion for YFP "Citrine" at its N-terminus, CIT-FYVE (Fig. 4-2A). Expression of CIT-FYVE was observed throughout the asexual stages as completely cytosolic (Fig. 4-2E, data not shown). Therefore, the FYVE domain alone is not sufficient for FV membrane association. In addition, parasites expressing CIT-FYVE did not exhibit any growth defect or morphological changes. These data suggest that the FYVE domain alone cannot interact with endogenous PfFCP or its effectors.

CIT-PfFCP forms a dimer with endogenous PfFCP in vivo

Identifying interacting partners of PfFCP is important for understanding its function in parasites. Recombinant PfFCP has been reported to form a homodimer *in vitro* likely through its coiled-coil domain [38]. Whether this interaction is relevant for its function in parasites has yet to be ascertained. As a dimer, PfFCP could function similarly to the mammalian protein early endosome autoantigen 1 (EEA1), which tethers vesicle traffic at the early endosome [44-47]. However, dimerization *in vitro* does not mean PfFCP functions as such in cells. The functional equivalent of EEA1 in yeast, Vac1, is not known to self-dimerize but rather forms a multiprotein complex and associates with the prevacuolar membrane by binding to a Q_A-SNARE, Pep12 [48,49]. Either of these models could be applicable to PfFCP.

To identify protein-protein interactions of PfFCP, we performed an anti-GFP pull-down on total protein extract from parasites expressing CIT-PfFCP (clone F9) and wild type 3D7. Bound protein was then subjected to SDS-PAGE, followed by silver staining or colloidal coomassie (Fig. 4-3, data not shown). Three unique bands present in the CIT-PfFCP sample but

not in wild type were detected and identified by mass spectrometry to be CIT-PfFCP, untagged PfFCP and free YFP "Citrine" (for details see Table 4-1). No other parasite proteins where found. These results indicate that CIT-PfFCP likely interacts with itself and/or endogenous PfFCP to form a dimer at the FV membrane. We did not observe free YFP in live cells (Fig. 4-2B and 4-2C), but it may be a minor component and not detectable in the presence of higher concentrations around the FV. Free YFP could also be produced from proteolytic cleavage of CIT-PfFCP during sample processing. The significance of these results is elaborated in the Discussion.

Truncated PfFCP lacking the FYVE-domain exerts a lethal dominant negative phenotype

McIntosh, et al. found that expression of a truncated PfFCP lacking the FYVE domain acted as a dominant negative mutant [38], resulting in developmentally arrested trophozoite-stage parasites. Further study of the dominant negative effect was limited by the small size of affected parasites and lack of regulation; this necessitated the use of inefficient transient transfection. Further study of this PfFCP dominant negative could reveal important details about the protein's interactions and functions within the parasite. Therefore, we sought to analyze the dominant negative effect of truncated PfFCP in detail using stable integration techniques.

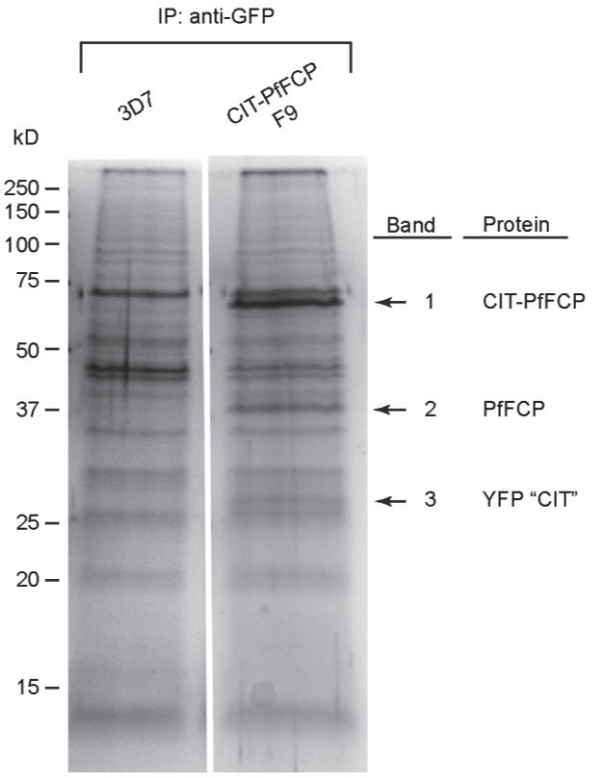

Figure 4-3: CIT-PfFCP forms a dimer with endogenous PfFCP in parasites.
Immunoprecipitation of CIT-PfFCP from clone F9 parasites. The immunoprecipitated proteins were analyzed by SDS-PAGE, silver staining and mass spectrometry. CIT-PfFCP, PfFCP, and YFP "Citrine" were detected in the CIT-PfFCP lane.

Table 4-1: CIT-PfFCP pull-down peptides identified by MS/MS

Band Size	Open Reading Frame	Residues	Peptide Sequence[1]	Observed Mass	Calculated Mass (Mr)	Mascot Individual Ion Score[2]
25 kD	YFP "Citrine"	86-96	KSAMPEGYVQER	1266.45	1265.57	42/62
		86-96	KSAmPEGYVQER[3]	1282.43	1281.57	26/62
		97-107	RTIFFKDDGNYK	1347.5	1346.65	78/62
		110-122	RAEVKFEGDTLVNR	1477.61	1476.76	93/62
37 kD	PfFCP	60-75	RACGNVFCSNCSDNKIK	1873.65	1872.79	85/62
		76-84	KISEYSYSEK	1105.42	1104.5	42/62
		76-86	KISEYSYSEKVR	1360.58	1359.67	58/62
		96-110	RSSPQTLLLQEDLGAR	1627.75	1626.86	148/62
		96-111	RSSPQTLLLQEDLGARK	1755.84	1754.95	101/62
		208-214	RNHEIQQK	896.383	895.451	46/62
75 kD	PfFCP	76-84	KISEYSYSEK	1105.44	1104.5	58/62
		96-110	RSSPQTLLLQEDLGAR	1627.79	1626.86	110/62
		96-111	RSSPQTLLLQEDLGARK	1755.88	1754.95	69/62
	YFP "Citrine"	80-85	KQHDFFK	821.345	820.387	35/62
		86-96	KSAMPEGYVQER	1266.52	1265.57	54/62
		86-96	KSAmPEGYVQER[3]	1282.5	1281.57	42/62
		97-107	RTIFFKDDGNYK	1347.58	1346.65	88/62
		110-122	RAEVKFEGDTLVNR	1477.7	1476.76	100/62
		114-122	KFEGDTLVNR	1050.47	1049.51	38/62

[1]Cleavage occurs after underlined residue.
[2]Scores shown with associated threshold score for p(match) < 0.05.
[3]Oxidized methionine residues are indicated by lower case.

Given the toxic effects of truncated mutants of PfFCP, we assumed that stable expression of PfFCP without the FYVE domain (PfFCPΔFYVE) from a transposon would not be tolerated. Based on previous success with regulated PfRab7 dominant negative mutants (Chapter 3), we attempted to express PfFCPΔFYVE as a fusion to an N-terminal *E. coli* DHFR destabilization domain (DD) [50]. Stabilization of the DD and its fusion partners can be achieved by addition of trimethoprim, which prevents their proteolytic degradation in a concentration dependent manner [51]. This construct would allow toxic PfFCP mutants to be "turned on" at different stages of parasite development and to different degrees. We also included an HA epitope tag to assist with quantification or localization studies and a human dihydrofolate reductase (hDHFR) expression cassette as a selectable marker and to provide resistance to trimethoprim. Transposable expression cassettes for full length DD-HA-PfFCP and dominant negative DD-HA-PfFCPΔFYVE under the control of the PfFCP promoter were generated and transfected into wild-type 3D7 parasites (Fig. 4-S1E and 4-S1F). To ensure that DD-HA-PfFCPΔFYVE was expressed sufficiently to produce observable effects, we constructed a second cassette with the potentially stronger *P. falciparum* aminopeptidase N (PfAMPN) promoter (unpublished data). To test if the C-terminal domain was necessary for membrane targeting, a similar transposable cassette was generated to express PfFCP with a C-terminal truncation and internal HA tag, DD-PfFCPΔCterm-HA. Parasites with each of the four transposable expression cassettes were obtained and screened for their sensitivity to trimethoprim. For screening, asynchronous transfected populations were cultured in media containing 10 μM trimethoprim or equivalent DMSO and monitored for several cycles using blood smears. Transfected parasite populations exhibiting morphological changes or lower parasitemia in trimethoprim than in DMSO were synchronized and screened again to confirm the effect. Although parasites expressing DD-HA-

PfFCP and DD-PfFCPΔCterm-HA thrived in trimethoprim-containing medium, those expressing DD-HA-PfFCPΔFYVE under control of either promoter exhibited morphological changes and a slower growth rate (data not shown).

Given that *piggyBac* transposase is not directed at a specific site in the parasite genome, and more than one transposition event can occur within a single parasite [52,53], protein expression within a transfected population will not be homogenous. Therefore, to control for multiple genotypes present, clonal lines of parasites expressing both DD-HA-PfFCP (A10) and DD-HA-PfFCPΔFYVE (C5 with the PfFCP promoter and B11 with the PfAMPN promoter) were produced and their genotype determined by Southern blot (Fig. 4-S1E). In clone A10, as well as in all other DD-HA-PfFCP clones (data not shown), a single transposition event had occurred (Fig. 4-S1F). In contrast to clones with a regulatable full length PfFCP, both trimethoprim sensitive DD-HA-PfFCPΔFYVE clonal lines had undergone multiple transposition events, four for the PfFCP promoter (C5) and two for the PfAMPN promoter (B11). Clones with fewer cassettes were likely missed by the stringency of our trimethoprim sensitivity screen.

Overexpression of DD-HA-PfFCP, whether truncated or wild type, may disrupt vesicle dynamics and be harmful to parasites. At the trimethoprim concentrations used the drug itself or even the solvent DMSO could cause toxic side effects. To control for these factors, trimethoprim (or equivalent DMSO) was added to synchronous ring-stage parasites from three different lines; their growth rate was analyzed by flow cytometry and blood smears (Fig. 4-4). In addition to conditionally regulated DD-HA-PfFCPΔFYVE (C5) and DD-HA-PfFCP (A10) lines, we included a modified parental parasite line, 3D7 attB. This line contains an hDHFR expression cassette within the *cg6* gene [54] and serves as a control for trimethoprim toxicity.

As predicted, 3D7 attB was resistant to trimethoprim up to 100 μM, the highest concentration tested, indicating that a single hDHFR expression cassette provided complete protection (Fig. 4-4A). Similarly, DD-HA-PfFCP (A10) expressing parasites grew in all trimethoprim concentrations at a rate comparable to 3D7 attB. DD-HA-PfFCPΔFYVE (C5), however, prevented parasite reinvasion in a concentration-dependent manner with an apparent IC_{50} of 720 ± 50 nM (Fig. 4-4A). From these data, we conclude that DMSO, trimethoprim and conditionally overexpressed full length PfFCP do not negatively affect parasite growth; only stabilization of the dominant negative results in a clear reduction in fitness.

To further study the mechanism by which the dominant negative prevents reinvasion and kills parasites, trimethoprim was added to synchronous ring-stage DD-HA-PfFCPΔFYVE (C5) expressing parasites and repeated again every 12 hrs. Changes in parasite morphology and parasitemia were examined at each time point (Fig. 4-4B). Parasites did not progress or reinvade if trimethoprim was added at or before 24 hrs, which corresponds to the trophozoite stage. Development appeared to be stalled during mid-trophozoite stages in dead and dying parasites, and exhibited other unusual characteristics. Many appeared "empty" or "hollow". Older parasites sometimes appeared vacuolarized. Parasites also contained compact, multiple, FVs with abnormally small, round hemozoin crystals. Together these data indicated that the dominant negative DD-HA-PfFCPΔFYVE interferes with an important process during the trophozoite stage, which affects the FV and potentially inbound traffic.

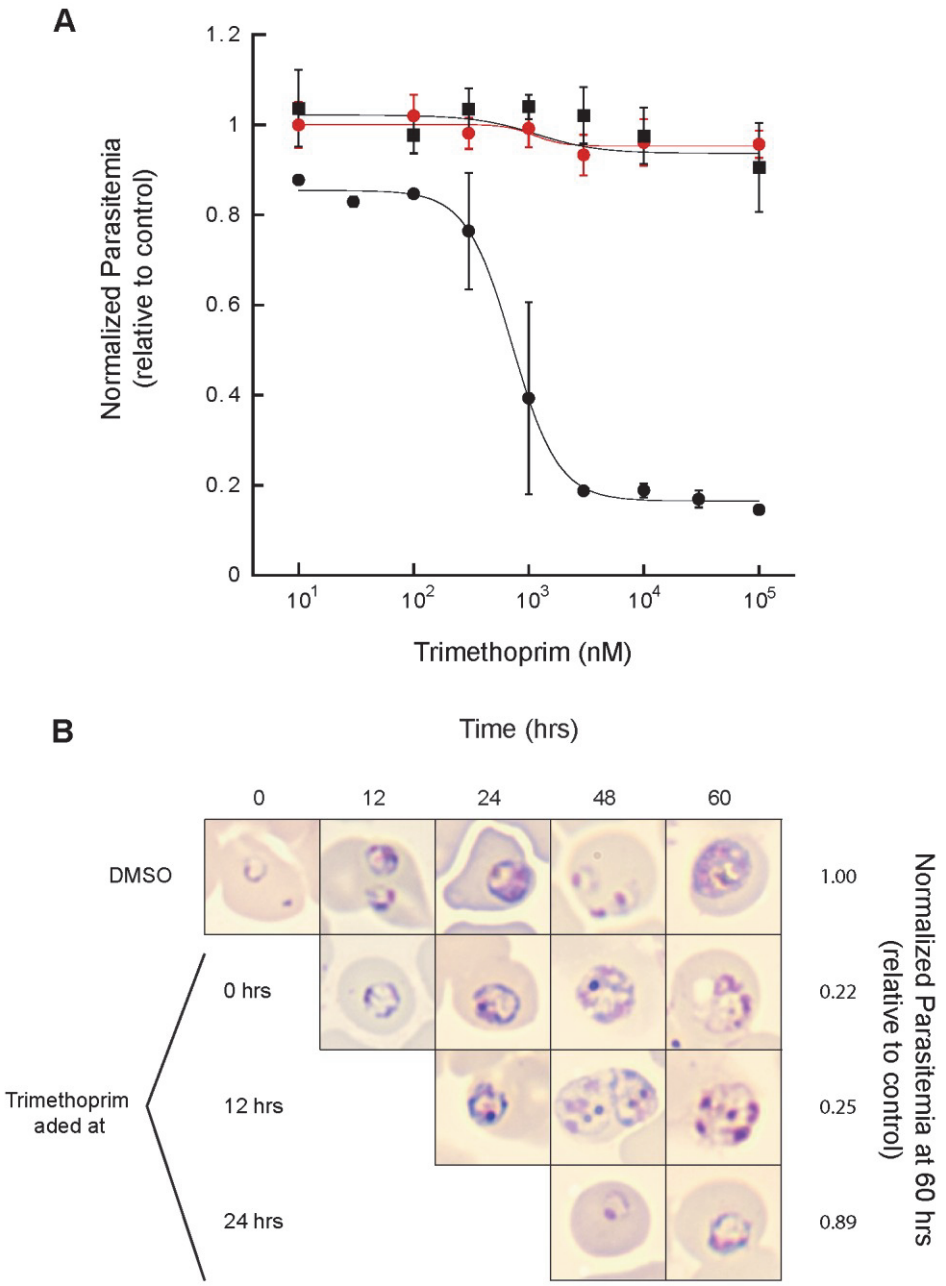
A
Normalized Parasitemia
(relative to control)
1.2
1
0.8
0.6
0.4
0.2
0
10^1
10^2
10^3
10^4
10^5
Trimethoprim (nM)
B
Time (hrs)
0
12
24
48
60
DMSO
1.00
0 hrs
0.22
Trimethoprim
aded at
12 hrs
0.25
24 hrs
0.89
Normalized Parasitemia at 60 hrs
(relative to control)

Figure 4-4 (previous page): Activation of the regulatable dominant negative mutant DD-HA-PfFCPΔFYVE causes parasite growth to stall at trophozoite stage.
A) Normalized parasitemia of 3D7 attB (red circles), DD-HA-PfFCP (A10) (black squares), and DD-HA-PfFCPΔFYVE (C5) (black circles) expressing parasites in the presence of trimethoprim (0 to 100 μM). "Normalized parasitemia" on the ordinate is the parasitemia divided by the parasitemia for the same culture in equivalent DMSO. Values are means ± standard deviation of the mean of at least three samples. B) The effect of trimethoprim addition at different stages on the intraerythrocytic development of DD-HA-PfFCPΔFYVE (C5) was monitored. Control medium contained only DMSO. The parasite culture medium was exchanged for medium containing 10 μM trimethoprim at 0 hrs, 12 hrs, and 24 hrs. Each panel shows the morphology of the intraerythrocytic parasite in each treatment at the indicated time. Normalized parasitemia at 60 hrs is indicated at right for each lane.

The C-terminal region of PfFCP but not the FYVE domain is necessary for membrane association

To understand how addition of trimethoprim results in a dominant negative effect, we attempted to localize the protein fusion in parasites expressing regulated PfFCP and its variants. Comparative immunofluorescence assays were performed after parasites were cultured, with trimethoprim or DMSO, for 22 to 24 hrs (Fig. 4-5A). In the presence of stabilizing ligand, DD-HA-PfFCPΔFYVE was present around the FV. This was similar to DD-HA-PfFCP. In addition, puncta in nascent merozoites were observed in DD-HA-PfFCP expressing parasites when using solvent fixation (Fig. 4-S2B). This indicates that puncta in CIT-PfFCP may not be an artifact. In contrast to the other constructs, DD-PfFCPΔCterm-HA exhibited a cytosolic punctate distribution characteristic of protein aggregation. Its inability to associate with the FV membrane reveals why this construct does not act as a dominant negative. In the absence of trimethoprim, the majority of parasites expressing the regulatable full length or dominant negative mutant were not fluorescent, or had fluorescence distributed in regions of the parasite other than the FV (data

not shown). In a few DD-HA-PfFCPΔFYVE expressing parasites we found fluorescence around the FV (data not shown), suggesting that the fusion is stable even in the absence of ligand.

These results suggest that the FYVE domain in PfFCP is not necessary for membrane association and that other interactions at the FV are required. We suspect formation of a dimer with endogenous PfFCP may be sufficient for FV membrane association. In this model, the dominant negative mutant continues to associate with PfFCP, but the complex is not fully functional, resulting in a dominant negative phenotype. Removal of DD-PfFCPΔCterm-HA from the FV renders the PfFCP variant ineffective as a dominant negative mutant. Surprisingly, in a small minority of parasites both DD-HA-PfFCP and DD-HA-PfFCPΔFYVE could be found around the FV in the absence of trimethoprim. Therefore, both fusions may be inherently stable. This was confirmed by an anti-HA immunoblot of lysate from parasites expressing DD-HA-PfFCPΔFYVE after a 6 hr incubation with various trimethoprim concentrations or DMSO control (Fig. 4-5B). Given that the addition of trimethoprim to DD-HA-PfFCP and DD-HA-PfFCPΔFYVE does not provide greater protein stability as predicted, it may induce a conformational change which allows either fusion to associate with the FV membrane, or makes the epitope tag available to anti-HA antibodies. This conformational change could also be responsible for the dominant negative trimethoprim-dependent effects on vesicle trafficking.

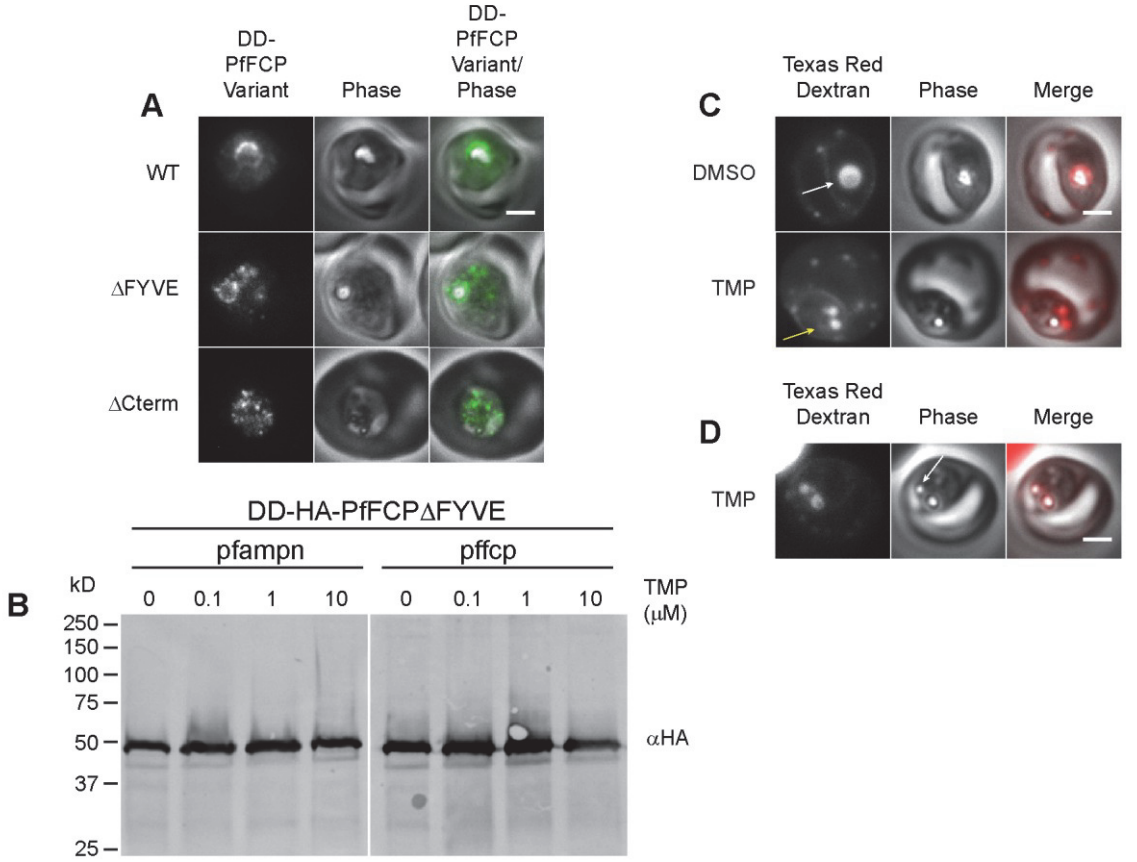

Figure 4-5: The dominant negative mutant DD-HA-PfFCPΔFYVE localizes to the FV membrane and alters of hemoglobin trafficking. A) Localization of regulatable HA-tagged DD-PfFCP variants. DD-HA-PfFCP-, DD-HA-PfFCPΔFYVE-, and DD-HA-PfFCPΔCterm-HA-expressing paraformaldehyde-fixed parasites after incubation for 24 hrs from ring stage in 10 μM trimethoprim In merged images, anti-HA antibody fluorescence is pseudocolored green. B) Immunoblot analysis DD-HA-PfFCPΔFYVE under control of PfAMPN (clone B11) or PfFCP (clone C5) promoter expressing parasites. Synchronous trophozoite parasites were incubated for 6 hrs with DMSO, 0.1, 1 or 10 μM trimethoprim (TMP) before saponin treatment and lysis in SDS-loading buffer before loading. Sizes of molecular mass markers are indicated in kD. C) DD-HA-PfFCPΔFYVE (C5) parasites purified from uninfected RBCs by magnetic column and allowed to invade in Texas Red dextran-containing resealed RBCs. Images taken 24 hrs after ring-stage addition of 10 μM trimethoprim (TMP) or equivalent DMSO. Texas Red dextran accumulated in the FV (white arrow) in DMSO, but distribution was altered in trimethoprim treated parasites (yellow arrow). D) Images show that in some parasites hemozoin crystals developed in compartment other than the FV (white arrow). In merged images, Texas Red dextran fluorescence is pseudocolored red. Scale bar, 2 μm.

PfFCP is a regulator of hemoglobin vesicle fusion to the food vacuole

We have found that both full length PfFCP and its truncated dominant negative mutant surround the FV, the primary site of hemoglobin catabolism. Host cell cytoplasm, containing mostly hemoglobin, is endocytosed through the cytostome inside double-membrane vesicles [55]. These fuse with the FV membrane to release their cargo [55]. Given that PfFCP is located at the FV membrane and that the PfFCP dominant negative mutant affects FV morphology, we suspect that PfFCP plays a role in vesicle transport to the FV. To test whether PfFCP is involved in the transport of host cytoplasm to the FV, synchronous DD-HA-PfFCPΔFYVE (C5) schizonts were purified by a magnetic column and then allowed to invade Texas Red Dextran loaded erythrocytes. After progression to rings, parasites were incubated with trimethoprim or equivalent DMSO for 24 hrs to induce the regulatable dominant negative mutant. In the control parasites, fluorescence was primarily observed within the hemozoin-containing FV (Fig. 4-5C). When incubated with trimethoprim, unusual staining was observed. Texas Red fluorescence was no longer within one large FV, but found in several smaller compartments and did not always overlap with the hemozoin crystal (Fig. 4-5C). In parasites where they did overlap, multiple hemozoin crystals were present (Fig. 4-5D). The addition of trimethoprim to the dominant negative mutant did not appear to prevent initial endocytosis or hemoglobin catabolism but rather seemed to disrupt the normal development of the FV during the trophozoite stage.

Dominant negative PfFCP alters distribution of a food vacuole hydrolase

Hemoglobin catabolism occurs as a stepwise process involving multiple proteases that must be expressed and transported to the FV [56-58]. Plasmepsin II (PM2) is one of these FV enzymes which catalyses the release of globin peptides from endocytosed hemoglobin [59]. It is

initially expressed as a transmembrane pro-protein (proPM2) and thought to be transported to the FV via cytostome-derived vesicles [60]. Under acidic conditions in the FV, PM2 undergoes autocatalytic maturation [60] or processing by other proteases [61], and is released in a soluble form into the lumen. If expressed as a fusion to green (or yellow) fluorescent protein, these fusion partners are cleaved and released into the FV lumen upon protein maturation. This multi-step environmentally sensitive maturation process makes PM2 an excellent, biologically relevant, tracer for monitoring biosynthetic cargo towards the FV and for FV acidity and integrity.

To monitor FV trafficking and structural integrity in live parasites, the endogenous PM2 locus was modified to encode a C-terminal fusion to the enhanced yellow fluorescent protein (YFP). For this experiment we used both the YFP variant “Citrine" (CIT) and “10C.” The YFP variant "Citrine" was developed in part to improve fluorescence intensity and stability in a wider variety of environments [40]. It contains the single mutation Gln69Met from its parental EYFP, which confers a pKa of 5.7, resulting in a larger proportion of the population remaining fluorescent in acidic environments [40], such as the parasite FV at pH 5.5 [62]. In an earlier variant of YFP, termed “10C,” [63] Gln at position 69 results in a much higher pKa of 6.3-7.1 (dependent on halide ion concentration [64,65]), causing the majority YFP "10C" to be much less fluorescent at pH 5.5 [40,65].

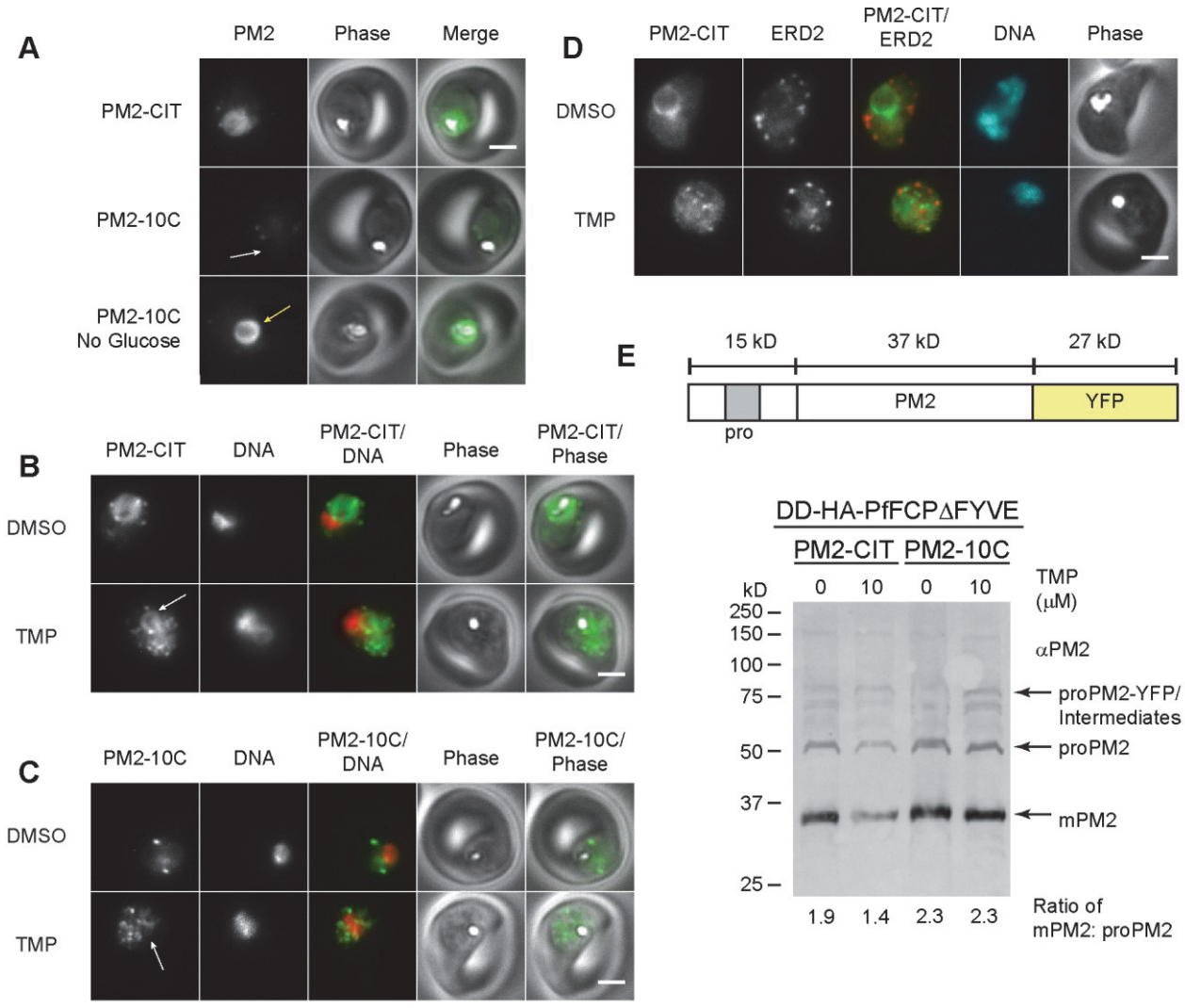

Figure 4-6: Induction of DD-HA-PfFCPΔFYVE with trimethoprim alters distribution of the FV hydrolase, plasmepsin II (PM2). A) Wide-field epifluorescence images of live parasites expressing PM2-CIT, PM2-10C in RPMI medium and PM2-10C after a 4 hr incubation in RPMI medium lacking glucose. B and C) Wide-field epifluorescence images of live parasites expressing PM2-CIT/DD-HA-PfFCPΔFYVE (B3) or B) PM2-10C/DD-HA-PfFCPΔFYVE (B11) in the presence of DMSO (top) or trimethoprim (TMP) (bottom). Arrows indicate the location of the FV in trimethoprim treated parasites. In merged images, PM2-YFP fluorescence is pseudocolored green and Hoechst 33342 (DNA) fluorescence is pseudocolored red. D) Colocalization of PM2-CIT and ERD2 (*cis*-Golgi) marker in PM2-CIT/DD-HA-PfFCPΔFYVE-expressing paraformaldehyde-fixed parasites after 24 hr incubation from ring stage in DMSO (top) or trimethoprim (bottom). In merged images, PM2-CIT fluorescence is pseudocolored green, ERD2 fluorescence is pseudocolored red and Hoechst 33342 (DNA) fluorescence is pseudocolored cyan. Scale bar, 2 μm. E) (Top) Schematic representation of the proPM2–YFP fusion. The propiece is shown with the single transmembrane domain (grey). proPM2–YFP is proteolytically processed twice to generate mPM2. Schematic is not drawn to scale. (Bottom)

Immunoblot analysis of PM2-CIT/DD-HA-PfFCPΔFYVE or PM2-10C/DD-HA-PfFCPΔFYVE expressing parasites synchronized at ring-stage and incubated with 10 μM trimethoprim or DMSO for 24 hrs before saponin treatment and lysis in SDS-loading buffer before loading. Ratio of intensity of the 37 kD band (mPM2) and the 50 kD band (proPM2) for each sample is at the bottom. Differences in intensity between PM2-CIT with and without trimethoprim were within experimental error. Sizes of molecular mass markers are indicated in kD.

Parasites with the desired modification were obtained and clonal lines generated. PM2-CIT fluorescence could be found in the FV and cytosolic punctate structures that are likely to be cytostomal-derived vesicles [60] (Fig. 4-6A). This was an identical distribution to the published distribution of PM2-GFP [60]. In parasites expressing PM2-10C, punctate structures remained, but FV fluorescence had disappeared (Fig. 4-6A). To determine if PM2-10C is still transported to the FV but remains “invisible” due to the acidic environment, the FV was alkalized by culturing parasites in the absence of glucose and thus ATP [66] for 4 hrs. In this environment, parasites lose the ability to regulate both their cytosolic and FV pH [67,68], which quickly equilibrate with the neutral medium. In these PM2-10C-expressing parasites the FV fluorescence was restored (Fig. 4-6A). From these data we determined that the fusion to the YFP variant “10C” versus "Citrine" has no effect on trafficking, but will have substantially lower fluorescence intensity in the acidic environment of the FV.

To determine if the dominant negative PfFCP mutant affects trafficking of FV enzymes, a DD-HA-PfFCPΔFYVE transposable expression cassette under control of the PfFCP or PfAMPN promoter (Fig. 4-2A) was introduced into the genome of the parasite lines expressing PM2 as a fusion to YFP, either the variant "Citrine" (PM2-CIT) or "10C" (PM2-10C) (Fig. 4-6A). Trimethoprim-sensitive clonal parasite lines with the PfFCP promoter in PM2-CIT (B3) and the PfAMPN promoter in PM2-10C (B11) were obtained. Synchronous ring-stage parasites from both lines were incubated with trimethoprim or DMSO for 22 hrs, after which morphological

changes were observed as have been described above. In the presence of DMSO, PM2-CIT (B3) fluorescence was primarily within the FV with peripheral puncta (Fig. 4-6B); this is identical to what was previously observed with PM2-CIT alone and PM2-GFP (Fig. 4-6A, [60]). In PM2-10C (B11), little fluorescence was detected in the FV, but peripheral puncta remained (Fig. 4-6A and 4-6C). After 22 hrs in the presence of trimethoprim, PM2-CIT was still found in the shrunken FV, whereas with PM2-10C FV fluorescence was not observed (Fig. 4-6B and 4-6C, arrows). Outside of the FV, however, PM2-CIT (and PM2-10C) distribution changed dramatically from several vesicles around the periphery to a multitude of potentially smaller vesicles throughout the cytosol, perhaps indicating fragmentation or increased vesicle production.

The cytosolic punctate pattern of PM2-CIT (and PM2-10C) in the presence of trimethoprim is similar to that of the parasite Golgi apparatus. Given that PM2 is transported through the secretory system [60], this pattern could be explained by a fraction of the PM2-YFP population stalled at the Golgi apparatus or endosome. To investigate if PM2-YFP vesicles colocalize with the Golgi apparatus, we performed immunofluorescence analysis using the *cis*-Golgi marker, ERD2, but found no evidence of colocalization with PM2-CIT or PM2-10C after trimethoprim or DMSO incubation (Fig. 4-6D, data not shown). We do not have an antibody for the parasite endosome, but given that it is found adjacent to the Golgi apparatus (Chapter 3), it is unlikely that PM2-YFP is in this compartment either. We conclude that PM2-YFP puncta represent a population of vesicles that is unable to fuse with the FV.

PM2-10C fluorescence in the trimethoprim-induced vesicles indicates that they are not acidic and therefore a portion of PM2 may remain as an unprocessed proprotein. To determine if PM2 is processed after an extended incubation with trimethoprim, synchronous ring-stage

parasites expressing PM2-CIT (and PM2-10C) with DD-HA-PfFCPΔFYVE were cultured in trimethoprim or DMSO for 24 hours and PM2 processing was determined by quantitative anti-PM2 immunoblot (Fig. 4-6E, [57,60]). Mature PM2 (mPM2) and unprocessed PM2 (proPM2) without a YFP tag were determined by band size to be the primary species observed at 37 and 52 kDa, respectively. The ratio between these two species was the same with and without trimethoprim, indicating that the dominant negative mutant had no effect on this step in processing (Fig. 4-6E). Bands at the size of proPM2-CIT/10C and processing intermediates were also detected but were not a major species in any sample.

From these observations it appears that DD-HA-PfFCPΔFYVE does not prevent PM2 processing. The small PM2-CIT/10C vesicles suggest that fusion to the FV is partially inhibited. Surprisingly, given PM2-10C fluorescence, these vesicles are not acidic, but the majority of PM2 appears to be present in its fully processed form. The cytosolic vesicles may contain only a minor fraction of total PM2 in the parasite. Alternatively, processing of proPM2-CIT/10C may still occur in these neutral vesicles more slowly by other proteases [61]. Further analysis using pulse-chase techniques will be necessary to determine if the dominant negative mutant slows PM2 maturation, and if PfFCP has a role in FV hydrolase processing.

Discussion

The process of hemoglobin endocytosis and subsequent vesicle-mediated sorting mechanisms have implications for antimalarial drug delivery and activation [21,22]. Homologs of several "classical" clathrin mediated endocytic components, including AP-2 and dynamin, have been implicated in hemoglobin uptake [15-17,21]. In this study we have presented evidence that the *P. falciparum* FYVE-domain containing protein, PfFCP, plays a role in trafficking of

cargo en route to the FV throughout the intraerythrocytic blood stage. Our localization studies place PfFCP at the FV membrane. We suspect it lies on the cytosolic face where it can bind resident PI3P through its FYVE domain [2]. Formation of a homodimer likely increases binding affinity for the phosphoinositide through the avidity effect, as the FYVE domain alone is not sufficient for membrane association (Fig. 4-2G).

Our results on the localization of PfFCP to the FV membrane conflict with studies by McIntosh, et al. [38]. Here we have ascertained the distribution of PfFCP using constructs with multiple tags in both live and fixed cells using stable integration techniques in an attempt to mitigate reliance on potentially artifactual results by using one strategy alone. We reason that some of the differences between our results and published results are attributable to variations in fixation protocols, which can alter the structural integrity of the sample [69,70]. Unfortunately, we were unable to obtain a sample of anti-PfFCP antisera [38] to test using our fixation conditions, but we did perform immunofluorescence assays with our DD-HA-PfFCP line using the published methods by McIntosh, et al. [38,39]. We found that the FV membrane was no longer intact in many parasites and DD-HA-PfFCP could be misread as localizing within the FV lumen (Fig. 4-S2C). Neither luminal nor cytosolic orientation can be ruled out given that our CIT-PfFCP construct cannot differentiate between the two. Live cell imaging of PfFCP as a fusion to a pH-sensitive reporter, like YFP "10C," will help to clarify this question.

Introduction of a dominant negative mutant of PfFCP slowed or disrupted traffic headed to the FV, resulting in a morphological change in the organelle itself, and changes to both endocytic and biosynthetic cargo distributions. Parasites in which DD-HA-PfFCPΔFYVE was induced were unable to mature beyond the trophozoite stage. The trophozoite stage specificity of the dominant negative mutant is an interesting result, and may indicate that PfFCP is especially

important at this stage in parasite development. Given that both PfAMPN and PfFCP have peak expression during the early trophozoite stage [71-73], the dominant negative effects we observe may be a result of higher transcription levels rather than the importance of PfFCP during that stage. The use of ring or schizont specific promoters to drive expression of the DD-HA-PfFCPΔFYVE would be necessary to fully explore this possibility. Even when using ring-stage specific promoters, we may still observe a delayed effect. For dominant negative effects to manifest DD-HA-PfFCPΔFYVE must out-compete the endogenous PfFCP to form nonfunctional dimers. In our current constructs, regardless of when trimethoprim is added, an effect is not observed until the trophozoite stage. This delay may be due to "residual" PfFCP, inherited from the parental parasite, as seen with CIT-PfFCP in merozoites and young rings.

PfFCP shares several domains with the mammalian early endosome autoantigen (EEA1) and its yeast functional equivalent, Vac1, which are involved in vesicle tethering prior to SNARE-mediated fusion at the early and late endosome respectively [47]. Both proteins contain FYVE and coiled-coil domains [35,48], which promote targeting to PI3P on the membrane and facilitate protein-protein interactions [74]. The two proteins form different functional complexes, however. Mammalian EEA1 forms a homodimer through its coiled-coil domain [45]. As a dimer, EEA1 possesses the increased binding affinity for PI3P required for tethering function [36]. If its FYVE domain is mutated and unable to bind PI3P, EEA1 cannot associate with the early endosome membrane [43,75]. The N-terminal zinc finger and FYVE domain also bind to the early endosome enriched small GTPase Rab5 [76]. In contrast, yeast Vac1 acts in conjunction with a multiprotein complex at the late endosomal membrane [49,77], whose members include a Q_A-SNARE (Pep12), Rab5 homolog (Vps21), PI3 Kinase (Vps34) and Sec1 homolog (Vps45) [48,77]. Vac1 does not require a complete complex or a FYVE domain to be membrane

associated, but a functional complex is required for vacuole hydrolases and internalized proteins to reach the vacuole [48,49,78].

Given that the PfFCP dominant negative mutant remains associated with the FV membrane and forms a homodimer, PfFCP appears to share properties with both EEA1 and Vac1. It is likely that the dominant negative disrupts vesicle fusion through formation of a non-functional complex with endogenous PfFCP. Membrane association may be facilitated by unidentified proteins, such as the small GTPase Rab5 (or Vps21 in yeast). Three isoforms of Rab5 have been identified in the *P. falciparum* genome [79], but their distributions have not been reported. We did not detect any Rab5 isoforms in our pull-down assay, but this may be due to the transient nature of the interaction with PfFCP. In yeast, the Vac1-Vps21 interaction was only detected with a constitutively active Q66L mutant of Vps21 [49]. The use of constitutively active mutants of PfRab5 isoforms may also be necessary to detect PfFCP-PfRab5 interaction.

Induction of the dominant negative mutant by trimethoprim did not stop all vesicle fusion at the FV in the parasite. Initial FV formation may occur before the dominant negative effect can manifest; this is either due to the promoters driving expression or the presence of endogenous PfFCP very early in the parasite life cycle. Some later fusion events may be permitted by a PfFCP-independent pathway. One possible fusion factor is the CORVET core complex, which is thought to catalyze the assembly of SNAREs at the early endosome in mammals and yeast [80]. CORVET has a role independent of EEA1 on Rab5-positive membranes [80,81]. This has lead to the theory that EEA1 and Vac1p facilitate endocytic vesicle fusion, whereas CORVET is involved in homotypic fusion at the endosome [80]. Homologs of the four subunits in its "Class C" core are encoded in the *P. falciparum* genome but have to our knowledge not been characterized [82]. In the parasite, this could result in the effects we see: production of smaller

compartments separate from the FV, but with similar content wherein hemoglobin catabolism can continue albeit inefficiently.

The study of PfFCP and its dominant negative have brought to light interesting questions about the nature of the parasite endocytic system, and its connection to the FV that may prove challenging to answer. Our study on the parasite retromer cargo selective complex showed that *P. falciparum* possesses an endosome in close opposition to nascent rhoptries and suggests that it is involved in transport to apical secretory organelles (Chapter 3). We found no evidence of an early endosome or an endosome maturation pathway, however. Despite being both acidic and a site of proteolytic degradation, we propose that, based on our results, the FV may be thought of as a terminal early endosome. We have found no evidence yet that the FV endocytic pathway intersects with the *P. falciparum* PfRab7 and retromer complex-labeled endosome. Further study of PfFCP and its effectors portend other exciting finds about the evolution of these unique protozoa with implications for anti-malarial targets and drug development.

Experimental Procedures

Construction of Plasmids for P. falciparum Transfection

Plasmids for the generation of a chimera between the chromosomal copy of plasmepsin II (PM2) and that of yellow fluorescent protein (YFP) variant "Citrine" (CIT) or "10C" through single-crossover homologous recombination were produced, as described in [83], to yield pPM2CIT1-1 and pPM210C. Briefly, the coding sequence for green fluorescent protein [84] was converted to YFP "Citrine" or YFP "10C" by introducing mutations A65G/Q69M/T203Y and A65G/T203Y, respectively using the QuikChange mutagenesis kit (Stratagene). The two YFP sequences were introduced into the AvrII/NotI sites of the plasmid pPM2GT [60] to produce

pPM2CIT1-1 [83] and pPM210C. To similarly modify the PfFCP chromosomal locus, a 3' fragment of the PfFCP coding sequence (basepairs 31 to 975), excluding the stop codon, was PCR amplified from *P. falciparum* 3D7 genomic DNA using oligos 439/440 (all oligonucleotide sequences referred to in this section are listed in Supplemental Table 4-S1). The PCR product was cloned into the XhoI and AvrII sites of pPM2CIT2 [83] to yield pPfFCP-CIT (Fig. 4-S1A).

Plasmids for transposon-based expression were constructed from pSD-DHFR (Chapter 3). To generate an expression cassette for CIT-PfFCP, the complete coding sequence of PfFCP (including the start and stop codon) was PCR amplified from 3D7 genomic DNA using oligos 552/553, and introduced into the AvrII/NotI sites of pSD-DHFR. The sequence for YFP variant "Citrine" (encoding for the last 15nt of the PfFCP 5' UTR and a C-terminal Softtag but no stop codon) was amplified using oligos 534/535 from pPM2CIT2 [83] and cloned into the XhoI/AvrII sites. Approximately 800 nucleotides of the 5' UTR of PfFCP were PCR amplified using oligos 532/533 and introduced into the XmaI/XhoI sites to yield pCIT-PfFCP. To generate an expression cassette for YFP fused to the N-terminal region including the entire FYVE domain of PfFCP, the first 300 nucleotides of PfFCP were PCR amplified from 3D7 genomic DNA using oligos 552/677 and cloned into AvrII/NotI sites of pCIT-PfFCP to yield pCIT-FYVE.

To generate an expression cassette for PfFCP with an internal HA tag, an N-terminal fragment (bases 1 to 453) of the coding sequence was PCR amplified from 3D7 genomic DNA to encode a C-terminal HA tag using oligos 555/556 and cloned into XhoI/AvrII sites of pDD-mCherry-PfRab7 (Chapter 3). Lastly, the C-terminal fragment (bases 454 to 978) was also PCR amplified from 3D7 genomic DNA using oligos 557/553 and cloned into AvrII/NotI sites to yield pPfFCP-IntHA.

To generate all regulatable expression cassettes, the *E. coli* DHFR destabilization domain (DD) coding sequence (omitting the stop codon) was PCR amplified from pBMN DHFR (DD)-YFP [50] using oligos 470/471 and cloned into XhoI/AvrII sites of pSD-DHFR. Approximately 800 nucleotides of the 5' UTR of PfFCP was PCR amplified using oligos 532/533 and cloned into XmaI/XhoI sites. The full length PfFCP coding sequence and a truncated fragment without the FYVE domain (bases 208 to 978) were PCR amplified from 3D7 genomic DNA to include an N-terminal HA tag using oligos 554/553 and 601/553 respectively. The coding sequence of PfFCP truncated at the C-terminus was PCR amplified from pPfFCP-IntHA using oligos 682/678 and digested with SpeI/NotI. All three were cloned into AvrII/NotI sites, yielding pDD-HA-PfFCP, pDD-HA-PfFCPΔFYVE, and pDD-PfFCPΔCterm-HA. Finally, the hDHFR cassette in selected transposon expression constructs was excised from the BglII/EcoRI sites and replaced with a yDHOD expression cassette amplified from pUF-1 [85] with oligos 501/502 to yield pDD-HA-PfFCP-yDHOD, pDD-HA-PfFCPΔFYVE-yDHOD, and pDD-PfFCPΔCterm-yDHOD. Another plasmid carrying the PfFCPΔFYVE expression cassette with transcription driven by the promoter sequence of *P. falciparum* M1-family aminopeptidase (GeneID PF3D7_1311800) was constructed by replacing the PfFCP 5' UTR with a PCR product (oligos 569/151) containing bases -800 to -15 of the PfAMPN 5' UTR to yield pPfAMPNp- pDD-HA-PfFCPΔFYVE and pPfAMPNp- pDD-HA-PfFCPΔFYVE-yDHOD.

All coding sequences that were subjected to PCR amplification were verified by DNA sequencing. Plasmids used in this study are listed in Table 4-S2.

Parasite Culture and Transfection

P. falciparum 3D7 parasites were cultured as described in (Krai_2014/Chapter 3). Briefly, parasites were grown in human O^+ erythrocytes (Interstate Blood Bank; 2% hematocrit) in RPMI 1640 medium (Life Technologies) supplemented with 27 mM sodium bicarbonate, 11 mM, glucose, 0.37 mM hypoxanthine, 10 μg/ml gentamicin, and 5 g/liter Albumax I (Invitrogen). Parasites were synchronized by 5% sorbitol treatment. Parasites used for immunoblotting were isolated from intact red blood cells by treatment with 1.5 mg/ml saponin in phosphate buffered saline (PBS).

To introduce plasmids for genomic integration at the PfFCP locus, ring-stage 3D7 parasites were transfected with 100 μg of plasmid containing pPfFCP-CIT. Transfected parasites were selected with 10 nM WR99210. Drug-resistant parasites were subjected to a drug cycling protocol whereby parasites were cultured without selection for 3 weeks followed by re-selection. To introduce plasmids carrying expression cassettes on the *piggyBac* transposon, uninfected erythrocytes were transfected with 100 μg of transposon-containing plasmid and 50 μg of the helper plasmid pHTH [53]. Late-stage parasites were purified using a MACS magnetic column (Miltenyl Biotec) and transfected erythrocytes were seeded with 2.5-5 x 10^5 parasites/mL. Drug selection with WR99210 (2.5-10 nM) or DSM-1 (1.5 μM) was initiated two days after transfection and drug-resistant parasites appeared after about 18 days. Clonal parasite lines were generated by limited dilution.

Parasite Growth Assays

Synchronous ring stage parasites were split for treatment with in various trimethoprim concentrations at 0.1% DMSO, 0.1% DMSO or complete medium alone and

seeded at 1 to 5% parasitemia. At each time point, 100 µL of culture was fixed in an equivalent volume of 0.1% glutaraldehyde in PBS. Parasites were permeabilized by 5 min incubation with 0.25% Triton X-100 detergent in PBS. DNA content was determined by staining with 400 nM YOYO-1 (Invitrogen) in PBS, followed by resolution in BD Accuri C6 Flow Cytometer (BD Biosciences, San Jose, CA). Data acquisition and analysis were performed using BD Accuri CFlow Plus 1.0 (BD Biosciences, San Jose, CA) and Kaleidagraph 4.1 (Synergy Software, Reading, PA). Parasite morphology was determined by microscopic analysis after smearing and staining. Briefly, smears were fixed in methanol for a few seconds, then stained with PROTOCOL Hema 3 Giemsa stain (Fisher) and washed with distilled water. Smears were allowed to fully dry before by microscopy (magnification X 100) with immersion oil.

Southern Blot Analysis

Genomic DNA was isolated from saponin-treated parasites using the QiaAmp DNA Mini kit (Qiagen) and digested with one or two restriction enzymes as indicated in Fig. 4-S1. DNA fragments were resolved on a 0.75% agarose gel, transferred to positively charged nylon membrane and hybridized to labeled probes overnight. Probe labeling and detection were carried out using the AlkPhos direct labeling kit (GE Biosciences) according to the manufacturer's instructions on film.

Immunofluorescence assays and live cell imaging

For live cell imaging, cultured parasites were resuspended and placed under a coverslip following a short (<30 minute) incubation with the vital nuclear stain Hoechst 33342 (5 µM). For immunofluorescence assays, parasites were fixed and permeabilized as described previously [83]

and incubated with mouse anti-HA antibodies (Covance) diluted to 0.5 μg/mL, or rabbit anti-ERD2 (MR4) [86] diluted to 1:500 followed by a Alexa 594 conjugated mouse secondary antibody diluted to 2 μg/mL (Invitrogen). Cells were placed under a coverslip after addition of vital nuclear stain Hoechst 33342 (1 μM) or mounted on polyethylenimine-coated cover slip using Prolong Gold with DAPI (Invitrogen). For hemoglobin uptake assay, synchronous late-stage parasites expressing DD-HA-PfFCPΔFYVE (C5) were purified using a MACS magnetic column (Miltenyl Biotec) and allowed to invade uninfected erythrocytes loaded with lysine flexible 10K MW Texas Red Dextran (Life Technologies). Parasites were then incubated with 10 μM trimethoprim or equivalent DMSO for 24 hrs before imaging. For PM2-10C images, medium was exchanged for RPMI without glucose and allowed to incubate for 4 hrs under normal culture conditions before images were taken. Images were collected on a Zeiss AxioImager equipped with an MRm Axiocam digital camera using a 100×/1.4NA objective lens. All images were converted to TIF files and contrast was adjusted using Adobe Photoshop CS6.

Immunoblotting

For protein analysis parasites expressing PfFCPp-DD-HA-PfFCPΔFYVE (clone C5), PfAMPNp-DD-HA-PfFCPΔFYVE (clone B11), PM2-CIT/ PfFCPp-DD-HA-PfFCPΔFYVE (clone B3), PM2-10C/PfAMPNp-DD-HA-PfFCPΔFYVE (clone B11) were harvested by saponin treatment. Parasite pellets were washed in cold 1X PBS supplemented with protease inhibitors (10 μM E-64, 10 μM pepstatin A, 1 mM 4-(2-aminoethyl) benzenesulfonyl fluoride). Parasites were lysed by boiling in SDS sample buffer for 10 min. Lysate was cleared of hemozoin by 15 min at 17k x g centrifugation and analyzed by immunoblotting with anti-HA mouse antibody (Covance) diluted 1:1,000 to 1 μg/mL or anti-PM2 rabbit antibody 737 [57] diluted 1:5000.

Signal was detected by chemiluminescence using horseradish peroxidase-conjugated anti-rabbit or anti-mouse secondary antibodies. Blots were developed using ECL Plus (GE Biosciences) and imaged Storm 860 imager (GE Biosciences).

YFP-PfFCP Pull-down

For PfFCP pull-down, wild-type 3D7 and YFP-PfFCP (clone F9) expressing parasites were harvested by saponin treatment and lysed in 10 mM HEPES-KOH, pH 7.5, 140 mM NaCl, 5mM KCl, 2mM $MgCl_2$ and 1% Triton-X 100 supplemented with protease inhibitors (10 μM E-64, 10 μM pepstatin A, 10 μM bestatin and 1 mM 4-(2-aminoethyl) benzenesulfonyl fluoride). Lysate was spun for 5 min at 604 x *g* at 4 °C. Chromotek-GFP-Trap Magnetic Beads (Allele Biotech) (wet volume 50 μL) were equilibrated in lysis buffer before incubation with parasite lysate for 1 hr at 4°C. After washing the beads three times with lysis buffer, bound protein was eluted with SDS sample buffer and boiled for 10 min. Bound protein was also analyzed by 10.5–14% SDS–PAGE (Bio-Rad) followed by GelCode Blue Colloidal Coomassie (Thermo Scientific). Unique protein bands in YFP-PfFCP (F9) bound fraction were excised and identified by mass spectrometry.

Acknowledgements

We are grateful to Dr. Richard Helm and Keith Ray for performing mass spectrometry analysis, Dr. Tom Wandless for generously supplying *E. coli* DHFR DD plasmids, Dr. Akhil Vaidhya for yDHOD expression plasmids and for DSM-1 compound. We also thank D. Jacobus (Jacobus Pharmaceuticals) for WR99210. PfERD2 antiserum was obtained through the MR4 as part of the BEI Resources Repository, NIAID, NIH: PfERD2 Rabbit Antiserum, MRA-1,

deposited by J. H. Adams. We also thank Dr. Maria Cassera for use of her equipment to photograph blood smears. This work was supported by the Department of Biochemistry at Virginia Tech and NSF S-STEM Graduate Scholarship.

. **References**

1. Abu Bakar N, Klonis N, Hanssen E, Chan C, Tilley L (2010) Digestive-vacuole genesis and endocytic processes in the early intraerythrocytic stages of Plasmodium falciparum. J Cell Sci 123: 441-450.
2. Tawk L, Chicanne G, Dubremetz JF, Richard V, Payrastre B, et al. (2010) Phosphatidylinositol 3-phosphate, an essential lipid in Plasmodium, localizes to the food vacuole membrane and the apicoplast. Eukaryot Cell 9: 1519-1530.
3. Organization WH (2012) World Malaria Report 2012. In: Organization WH, editor. Geneva, Switzerland: World Health Organization (WHO).
4. Reilly HB, Wang H, Steuter JA, Marx AM, Ferdig MT (2007) Quantitative dissection of clone-specific growth rates in cultured malaria parasites. Int J Parasitol 37: 1599-1607.
5. Dasari P, Reiss K, Lingelbach K, Baumeister S, Lucius R, et al. (2011) Digestive vacuoles of Plasmodium falciparum are selectively phagocytosed by and impair killing function of polymorphonuclear leukocytes. Blood 118: 4946-4956.
6. Krugliak M, Zhang J, Ginsburg H (2002) Intraerythrocytic Plasmodium falciparum utilizes only a fraction of the amino acids derived from the digestion of host cell cytosol for the biosynthesis of its proteins. Mol Biochem Parasitol 119: 249-256.
7. Loria P, Miller S, Foley M, Tilley L (1999) Inhibition of the peroxidative degradation of haem as the basis of action of chloroquine and other quinoline antimalarials. Biochem J 339 (Pt 2): 363-370.
8. Liu J, Istvan ES, Gluzman IY, Gross J, Goldberg DE (2006) Plasmodium falciparum ensures its amino acid supply with multiple acquisition pathways and redundant proteolytic enzyme systems. Proc Natl Acad Sci U S A 103: 8840-8845.
9. Martin RE, Kirk K (2007) Transport of the essential nutrient isoleucine in human erythrocytes infected with the malaria parasite Plasmodium falciparum. Blood 109: 2217-2224.
10. Lew VL, Tiffert T, Ginsburg H (2003) Excess hemoglobin digestion and the osmotic stability of Plasmodium falciparum-infected red blood cells. Blood 101: 4189-4194.
11. Rosenthal PJ (2011) Falcipains and other cysteine proteases of malaria parasites. Adv Exp Med Biol 712: 30-48.
12. Goldberg DE (2013) Complex nature of malaria parasite hemoglobin degradation [corrected]. Proc Natl Acad Sci U S A 110: 5283-5284.
13. Rosenthal PJ (1995) Plasmodium falciparum: effects of proteinase inhibitors on globin hydrolysis by cultured malaria parasites. Exp Parasitol 80: 272-281.
14. Olson JE, Lee GK, Semenov A, Rosenthal PJ (1999) Antimalarial effects in mice of orally administered peptidyl cysteine protease inhibitors. Bioorg Med Chem 7: 633-638.
15. Zhou HC, Gao YH, Zhong X, Wang H (2009) Dynamin like protein 1 participated in the hemoglobin uptake pathway of Plasmodium falciparum. Chin Med J (Engl) 122: 1686-1691.

16. Li H, Han Z, Lu Y, Lin Y, Zhang L, et al. (2004) Isolation and functional characterization of a dynamin-like gene from Plasmodium falciparum. Biochem Biophys Res Commun 320: 664-671.
17. Charneau S, Bastos IM, Mouray E, Ribeiro BM, Santana JM, et al. (2007) Characterization of PfDYN2, a dynamin-like protein of Plasmodium falciparum expressed in schizonts. Microbes Infect 9: 797-805.
18. Parish LA, Rayner JC (2009) Plasmodium falciparum secretory pathway: characterization of PfStx1, a plasma membrane Qa-SNARE. Mol Biochem Parasitol 164: 153-156.
19. Ayong L, DaSilva T, Mauser J, Allen CM, Chakrabarti D (2011) Evidence for prenylation-dependent targeting of a Ykt6 SNARE in Plasmodium falciparum. Mol Biochem Parasitol 175: 162-168.
20. Ayong L, Pagnotti G, Tobon AB, Chakrabarti D (2007) Identification of Plasmodium falciparum family of SNAREs. Mol Biochem Parasitol 152: 113-122.
21. Henriques G, Martinelli A, Rodrigues L, Modrzynska K, Fawcett R, et al. (2013) Artemisinin resistance in rodent malaria--mutation in the AP2 adaptor mu-chain suggests involvement of endocytosis and membrane protein trafficking. Malar J 12: 118.
22. Klonis N, Crespo-Ortiz MP, Bottova I, Abu-Bakar N, Kenny S, et al. (2011) Artemisinin activity against Plasmodium falciparum requires hemoglobin uptake and digestion. Proc Natl Acad Sci U S A 108: 11405-11410.
23. Elliott DA, McIntosh MT, Hosgood HD, 3rd, Chen S, Zhang G, et al. (2008) Four distinct pathways of hemoglobin uptake in the malaria parasite Plasmodium falciparum. Proc Natl Acad Sci U S A 105: 2463-2468.
24. Lazarus MD, Schneider TG, Taraschi TF (2008) A new model for hemoglobin ingestion and transport by the human malaria parasite Plasmodium falciparum. J Cell Sci 121: 1937-1949.
25. Hanssen E, McMillan PJ, Tilley L (2010) Cellular architecture of Plasmodium falciparum-infected erythrocytes. Int J Parasitol 40: 1127-1135.
26. Ehlgen F, Pham JS, de Koning-Ward T, Cowman AF, Ralph SA (2012) Investigation of the Plasmodium falciparum food vacuole through inducible expression of the chloroquine resistance transporter (PfCRT). PLoS One 7: e38781.
27. Traub LM (2009) Tickets to ride: selecting cargo for clathrin-regulated internalization. Nat Rev Mol Cell Biol 10: 583-596.
28. Brocker C, Engelbrecht-Vandre S, Ungermann C (2010) Multisubunit tethering complexes and their role in membrane fusion. Curr Biol 20: R943-952.
29. Weinberg J, Drubin DG (2012) Clathrin-mediated endocytosis in budding yeast. Trends Cell Biol 22: 1-13.
30. Ungewickell EJ, Hinrichsen L (2007) Endocytosis: clathrin-mediated membrane budding. Curr Opin Cell Biol 19: 417-425.
31. Misra S, Miller GJ, Hurley JH (2001) Recognizing phosphatidylinositol 3-phosphate. Cell 107: 559-562.
32. Bhattacharjee S, Speicher KD, Stahelin RV, Speicher DW, Haldar K (2012) PI(3)P-independent and -dependent pathways function together in a vacuolar translocation sequence to target malarial proteins to the host erythrocyte. Mol Biochem Parasitol 185: 106-113.
33. Bhattacharjee S, Stahelin RV, Speicher KD, Speicher DW, Haldar K (2012) Endoplasmic reticulum PI(3)P lipid binding targets malaria proteins to the host cell. Cell 148: 201-212.

34. Lemmon MA (2008) Membrane recognition by phospholipid-binding domains. Nat Rev Mol Cell Biol 9: 99-111.
35. Kutateladze TG (2007) Mechanistic similarities in docking of the FYVE and PX domains to phosphatidylinositol 3-phosphate containing membranes. Prog Lipid Res 46: 315-327.
36. Kutateladze TG (2006) Phosphatidylinositol 3-phosphate recognition and membrane docking by the FYVE domain. Biochim Biophys Acta 1761: 868-877.
37. Gillooly DJ, Simonsen A, Stenmark H (2001) Cellular functions of phosphatidylinositol 3-phosphate and FYVE domain proteins. Biochem J 355: 249-258.
38. McIntosh MT, Vaid A, Hosgood HD, Vijay J, Bhattacharya A, et al. (2007) Traffic to the malaria parasite food vacuole: a novel pathway involving a phosphatidylinositol 3-phosphate-binding protein. J Biol Chem 282: 11499-11508.
39. Vaid A, Ranjan R, Smythe WA, Hoppe HC, Sharma P (2010) PfPI3K, a phosphatidylinositol-3 kinase from Plasmodium falciparum, is exported to the host erythrocyte and is involved in hemoglobin trafficking. Blood 115: 2500-2507.
40. Griesbeck O, Baird GS, Campbell RE, Zacharias DA, Tsien RY (2001) Reducing the environmental sensitivity of yellow fluorescent protein. Mechanism and applications. J Biol Chem 276: 29188-29194.
41. Miyawaki A, Griesbeck O, Heim R, Tsien RY (1999) Dynamic and quantitative Ca2+ measurements using improved cameleons. Proc Natl Acad Sci U S A 96: 2135-2140.
42. Lawe DC, Patki V, Heller-Harrison R, Lambright D, Corvera S (2000) The FYVE domain of early endosome antigen 1 is required for both phosphatidylinositol 3-phosphate and Rab5 binding. Critical role of this dual interaction for endosomal localization. J Biol Chem 275: 3699-3705.
43. Stenmark H, Aasland R, Toh BH, D'Arrigo A (1996) Endosomal localization of the autoantigen EEA1 is mediated by a zinc-binding FYVE finger. J Biol Chem 271: 24048-24054.
44. Simonsen A, Lippe R, Christoforidis S, Gaullier JM, Brech A, et al. (1998) EEA1 links PI(3)K function to Rab5 regulation of endosome fusion. Nature 394: 494-498.
45. Callaghan J, Simonsen A, Gaullier JM, Toh BH, Stenmark H (1999) The endosome fusion regulator early-endosomal autoantigen 1 (EEA1) is a dimer. Biochem J 338 (Pt 2): 539-543.
46. Mills IG, Jones AT, Clague MJ (1998) Involvement of the endosomal autoantigen EEA1 in homotypic fusion of early endosomes. Curr Biol 8: 881-884.
47. Christoforidis S, McBride HM, Burgoyne RD, Zerial M (1999) The Rab5 effector EEA1 is a core component of endosome docking. Nature 397: 621-625.
48. Peterson MR, Burd CG, Emr SD (1999) Vac1p coordinates Rab and phosphatidylinositol 3-kinase signaling in Vps45p-dependent vesicle docking/fusion at the endosome. Curr Biol 9: 159-162.
49. Tall GG, Hama H, DeWald DB, Horazdovsky BF (1999) The phosphatidylinositol 3-phosphate binding protein Vac1p interacts with a Rab GTPase and a Sec1p homologue to facilitate vesicle-mediated vacuolar protein sorting. Mol Biol Cell 10: 1873-1889.
50. Iwamoto M, Bjorklund T, Lundberg C, Kirik D, Wandless TJ (2010) A general chemical method to regulate protein stability in the mammalian central nervous system. Chem Biol 17: 981-988.

51. Muralidharan V, Oksman A, Iwamoto M, Wandless TJ, Goldberg DE (2011) Asparagine repeat function in a Plasmodium falciparum protein assessed via a regulatable fluorescent affinity tag. Proc Natl Acad Sci U S A 108: 4411-4416.
52. Balu B, Chauhan C, Maher SP, Shoue DA, Kissinger JC, et al. (2009) piggyBac is an effective tool for functional analysis of the Plasmodium falciparum genome. BMC Microbiol 9: 83.
53. Balu B, Shoue DA, Fraser MJ, Jr., Adams JH (2005) High-efficiency transformation of Plasmodium falciparum by the lepidopteran transposable element piggyBac. Proc Natl Acad Sci U S A 102: 16391-16396.
54. Nkrumah LJ, Muhle RA, Moura PA, Ghosh P, Hatfull GF, et al. (2006) Efficient site-specific integration in Plasmodium falciparum chromosomes mediated by mycobacteriophage Bxb1 integrase. Nat Methods 3: 615-621.
55. Francis SE, Gluzman IY, Oksman A, Knickerbocker A, Mueller R, et al. (1994) Molecular characterization and inhibition of a Plasmodium falciparum aspartic hemoglobinase. EMBO J 13: 306-317.
56. Dasaradhi PV, Korde R, Thompson JK, Tanwar C, Nag TC, et al. (2007) Food vacuole targeting and trafficking of falcipain-2, an important cysteine protease of human malaria parasite Plasmodium falciparum. Mol Biochem Parasitol 156: 12-23.
57. Francis SE, Banerjee R, Goldberg DE (1997) Biosynthesis and maturation of the malaria aspartic hemoglobinases plasmepsins I and II. J Biol Chem 272: 14961-14968.
58. Subramanian S, Sijwali PS, Rosenthal PJ (2007) Falcipain cysteine proteases require bipartite motifs for trafficking to the Plasmodium falciparum food vacuole. J Biol Chem 282: 24961-24969.
59. Gluzman IY, Francis SE, Oksman A, Smith CE, Duffin KL, et al. (1994) Order and specificity of the Plasmodium falciparum hemoglobin degradation pathway. J Clin Invest 93: 1602-1608.
60. Klemba M, Beatty W, Gluzman I, Goldberg DE (2004) Trafficking of plasmepsin II to the food vacuole of the malaria parasite Plasmodium falciparum. J Cell Biol 164: 47-56.
61. Drew ME, Banerjee R, Uffman EW, Gilbertson S, Rosenthal PJ, et al. (2008) Plasmodium food vacuole plasmepsins are activated by falcipains. J Biol Chem 283: 12870-12876.
62. Klonis N, Tan O, Jackson K, Goldberg D, Klemba M, et al. (2007) Evaluation of pH during cytostomal endocytosis and vacuolar catabolism of haemoglobin in Plasmodium falciparum. Biochem J 407: 343-354.
63. Ormo M, Cubitt AB, Kallio K, Gross LA, Tsien RY, et al. (1996) Crystal structure of the Aequorea victoria green fluorescent protein. Science 273: 1392-1395.
64. Llopis J, McCaffery JM, Miyawaki A, Farquhar MG, Tsien RY (1998) Measurement of cytosolic, mitochondrial, and Golgi pH in single living cells with green fluorescent proteins. Proc Natl Acad Sci U S A 95: 6803-6808.
65. McAnaney TB, Zeng W, Doe CF, Bhanji N, Wakelin S, et al. (2005) Protonation, photobleaching, and photoactivation of yellow fluorescent protein (YFP 10C): a unifying mechanism. Biochemistry 44: 5510-5524.
66. Sherman IW (1998) Malaria : parasite biology, pathogenesis, and protection. Washington, DC: ASM Press.
67. Saliba KJ, Kirk K (1999) pH Regulation in the Intracellular Malaria Parasite, Plasmodium falciparum : H+ EXTRUSION VIA A V-TYPE H+-ATPase. Journal of Biological Chemistry 274: 33213-33219.

68. Saliba KJ, Allen RJW, Zissis S, Bray PG, Ward SA, et al. (2003) Acidification of the Malaria Parasite's Digestive Vacuole by a H+-ATPase and a H+-pyrophosphatase. Journal of Biological Chemistry 278: 5605-5612.
69. Tonkin CJ, van Dooren GG, Spurck TP, Struck NS, Good RT, et al. (2004) Localization of organellar proteins in Plasmodium falciparum using a novel set of transfection vectors and a new immunofluorescence fixation method. Mol Biochem Parasitol 137: 13-21.
70. Allan VJ (2000) Protein localization by fluorescent microscopy : a practical approach. Oxford ; New York: Oxford University Press. xxiv, 231 p. p.
71. Le Roch KG, Zhou Y, Blair PL, Grainger M, Moch JK, et al. (2003) Discovery of gene function by expression profiling of the malaria parasite life cycle. Science 301: 1503-1508.
72. Bartfai R, Hoeijmakers WA, Salcedo-Amaya AM, Smits AH, Janssen-Megens E, et al. (2010) H2A.Z demarcates intergenic regions of the *Plasmodium falciparum* epigenome that are dynamically marked by H3K9ac and H3K4me3. PLoS Pathog 6: e1001223.
73. Bozdech Z, Llinas M, Pulliam BL, Wong ED, Zhu J, et al. (2003) The transcriptome of the intraerythrocytic developmental cycle of *Plasmodium falciparum*. PLoS Biology 1: 85-100.
74. Kutateladze TG, Ogburn KD, Watson WT, de Beer T, Emr SD, et al. (1999) Phosphatidylinositol 3-phosphate recognition by the FYVE domain. Mol Cell 3: 805-811.
75. Gaullier JM, Ronning E, Gillooly DJ, Stenmark H (2000) Interaction of the EEA1 FYVE finger with phosphatidylinositol 3-phosphate and early endosomes. Role of conserved residues. J Biol Chem 275: 24595-24600.
76. Mishra A, Eathiraj S, Corvera S, Lambright DG (2010) Structural basis for Rab GTPase recognition and endosome tethering by the C2H2 zinc finger of Early Endosomal Autoantigen 1 (EEA1). Proc Natl Acad Sci U S A 107: 10866-10871.
77. Bowers K, Stevens TH (2005) Protein transport from the late Golgi to the vacuole in the yeast Saccharomyces cerevisiae. Biochim Biophys Acta 1744: 438-454.
78. Webb GC, Zhang J, Garlow SJ, Wesp A, Riezman H, et al. (1997) Pep7p provides a novel protein that functions in vesicle-mediated transport between the yeast Golgi and endosome. Mol Biol Cell 8: 871-895.
79. Quevillon E, Spielmann T, Brahimi K, Chattopadhyay D, Yeramian E, et al. (2003) The Plasmodium falciparum family of Rab GTPases. Gene 306: 13-25.
80. Balderhaar HJ, Ungermann C (2013) CORVET and HOPS tethering complexes - coordinators of endosome and lysosome fusion. J Cell Sci 126: 1307-1316.
81. Cabrera M, Arlt H, Epp N, Lachmann J, Griffith J, et al. (2013) Functional separation of endosomal fusion factors and the class C core vacuole/endosome tethering (CORVET) complex in endosome biogenesis. J Biol Chem 288: 5166-5175.
82. Koumandou VL, Dacks JB, Coulson RM, Field MC (2007) Control systems for membrane fusion in the ancestral eukaryote; evolution of tethering complexes and SM proteins. BMC Evol Biol 7: 29.
83. Dalal S, Klemba M (2007) Roles for two aminopeptidases in vacuolar hemoglobin catabolism in Plasmodium falciparum. J Biol Chem 282: 35978-35987.
84. Cormack BP, Valdivia RH, Falkow S (1996) FACS-optimized mutants of the green fluorescent protein (GFP). Gene 173: 33-38.

85. Ganesan SM, Morrisey JM, Ke H, Painter HJ, Laroiya K, et al. (2011) Yeast dihydroorotate dehydrogenase as a new selectable marker for Plasmodium falciparum transfection. Mol Biochem Parasitol 177: 29-34.
86. Elmendorf HG, Haldar K (1993) Identification and localization of ERD2 in the malaria parasite Plasmodium falciparum: separation from sites of sphingomyelin synthesis and implications for organization of the Golgi. EMBO J 12: 4763-4773.

Supplementary Information

Figure 4-S1 (following pages): Genotype analysis of transfected parasite lines. A) Parasite line expressing PfFCP-CIT following single-crossover recombination with pPfFCP-CIT. B and C) Two clonal parasite lines (F9 and B8) transfected with a plasmid carrying a transposable CIT-PfFCP expression cassette. D) Parasites transfected with a plasmid carrying a transposable PfFCP-IntHA expression cassette. E) Two clonal parasite lines (B11 and C5) transfected with a plasmid carrying a DD-HA-PfFCPΔFYVE transposable expression cassette under control of the PfAMPN and PfFCP promoter, respectively. F) One clonal parasite line (A10) transfected with a plasmid carrying a transposable DD-HA-PfFCP expression cassette. For all panels, a schematic diagram of the product of recombination or transposition is provided on the left. The predicted sizes of DNA fragments upon digestion with the indicated restriction enzyme are shown. The red (or blue) bar indicates the position of the probe used for Southern blotting. "X" indicates the expected site(s) of homologous recombination, where applicable. Figures are not drawn to scale. Southern blots of genomic DNA of parental and transformed parasite lines are shown on the right. Each blot was performed on a single membrane. For clarity, some lanes are shown as individual strips but all strips originate from the same exposure. Sizes of DNA markers in kilobases are indicated at left. Arrows at right identify the positions of the expected bands. Bands identified with an asterisk "*" are presumably products of restriction enzyme star activity. The presence of "plasmid" likely reflects the integration of concatameric episomes. Abbreviations: CIT, yellow fluorescent protein "Citrine"; hDHFR, human dihydrofolate reductase; CD, cytosine deaminase; DD, *E. coli* DHFR destabilization domain; HA, hemagglutinin epitope tag.

Figure 4-S1 (continued)

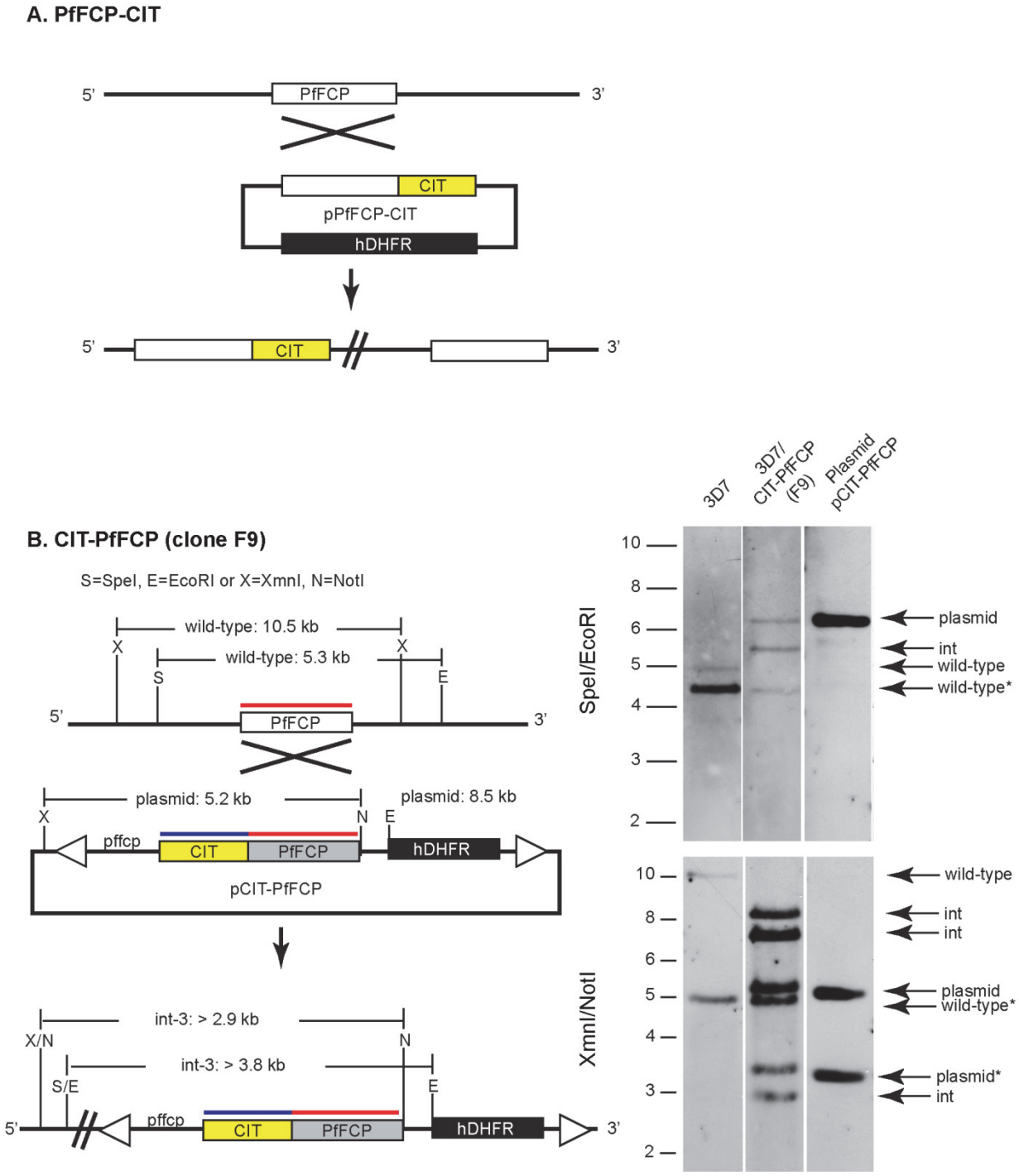

Figure 4-S1 (continued)

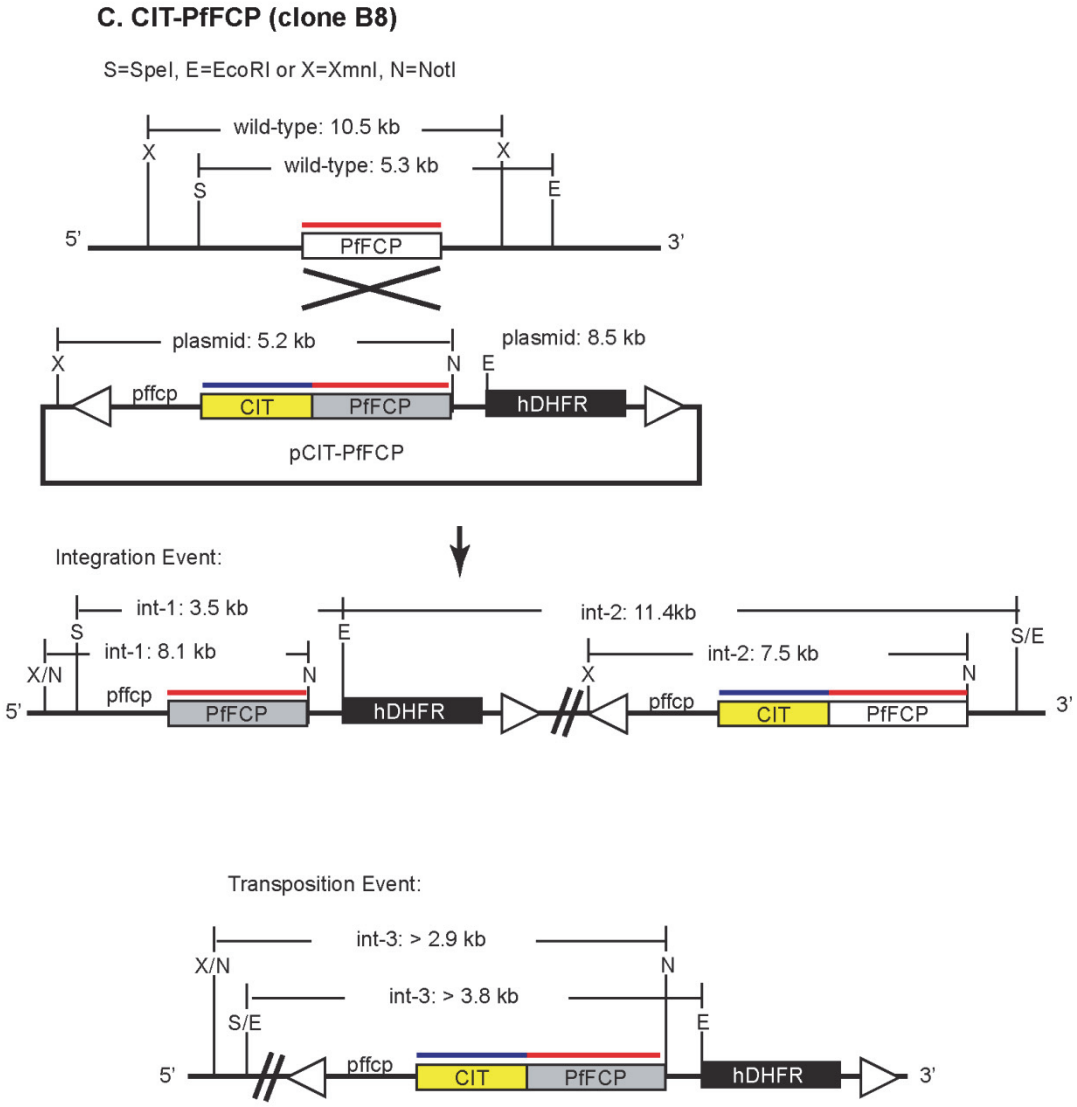

Figure 4-S1 (continued)

C. CIT-PfFCP (clone B8) (Continued)

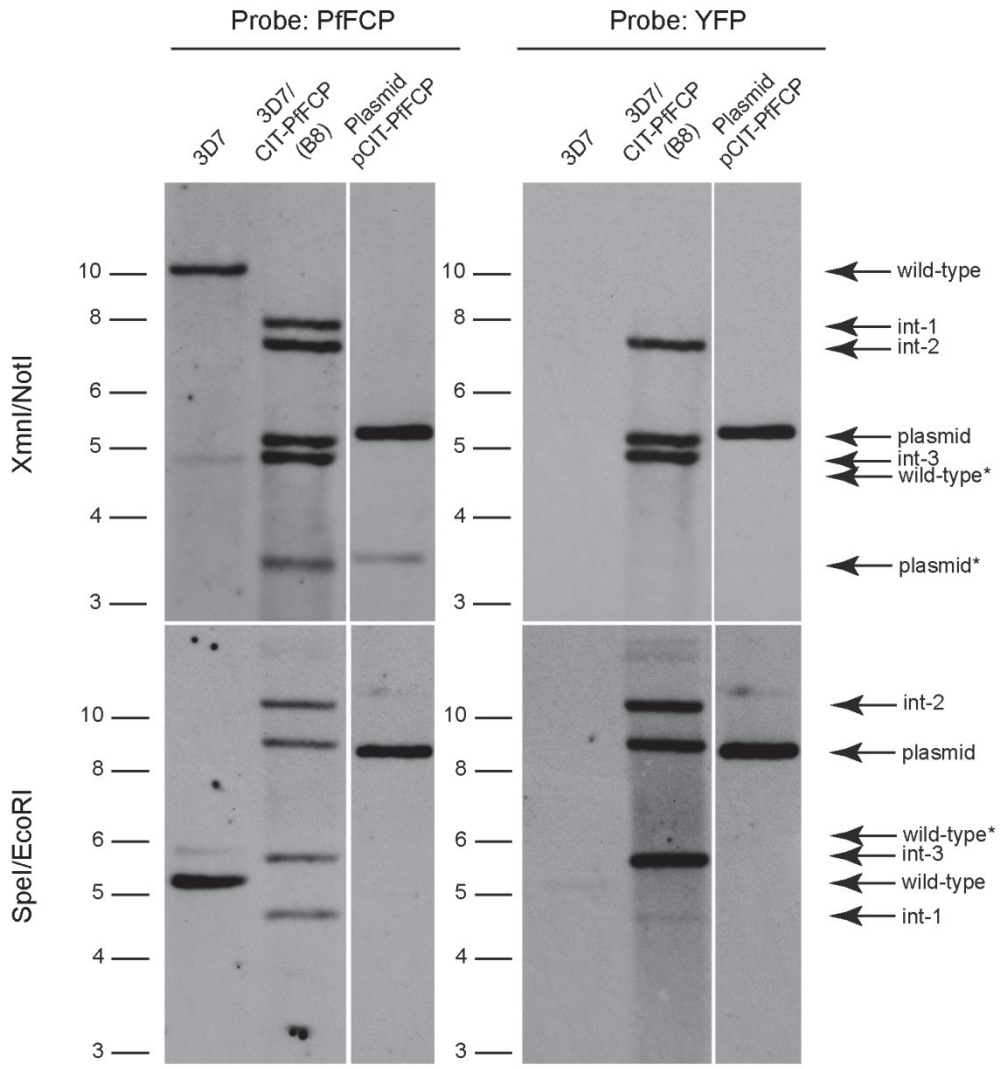

Figure 4-S1 (continued)

D. PfFCP-IntHA

X=XmnI, N=NotI, S=SpeI, E=EcoRI

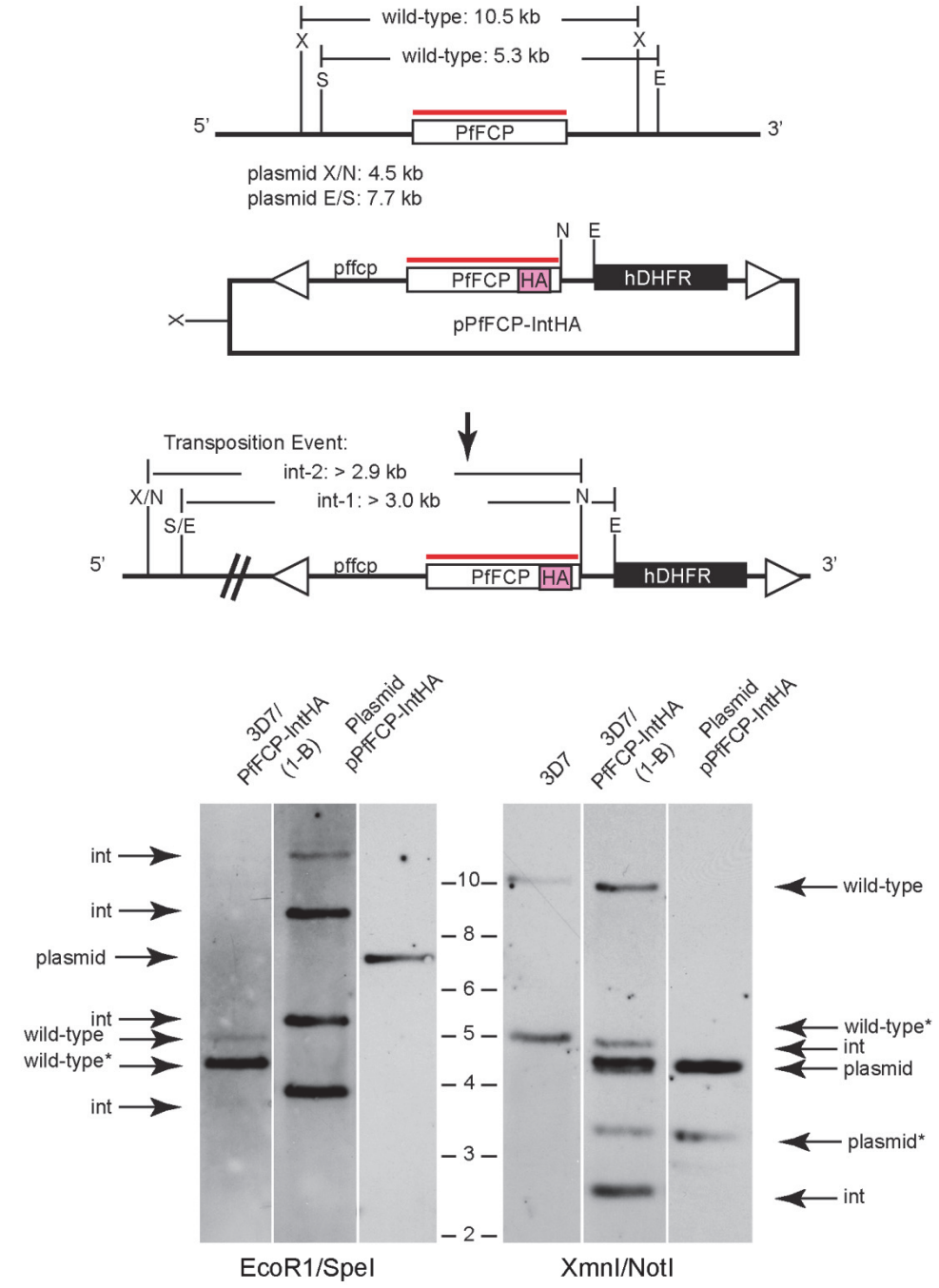

Figure 4-S1 (continued)

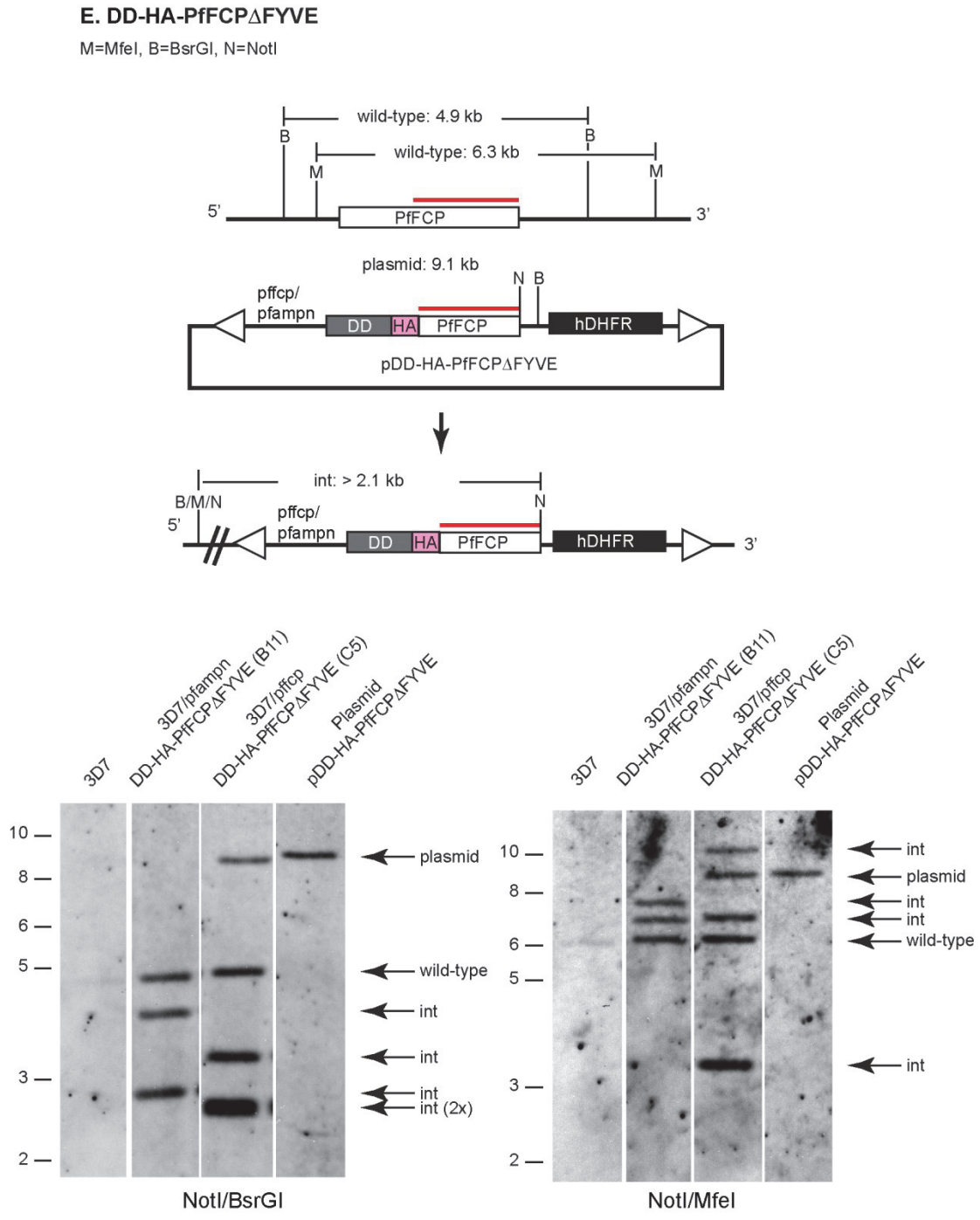

Figure 4-S1 (continued)

F. DD-HA-PfFCP

M=MfeI, B=BsrGI, N=NotI

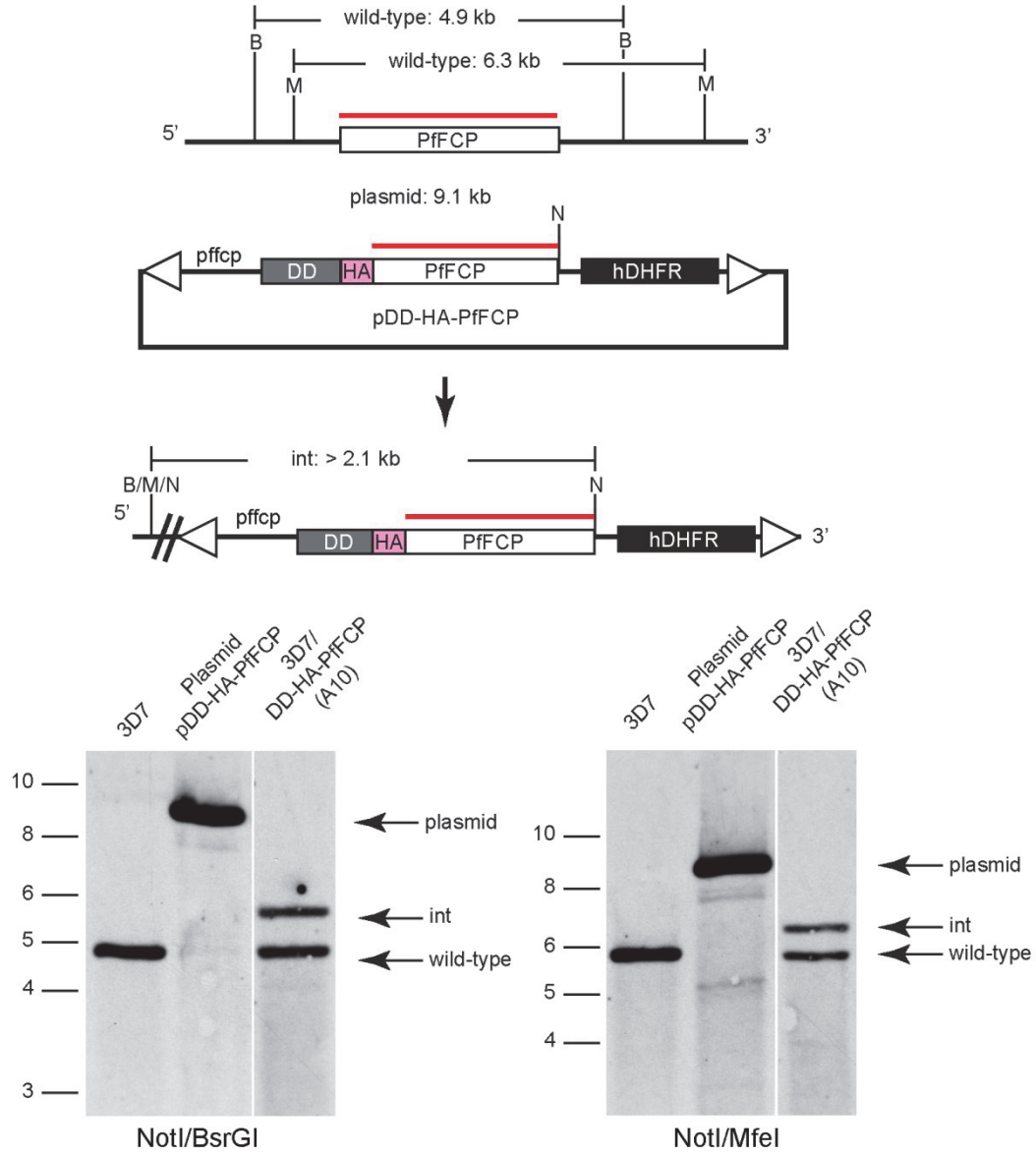

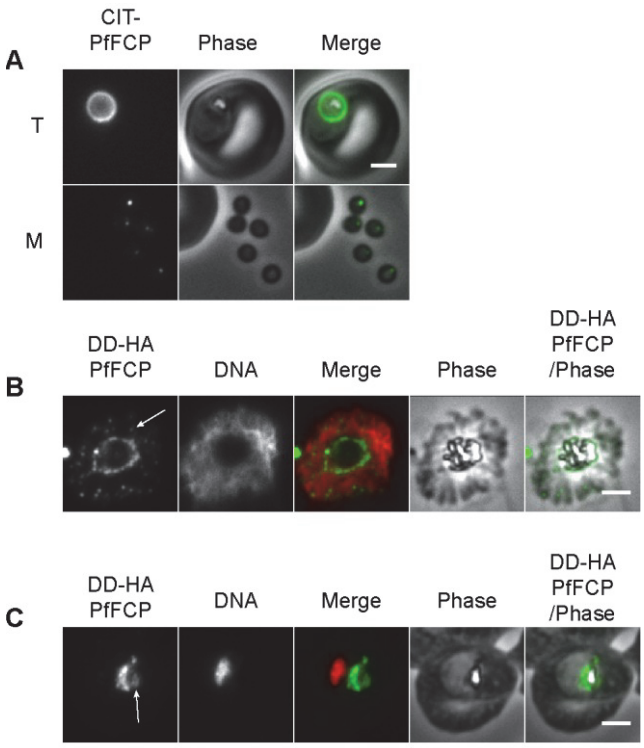

Figure 4-S2: Images of alternate PfFCP lines and fixation conditions. A and B) Wide-field epifluorescence images of fixed parasites expressing DD-HA-PfFCP (A10) after 24 hr incubation with 10 μM trimethoprim. Parasites were fixed in C) dry ice/methanol or D) 4 °C methanol for 10 min as directed in [79]. Punctate structures and FV lumen fluorescence are indicated with white arrows

Table 4-S1: Sequences of oligonucleotides used in this study. Restriction sites are underlined. RE, restriction endonuclease; UTR, untranslated region; YFP, yellow fluorescent protein; DD, destabilization domain; HA, hemagglutinin epitope tag.

Name	Oligonucleotide Sequence (5' to 3')	RE site	Purpose
569 151	GTACGCCCGGGAATAAATTATTTCTATTGATATAACAATAC GTACGCTCGAGTATATAAAAAAAAAAAAATTAAATAAAAATTA	XmaI XhoI	PCR: PfAMPN 5' UTR (bases -800 to -15
439 440	GCACGCTCGAGGGTAGCCCATCAGATTCTCTAAATG GCACGCCTAGGCATAATATTACACATTCTTCTCTGACAT	XhoI AvrII	PCR: PfFCP for C-term. YFP Fusion (bases 31 to 978)
470 471	GTACGCTCGAGCTTAAAAGAATAATAATGATCAGTCTGATTGCGGCGTTAG GTACGCCTAGGTCCTCCTCCTCCTCCCCGCCGCTCCAGAATCTCAAAGC	XhoI AvrII	PCR: ecDHFR-DD and 15nt Vps35 5' UTR (bases 1 to 477)
501 502	CTACGAGATCTCATTTTGTAAAAAAAATTAAAATATATTTATAT CTACGGAATTCTTTAATAAATATGTTCTTATATATAATGAG	BglII EcoRI	PCR: yDHOD expression cassette
532 533	GTACGCCCGGGTAAACCTCATAACAACTTTGTGTGC GTACGCTCGAGTTAAAAATTTATATATAATATATATATTATAT	XmaI XhoI	PCR: PfFCP 5'UTR bases (-820 to -15)
534 535	GCACGCTCGAGTGTATTTATATATATATGAGTAAAGGAGAAGAACTTTTC GCACGCCTAGGACTTCCTCCTAATCCTGCATTTAATAATTC	XhoI AvrII	PCR: YFP with 15nt PfFCP 5' UTR
552 553	GCACGCCTAGGATGTTAAATTCTAAAGAGAAGGAAGT GCACGGCGGCCGCTTACATAATATTACACATTCTTCTCTG	AvrII NotI	PCR: PfFCP bases 1 to 978
554	GTACGCTCGAGTGTATTTATATATATATGTATCCATATGATGTACCAGATTA TGCATTAAATTCTAAAGAGAAGGAAGTAAATG	XhoI	PCR: PfFCP with N-terminal HA tag
555 556	GTACGCTCGAGTGTATTTATATATATATGTTAAATTCTAAAGAG GTACGCCTAGGTGCATAATCTGGTACATCATATGGATAACCACCATCGGTGT TATCTGTATTATTCAAAA	XhoI AvrII	PCR: PfFCP with internal HA tag (bases 1 to 453
557	GTACGCCTAGGAATACAGATGTTCTTTCTTTATTAAAAAG	AvrII	PCR: PfFCP with internal HA tag (bases 454 to 978)
601	GTACGCCTAGGTATCCATATGATGTACCAGATTATGCAGAAAGATCTTCTCC TCAAACTTTATTATTAC	AvrII	fwd, N-terminal truncation of PfFCP for DN
677	GCACGGCGGCCGCTTAAGTTTGAGGAGAAGATCTTTCCATAAAAC	NotI	PCR: PfFCP FYVE domain
682 678	GCACGACTAGTATGTTAAATTCTAAAGAGAAGGAAGT GCACGGCGGCCGCTTATGAAGAAGAACTTGTATTTGTCATAGAG	SpeI NotI	PCR: PfFCP C-terminal truncation (bases 208 to 978)

Table 4-S2: Plasmids constructed in this study. YFP, yellow fluorescent protein; DD, *E. coli* dihydrofolate reductase destabilization domain; HA, hemagglutinin epitope tag; RFP, red fluorescent protein; hDHFR, human dihydrofolate reductase; yDHOD, *yeast* dihydroorotate dehydrogenase; DKO, double-crossover knockout.

Name of Plasmid	Promoter	Tag	Modification	Drug Resistance	Integration
pPfFCP-CIT	N/A	YFP "Citrine"	N/A	hDHFR	Homologous Recombination
pCIT-PfFCP	PfFCP 5' UTR	YFP "Citrine"	N/A	hDHFR	*piggyBac* Transposon
pCIT-FYVE	PfFCP 5' UTR	YFP "Citrine"	N-terminal fragment	hDHFR	*piggyBac* Transposon
pPfFCP-IntHA	PfFCP 5' UTR	HA	Internal epitope tag	hDHFR	*piggyBac* Transposon
pDD-HA-PfFCP	PfFCP 5' UTR	HA	N/A	hDHFR	*piggyBac* Transposon
pDD-HA-PfFCP-yDHOD	PfFCP 5' UTR	HA	N/A	yDHOD	*piggyBac* Transposon
pDD-HA-PfFCPΔFYVE	PfFCP 5' UTR	HA	N-terminal truncation	hDHFR	*piggyBac* Transposon
pDD-HA-PfFCPΔFYVE-yDHOD	PfFCP 5' UTR	HA	N-terminal truncation	yDHOD	*piggyBac* Transposon
pDD-PfFCPΔCterm-HA	PfFCP 5' UTR	HA	C-terminal truncation/ Internal epitope tag	hDHFR	*piggyBac* Transposon
pDD-PfFCPΔCterm-HA-yDHOD	PfFCP 5' UTR	HA	C-terminal truncation/ Internal epitope tag	yDHOD	*piggyBac* Transposon
pPfAMPNp- pDD-HA-PfFCPΔFYVE	PfAMPN 5' UTR	HA	N-terminal truncation	hDHFR	*piggyBac* Transposon
pPfAMPNp- pDD-HA-PfFCPΔFYVE-yDHOD	PfAMPN 5' UTR	HA	N-terminal truncation	yDHOD	*piggyBac* Transposon

CHAPTER 5:

Summary and Conclusions

The parasites of *Plasmodium* spp. have unique trafficking needs during their asexual stages in the human host. *P. falciparum* has evolved to invade human erythrocytes and efficiently endocytose host hemoglobin to its acidic degradative food vacuole. It also transports recently synthesized parasite proteins to an array of parasite specific compartments, including the FV and the apical organelles. The work presented in this dissertation provides a basis for understanding evolutionarily conserved roles of proteins involved in trafficking, as well as those specific to the parasite.

For the first time, we have identified an endosomal compartment in *P. falciparum* by investigating the presence of endosomal protein homologs of the retromer cargo-selective complex and the small GTPase Rab7 (Chapter 3). We have found that these proteins are synthesized throughout the asexual blood stage and have localized them to punctate structures near, but separate, from the Golgi apparatus. We attempted to investigate the function of both retromer and PfRab7 through various methods, but found them intractable to disruption. This indicates that they are very important to parasite proliferation and development. We also identified a homolog of a retromer recycled sorting receptor, PfSortilin, which localizes to the Golgi apparatus. While functional analysis proved unsuccessful, these descriptive studies along with those done in related species [1] are suggestive of a retromer-mediated sorting pathway to the rhoptries, a secretory apical organelle involved in host invasion.

We have also determined the distribution of the potential EEA1 homolog, PfFCP, to FV membrane where it participates in FV vesicle fusion. Typically, mammalian FYVE-domain

proteins have been localized to the early endosome [2], a weakly acidic (pH 6.8-5.9) sorting organelle [3]. The presence of PfFCP on the membrane of an acidic (pH 5.5) degradative compartment is unusual [4]. Induction of a regulatable PfFCP dominant negative resulted in missorting of endocytic and biosynthetic traffic bound for FV. We showed that PfFCP forms a dimer *in vivo* and thus the dominant negative effects are most likely the result of interference from a nonfunctional heterodimer. Taken together these data are consistent with PfFCP binding PI3P and facilitating vesicle tethering at the FV membrane. Further investigation will be necessary to prove this function, however. Tethering likely requires additional protein partners that were not found in this study due to weak or transient interactions that may require different experimental conditions. In addition, the function of the C-terminus and how it facilitates membrane association are especially interesting.

This study focused on cytosolic proteins that associate with two structures: the parasite endosome and the food vacuole that share characteristics with the mammalian late and early endosome, respectively. Evolutionary adaptation and the unique needs of the parasite resulted in protein trafficking pathways that resemble those in other eukaryotes but with key differences (Fig. 5-1). The early secretory pathway is highly conserved. Biosynthetic cargo enters the ER via the translocon complex and is transported through to the Golgi apparatus (Fig. 5-1A). There, trafficking defaults to the PV (Fig. 5-1B) and proteins can be translocated beyond the PVM into the host erythrocyte (Fig. 5-1C). Trafficking within the PM may take several routes.

In Chapter 3, we found evidence of a receptor-mediated pathway from the Golgi apparatus that passes through an intermediate compartment we called the parasite endosome (Fig. 5-1D). Currently, the only receptor identified along this pathway is PfSortilin, a parasite homolog of sortilin/Vps10. The most likely candidate for recycling of PfSortilin is a protein coat

complex known as retromer, a PfRab7 effector. Both retromer and PfRab7 have been localized to the parasite endosome. Close association between the parasite endosome and nascent rhoptries, as well as studies on the PfSortilin homolog in *T. gondii* [1], are consistent with endosome involvement in trafficking to the apical organelles, especially the rhoptries (Fig. 5-1E). Our observations agree with the current understanding of rhoptry formation by vesicle budding and fusion from the late endosome to produce potentially acidic compartments [5-7]. It does not appear, however, that early endosome maturation process is involved. The parasite endosome may play a role similar to the mammalian late endosome or trans-Golgi network.

Hemoglobin endocytosis and delivery to the FV has been studied by many groups, and the body of evidence is consistent with vesicle-mediated transport (Fig. 5-1F). Host erythrocyte cytoplasm is brought into the parasite through a specialized pore, known as a cytostome, into double membrane-bound vesicles that fuse to the FV membrane. There the hemoglobin is catabolized and toxic heme sequestered in a crystalline lattice known as hemozoin. Curiously, the FV membrane is labeled with the early endosome characteristic phosphoinositide, PI3P. In Chapter 4, we described our characterization of PfFCP, a FYVE domain containing protein located around the FV and nearby compartments. Given the domain organization of PfFCP, and that it forms a dimer *in vivo*, we suspect that PfFCP is involved with vesicle fusion at the FV membrane with the assistance of accessory proteins that have yet to be identified. Traffic to the food vacuole for synthesized proteins is not as well characterized. There is evidence that dipeptidyl aminopeptidase I, PfDPAP1, and plasmepsin II, PM2, traverse the PV en route to the FV (Fig. 5-1G) [8,9]. The FV hydrolase, plasmepsin II (PM2), is trafficked to compartments near the PPM and enters the FV through vesicle fusion (Fig. 5-1H) [9], but the existence of a direct pathway to the FV cannot be ruled out (Fig. 5-1I). From its membrane characteristics and

trafficking pathways, the food vacuole now more closely resembles an early endosome, the initial site of endocytic sorting. To our knowledge, there are no reports of post-FV trafficking as one would expect from an early endosome (Fig. 5-1J). Therefore, we hypothesize that the *P. falciparum* FV acts as a novel terminal early endosome.

In *P. falciparum,* we find many conserved components and trafficking pathways that have been characterized in model mammalian and yeast systems. The unique needs of the intraerythrocytic parasite demanded some changes, however. While these differences are interesting in their own right from an evolutionary perspective, they are also potential new targets to be exploited for anti-malarial drug development.

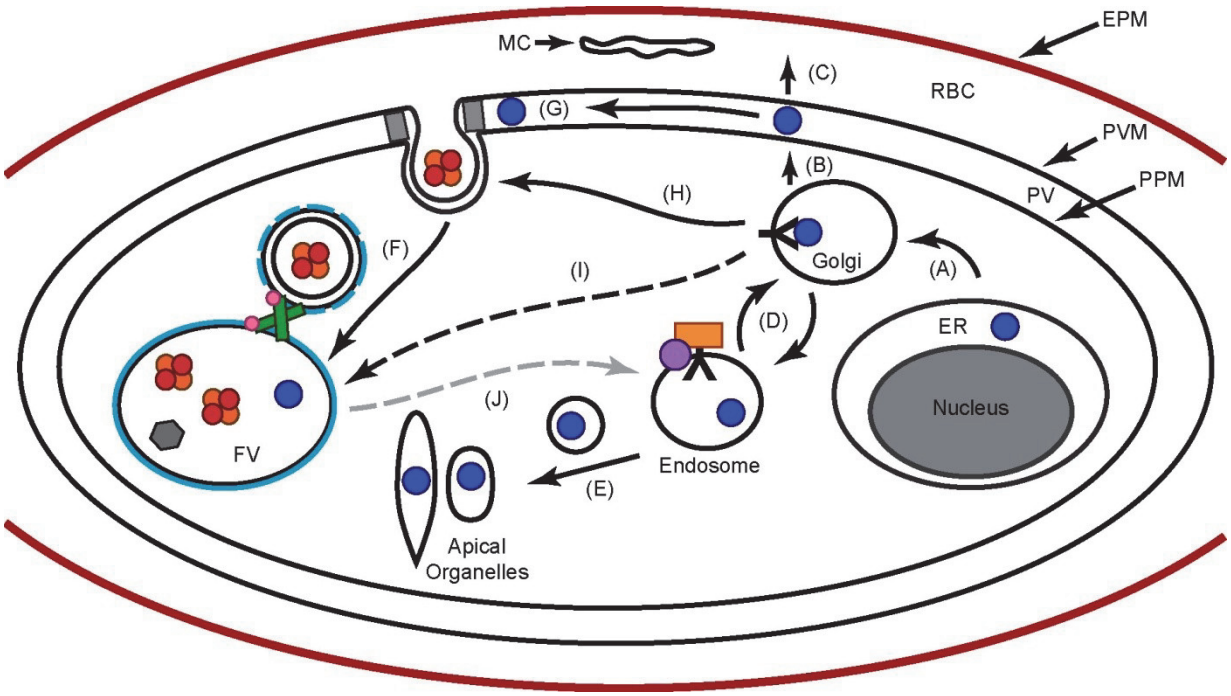

Figure 5-1: A model of protein trafficking within the malaria parasite, *P. falciparum*. The asexual parasite resides within the erythrocyte plasma membrane (EPM) of its host cell (RBC) surrounded by the RBC-derived parasitophorous vacuole membrane (PVM). A protein (blue circle) enters the secretory pathway at the ER. Transport to the Golgi apparatus is COPII-mediated (A). Default trafficking transports proteins passed the parasite plasma membrane (PPM) to the parasitophorous vacuole (PV) (B) where it can then be translocated through the PVM into the RBC, EPM (red line), or Maurer's clefts (MC) (C). The retromer cargo-selective complex (orange rectangle) and PfRab7 GTPase (purple circle) were localized to the parasite endosome where they likely assist in recycling of the sorting receptor, PfSortilin (black "Y") (D). Current evidence indicates that the endosome and PfSortilin are involved with trafficking to the apical organelles (E). Transport of hemoglobin (red/orange circles) to the FV occurs through a vesicle-mediated process (F) at the cytostome (grey rectangles). The location of PfFCP (green rectangles) most likely binds PI3P (blue circles) at the FV and possible associated compartments to facilitate vesicle docking. Other proteins (pink circles), such as a PfRab5 homolog, may also be involved but was not found in our pull-down. Trafficking to the FV may occur through the PV (G), hemoglobin vesicles (H) or by direct transport (I). No evidence of FV to endosome transport (J) has been found.

References

1. Sloves PJ, Delhaye S, Mouveaux T, Werkmeister E, Slomianny C, et al. (2012) *Toxoplasma* sortilin-like receptor regulates protein transport and is essential for apical secretory organelle biogenesis and host infection. Cell Host Microbe 11: 515-527.
2. Kutateladze TG (2006) Phosphatidylinositol 3-phosphate recognition and membrane docking by the FYVE domain. Biochim Biophys Acta 1761: 868-877.
3. Huotari J, Helenius A (2011) Endosome maturation. EMBO J 30: 3481-3500.
4. Klonis N, Tan O, Jackson K, Goldberg D, Klemba M, et al. (2007) Evaluation of pH during cytostomal endocytosis and vacuolar catabolism of haemoglobin in Plasmodium falciparum. Biochem J 407: 343-354.
5. Bannister LH, Hopkins JM, Fowler RE, Krishna S, Mitchell GH (2000) Ultrastructure of rhoptry development in *Plasmodium falciparum* erythrocytic schizonts. Parasitology 121: 273-287.
6. Ngo HM, Yang M, Joiner KA (2004) Are rhoptries in Apicomplexan parasites secretory granules or secretory lysosomal granules? Mol Microbiol 52: 1531-1541.
7. Kats LM, Cooke BM, Coppel RL, Black CG (2008) Protein trafficking to apical organelles of malaria parasites - building an invasion machine. Traffic 9: 176-186.
8. Klemba M, Gluzman I, Goldberg DE (2004) A Plasmodium falciparum dipeptidyl aminopeptidase I participates in vacuolar hemoglobin degradation. J Biol Chem 279: 43000-43007.
9. Klemba M, Beatty W, Gluzman I, Goldberg DE (2004) Trafficking of plasmepsin II to the food vacuole of the malaria parasite Plasmodium falciparum. J Cell Biol 164: 47-56.

APPENDIX A:

Biochemical characterization of *Plasmodium falciparum* dipeptidyl aminopeptidase 1

Reprinted from Molecular and Biochemical Parasitology, Vol 176, Flora Wang*, Priscilla Krai*, Edgar Deu, Brittney Bibb, Conni Lauritzen, John Pedersen, Matthew Bogyo, Michael Klemba. "Biochemical characterization of *Plasmodium falciparum*dipeptidyl aminopeptidase 1," pp. 10-20, Copyright (2011), with permission from Elsevier.

* These authors contributed equally to this work.

Author Contributions:

Flora Wang (Virginia Tech) developed the method for recombinant DPAP1 production and assess specificity of DPAP1 and human CatC with a positional scanning library.

Priscilla Krai (Virginia Tech) purified native DPAP1, characterized steady state kinetics for substrates and inhibitors.

Brittney Bibb (Virginia Tech) assisted with development of recombinant DPAP1.

Edgar Deu and Matthew Bogyo (Stanford University School of Medicine) provided a set of novel fluorogenic DPAP1/CatC substrates.

Conni Lauritzen and John Pedersen (Unizyme Laboratories A/S) provided recombinant human CatC and inhibitors.

Michael Klemba (Virginia Tech) oversaw and directed research, and wrote the article.

Abstract

Dipeptidyl aminopeptidase 1 (DPAP1) is an essential food vacuole enzyme with a putative role in hemoglobin catabolism by the erythrocytic malaria parasite. Here, the biochemical properties of DPAP1 have been investigated and compared to those of the human ortholog cathepsin C. To facilitate the characterization of DPAP1, we have developed a method for the production of purified recombinant DPAP1 with properties closely resembling those of the native enzyme. Like cathepsin C, DPAP1 is a chloride-activated enzyme that is most efficient in catalyzing amide bond hydrolysis at acidic pH values. The monomeric quaternary structure of DPAP1 differs from the homotetrameric structure of cathepsin C, which suggests that tetramerization is required for a cathepsin C-specific function. The S1 and S2 subsite preferences of DPAP1 and cathepsin C were profiled with a positional scanning synthetic combinatorial library. The S1 preferences bore close similarity to those of other C1-family cysteine peptidases. The S2 subsites of both DPAP1 and cathepsin C accepted aliphatic hydrophobic residues, proline, and some polar residues, yielding a distinct specificity profile. DPAP1 efficiently catalyzed the hydrolysis of several fluorogenic dipeptide substrates; surprisingly, however, a potential substrate with a P2-phenylalanine residue was instead a competitive inhibitor. Together, our biochemical data suggest that DPAP1 accelerates the production of amino acids from hemoglobin by bridging the gap between the endopeptidase and aminopeptidase activities of the food vacuole. Two reversible cathepsin C inhibitors potently inhibited both recombinant and native DPAP1, thereby validating the use of recombinant DPAP1 for future inhibitor discovery and characterization.

Introduction

Human malaria is caused by five species of the genus *Plasmodium*, with most of the 1-2 million annual deaths attributable to *P. falciparum*. The pathology of malaria arises from infection of host erythrocytes by the parasite. One intriguing feature of the host cell-parasite relationship during this stage is the endocytosis and catabolism of up to 75% of erythrocyte hemoglobin by *P. falciparum* [1,2]. Hemoglobin is taken up through the cytostome and delivered to an acidic compartment called the food vacuole or digestive vacuole. Three classes of endopeptidases have been implicated in the hydrolysis of globin into oligopeptides in the food vacuole: aspartic proteases (plasmepsins I, II and IV and the active-site variant histo-aspartic protease), cysteine proteases (falcipain-2, -2' and -3) and a metalloprotease (falcilysin) [3]. Inhibitors of the first two classes kill parasites and, in the case of cysteine protease inhibitors, lead to the accumulation of undegraded hemoglobin in the food vacuole [4]. In light of this evidence, enzymes that catalyze hemoglobin catabolism are regarded as attractive targets for new anti-malarial drugs.

The endopeptidases described above do not efficiently release small peptides or amino acids from globin oligopeptides; rather, exopeptidases are required for this task. A cysteine exopeptidase termed dipeptidyl aminopeptidase 1 (DPAP1) is located in the *P. falciparum* food vacuole [5]. We hypothesize that this enzyme reduces the oligopeptide products of endopeptidase cleavage to dipeptides, thereby generating substrates for the vacuolar aminopeptidase PfA-M1 [6]. Attempts to disrupt the DPAP1 gene have been unsuccessful, which suggests that the enzyme makes an important contribution to hemoglobin catabolism during the intraerythrocytic cycle [5]. Although DPAP1 is one of three related DPAP enzymes encoded in the parasite genome, current evidence suggests that only DPAP1 resides in the food vacuole. In

contrast to DPAP1, DPAP3 is expressed late in the asexual replication cycle [7]. Abrogation of DPAP3 activity with a specific inhibitor implicates this enzyme in parasite egress [7]. DPAP2 (gene ID PFL2290w) does not appear to be expressed during asexual erythrocytic replication (unpublished observations). Together, these results suggest that the design of inhibitors that block both DPAP1 and DPAP3 could be a desirable anti-malarial strategy as the simultaneous impairment of two distinct, critical pathways would not only kill the parasite but could also delay the onset of resistance.

Mammals possess a single DPAP1 ortholog, termed cathepsin C or dipeptidyl peptidase I (to avoid confusion with DPAP1, the mammalian enzyme is referred to here as cathepsin C). Cathepsin C has two distinct roles. First, it contributes to general protein catabolism within the lysosome. Second, the enzyme is found in secretory granules of immune effector cells (cytotoxic lymphocytes, mast cells and neutrophils) where it activates granular serine proteases by removing an inhibitory N-terminal dipeptide sequence [8-10]. Its role as a mediator of inflammatory processes has made cathepsin C an appealing target for the development of drugs against some inflammation-based pathologies [11,12].

Cathepsin C and DPAP1 are members of the large C1 family of cysteine endo- and exopeptidases, of which papain is the archetypal member. Papain is comprised of a prodomain, which is proteolytically removed to generate the mature enzyme, and two catalytic domains. In the case of cathepsin C, the polypeptide of the catalytic domains is cleaved into “heavy” and “light” chains. An additional domain, termed the exclusion domain or the residual pro-part, is found in cathepsin C and its orthologs and positions substrates such that peptide bond hydrolysis occurs between the second and third residues [13,14]. Two other structural features, tetramerization and binding of a monovalent anion in the S2 pocket, differentiate cathepsin C

from other C1-family exo- and endopeptidases [13,14]. (The nomenclature of Schechter and Berger [15] is used here to identify substrate residues (P1, P2 etc.) and the corresponding enzyme subsites (S1, S2 etc.) with which they interact.) While it is reasonable to presume that these latter two variations on the papain scaffold enhance the ability of cathepsin C to carry out its biological roles, their contribution to cathepsin C function remains enigmatic.

The aim of the studies presented here is to elaborate the biochemical properties of DPAP1 for the purpose of further understanding its role in the malaria parasite and of establishing the similarities and differences between this enzyme and its human homolog cathepsin C. Toward this goal, we have compared the oligomerization state, chloride activation and pH-activity relationship of DPAP1 to those of cathepsin C. We have also generated a detailed profile of the subsite specificities of both DPAP1 and cathepsin C for the two substrate residues upstream of the scissile bond. These specificities were then further defined through kinetic characterization of these enzymes with a set of P2-diverse fluorogenic dipeptide substrates and with two established cathepsin C inhibitors. To accomplish these studies, we have developed a method for the recombinant production and *in vitro* activation of DPAP1.

Results

Purification of native DPAP1.

To obtain material for biochemical characterization, we first attempted to purify DPAP1 from saponin-treated trophozoite-stage parasites. As described previously [5], a three-column protocol yielded highly purified native DPAP1; however, yields of enzyme were low and activity was unstable, probably due to the adsorption of the minute quantities of the enzyme to surfaces. By modifying the purification protocol to consist of two (instead of three) chromatographic

steps, sufficient native enzyme for the studies described here was obtained; however, the resulting enzyme preparation contained many other polypeptides (data not shown).

Generation and activation of recombinant DPAP1.

To produce greater quantities of DPAP1 at higher purity, we have developed a method for the production of recombinant enzyme by expression in *Escherichia coli*. We took into consideration three factors that would likely be important for generating recombinant DPAP1 with native-like qualities. First, expression of the protein in soluble form would be required for proteolytic removal of the proregion *in vitro*. Second, the amino terminus of the exclusion domain would have to begin with a specific sequence (Fig. A-1A). Crystal structures of cathepsin C reveal that the amino-terminal Asp residue of the exclusion domain forms a critical interaction through its sidechain carboxylate with the amino group of the substrate [13,14,16]. The homologous residue in DPAP1 (Asp28) likely plays an identical role. Thus, the exclusion domain of recombinant DPAP1 should begin at Asp28. Third, the internal proregion (also called the activation peptide) would have to be proteolytically removed to fully activate the enzyme (Fig. A-1A). In the case of recombinant cathepsin C, excision of the proregion results in a 2000-fold increase in activity [17].

Prior reports of expression in *E. coli* of soluble, active *P. falciparum* peptidases as fusions to the C-terminus of maltose binding protein (MBP) [18,19] motivated us to attempt expression of an MBP-DPAP1 chimera (Fig. A-1). A hexahistidine tag was placed at the C-terminus to permit a second mode of affinity purification. To generate the presumed native N-terminal sequence of the exclusion domain, a modified tobacco etch virus (TEV) protease cleavage site was introduced between MBP and DPAP1 in which the preferred Gly or Ser

residue in the last position is replaced with Asp (Fig. A-1A). Cleavage of this modified sequence would result in an exclusion domain N-terminus that begins with Asp28. Aspartate is tolerated in the last position of the TEV protease cleavage sequence, although cleavage efficiency is somewhat reduced [20].

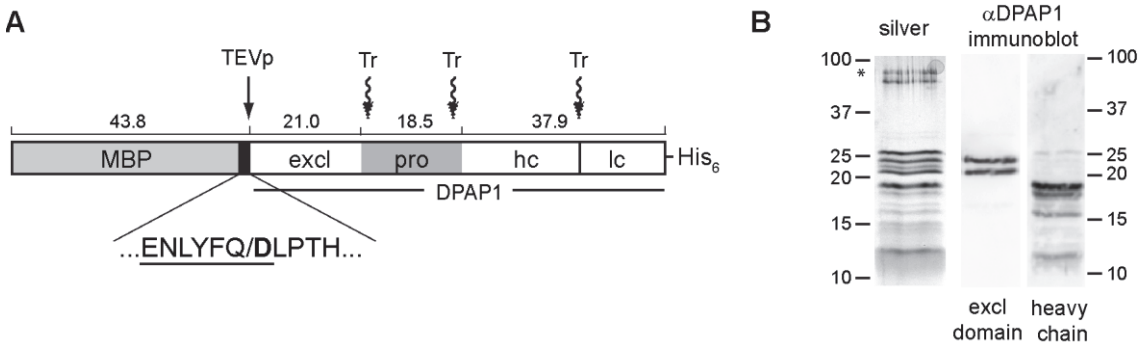

Figure A-1: (A) Schematic diagram of the recombinant MBP-DPAP1-His_6 fusion. The white boxes indicate those regions of DPAP1 found in the mature protein, namely the exclusion domain (excl) and catalytic region, the latter being proteolytically cleaved to generate a heavy chain (hc) and a light chain (lc). The gray box within the DPAP1 sequence is the proregion (pro), the boundaries of which are not precisely known but were estimated from a sequence alignment with cathepsin C [5]. The black box represents the linker between MBP and DPAP1. The sequence below shows the TEV protease recognition sequence (underlined) with the cleavage site indicated by "/". The resulting N-terminal Asp residue is shown in bold. The approximate positions of trypsin (Tr) cleavage are indicated with wavy arrows. Additional/alternate cleavage sites (not shown) give rise to size heterogeneity in the mature DPAP1 polypeptides. The hexahistidine tag is retained in the mature recombinant protein. Predicted polypeptide sizes are shown above the boxes in kDa. (B) Analysis of purified rDPAP1 by reducing SDS-PAGE. Left panel: silver stain. Contaminating proteins (probably keratins) are indicated with an asterisk. Right panels: immunoblots using antibodies that recognize the exclusion domain ("excl domain") or the heavy chain. Sizes of markers are given in kDa.

MBP-DPAP1-His_6 was expressed in soluble form in *E. coli* and was purified by immobilized metal affinity chromatography (IMAC). Cleavage at the TEV protease recognition site between MBP and DPAP1 was carried out using an MBP-TEV protease fusion [21], which permitted the separation of DPAP1-His_6 from MBP-containing species (cleaved MBP, uncleaved MPB-DPAP1-His_6 and MBP-TEV protease) by interaction of the latter with amylose resin. Most

of the cleaved DPAP1-His_6 sedimented upon high-speed centrifugation, a result that is likely due to the formation of aggregates of incorrectly folded protein. The formation of disulfide bonds may be a limiting factor in the folding of DPAP1 in the *E. coli* cytosol, as soluble enzyme was only obtained when MPB-DPAP1-His_6 was produced in a *trxB/gor E. coli* strain that yields higher levels of disulfide bond formation in the cytosol [22]. Based on a sequence alignment with cathepsin C, three of the five disulfide bonds in the latter protein are expected to be conserved in DPAP1 (not shown).

The identities of the endoproteases that excise the DPAP1 proregion and cleave the catalytic region into heavy and light chains *in vivo* are unknown. We attempted to mimic the *in vivo* proteolytic events by treating recombinant DPAP1 with commercially-available peptidases. Trypsin and papain were chosen as one (trypsin) is relatively selective at the P1 position while the other (papain) is not; thus, it was expected that each would produce a distinct spectrum of cleavages in recombinant DPAP1. In addition, papain has been successfully used to activate recombinant cathepsin C [23]. Incubation of DPAP1-His_6 with either protease resulted in a moderate (2 to 3-fold) increase in activity. When the kinetics of hydrolysis of the DPAP1 substrate Pro-Arg-AMC [5] by trypsin-treated DPAP1-His_6, papain-treated DPAP1-His_6 and native DPAP1 was compared, the trypsin-activated enzyme exhibited a hyperbolic relationship between initial velocity and substrate concentration, like that of the native enzyme (Fig. A-S1). In contrast, the papain-activated enzyme reproducibly exhibited substrate inhibition (Fig. A-S1). Thus, we selected the trypsin-activated DPAP1-His_6 (referred to from here on as "rDPAP1") for further characterization. rDPAP1 was further purified by metal affinity and gel filtration chromatography.

Highly purified rDPAP1 contains an ensemble of polypeptides with sizes between ~12 and ~27 kDa (Fig. A-1B). Immunoblotting with antibodies that recognize the exclusion domain or the heavy chain of the catalytic region revealed heterogeneous processing of rDPAP1 by trypsin (Fig. A-1B). The exclusion domain appeared as a doublet of 21 and 23 kDa species. The heavy chain was represented by four major polypeptides ranging in size from 12 to 18 kDa. Other bands appearing in this size range could be light chain polypeptides, for which an antibody is not available. A time course of trypsin activation indicated that, under the conditions employed here, the observed ensemble of polypeptides was stable over time (Fig. A-S2), which suggests that the size heterogeneity of the exclusion domain and heavy chain is not simply due to incomplete proteolysis. The ~27 kDa band detected by silver staining was not recognized by either antibody (Fig. A-1B). This polypeptide is unlikely to correspond to the excised prodomain (predicted size of 18.5 kDa) but could be a C-terminal fragment of DPAP1 (the heavy chain antibody recognizes a peptide epitope 31 kDa from the C-terminus). Since trypsin is predicted to have a molecular mass of ~27 kDa, we assessed whether trypsin activity is present in the rDPAP1 preparation. Using a fluorogenic trypsin substrate and 10-fold more protein than typically included in a DPAP1 assay, no trypsin activity could be detected under the conditions of the standard DPAP1 assay or of an optimized trypsin assay (see Materials and Methods). Therefore we conclude that the 27 kDa band corresponds to a C-terminal fragment of DPAP1 or to inactive trypsin.

DPAP1 quaternary structure.

One feature that distinguishes mature mammalian cathepsin C from other C1-family cysteine peptidases is its tetrameric quaternary structure consisting of a dimer of dimers [13,14].

To determine whether DPAP1 forms a tetramer at physiologically relevant pH values, the apparent molecular mass of the native enzyme was determined by gel filtration chromatography at pH 6 and was found to be 51 kDa (Fig. A-2A). Because the sites of *in vivo* proenzyme cleavage are not known, the predicted molecular mass of the native enzyme cannot be precisely calculated; however, if the boundaries of the proenzyme are assumed to be similar to those of cathepsin C [5], a molecular mass of 59 kDa can be estimated for mature native DPAP1. Thus, the migration of the enzyme on a gel filtration column is consistent with a monomeric rather than a tetrameric structure. In contrast, under the same elution conditions recombinant cathepsin C migrated with an apparent molecular mass of 153 kDa (Fig. A-2A), which is close to the value of 140 kDa that was previously reported for this enzyme [17].

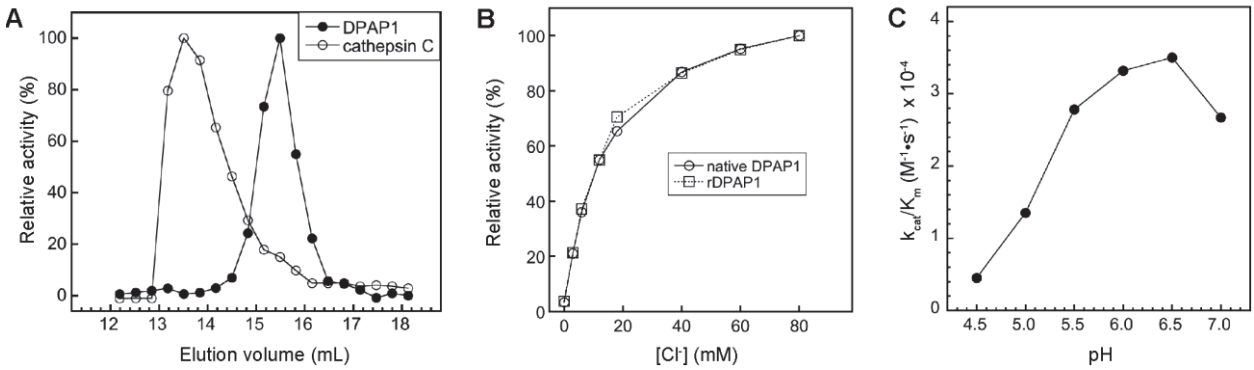

Figure A-2: (A) Elution of native DPAP1 (filled circles) and cathepsin C (open circles) from a Superdex 200 gel filtration column in 50 mM Na-MES pH 6, 200 mM NaCl and 1 mM EDTA. For each protein, activities in fractions are shown as percent relative activity with the highest activity set to 100%. (B) Activation of native (circles) and recombinant DPAP1 (squares) by chloride at pH 6.0. Ionic strength was held constant with Na_2SO_4. Activity values are expressed as relative activity with the highest activity set at 100%. Data points are the average of duplicate assays. (C) The catalytic efficiency (k_{cat}/K_m) of recombinant DPAP1 within the pH range 4.5 to 7.0 with the substrate Pro-Arg-AMC. Chloride concentration (30 mM) and total ionic strength (100 mM) were held constant at all pH values.

Activation of DPAP1 by chloride.

Cathepsin C appears to be unique among C1-family cysteine peptidases in exhibiting activation by univalent anions, of which halide ions such as chloride are the most potent activators [24,25]. To assess whether such activation is a conserved feature of cathepsin C-like dipeptidases, we examined the effects of chloride concentration on DPAP1 activity. Preliminary experiments indicated that DPAP1 activity was sensitive to changes in ionic strength (data not shown); therefore, in the analysis of chloride activation, ionic strength was held constant with sodium sulfate (the divalent sulfate anion does not activate cathepsin C [25]). To deplete chloride from stock solutions of DPAP1, native and recombinant enzyme were extensively dialyzed against chloride-free buffer. In both cases, strong activation was observed upon the addition of millimolar concentrations of chloride to enzyme assays (Fig. A-2B). Around 3% activity was observed in the absence of added chloride (relative to activity in 80 mM Cl^-). To determine whether this was due to incomplete dialysis of chloride from the DPAP1 stock, native DPAP1 was purified by gel filtration chromatography in chloride-free buffer. This preparation retained a similar level of residual activity (data not shown). These results are most consistent with a hyperbolic activation mechanism for chloride ion in which the enzyme does not exhibit an absolute chloride requirement for either substrate binding or turnover [26]. However, it is formally possible that chloride is essential for binding and/or turnover (i.e., chloride is an essential activator) but has not been completely eliminated from the assay solution or from the enzyme. For practical purposes, a chloride concentration of 30 mM was found to be an optimal balance between the activation of DPAP1 by chloride and the suppression of activity as ionic strength increases. Thus, this concentration was routinely used in DPAP1 assays.

DPAP1 is an efficient catalyst at acidic pH.

If DPAP1 is a catalyst of peptide bond hydrolysis in the food vacuole, it should function efficiently at the acidic lumenal pH of this organelle. The efficiency of rDPAP1 catalysis of Pro-Arg-AMC hydrolysis in the pH range 4.5 to 7.0 was determined at constant chloride concentration and ionic strength (Fig. A-2C). The pH-activity profile has an apparent bell shape that resembles those of cathepsin C [27-29]. Catalytic efficiency (k_{cat}/K_m) was highest in the pH range 6.0 – 6.5 but was also substantial at pH 5.5, which is within the range of several estimates of food vacuole pH [30-33]. These data are therefore consistent with a catalytic role for DPAP1 in peptide hydrolysis in the malarial food vacuole. The bell-shaped pH-activity profile of C1 family peptidases such as papain has been attributed to protonation of the active site cysteine (acidic arm) and deprotonation of the histidine sidechain that ion pairs with the catalytic cysteine (basic arm) [34]. While that may be the case for DPAP1 and cathepsin C as well, it should be noted that the substrate contains a free a-amino group that ionizes with a pK_a of ~8 [35] and that the affinity of chloride for cathepsin C shows a pH dependence, with higher affinity at lower pH [36].

S1 and S2 subsite specificities of DPAP1 and cathepsin C.

The specificities of peptidases are dictated in large part by the interactions of substrate sidechains with cavities or surfaces of the enzyme, which are referred to as subsites. Structures of C1-family cysteine peptidases complexed with inhibitors have revealed that enzyme interactions are most substantial with the P1, P2 and P3 residues on the N-terminal side of the scissile bond and with the P1' and P2' residues on the C-terminal side [37,38]. In the case of the dipeptidyl aminopeptidases DPAP1 and cathepsin C, the S3 subsite is occluded by the exclusion

domain; therefore, the S1 and S2 subsites are major determinants of substrate specificity. Using a positional scanning synthetic combinatorial library, we have profiled the S1 and S2 subsite specificities of DPAP1 and human cathepsin C to investigate: i) whether DPAP1 accepts a wide range of amino acid residues in the first two positions of the substrate, which would support a general role for DPAP1 in peptide catabolism in the *P. falciparum* food vacuole; and ii) whether the subsite preferences of DPAP1 have diverged from those of cathepsin C, perhaps indicating functional specialization of the former as an enzyme dedicated to the catabolism of hemoglobin peptides. The latter point is also clearly of interest if we wish to design inhibitors that are specific for the parasite enzyme over that of the human host.

Positional scanning libraries (PSL) are powerful tools with which to profile the subsite specificities of peptidases [39]. Here, we have employed a fluorogenic dipeptidyl-7-amido-4-carbamoylcoumarin (dipeptide-ACC) PSL (Fig. A-3A) to explore the S1 and S2 subsite preferences of native and recombinant DPAP1 and of human cathepsin C. This PSL has been previously used to profile the specificities of the serine dipeptidyl peptidases II, IV and VII [40]. The PSL is divided into two sub-libraries, the structures of which are depicted in Fig. A-3A. In each sub-library, one position (P1 or P2) is varied to contain each of twenty amino acids (all of the standard proteinogenic amino acids except cysteine plus norleucine, which is abbreviated Nle here). The other position in the dipeptide is occupied by an equimolar mixture of these same 20 amino acids, which reduces the influence of sidechain interactions between adjacent substrate residues on the observed preferences [39]. We first compared the subsite preferences of native DPAP1 and cathepsin C. Then, to validate the use of rDPAP1 in biochemical studies, its specificity profile was compared to that of the native enzyme.

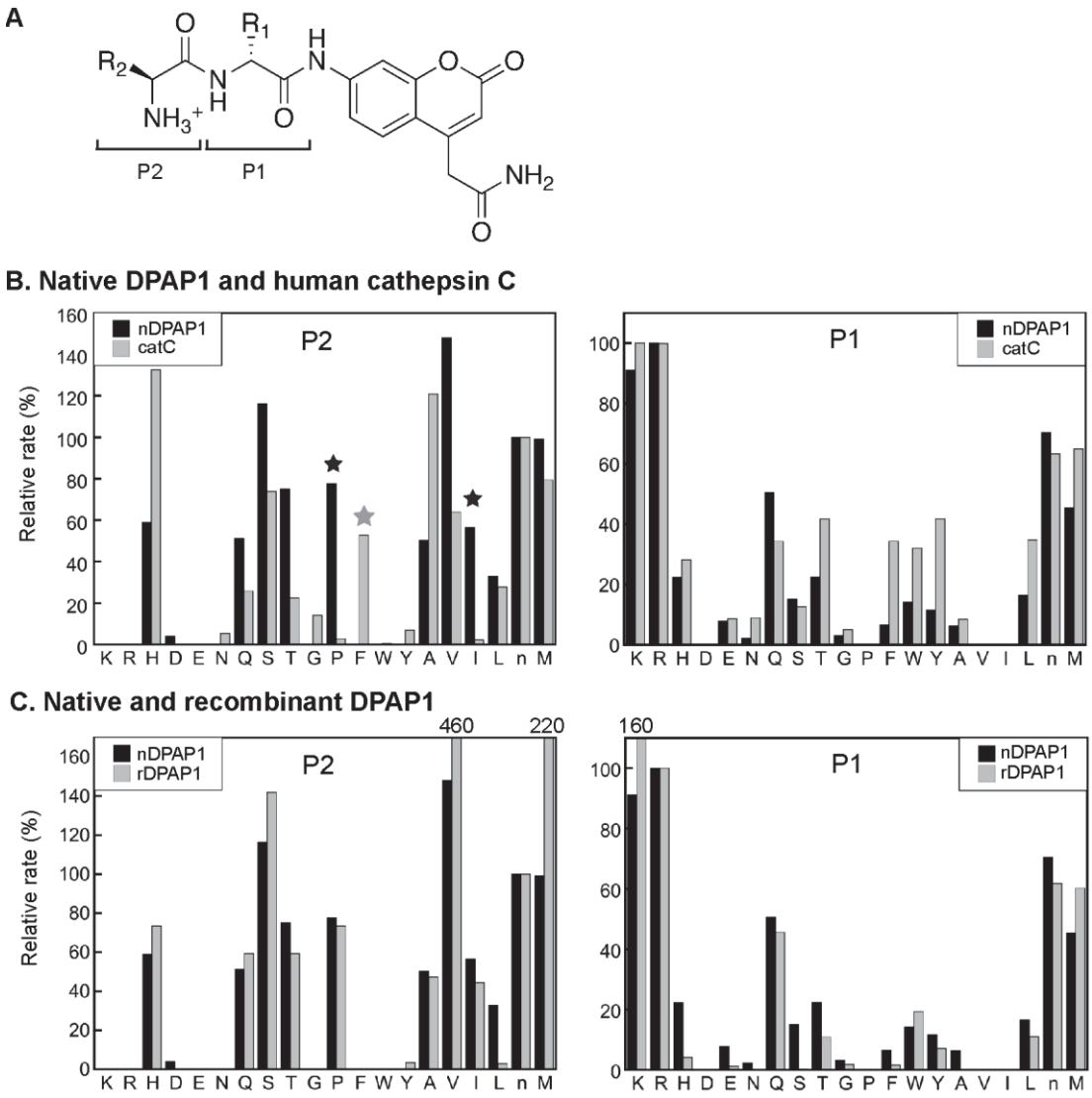

Figure A-3: S1 and S2 specificity profiles of DPAP1 and cathepsin C. (A) Structure of the dipeptidyl-ACC positional scanning library. The P1 and P2 residues are indicated. In the P1 sublibrary, the each member contains a defined residue at the P1 position (the identities of which are indicated in the x-axis labels of the right panels of (B) and (C)) and the P2 position consists of an equimolar mixture of 20 amino acids. In the P2 sublibrary, the P2 position is defined (indicated in the x-axis labels of the left panels of (B) and (C)) and the P1 position is an equimolar mixture. (B) S1 and S2 specificities of native DPAP1 (black bars) and cathepsin C (gray bars). Data are reported as relative rates with those for Arg (P1 dataset) and norleucine (P2 dataset) set to 100%. The P1 or P2 amino acid is indicated with single-letter code, with n representing norleucine. Black stars indicate members of the P2 sublibrary that are substantially better substrates for DPAP1 compared to cathepsin C; a grey star indicates the P2 sublibrary member that is a much better substrate for cathepsin C than DPAP1. Each data point is the average of duplicate assays. nDPAP1, native DPAP1; catC, cathepsin C. (C) Comparison of the S1 and S2 specificities of recombinant DPAP1 with those of the native enzyme. Normalization of rates was as in (B). Values of rates that are off-scale are indicated above the graphs. rDPAP1, recombinant DPAP1. Each data point is the average of duplicate assays.

The S1 subsite specificities of native DPAP1 and cathepsin C are shown in Fig. A-3B (right panel). The relative preferences are similar: both enzymes prefer unbranched residues (Arg, Lys, Met and Nle) at this position. Consistent with previous observations with cathepsin C [25,41], peptides with Ile or Pro in the P1 position were not hydrolyzed. As this is also the case for Val, it appears that b-branched amino acids are not readily accommodated in the S1 subsite of either enzyme. Acidic residues, Ala and Gly in the P1 position also made for poor substrates.

The S2 subsite of cysteine peptidases is typically the most restrictive of the subsites upstream of the scissile bond [37,38]. The S2 preferences of native DPAP1 and cathepsin C are shown in Fig. A-3B, left panel. Aliphatic (but not aromatic) hydrophobic residues generally made for good substrates for both enzymes. DPAP1 and cathepsin C also exhibited a preference for the small hydrophilic residues Ser and Thr as well as the larger sidechains of Gln and His at the P2 position. Substrates with the cationic sidechains of Arg and Lys at the P2 position were not detectably hydrolyzed by either DPAP1 or cathepsin C, an observation that is consistent with previous reports for cathepsin C [25,41,42]. The specificity profiles for DPAP1 and cathepsin C appear to be distinct from those of other C1-family cysteine proteases for which PSL data are available (see Discussion).

Although the S2 specificities of DPAP1 and cathepsin C were broadly similar, there were a few P2 residues that were much more highly preferred by one enzyme. In the case of DPAP1, Pro and Ile were much more favorable substrates (in a relative sense) than they were with cathepsin C (Fig. A-3B, left, black stars). On the other hand, a dipeptide containing a P2 Phe residue made for a good cathepsin C substrate but was not detectably hydrolyzed by DPAP1 (Fig. A-3B, left, gray star). These data suggest that there are differences in the accommodation of

certain substrate P2 residues within the S2 subsites of the two enzymes. This possibility was further explored with defined substrates.

The S1 and S2 specificities observed with native DPAP1 were reproduced with the recombinant enzyme (Fig. A-3C, right and left panels respectively). Importantly, the S2 specificity profile noted above (aliphatic hydrophobic, small hydrophilic, Pro, Gln and His) was observed in the recombinant enzyme. For unknown reasons, a few residues appeared to be much more highly preferred by the recombinant enzyme compared to native DPAP1; for example, relative rates with P2 Val and Met were 3.1- and 2.2-fold higher for recombinant enzyme over native (Fig. A-3C). Kinetic analysis of a dipeptide substrate incorporating a P2 Val residue suggests that these outliers are probably in error.

Kinetic analysis of DPAP1 and cathepsin C.

To further investigate the differences in S2 substrate specificities between DPAP1 and cathepsin C noted above, we determined the kinetics of hydrolysis of a panel of fluorogenic dipeptide substrates with a fixed P1 Arg residue and variable P2 residues. Arg was selected as the P1 residue because it is highly preferred by both enzymes. P2 residues were selected that, based on the PSL results, appeared to be preferred by: i) both enzymes (Val); ii) DPAP1 only (Ile, Pro); or iii) cathepsin C only (Phe), or were disfavored by both enzymes (Arg).

rDPAP1 catalyzed the hydrolysis of the P2-Pro, -Val and -Ile substrates (Table 1). The rank order of catalytic efficiency (k_{cat}/K_m) followed that predicted from the PSL data: Val>Pro>Ile. The K_m and k_{cat} values varied much more widely for these three substrates than the k_{cat}/K_m values; for example, Ile-Arg-ACC exhibited a 5-fold lower K_m and a 10-fold lower k_{cat} than Val-Arg-ACC, resulting in a two-fold change in k_{cat}/K_m. To validate these results obtained

with rDPAP1, the kinetics of hydrolysis of Pro-Arg-AMC and Val-Arg-ACC by partially purified native DPAP1 was examined. Differences in K_m values for the two enzymes were within experimental error in both cases (Table 1). The k_{cat} values (and therefore k_{cat}/K_m values) were 3- to 5-fold lower for recombinant DPAP1; possible reasons for this are given in the Discussion. Consistent with the PSL data, no hydrolysis was observed for the substrates Phe-Arg-ACC and Arg-Arg-ACC at concentrations up to 500 μM by either recombinant or native DPAP1.

Table A-1: Kinetic parameters for hydrolysis of fluorogenic dipeptide substrates.

Substrate	Enzyme	K_m (μM)[a]	k_{cat} (s^{-1})[a]	k_{cat}/K_m ($M^{-1}•s^{-1}$)[a]	K_i (μM)
Pro-Arg-AMC	nDPAP1	84 ± 9	6.2 ± 0.4	(7.4 ± 0.2) x 10^4	
	rDPAP1	79 ± 2	1.8 ± 0.1	(2.3 ± 0.1) x 10^4	
	cathepsin C	130 ± 10	490 ± 10	(3.6 ± 0.1) x 10^6	
Val-Arg-ACC	nDPAP1	21 ± 2	3.5 ± 0.1	(1.7 ± 0.1) x 10^5	
	rDPAP1	20 ± 1	0.72 ± 0.02	(3.7 ± 0.1) x 10^4	
	cathepsin C	51 ± 8	180 ± 10	(3.6 ± 0.3) x 10^6	
Ile-Arg-ACC	rDPAP1	3.9 ± 0.2	0.072 ± 0.003	(1.9 ± 0.1) x 10^4	
	cathepsin C	28 ± 2	17 ± 1	(6.3 ± 0.4) x 10^5	
Phe-Arg-ACC	nDPAP1	NH[b]	NH	NH	
	rDPAP1	NH	NH	NH	2.2
	cathepsin C	ND[c]	ND	ND	

[a] Values are reported as means and standard deviations from triplicate data sets for each substrate/enzyme combination. [b] NH, no hydrolysis. [c] ND, kinetic parameters were not determined due to substrate inhibition.

Cathepsin C catalyzed the hydrolysis of substrates with P2-Phe, -Pro, -Val and -Ile substrates. For the latter three, the rank order of catalytic efficiency was Val, Pro > Ile (Table A-1). Values of k_{cat}/K_m were in the range (10^6 – 10^7 $M^{-1}•s^{-1}$) of those reported previously for similar

substrates [41]; these values were up to 50-fold greater than those of DPAP1. Surprisingly, the expected selectivity for a P2-Val over a P2-Pro residue was not apparent in the context of a P1-Arg residue. In the case of Phe-Arg-ACC, substrate inhibition was observed (Fig. A-S3); therefore, kinetic constants for Phe-Arg-ACC turnover were not determined. As with DPAP1, no turnover of Arg-Arg-AMC was observed.

Given the inhibition of cathepsin C observed with Phe-Arg-ACC, we investigated whether this compound could inhibit DPAP1. Phe-Arg-ACC was a potent inhibitor of the hydrolysis of Pro-Arg-AMC catalyzed by rDPAP1. Dixon analysis yielded a K_i of 2.2 mM and indicated that the inhibition was purely competitive (data not shown). Thus, Phe-Arg-ACC appears to interact with DPAP1 in a conformation that is unproductive for catalysis and that blocks the binding of other substrates.

Inhibition of DPAP1 by semicarbazide- and nitrile-containing peptide analogs

Peptide analogs containing semicarbazide and nitrile pharmacophores have been shown to be effective reversible inhibitors of C1-family cysteine proteases including cathepsin C [11,12,43]. To further validate recombinant DPAP1 as a reagent for small-molecule inhibitor discovery, we have determined the inhibition constants of two established cathepsin C inhibitors (Fig. A-4; [11,43]) for native and recombinant DPAP1. Both were potently inhibited with sub-nanomolar K_i values for the semicarbazide **1** and single-digit nanomolar K_i values for the peptide nitrile **2** (Fig. A-4 and Fig. A-S4). Importantly, for each inhibitor the differences in the K_i values for native and recombinant DPAP1 were within experimental error. We also determined inhibition constants for cathepsin C under the assay conditions used for DPAP1. The semicarbazide **1** was a slow, tight-binding inhibitor of cathepsin C and was analyzed accordingly

(see Supplementary Methods and Fig. A-S4). The K_i values of both inhibitors for cathepsin C (Fig. A-4) were within an order of magnitude of the respective K_i values for DPAP1, an observation that underscores the potential difficulty of developing peptide-based compounds that specifically inhibit DPAP1 over its host homolog.

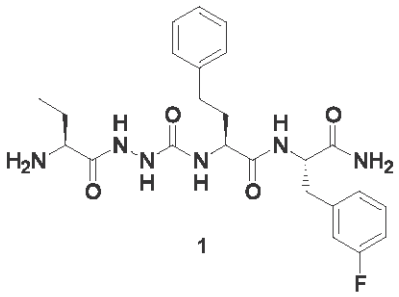

1

	K_i (nM)
rDPAP1	0.70 ± 0.10
nDPAP1	0.63 ± 0.05
catC	0.16 ± 0.01

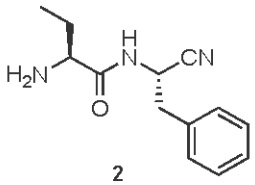

2

	K_i (nM)
rDPAP1	8.7 ± 0.9
nDPAP1	8.4 ± 0.3
catC	24 ± 11

Figure A-4: K_i values for inhibition of native DPAP1 (nDPAP1), recombinant DPAP1 (rDPAP1) and cathepsin C (catC) by peptide analogs containing semicarbazide (1) and nitrile (2) pharmacophores.

Discussion

To obtain biochemical quantities of highly purified DPAP1, we developed a method for the production of recombinant DPAP1 in *E. coli* and for its processing and activation *in vitro*. Mature rDPAP1 was obtained by limited cleavage of proDPAP1 with bovine pancreatic trypsin which resulted in removal of the proregion between the exclusion domain and the catalytic domains as well as cleavage of the catalytic domains into heavy and light chains. Heterogeneity of the exclusion domain and heavy chain of rDPAP1 was observed following trypsin treatment. Alternate processing sites have been observed in the heavy chain of native DPAP1 [5] and in the

exclusion domain of native cathepsin C [44], the functional significance of which is unknown. It was important to consider whether contaminating trypsin activity could confound the data obtained with rDPAP1. We were unable to detect trypsin activity using a trypsin substrate (which is a more sensitive probe of trypsin activity than the DPAP1 substrates used here) and 10-fold more protein than was typically added to DPAP1 assays. Thus, the presence of active trypsin, if any, in the rDPAP1 preparation appears to be below the limit of detection of our assays.

The biochemical attributes of rDPAP1 were validated against a partially purified preparation of native enzyme. Several key enzymatic properties were recapitulated with the recombinant enzyme, including activation by chloride ion, highly similar S1 and S2 subsite preferences, essentially identical K_m values with two fluorogenic dipeptide substrates and nearly identical inhibition constants for two reversible inhibitors with distinct pharmacophores. The one substantive difference between them is the ~4-fold lower k_{cat} values for rDPAP1. Possible explanations for this difference include inaccuracies in the immunoblot-based quantitation of native DPAP1, the presence of inactive enzyme in the recombinant preparation, or subtle structural changes deriving from differences in polypeptide processing *in vivo* and *in vitro*. With this one caveat in mind, the results presented here validate the use of recombinant DPAP1 for inhibitor screening and assessment.

A number of characteristics distinguish cathepsin C from its brethren in the C1 cysteine peptidase family: a homotetrameric structure, the presence of the exclusion domain, and activation by chloride. Our comparison of divergent (protozoan and metazoan) homologs sheds light on those features that are conserved (the presence of an exclusion domain and chloride activation) and highlights that which is unique to the mammalian enzyme (a tetrameric

quaternary structure). The exclusion domain of cathepsin C is an autonomously-folding b-barrel with structural similarity to a metalloprotease inhibitor from *Erwinia chrysanthemi* [14]. It defines amino-dipeptidase activity by interacting with the amino terminus of the substrate and thereby preventing endopeptidase activity [13,14,16]. In mature DPAP1, the exclusion domain almost certainly serves the same purpose. The exclusion domain of cathepsin C also acts as a chaperone to facilitate folding of the catalytic region [45]. Whether it has a similar chaperone function in DPAP1 remains to be determined. The observation of chloride activation in DPAP1 suggests that this property was present in an ancestral cathepsin C pre-dating divergence of the protozoan and metazoan lineages. The activating chloride ion is most likely that observed at the bottom of the S2 pocket in the x-ray crystal structures of rat and human cathepsin C [13,14]. Consistent with this notion, the one residue that co-ordinates the chloride ion with its sidechain, Tyr323, is conserved in DPAP1. It has been proposed that the bound chloride ion stabilizes helix 3 of cathepsin C by interacting with the helix dipole [13].

The proenzyme form of mammalian cathepsin C is a dimer that associates to form a dimer of dimers (i.e., a homotetramer) upon maturation [17]. Based on its mobility on a gel filtration column, DPAP1 appears to be a monomeric enzyme, as are other C1-family peptidases; however, we cannot rule out the possibility that DPAP1 forms a tetramer at higher concentration or under different environmental conditions. The reasons for the unusual quaternary organization of cathepsin C have been somewhat of a mystery. It has been suggested that tetramerization stabilizes the association of the exclusion domain with the two catalytic domains [13]. Our results indicate that tetramerization is not a structural requirement for this interaction and that the acquisition of a tetrameric structure probably occurred following divergence of the protozoan and metazoan lineages. One possibility is that the tetrameric structure enhances the affinity

and/or specificity of cathepsin C for its protein substrates (the immune cell serine proteases granzyme A and B, mast cell chymase and neutrophil elastase, cathepsin G and proteinase 3 [8-10]) by providing interaction sites separate from the active site.

The S1 subsite preferences of DPAP1 and cathepsin C, as revealed by PSL analysis, are similar to those of other C1 family endo- and exopeptidases for which similar data exist [46-48]. This is likely due to the paucity of interactions between the P1 residue sidechain and the enzyme domain that defines the S1 site [37], which in turn offers little opportunity to tune the specificity of this site. In contrast, the S2 subsite of C1-family peptidases is the only one that forms a pocket and is generally the most discriminating of the subsites [37,38]. In many cases, the S2 subsite exhibits a strong preference for hydrophobic sidechains which can be further divided into a preference for aromatic (e.g., cathepsin L) or aliphatic (e.g. cathepsin S) sidechains. The S2 subsite of cathepsin B has a comparatively broad specificity, in part due to the presence of a glutamate sidechain at the bottom of the S2 pocket that can interact with positively charged P2 sidechains [49]. The S2 preferences of DPAP1 and cathepsin C fall in between those of cathepsin S and cathepsin B. While aliphatic hydrophobic P2 sidechains are clearly preferred over aromatic sidechains, polar residues such as His, Ser, Thr and Gln are accepted as readily. However, in contrast to cathepsin B, substrates with Arg or Lys at the P2 position are not cleaved by DPAP1 or cathepsin C. A bias against aromatic and basic P2 sidechains by DPAP1 was also observed with a P2-diverse library of dipeptide vinyl sulfone inhibitors [7]. Crystal structures of cathepsin C have revealed a bound chloride ion at the bottom of the S2 pocket [13,14] with several water molecules filling the pocket. These water molecules may stabilize the binding of substrates with small polar residues such as Ser and Thr in the S2 pocket through hydrogen bonding. A

relatively broad S2 specificity is probably advantageous in enabling the efficient hydrolysis of sequence-diverse substrates in the lysosome (cathepsin C) or the food vacuole (DPAP1).

The ability of DPAP1 and cathepsin C to catalyze the hydrolysis of substrates with a P2 proline residue has been reported previously [5,25,41,50] and was confirmed in our PSL analysis. Substrates with a P2 proline residue are generally not cleaved by C1 family cysteine proteases, prominent exceptions being cathepsin K [46,51,52] and cathepsin L2 from the trematode *Fasciola hepatica* [53]. Mutagenic analysis has revealed that two residues in the S2 pocket of cathepsin K contribute to the acceptance of a P2 proline residue: Tyr67 and Leu205 (papain numbering; [52,54]). The homologous residues are Phe and Gln in DPAP1 and Phe and Ile in cathepsin C. In contrast, the homologous residues in cathepsin L, which does not efficiently cleave substrates with a P2 proline residue, are Leu and Ala. Thus, these two S2 subsite residues in DPAP1 and cathepsin C are much closer in character to those in cathepsin K. This observation suggests that the S2 subsites of DPAP1/cathepsin C and cathepsin K have evolved in a similar fashion to permit the efficient hydrolysis of substrates with a P2 proline residue. Consistent with this analysis, Arastu-Kapur *et al* have shown that a dipeptide vinyl sulfone inhibitor with a P2 proline residue exhibits high specificity for DPAP1 over the *P. falciparum* cysteine peptidases DPAP3 and falcipain-2 and -3 [7].

Despite the overall similarities in the S2 preferences of DPAP1 and cathepsin C, a few pronounced differences stood out. To further explore the S2 preferences of DPAP1 and cathepsin C, we assayed a P2-diverse panel of substrates with a highly-preferred P1 residue (Arg) to define in kinetic terms the differences in specificity observed with the positional scanning library. These experiments supplemented the PSL data by revealing large variations in k_{cat} and K_m values that

were not apparent from the relative rates of cleavage of the PSL members and by identifying substrate inhibition as a contributor to the observed S2 specificities.

Considering the k_{cat}/K_m values for DPAP1 (Table A-1), the trends observed with the PSL held up in the kinetic analysis, at least in a qualitative sense. With cathepsin C, a P2-Pro residue was predicted by the PSL data to make for a poor substrate in comparison to P2-Val. However, Pro-Arg-AMC and Val-Arg-ACC were hydrolyzed by cathepsin C with comparable catalytic efficiencies. This finding contrasts with a previous study showing a 10-fold increase in k_{cat}/K_m for the hydrolysis of Val-Phe-AMC relative to that of Pro-Phe-AMC [41], which is more in line with expectation from the PSL data. This discrepancy might be explained by the presence of positive co-operativity between P2-Pro and P1-Arg sidechains that does not exist with a P1-Phe or a randomized P1 substrate. It is also possible that differences in the structures of the ACC and AMC fluorophores could affect the relative k_{cat}/K_m values.

Cathepsin C was a substantially better catalyst than DPAP1. k_{cat}/K_m values for the hydrolysis of Pro-Arg-AMC and Val-Arg-ACC were over an order of magnitude higher for cathepsin C. One trivial explanation for this observation would be that the DPAP1 preparations contain a substantial fraction of catalytically dead enzyme. Given the low concentrations of both native and recombinant DPAP1 in the preparations described here, titration of active enzyme with an inhibitor was not feasible. However, the reasonable concordance of k_{cat}/K_m values for native and recombinant DPAP1, which were prepared in very different ways, lends confidence that these are not artifactually low.

Phe-Arg-ACC inhibited both DPAP1 and cathepsin C. DPAP1 activity was competitively inhibited with a low micromolar K_i and no substrate turnover was observed. In the case of cathepsin C, substrate turnover occurred with substrate inhibition at higher concentrations. These

results indicate that the apparent "preference" of cathepsin C for a P2 phenylalanine residue (compared with DPAP1) that was observed in the PSL profile cannot simply be attributed to differences in accommodation of this sidechain in the S2 subsites of the two enzymes. The inhibition of cathepsin C by phenylalanine-containing compounds was reported over 50 years ago by Fruton and Mycek [50], who found that phenylalaninamide, DL-Phe-Gly and L-Phe-L-Phe competitively inhibited cathepsin C. Taken together, these observations indicate that a phenylalanyl moiety, in certain contexts, can interact with DPAP1 and cathepsin C in a manner that is unproductive for catalysis.

In conclusion, the relatively broad S1 and S2 specificities of DPAP1 and its high catalytic efficiency at acidic pH are consistent with a key role in peptide turnover in the food vacuole. A chloride concentration inside the parasite of 48 mM [55] is adequate for DPAP1 activation. We envision DPAP1 acting on a wide range of sequence-diverse oligopeptides that are generated by the action of endopeptidases on globin polypeptides. The dipeptides produced through DPAP1 catalysis could then be hydrolyzed into two amino acids by the vacuolar aminopeptidase PfA-M1 [6]. Thus, DPAP1 likely accelerates the rate of production of amino acids from globin by increasing the concentration of PfA-M1 substrates. Conversely, PfA-M1 could remove from the amino termini of oligopeptides those residues that prohibit DPAP1 cleavage (for example, Arg or Lys), thereby preventing the accumulation of such "blocked" peptides. We have proposed a similar role for *P. falciparum* aminopeptidase P with respect to proline-containing substrates [6]. Our data suggest that inhibitors that block DPAP1 will impede the production of amino acids from hemoglobin and may have anti-malarial activity; however, it appears that the design of an inhibitor that is highly selective for DPAP1 over cathepsin C will be a challenge.

Experimental Procedures

Substrates and inhibitors

Phe-Arg-AMC and Arg-Arg-AMC were obtained from Bachem. To synthesize Val-Arg-ACC, Ile-Arg-ACC, Phe-Arg-ACC and Pro-Nle-ACC, N-fluorenylmethyloxycarbonyl-7-amino-4-carbamoylmethylcoumarin (N-Fmoc-ACC; a gift of Jonathan A. Ellman) was linked to Rink Amide AM polystyrene resin and the P1 residue was coupled to the ACC-resin as described [56]. The second Fmoc-protected amino acid was linked using standard *N,N*-diisopropylcarbodiimide /1-hydroxybenzotriazole coupling conditions. After Fmoc deprotection of the N-terminal amine with 20% piperidine, treatment with trifluoroacetic acid/water/triisopropylsilane (95:2.5:2.5) resulted in the cleavage of fully deprotected dipeptide-ACC substrates. Substrates were purified by high pressure liquid chromatography on a C18 reverse phase column with a gradient of 5 to 60% acetonitrile in water and 0.1 % trifluoroacetic acid. The purity of the collected fractions was assessed by liquid chromatography-mass spectrometry. All substrates were at least 95% pure.

The inhibitor Pro-Arg-fluoromethylketone was custom synthesized by Enzyme Product Systems. Bestatin and *trans*-epoxysuccinyl-L-leucylamido(4-guanidino)butane (E-64) were obtained from Sigma-Aldrich and 4-(2-Aminoethyl)-benzenesulfonyl fluoride hydrochloride (AEBSF) was obtained from Roche Applied Science. Synthesis of the cathepsin C inhibitors 1-(2*S*-2-aminobutanoyl)-4-{2*S*-*N*-[2*S*-3-(m-fluorophenyl)propan-2-yl-amide]-4-phenylbutan-2-yl-amide}7semicarbazide (compound **1** in Fig. A-4) and *S*-2-aminobutyryl-phenylalanine-nitrile (compound **2** in Fig. A-4) has been described previously [11,43].

Purification of native DPAP1

Native DPAP1 was purified from saponin-treated parasites as previously described [5] with the modification that two rather than three column steps were employed, resulting in higher yield. Briefly, clarified parasite lysate prepared in 20 mM bis-tris•HCl pH 6.0 was loaded onto a MonoQ 5/50 GL column (GE Biosciences) equilibrated in the same buffer. Bound protein was eluted with a linear gradient of 0 - 1 M NaCl. Fractions containing DPAP1 activity were pooled, concentrated and injected onto a Superdex 200 10/300 GL gel filtration column (GE Biosciences) equilibrated in 50 mM Tris-HCl pH 7.5, 200 mM NaCl and 1 mM EDTA. Active fractions were pooled, supplemented with 0.1% Triton X-100, 2 mM dithiothreitol and 10% glycerol, snap frozen, and stored at -80 °C.

Expression and purification of MBP-TEV protease

The S219V autoinactivation-resistant mutant of tobacco etch virus protease was expressed as a fusion with maltose binding protein from plasmid pRK1043 [21]. The plasmid was transformed into *E. coli* strain Rosetta2 (EMD Biosciences) and grown in Luria-Bertani broth containing 100 mg/mL ampicillin and 30 mg/mL chloramphenicol to an optical density at 600 nm of about 0.7, at which point the temperature was reduced to 30 °C and 1 mM isopropyl β-D-1-thiogalactopyranoside was added. Cells were harvested 4 hours later by centrifugation. MBP-TEV protease was purified by resuspending the cell pellet in 50 mM HEPES pH 7.5, 200 mM NaCl and 1 mM EDTA, 100 mM AEBSF and 1 mg/mL lysozyme and incubating on ice for 30 minutes. Cells were disrupted by sonication and the lysate was clarified by two rounds of centrifugation at 15 000 g for 10 minutes at 4 °C. The clarified lysate was loaded onto an amylose column (New England Biologicals) equilibrated in 50 mM HEPES pH 7.5, 200 mM

NaCl, 1 mM EDTA. MBP-TEV protease was eluted with the same buffer supplemented with 1 M a-methylglucopyranoside. Fractions containing TEV protease were pooled, dialyzed overnight at 4 °C against 50 mM HEPES pH 8.2, 200 mM NaCl, 5 mM dithiothreitol, 1 mM EDTA and 10% glycerol, snap frozen in liquid nitrogen and stored at -80 °C. Because dithiothreitol inhibited DPAP1 activation, MBP-TEV protease was dialyzed against 50 mM HEPES pH 8.2, 200 mM NaCl, 1 mM reduced glutathione, 1 mM EDTA and 10% glycerol prior to addition to MBP-DPAP1-His_6.

Cloning, expression, purification and activation of recombinant DPAP1-His_6

The DPAP1 coding sequence was PCR amplified from the genomic DNA of *P. falciparum* clone 3D7 using primers 5'-GCACG*GAATTC*GAAAACCTGTATTTTCAGGATTTACCAACCCATGTAGAAAC (EcoRI site is in italics, TEV protease recognition sequence is underlined) and 5'-GCACG*CTGCAG*TTAATGATGATGATGATGATGATTTCCTAATTCCTTTTGCATTT (PstI site is in italics, hexahistidine tag is underlined). The PCR product was digested with EcoRI and PstI and cloned into the same sites in pMAL-c2x (New England Biolabs) which generated the MBP-DPAP1-His_6 chimera. Coding sequences were verified by DNA sequencing.

The MBP-DPAP1-His_6 expression plasmid was transformed into a *trxB/gor* strain of *E. coli* (Rosetta-gami 2; EMD Biosciences). Bacteria were grown at 37 °C in Luria-Bertani broth containing 100 mg/mL ampicillin to an optical density at 600 nm of about 0.7, at which point the temperature was reduced to 25 °C. After 20 minutes, protein expression was induced by adding 0.3 mM isopropyl β-D-1-thiogalactopyranoside and shaking for 6 hours. Bacteria were collected by centrifugation and stored at -80 °C.

To purify MBP-DPAP1-His_6, pellets of induced *E. coli* were resuspended in 15 mL of 20 mM NaH_2PO_4 pH 7.5, 500 mM NaCl, 30 mM imidazole (immobilized metal affinity chromatography (IMAC) buffer) containing 1 mg/mL hen egg white lysozyme and incubated on ice for 30 minutes. Bacteria were disrupted by sonication and cell debris was removed by two rounds of centrifugation at 20,000 g for 40 minutes at 4 °C. The cleared supernatant was loaded onto an Ni(II)-charged immobilized metal affinity column equilibrated in IMAC buffer. The column was washed extensively and bound protein was eluted with a gradient of 30 - 500 mM imidazole. Fractions containing MBP-DPAP1-His_6 were pooled and stored at 4 °C.

Cleavage of MBP from MBP-DPAP1-His_6 was achieved by incubating MBP-DPAP1-His_6 with purified MBP-TEV protease (100 µg/mL) overnight at room temperature in 10 mM Tris-HCl pH 8, 1 mM reduced glutathione, 0.3 mM oxidized glutathione and 0.5 mM EDTA. To separate DPAP1-His_6 from cleaved MBP, uncleaved MBP-DPAP1-His_6 and MBP-TEV protease, amylose resin (New England Biolabs) was added, the mixture was rocked gently for 30 minutes at room temperature and the supernatant containing DPAP1-His_6 was recovered by centrifugation. To excise the internal DPAP1 proregion, bovine pancreatic trypsin (Sigma, T1426) was added at a concentration of 1.5 µg/mL for 90 minutes at room temperature after which trypsin was inactivated by adding 0.5 mM AEBSF. DPAP1-His_6 was separated from trypsin and peptide fragments by IMAC as described above. Active fractions were pooled, concentrated and purified on a Superdex 200 gel filtration column equilibrated with 50 mM Tris-HCl pH 8, 200 mM NaCl and 1 mM EDTA. Fractions with active enzyme were pooled, supplemented with 10% glycerol and 2 mM dithiothreitol, snap frozen in liquid nitrogen and stored at -80 °C. Upon thawing, Triton X-100 was added at 0.1% to preserve full activity. The yield of purified, activated recombinant DPAP1 was about 30 µg per liter of induced *E. coli*

culture. Immunoblot analysis of recombinant DPAP1 was accomplished using a monoclonal antibody that recognizes the exclusion domain (304.4.2.2) and an anti-peptide polyclonal antibody (1502) that recognizes a 14-amino acid peptide sequence in the heavy chain [5].

Trypsin activity assays

Potential trypsin contamination of purified recombinant DPAP1 was assayed against the endopeptidase substrate N-(carbobenzyloxy)-L-phenylalanyl-L-arginyl-7-amido-4-methylcoumarin (100 μM) in an optimized trypsin assay containing 50 mM Tris-HCl pH 8.0, 20 mM $CaCl_2$ or in the standard DPAP1 assay. Two microliters of recombinant DPAP1 stock were assayed, which represents a ten-fold excess over the amount of enzyme typically added to DPAP1 assays.

Expression and purification of human cathepsin C

Activated recombinant human cathepsin C was purified from baculovirus-infected insect cell culture medium as previously described [17]. The enzyme was stored in 50% glycerol at -20 °C.

Protein quantitation

Recombinant DPAP1 was quantified using the fluorescence-based NanoOrange assay (Invitrogen) according to the manufacturer's instructions. Fluorescence values of samples, matched buffer blanks and bovine serum albumin standards were read on a Spectramax M5e microplate fluorometer (Molecular Devices) with excitation at 470 nm, emission at 590 nm and a 570 nm cutoff filter. The amount of native DPAP1 in a partially purified preparation was

estimated by immunoblotting. Known amounts of recombinant protein (20 to 80 ng) were electrophoresed along with native DPAP1 on a 12% SDS-polyacrylamide gel. After blotting to nitrocellulose, DPAP1 was detected using the monoclonal antibody 304.2.4.4 ([5]; 1:100 dilution), an alkaline phosphatase-conjugated secondary antibody and ECL Plus. Fluorescence signal was recorded on a STORM 840 phosphorimager. Peak volumes were quantified using ImageQuant TL version 7.0 software (GE Bioscences). Because the monoclonal antibody recognizes two bands in recombinant DPAP1 (Fig. A-1), the volumes of these bands were summed to obtain a final integrated volume. The amount of native enzyme was determined from a standard curve plotted as peak volume *vs.* amount of rDPAP1. The R^2 value for the linear fit was 0.98.

Gel filtration analysis of quaternary structure

Native DPAP1 was purified as described above, dialyzed into 50 mM sodium-MES pH 6.0, 200 mM NaCl, 1 mM EDTA overnight at 4 °C and then injected onto a Superdex 200 gel filtration column equilibrated in the same buffer. Fractions of 0.33 mL were collected and assayed for DPAP1 activity as described previously. Recombinant cathepsin C was diluted into gel filtration buffer, concentrated and was analyzed as described for DPAP1. Molecular masses were estimated from a calibration curve generated with ferretin (440 kDa), catalase (232 kDa), aldolase (158 kDa), albumin (67 kDa), ovalbumin (43 kDa), chymotrypsinogen A (25 kDa) and ribonuclease A (14 kDa). The void volume was estimated with blue dextran 2000.

DPAP1 activity assays and effects of ionic strength and chloride

DPAP1 activity was routinely assayed at 25 °C in a volume of 200μmL in 50 mM sodium MES pH 6.0, 30 mM NaCl, 2 mM dithiothreitol, 1 mM EDTA, 0.1% Triton X-100, 10 μM bestatin (to inhibit any remaining aminopeptidase activity in partially purified native DPAP1) and, unless otherwise noted, 100 μM Pro-Arg-AMC. Changes in fluorescence were monitored with a Victor^3 microplate fluorometer (PerkinElmer) with an excitation filter of 380 nm (10 nm bandwidth) and an emission filter of 460 nm (25 nm bandwidth).

To evaluate the effect of chloride on DPAP1 activity, chloride was first depleted from native and recombinant DPAP1 by dialysis against 50 mM sodium MES pH 6.0, 1 mM EDTA and 0.1% Triton X-100 in Slide-A-Lyzer MINI dialysis cassettes with a 10,000 molecular weight cutoff (Pierce). Alternately, native DPAP1 was prepared by carrying out the gel filtration step of the purification in chloride-free buffer (50 mM sodium HEPES pH 7.5, 100 mM Na_2SO_4 and 1 mM EDTA). DPAP1 assays contained 50 mM sodium MES pH 6.0, 2 mM dithiothreitol, 1 mM EDTA, 0.1% Triton X-100 and 10 μM bestatin. The chloride concentration was varied from 0 – 80 mM by adding NaCl. The ionic strength was held constant by adding Na_2SO_4 such that the ionic strength contributed by NaCl and Na_2SO_4 totaled 100 mM in all assays. Prolyl-norleucyl-ACC, which lacks a chloride counterion, was used as the substrate (100 μM).

S1 and S2 profiling with a positional scanning library

The 40 members of the dipeptide-ACC positional scanning library were assayed at 25 °C in 50 mM sodium MES pH 6.0, 30 mM NaCl, 2 mM dithiothreitol, 1 mM EDTA and 10 μM substrate (diluted from a 1 mM stock in dimethylsulfoxide) in a volume of 100 μL. Since each substrate mixture consisted of 20 compounds, each compound was present in the assay at 0.5

μM. In assays containing partially purified native DPAP1, 1 μM bestatin and 1 μM E-64 were added to suppress aminopeptidase and falcipain activities, respectively. In addition, background rates were assessed using control assays containing native DPAP1 that had been pre-treated for 15 minutes with the irreversible inhibitor Pro-Arg-fluoromethylketone. For recombinant DPAP1 and cathepsin C, no background rate adjustment was made. Assays were conducted in duplicate. Fluorescence values were read in 96 well half-area microplates as described previously

Kinetic analysis of DPAP1 and cathepsin C activity and inhibition

Steady-state kinetic parameters for hydrolysis of fluorogenic dipeptide-AMC or -ACC substrates were determined at 25 °C by assaying DPAP1 and cathepsin C in 50 mM sodium MES pH 6.0, 2 mM dithiothreitol and 1 mM EDTA. The final concentration of chloride, including that carried over with the enzyme and dipeptide-AMC substrates, was maintained at 30 mM by addition of NaCl. Native DPAP1 assays also contained 10 mM bestatin to suppress any contaminating aminopeptidase activity. Substrate concentrations were varied from approximately $0.2K_m$ to $5K_m$. Enzyme concentrations were 0.3 nM native DPAP1, 0.8 nM rDPAP1 and 0.06 – 0.3 nM cathepsin C. At these concentrations, substrate consumption was less that 10% over the course of the assay. Fluorescence values were converted to AMC concentrations by reference to a standard AMC solution. Rates from dipeptide-ACC substrates were adjusted to reflect the 2.8-fold higher fluorescence of ACC over that of AMC [47]. Assays were conducted in triplicate. Rates were determined from the linear portions of the progress curves. In the case of DPAP1, rates were measured following a ~15 minute non-linear segment that may reflect reductive activation of the enzyme. Rates were fit by non-linear regression to the Michaelis-Menten equation $\upsilon = Vs/(K_m + s)$ using Kaleidagraph 4.1 (Synergy Software) where V is the limiting

velocity and *s* is substrate concentration. k_{cat} was calculated from the relationship $V = k_{cat}[E]$. The K_i for inhibition of DPAP1 by Phe-Arg-ACC was determined by the Dixon method [57]. Methods for the determination of K_i values for the inhibitors in Fig. A-4 are provided as Supplementary Methods.

To assess the effects of pH on catalytic efficiency, assays were carried out as described in the above paragraph with PR-AMC (0 – 500 μM) as substrate. Buffering capacity was provided by 50 mM sodium acetate (pH 4.5 and 5.0), sodium MES (pH 5.5, 6.0 and 6.5) or sodium HEPES (pH 7.0). Buffer pK_a values were adjusted for an ionic strength of 100 mM and a temperature of 25 °C [58]. Contributions of ionic buffer components to the ionic strength were calculated using the Henderson-Hasselbalch equation. Total ionic strength of the reactions was maintained at 100 mM by adding Na_2SO_4. Kinetic parameters were obtained from non-linear regression fits to the Michaelis-Menten equation. No substrate inhibition was observed at any pH value.

Acknowledgements

We wish to thank D. Waugh for the MBP-TEV expression plasmid, J. Ellman for the positional scanning library, D. Goldberg for anti-DPAP1 antibodies, M. Leyva in J. Ellman's laboratory for Fmoc-ACC, S. Dalal for constructing the DPAP1 expression plasmid and M. Drew for critique of the manuscript.

References

1. Krugliak M, Zhang J, Ginsburg H (2002) Intraerythrocytic Plasmodium falciparum utilizes only a fraction of the amino acids derived from the digestion of host cell cytosol for the biosynthesis of its proteins. Mol Biochem Parasitol 119: 249-256.

2. Loria P, Miller S, Foley M, Tilley L (1999) Inhibition of the peroxidative degradation of haem as the basis of action of chloroquine and other quinoline antimalarials. Biochem J 339 (Pt 2): 363-370.
3. Goldberg DE (2005) Hemoglobin degradation. Curr Top Microbiol Immunol 295: 275-291.
4. Rosenthal PJ, McKerrow JH, Aikawa M, Nagasawa H, Leech JH (1988) A malarial cysteine proteinase is necessary for hemoglobin degradation by *Plasmodium falciparum*. J Clin Invest 82: 1560-1566.
5. Klemba M, Gluzman I, Goldberg DE (2004) A Plasmodium falciparum dipeptidyl aminopeptidase I participates in vacuolar hemoglobin degradation. J Biol Chem 279: 43000-43007.
6. Dalal S, Klemba M (2007) Roles for two aminopeptidases in vacuolar hemoglobin catabolism in Plasmodium falciparum. J Biol Chem 282: 35978-35987.
7. Arastu-Kapur S, Ponder EL, Fonovic UP, Yeoh S, Garinger M, et al. (2008) Chemically mapping protease pathways involved in the regulation of erythrocyte rupture by the human malaria parasite *Plasmodium falciparum* Nat Chem Biol 4: 203-213.
8. Adkison AM, Raptis SZ, Kelley DG, Pham CT (2002) Dipeptidyl peptidase I activates neutrophil-derived serine proteases and regulates the development of acute experimental arthritis. J Clin Invest 109: 363-371.
9. Pham CT, Ley TJ (1999) Dipeptidyl peptidase I is required for the processing and activation of granzymes A and B *in vivo*. Proc Natl Acad Sci USA 96: 8627-8632.
10. Wolters PJ, Pham CT, Muilenburg DJ, Ley TJ, Caughey GH (2001) Dipeptidyl peptidase I is essential for activation of mast cell chymases, but not tryptases, in mice. J Biol Chem 276: 18551-18556.
11. Bondebjerg J, Fuglsang H, Valeur KR, Pedersen J, Naerum L (2006) Dipeptidyl nitriles as human dipeptidyl peptidase I inhibitors. Bioorg Med Chem Lett 16: 3614-3617.
12. Methot N, Rubin J, Guay D, Beaulieu C, Ethier D, et al. (2007) Inhibition of the activation of multiple serine proteases with a cathepsin C inhibitor requires sustained exposure to prevent pro-enzyme processing. J Biol Chem 282: 20836-20846.
13. Olsen JG, Kadziola A, Lauritzen C, Pedersen J, Larsen S, et al. (2001) Tetrameric dipeptidyl peptidase I directs substrate specificity by use of the residual pro-part domain. FEBS Lett 506: 201-206.
14. Turk D, Janjic V, Stern I, Podobnik M, Lamba D, et al. (2001) Structure of human dipeptidyl peptidase I (cathepsin C): exclusion domain added to an endopeptidase framework creates the machine for activation of granular serine proteases. EMBO J 20: 6570-6582.
15. Schechter I, Berger A (1967) On the size of the active site in proteases. I. Papain. Biochem Biophys Res Commun 27: 157-162.
16. Molgaard A, Arnau J, Lauritzen C, Larsen S, Petersen G, et al. (2007) The crystal structure of human dipeptidyl peptidase I (cathepsin C) in complex with the inhibitor Gly-Phe-CHN2. Biochem J 401: 645-650.
17. Dahl SW, Halkier T, Lauritzen C, Dolenc I, Pedersen J, et al. (2001) Human recombinant pro-dipeptidyl peptidase I (cathepsin C) can be activated by cathepsins L and S but not by autocatalytic processing. Biochemistry 40: 1671-1678.
18. Goh LL, Loke P, Singh M, Sim TS (2003) Soluble expression of a functionally active *Plasmodium falciparum* falcipain-2 fused to maltose-binding protein in *Escherichia coli*. Protein Expr Purif 32: 194-201.

19. Goh SL, Goh LL, Sim TS (2005) Cysteine protease falcipain 1 in *Plasmodium falciparum* is biochemically distinct from its isozymes. Parasitol Res 97: 295-301.
20. Kapust RB, Tozser J, Copeland TD, Waugh DS (2002) The P1' specificity of tobacco etch virus protease. Biochem Biophys Res Commun 294: 949-955.
21. Kapust RB, Tozser J, Fox JD, Anderson DE, Cherry S, et al. (2001) Tobacco etch virus protease: mechanism of autolysis and rational design of stable mutants with wild-type catalytic proficiency. Protein Eng 14: 993-1000.
22. Bessette PH, Aslund F, Beckwith J, Georgiou G (1999) Efficient folding of proteins with multiple disulfide bonds in the *Escherichia coli* cytoplasm. Proc Natl Acad Sci USA 96: 13703-13708.
23. Lauritzen C, Pedersen J, Madsen MT, Justesen J, Martensen PM, et al. (1998) Active recombinant rat dipeptidyl aminopeptidase I (cathepsin C) produced using the baculovirus expression system. Protein Expr Purif 14: 434-442.
24. McDonald JK, Reilly TJ, Zeitman BB, Ellis S (1966) Cathepsin C: a chloride-requiring enzyme. Biochem Biophys Res Commun 22: 771-775.
25. McDonald JK, Zeitman BB, Reilly TJ, Ellis S (1969) New observations on the substrate specificity of cathepsin C (dipeptidyl aminopeptidase I). Including the degradation of beta-corticotropin and other peptide hormones. J Biol Chem 244: 2693-2709.
26. Cornish-Bowden A (2004) Fundamentals of enzyme kinetics. London: Portland Press.
27. Dolenc I, Turk B, Pungercic G, Ritonja A, Turk V (1995) Oligomeric structure and substrate induced inhibition of human cathepsin C. J Biol Chem 270: 21626-21631.
28. Nagler DK, Tam W, Storer AC, Krupa JC, Mort JS, et al. (1999) Interdependency of sequence and positional specificities for cysteine proteases of the papain family. Biochemistry 38: 4868-4874.
29. Schneck JL, Villa JP, McDevitt P, McQueney MS, Thrall SH, et al. (2008) Chemical mechanism of a cysteine protease, cathepsin C, as revealed by integration of both steady-state and pre-steady-state solvent kinetic isotope effects. Biochemistry 47: 8697-8710.
30. Bennett TN, Kosar AD, Ursos LM, Dzekunov S, Singh Sidhu AB, et al. (2004) Drug resistance-associated pfCRT mutations confer decreased *Plasmodium falciparum* digestive vacuolar pH. Mol Biochem Parasitol 133: 99-114.
31. Klonis N, Tan O, Jackson K, Goldberg D, Klemba M, et al. (2007) Evaluation of pH during cytostomal endocytosis and vacuolar catabolism of hemoglobin in *Plasmodium falciparum*. Biochem J 407: 343-354.
32. Krogstad DJ, Schlesinger PH, Gluzman IY (1985) Antimalarials increase vesicle pH in *Plasmodium falciparum*. J Cell Biol 101: 2302-2309.
33. Kuhn Y, Rohrbach P, Lanzer M (2007) Quantitative pH measurements in *Plasmodium falciparum*-infected erythrocytes using pHluorin. Cell Microbiol 9: 1004-1013.
34. Storer AC, Menard R (1994) Catalytic mechanism in papain family of cysteine peptidases. Methods Enzymol 244: 486-500.
35. Fersht A (1999) Structure and mechanism in protein science. New York: W.H. Freeman and Company.
36. Cigic B, Pain RH (1999) Location of the binding site for chloride ion activation of cathepsin C. Eur J Biochem 264: 944-951.
37. McGrath ME (1999) The lysosomal cysteine proteases. Annu Rev Biophys Biomol Struct 28: 181-204.

38. Turk D, Guncar G, Podobnik M, Turk B (1998) Revised definition of substrate binding sites of papain-like cysteine proteases. Biol Chem 379: 137-147.
39. Schneider EL, Craik CS (2009) Positional scanning synthetic combinatorial libraries for substrate profiling. Methods Mol Biol 539: 59-78.
40. Leiting B, Pryor KD, Wu JK, Marsilio F, Patel RA, et al. (2003) Catalytic properties and inhibition of proline-specific dipeptidyl peptidases II, IV and VII. Biochem J 371: 525-532.
41. Tran TV, Ellis KA, Kam CM, Hudig D, Powers JC (2002) Dipeptidyl peptidase I: importance of progranzyme activation sequences, other dipeptide sequences, and the N-terminal amino group of synthetic substrates for enzyme activity. Arch Biochem Biophys 403: 160-170.
42. McGuire MJ, Lipsky PE, Thiele DL (1992) Purification and characterization of dipeptidyl peptidase I from human spleen. Arch Biochem Biophys 295: 280-288.
43. Bondebjerg J, Fuglsang H, Valeur KR, Kaznelson DW, Hansen JA, et al. (2005) Novel semicarbazide-derived inhibitors of human dipeptidyl peptidase I (hDPPI). Bioorg Med Chem 13: 4408-4424.
44. Cigic B, Krizaj I, Kralj B, Turk V, Pain RH (1998) Stoichiometry and heterogeneity of the pro-region chain in tetrameric human cathepsin C. Biochim Biophys Acta 1382: 143-150.
45. Cigic B, Dahl SW, Pain RH (2000) The residual pro-part of cathepsin C fulfills the criteria required for an intramolecular chaperone in folding and stabilizing the human proenzyme. Biochemistry 39: 12382-12390.
46. Choe Y, Leonetti F, Greenbaum DC, Lecaille F, Bogyo M, et al. (2006) Substrate profiling of cysteine proteases using a combinatorial peptide library identifies functionally unique specificities. J Biol Chem 281: 12824-12832.
47. Harris JL, Backes BJ, Leonetti F, Mahrus S, Ellman JA, et al. (2000) Rapid and general profiling of protease specificity by using combinatorial fluorogenic substrate libraries. Proc Natl Acad Sci USA 97: 7754-7759.
48. Subramanian S, Hardt M, Choe Y, Niles RK, Johansen EB, et al. (2009) Hemoglobin cleavage site-specificity of the *Plasmodium falciparum* cysteine proteases falcipain-2 and falcipain-3. PLoS ONE 4: e5156.
49. Jia Z, Hasnain S, Hirama T, Lee X, Mort JS, et al. (1995) Crystal structures of recombinant rat cathepsin B and a cathepsin B-inhibitor complex. Implications for structure-based inhibitor design. J Biol Chem 270: 5527-5533.
50. Fruton JS, Mycek MJ (1956) Studies on beef spleen cathepsin C. Arch Biochem Biophys 65: 11-20.
51. Garnero P, Borel O, Byrjalsen I, Ferreras M, Drake FH, et al. (1998) The collagenolytic activity of cathepsin K is unique among mammalian proteinases. J Biol Chem 273: 32347-32352.
52. Lecaille F, Choe Y, Brandt W, Li Z, Craik CS, et al. (2002) Selective inhibition of the collagenolytic activity of human cathepsin K by altering its S2 subsite specificity. Biochemistry 41: 8447-8454.
53. Dowd AJ, Smith AM, McGonigle S, Dalton JP (1994) Purification and characterisation of a second cathepsin L proteinase secreted by the parasitic trematode *Fasciola hepatica*. Eur J Biochem 223: 91-98.

54. Lecaille F, Chowdhury S, Purisima E, Bromme D, Lalmanach G (2007) The S2 subsites of cathepsins K and L and their contribution to collagen degradation. Protein Sci 16: 662-670.
55. Henry RI, Cobbold SA, Allen RJW, Khan A, Hayward R, et al. (2010) An acid-loading chloride transport pathway in the intraerythrocytic malaria parasite, *Plasmodium falciparum*. J Biol Chem 285: 18615-18626.
56. Maly DJ, Leonetti F, Backes BJ, Dauber DS, Harris JL, et al. (2002) Expedient solid-phase synthesis of fluorogenic protease substrates using the 7-amino-4-carbamoylmethylcoumarin (ACC) fluorophore. J Org Chem 67: 910-915.
57. Dixon M (1953) The determination of enzyme inhibitor constants. Biochem J 55: 170-171.
58. Ellis KJ, Morrison JF (1982) Buffers of constant ionic strength for studying pH-dependent processes. Methods Enzymol 87: 405-426.